#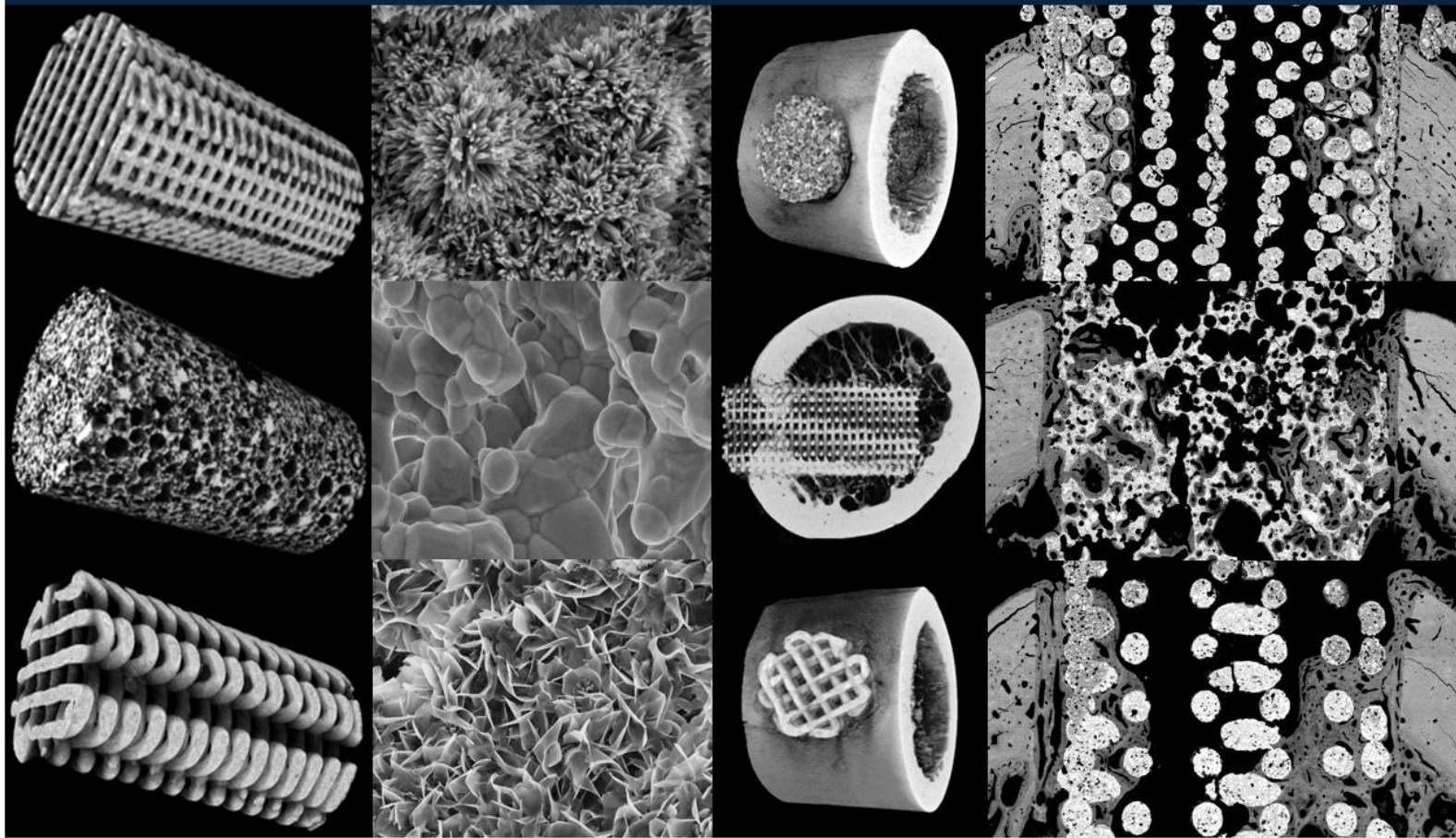 INTRINSIC OSTEOINDUCTION AND OSTEOGENESIS OF BIOMIMETIC CALCIUM PHOSPHATE SCAFFOLDS WITH DIFFERENT NANO-, MICRO- AND MACROPOROSITIES

ECTOPIC AND ORTHOTOPIC IMPLANTATION IN A CANINE MODEL

Albert Barba Serrahima
PhD Thesis

Maria Pau Ginebra Molins
Jordi Franch Serracanta

Intrinsic osteoinduction and osteogenesis of biomimetic calcium phosphate scaffolds with different nano-, micro- and macroporosities : ectopic and orthotopic implantation in a canine model

Albert Barba Serrahima

PhD Thesis

Doctoral Program of Biomedical Engineering

UNIVERSITAT POLITÈCNICA
DE CATALUNYA
BARCELONATECH
UPC

INTRINSIC OSTEOINDUCTION AND OSTEOGENESIS OF BIOMIMETIC CALCIUM PHOSPHATE SCAFFOLDS WITH DIFFERENT NANO-, MICRO- AND MACROPOROSITIES

ECTOPIC AND ORTHOTOPIC IMPLANTATION IN A CANINE MODEL

PhD Candidate: Albert Barba Serrahima

Supervisors: Prof. Maria Pau Ginebra Molins
Prof. Jordi Franch Serracanta

Biomaterials, Biomechanics and Tissue engineering Group

BIOMATERIALS,
BIOMECHANICS &
TISSUE ENGINEERING

Department of Material Science and Metallurgical Engineering

Universitat Politècnica de Catalunya

Barcelona, 2018

TABLE OF CONTENTS

CHAPTER 1

INTRODUCTION

CHAPTER 2 (Study I)

OSTEOINDUCTION BY FOAMED AND 3D-PRINTED CALCIUM PHOSPHATE SCAFFOLDS: EFFECT OF NANOSTRUCTURE AND PORE ARCHITECTURE

<u>CHAPTER 3</u> (Study II)

OSTEOGENESIS BY FOAMED AND 3D-PRINTED NANOSTRUCTURED CALCIUM PHOSPHATE SCAFFOLDS: EFFECT OF PORE ARCHITECTURE

<u>CHAPTER 4</u> (Study III)

OSTEOINDUCTION AND OSTEOGENSIS BY NANOSTRUCTURED CALCIUM PHOSPHATE SCAFFOLDS: EFFECT OF NANOCRYSTAL MORPHOLOGY AND CARBONATE DOPING

CHAPTER 5

CHAPTER 6

ANNEX

ABSTRACT

The development of synthetic bone substitutes with enhanced osteogenic properties is urged by the global ageing population. Sintered calcium-phosphate (CaP) ceramics are the most widely used synthetic biomaterials for bone regeneration. However, their clinical performance is inferior to those of autografts, which are still considered the gold standard, despite the serious drawbacks associated with the need of a harvesting surgery.

This thesis aims at providing new insights in the development of CaP biomaterials with intrinsic osteoinductive properties, that is, with the capacity to foster the differentiation of mesenchymal stem cells to bone forming cells, without the need of adding exogenous growth factors. Previous studies pointed to chemical composition, macropore architecture, microstructural topography and specific surface area (SSA) as critical factors in the intrinsic osteoinduction of biomaterials. However, only sintered ceramics with a limited range of porosities and low SSAs had been analyzed so far. In the present thesis, we were able to extend this range to the nanoscale by using biomimetic low-temperature processing routes. Foaming and 3D-printing methods allowed producing biomimetic CaP scaffolds with tailored macropore architectures together with controlled micro and nanoporosity and, hence, high SSAs.

In order to evaluate the intrinsic osteoinduction of this new family of biomimetic bone substitutes, nanostructured calcium deficient hydroxyapatite (CDHA) scaffolds with needle-like crystal morphology were implanted intramuscularly in a canine model, and compared with two sintered ceramics, namely biphasic calcium phosphate and beta-tricalcium phosphate (**Study I**). The results showed that the high reactivity of nanostructured biomimetic CDHA, combined with a spherical concave macroporosity of foamed scaffolds, accelerated and enhanced the osteoinduction potential beyond the limits of conventional, microstructured, sintered ceramics.

As a second step, the effect of macropore geometry of nanostructured CDHA on the bone healing capacity was analyzed. The same foamed and 3D-printed CDHA scaffolds were implanted intraosseoulsy in a canine model (**Study II**). Whereas nanostructured CDHA was shown to be highly osteoconductive irrespective of macropore geometry, a superior osteogenic capacity was observed in the foamed scaffolds, which correlated well with the higher intrinsic osteoinductive potential demonstrated previously. Moreover, foams showed a higher cell-mediated degradation than the 3D-printed constructs, with a simultaneous and progressive replacement of the scaffold by new bone, demonstrating that the control of macropore architecture allows tuning both material degradation and new bone formation.

Finally, aiming to further mimic the natural bone apatite, the effect of nanocrystal morphology (plate *vs.* needle) and carbonate doping on the intrinsic bioactivity of biomimetic CDHA was investigated. To this end, CDHA foams with different nanostructures (Coarse/Fine-CDHA) and carbonated CDHA foams were compared, both in canine ectopic and orthotopic implantation models (**Study III**). Fine-CDHA foams showed a superior osteoinduction and bone healing potential, as well as a higher degradation than Coarse-CDHA foams, suggesting that there is a threshold value in terms of SSA necessary to activate the cell-mediated resorption and the associated osteoinduction, which determines in turn the osteogenic capacity of the materials in a bony enviroment. Moreover, carbonate dopping of CDHA accelerated both intrinsic osteoinduction and bone healing, simultaneously increasing the cell-mediated resorption. Thus, the increased biomimetism of CDHA allowed the material to enter the natural bone remodelling cycle, this resulting in a tight synchronization between material degradation and bone formation, and ultimately, obtaining bone substitutes with enhanced bone regeneration potential.

RESUM

L'envelliment global de la població exigeix el desenvolupament de nous substituts ossis sintètics amb capacitats osteogèniques optimitzades. Tot i que les ceràmiques de fosfats de calci (CaP) sinteritzades són els biomaterials sintètics més utilitzats en regeneració òssia, la seva eficiència és inferior a la dels empelts d'os autòleg, els quals continuen sent el tractament de primera elecció malgrat presentar inconvenients importants associats a la necessitat d'una segona cirurgia.

Aquesta tesi té com a objectiu optimitzar el desenvolupament de biomaterials de CaP amb propietats osteoinductives, fet que estimula la diferenciació de cèl·lules mare mesenquimals a cèl·lules osteogèniques, sense l'ús de factors de creixement exògens. Estudis recents han identificat diferents factors crítics en l'osteoinducció intrínseca dels biomaterials com ara la composició química, la macroporositat, la microestructura i la superfície específica (SSA). Fins al moment, només s'han analitzat ceràmiques sinteritzades amb un rang limitat de porositats i SSAs. Tanmateix, en la present tesi s'ha aconseguit augmentar aquest rang a la nanoescala per mitjà de rutes de processament biomimètiques a baixes temperatures. L'escumat i la impressió 3D de CaP biomimètics, ha permès l'obtenció d'implants amb arquitectures macroporoses específicament modulades conjuntament amb micro i nanoporositats controlades, i per tant, amb SSAs significativament superiors.

Per tal d'avaluar l'osteoinducció intrínseca d'aquests nous materials biomimètics, es van implantar intramuscularment materials nanoestructurats (cristalls tipus agulla) de hidroxiapatita deficient en calci (CDHA) en un model caní, i es van comparar amb dues ceràmiques sinteritzades (**Estudi I**). Els resultats van mostrar que la gran reactivitat de la CDHA nanoestructurada, combinada amb una macroporositat esfèrica còncava de les escumes, van incrementar el potencial d'osteoinducció més enllà dels límits oferts per les ceràmiques sinteritzades microestructurades.

El segon pas va consistir en l'anàlisi de l'efecte de la geometria de la macroporositat dels materials de CDHA sobre la seva capacitat de consolidació òssia, implantant els materials escumats i els impresos en 3D a nivell intraossi en un model caní (**Estudi II**). Tot i que la CDHA nanoestructurada va demostrar ser altament osteoconductiva independentment de la geometria macroporosa, les escumes van mostrar una capacitat osteogènica superior, correlacionant-se directament amb el major potencial osteoinductiu intrínsec demostrat anteriorment. A més, les escumes van mostrar una reabsorció cel·lular superior als implants obtinguts per impressió 3D, substituint progressivament el material per nou os i, demostrant així que el control de l'arquitectura de la macroporositat permet adequar tant la degradació del material com fomentar la regeneració òssia.

Finalment, amb l'objectiu de mimetitzar encara més la fase mineral òssia, es va investigar l'efecte de la morfologia dels nanocristalls (placa *vs.* agulla) i del dopatge amb ions carbonat sobre la bioactivitat intrínseca de la CDHA biomimètica, implantant escumes de CDHA amb diferents nanoestructures (Coarse/Fine-CDHA) i escumes carbonatades a nivell ectòpic i ortotòpic en gos (**Estudi III**). Les escumes Fine-CDHA van mostrar un potencial osteoinductiu i osteogènic superiors, i una degradació incrementada respecte a les escumes Coarse-CDHA, suggerint que existeix una SSA mínima per activar la degradació cel·lular dels materials i la conseqüent resposta osteoinductiva, fet que determina la capacitat osteogènica dels materials en un defecte ossi. La carbonatació de la CDHA va accelerar tant el potencial osteoinductiu i osteogènic, com la degradació cel·lular dels materials, suggerint que l'increment del biomimetisme de la CDHA afavoreix la introducció del material dins del cicle de remodelació òssia, sincronitzant la seva degradació amb la neformació òssia, i obtenint així substituts ossis més eficaços.

ACKNOWLEDGEMENTS

SCOPE AND AIM OF THE THESIS

Bone has a high capacity for regeneration. However, it is not unlimited. Several conditions such as trauma, infection, cyst or tumour resection, bone resorption around implants, corrective ostectomies, avascular necrosis, osteoporosis and some specific systemic diseases hinder the natural potential of bone regeneration. In general, when a bone defect exceeds a critical size, it requires the use of a substrate (bone graft) to serve as a support and guide the action of bone regenerating cells. Nowadays, the progressive increase of life expectancy has led to a higher incidence of impaired healing situations due to osteoporosis, bone cancer and other degenerative bone diseases, which, moreover, are predicted to increase significantly over the coming years. In consequence, the number of bone-grafting procedures has also increased, becoming a remarkable public health issue.

Autologous bone grafting is still considered the gold standard treatment for bone regeneration. However, autografts present important drawbacks associated with the need of a harvesting surgery such as higher risk of side effects (infections, donor site pain), higher operative time and cost and the limited availability of bone graft.

To overcome these limitations and to tackle the high demands of a global ageing population, current efforts in the field of bone regeneration are centered in developing synthetic bone substitutes with enhanced performance. Calcium phosphates (CaPs) have been used since the 1970s as synthetic bone grafts due to their chemical resemblance to the inorganic fraction of bone tissue, showing a suitable biocompatibility, as well as, a good osteoconductivity. However, the bone healing capacity of the CaPs developed so far is still inferior to that of autologous bone grafts in terms of initiation of bone growth.

The combination of CaP scaffolds with either cells or growth factors has attracted much attention lately as a strategy to enhance their clinical performance. However, it raises safety, ethical, logistic and economic concerns, besides suffering from poor reproducibility and patient variability, making this strategy ineffective in the daily clinical practice. An attractive alternative lies in endowing intrinsic osteoinductive properties to these biomaterials by tuning their physico-chemical and structural properties. Although the mechanisms underlying CaPs material-associated osteoinduction are still not fully understood, there are some physico-chemical properties that are believed to play a key role, such as chemical composition, macropore architecture, microstructural topography and high SSA. However, most *in vivo* studies on osteoinduction of CaPs have been performed with sintered ceramics, where the high temperature processing precludes the introduction of nanoporosity and, hence, low specific SSAs are obtained. This leaves the hypothesis without a complete verification, and establishes the need to provide a full picture of the situation, by assessing the osteoinductive properties of CaP-based biomaterials with nanostructured features and higher SSA.

In this respect, we propose the use of biomimetic routes based on the self-setting reaction of calcium phosphate cements (CPCs) to obtain nanostructured CDHA scaffolds at physiological temperature, which do not simply mimic the composition and morphology of the bone mineral phase better than sintered ceramics, but also generate a porous structure with controlled micro and nanoporosity (needle-like or plate-like nanocrystals), and consequently, much higher SSAs. One additional advantage of CPCs is their simplicity in processing, which makes them extremely versatile and compatible with many techniques, such as 3D-printing technology or foaming

method. This allowed fabricating scaffolds with different macropore geometries and dimensions in a controlled way, while preserving the specific nanostructure typical of biomimetic ceramics. Moreover, crystal structure of CDHA allows for many ionic substitutions. Therefore, in order to further mimic biological apatite, CDHA can be synthesized incorporating the ion substitutions present in bone, such as carbonate.

The originality of this PhD Thesis is based on the possibility to tailor porosity at different levels (from the nano- to the macroscale) of biomimetic CaPs scaffolds, which significantly extends the range of textures analyzed so far, addressing more in-depth the effect of the nanostructure and macropore architecture on the intrinsic osteoinduction of CaPs.

Therefore, the main aim of this PhD Thesis is the *in vivo* evaluation of the intrinsic osteoinductive capacity of a new family of biomimetic nanostructured CaP-based biomaterials with different macropore architectures in a canine ectopic implantation model and to asses if there is a direct correlation with their capacity for repairing bone defects in a canine orthotopic implantation model.

The specific objectives to achieve the aforementioned goal are:

- Assess the effect of **nanostructural features** and **SSA** of CDHA scaffolds on the intrinsic osteoinduction capacity and the material resorption, by comparing them with sintered BCP and β-TCP ceramics with the same macrostructure (spherical concave macropores) but absence of nanostructure and significantly lower SSAs, in a canine intramuscular implantation model (Study I).

- Study the role of **macropore architecture** on the intrinsic osteoinduction capacity and material resorption, of nanostructured CDHA scaffolds with different macropore geometries (prismatic convex macropores *vs.* spherical concave macropores) and dimensions in a canine intramuscular implantation model (Study I); and to correlate these results with their bone healing capacity and material degradation patterns when implanted orthotopically (Study II).

- Assess the role of **nanocrystal morphology** and SSA on the osteoinduction capacity and material resorption of nanostructured scaffolds of CDHA with the same macropore architecture (spherical concave macropores) but with different nanocrystal morphologies (needle-like *vs.* plate-like nanocrystals) and different SSA, in a canine intramuscular implantation model; and to correlate these results with their bone healing capacity and material degradation patterns when implanted orthotopically (Study III).

- Investigate the effect of **carbonate doping** of nanostructured CDHA scaffolds on the intrinsic osteoinduction and degradation behaviour by comparing them with undoped nanostructured CDHA constructs with the same macrostructure (spherical concave macropores) in a canine ectopic implantation model; and to correlate these results with their bone healing capacity and material degradation patterns when implanted orthotopically (Study III).

ABBREVIATIONS

ACP	Amorphous calcium phosphate	**L/P**	Liquid to powder ratio
ALP	Alkaline phosphatase	**MMP**	Matrix metalloproteinase
α-TCP	Alpha-tricalcium phosphate	**MIP**	Mercury intrusion porosimetry
ATR	Attenuated total reflectance	**MSC**	Mesenchymal stem cell
DMEM	Dulbecco's Modified Eagle Medium	**Micro-CT**	Microcomputed tomography
BS-SEM	Backscattered scanning electron microscopy	**NSAID**	Nonsteroidal anti-inflammatory drug
BMU	Basic multicellular unit	**OCP**	Octacalcium phosphate
β-TCP	Beta-tricalcium phosphate	**Osx**	Osterix
BCP	Biphasic calcium phosphate	**OP**	Osteogenic protein
BMP	Bone morphogenetic protein	**OCN**	Osteocalcin
BSP	Bone sialoprotein	**ONN**	Osteonectin
BET	Brunauer-Emmett-Teller	**OPG**	Osteoprotegerin
CDHA	Calcium deficient hydroxyapatite	**OPN**	Osteopontin
CaP	Calcium phosphate	**PBS**	Phosphate buffered saline
CPC	Calcium phosphate cement	**PDGF**	Platelet derived growth factor
CO$_3$-CDHA	Carbonated calcium deficient hydroxyapatite	**PRP**	Platelet rich plasma
CD	Cluster of differentiation	**HEMA**	Hydroxyethyl methacrylate
Col I	Collagen type-I	**PG**	Proteoglycan
cDNA	Complementary DNA	**PGE$_2$**	Prostaglandin E2
CSF	Colony stimulating factor	**rMSC**	Rat mesenchymal stem cell
DBM	Demineralized bone matrix	**RP**	Rapid prototyping
DNA	Deoxyribonucleic acid	**ROS**	Reactive oxygen species
DCPA	Dicalcium phosphate anhydrous	**qPCR**	Quantitative polymerase chain reaction
DCPD	Dicalcium phosphate dihydrate	**RANK**	Receptor activator of nuclear factor κ B
FBS	Fetal bovine serum	**RANKL**	RANK ligand
FGF	Fibroblast growth factor	**RNA**	Ribonucleic acid
FN	Fibronectin	**Runx2**	Runt-related transcription factor 2
FC	Fold changes	**SSA**	Specific surface area
FDA	US Food and drug administration	**TRAP**	Tartrate-resistant acid phosphatase
FTIR	Fourier transform infrared spectroscopy	**TCPS**	Tissue-culture polystyrene
GAG	Glycosaminoglycan	**TGF**	Transforming growth factor
HA	Hydroxyapatite	**TNF-α**	Tumor necrosis factor alpha
Ihh	Indian hedgehog	**VEGF**	Vascular endothelial growth factor
IGF	Insulin-like growth factor	**VOI**	Volume of interest
IL	Interleukin	**XRD**	X-ray diffraction

Chapter 1

INTRODUCTION

Bone is a remarkable organ, as it has an inherent self-healing capacity without a fibrous scar formation under physiological conditions (when the defect size is not critical). The standard treatment for bone defects such as fractures consists of reduction and fixation of the fracture, acting as secondary aid to the self-regeneration process.[1] However, the treatment of critical-sized bone defects, defined as the defects with the minimum size that cannot be spontaneously healed, is still an unresolved clinical challenge in orthopedics, affecting over 20 million people annually worldwide. This leads to about 5 million orthopedic interventions every year, of which about 60% require bone grafting therapies.[2] Therefore, bone grafting has become a common procedure, bone being the most frequently transplanted tissue after blood.[3]

Moreover, improvement of life quality and the consequent increase in life expectancy are accompanied by an expanding demand for the repair of damaged and degraded organs and tissues. In connection to this, some experts predict that 30% of hospital beds will soon be occupied by osteoporosis patients[4] and consequently delayed healing and non-unions will occur more frequently as a result of the global ageing of the population.[5] Hence the imperative necessity to improve the existing strategies for bone regeneration.

In this context, biomimicry, defined as the creative innovation of specific solutions to human challenges by emulating nature's time-tested patterns and strategies, has been proven as a powerful approach in the development of bone substitutes. Biomimetic biomaterials can form intimate and functional interfaces with neighboring bone, fostering specific physiological processes required for bone regeneration such as angiogenesis, osteoclastogenesis, osteoinduction and osteoconduction.[6] The following sections will provide an overview of the basic concepts of bone tissue in order to better understand the rationale behind the design of biomimetic biomaterials to be used as bone substitutes. Moreover, the current strategies for bone regeneration will be presented, focusing especially on the osteoinductive biomaterials and, particularly, on the osteoinductive properties of calcium phosphate-based biomaterials (CaPs).

1.1 Bone function

Bone tissue provides structural support to the body for locomotion, serves as a protective cage for internal organs, and it also plays a key role in a wide number of physiological functions. Associated to this physiological workload, bone has been estimated to receive 10-20% of total cardiac output. The main physiological functions include haematopoiesis, endocrine regulation, acid-base balance, mineral reserve (mainly calcium and phosphate) and ion homeostasis. Bone also serves as storage for mesenquimals stem cells (MSCs) and growth factors that are essential for vital physiological events, such as bone healing among others.[1,7,8]

1.2 Bone composition

Bone is a complex and intimate biocomposite of a mineral phase and an organic phase. The inorganic to organic ratio is approximately 75 to 25 by weight (**Fig. 1.1A**) and 65 to 35 by volume.[2]
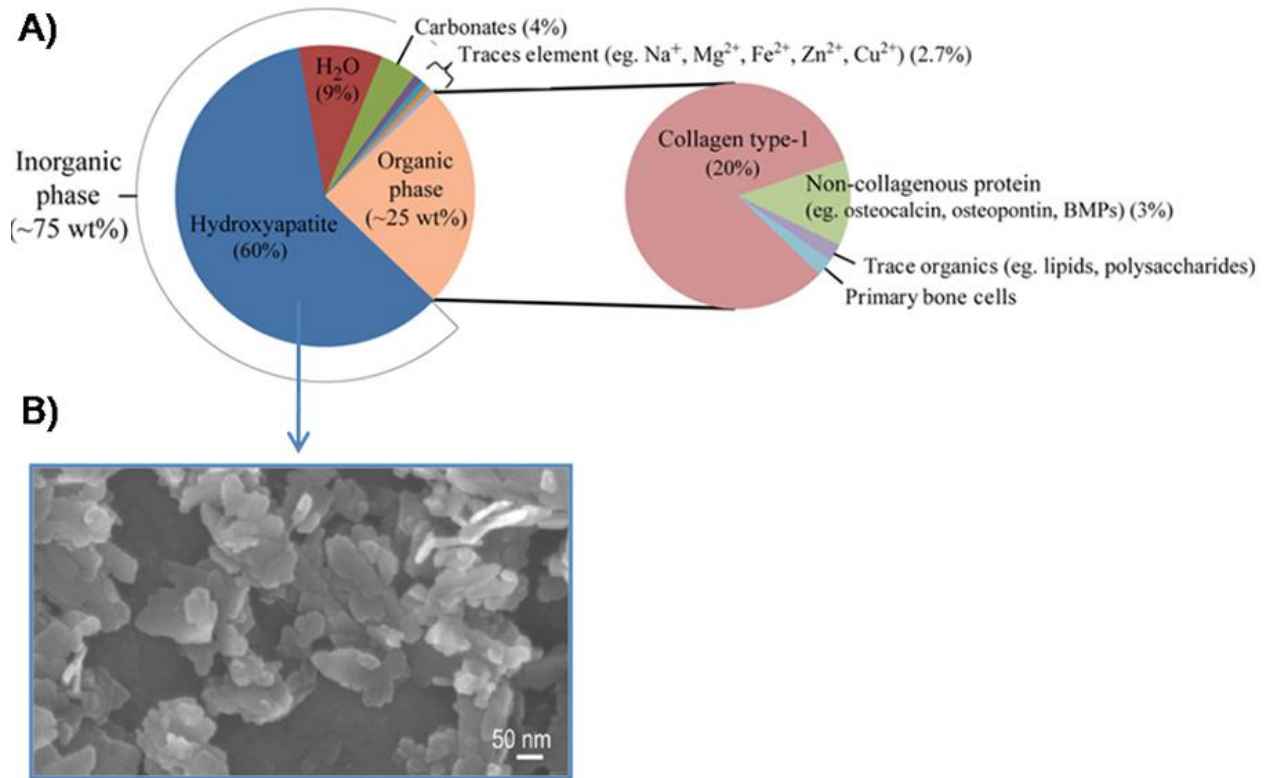
Figure 1.1. (A) Bone composition.[1] **(B)** Scanning electron microscope image of plate-shaped crystals of bone carbonate hydroxyapatite.[15]

Inorganic phase

The inorganic fraction of bone, also called dahlite, consists of a non-stoichiometric, carbonated calcium-deficient (Ca/P molar ratio lower than 1.67) and low-crystalline form of hydroxyapatite (HA).[10] Bone HA has an open crystal structure which allows several ionic substitutions such as Mg^{2+}, Fe^{2+}, Zn^{2+}, K^+, Na^+, $(HPO_4)^{2-}$, F^- and Cl^-, the most abundant being carbonate (CO_3^{2-}) substitution,[11,12] which accounts for 2-8 wt% depending on the age.[13] Specifically, the carbonate ions can substitute both hydroxyl or phosphate groups in the HA crystal lattice, originating the A-type and B-type carbonation, respectively. The B-type carbonate substitution prevails in the biological apatites of the different species.[13] Therefore, the bone apatite can be described as a carbonated calcium deficient hydroxyapatite (CO_3-CDHA) approximated by the formula: $(Ca,X)_{10}(PO_4,HPO_4,CO_3)_6(OH,Y)_2$, where X are cations ($Mg^{2+}$, Fe^{2+}, Zn^{2+}, K^+, Na^+) that can substitute for the calcium ions, and Y are anions (F^- and Cl^-) that can substitute for the hydroxyl group.[9] As above-mentioned, biological apatites are often described as poorly crystalline and non-stoichiometric since the presence of these ionic substitutions causes a decrease in the crystallite size, and a decrease in the Ca/P ratio below 1.67, which is the stoichiometric value of pure HA.[14] More specifically, bone apatite consists of nanometer-sized and irregularly shaped plate-like crystals (**Fig.1.1B**) of variable lengths (30-45 nm) and thickness (1.5-5 nm) discontinuously incorporated within the collagen fibrils of the organic matrix and mainly oriented with the c-axis in the direction of the fibril.[15] Bone inorganic phase also contains 9% of water.[15]

Organic phase

The organic matrix, also known as osteoid, is mainly composed of collagen type-I (80%). The remaining 20% is constituted by proteoglycans (PGs) and non-collagenous structural proteins such as osteocalcin (OCN), osteonectin (ONN), osteopontin (OPN), fibronectin (FN), glycoproteins, and bone sialoproteins (BSP).[16,17] Many of the proteins contained in the organic matrix are glycosylated, partially due to the presence of glycosaminoglycans (GAG). GAGs, which are assembled into PGs through a core protein, are long negatively charged heteropolysaccharides that occupy large areas providing many sites for interaction with various molecules such as growth factors and cytokines, crucial for several signaling pathways.[16,17] The bone organic phase also contains phospholipids, cells and growth factors.

1.3 Bone structure

Bone is a highly specialized form of connective tissue structured in a distinct hierarchical fashion. Weiner and Wagner described extensively the hierarchy of bone structure and established seven levels from the nano to the macroscale,[18] as shown in **Fig. 1.2**. The smallest scale level corresponds to tropocollagen molecules, which form collagen fibrils that are later mineralized by nanocrystals of CO_3-CDHA and arranged together forming a mineralized collagen fiber. These mineralized collagen fibers are then self-arrayed originating a twisted plywood-like structure called lamellae, which eventually wrap into concentric layers around a central canal called Haversian canal that contains blood vessels and nerves. Each Haversian canal is surrounded by varying number (5-20) of concentrically arranged lamellae of bone matrix forming an osteon or Harversian system, which is the fundamental functional unit of compact bone. Osteons are around 200 to 250 μm in diameter and run parallel to the long axis of bone.[19]
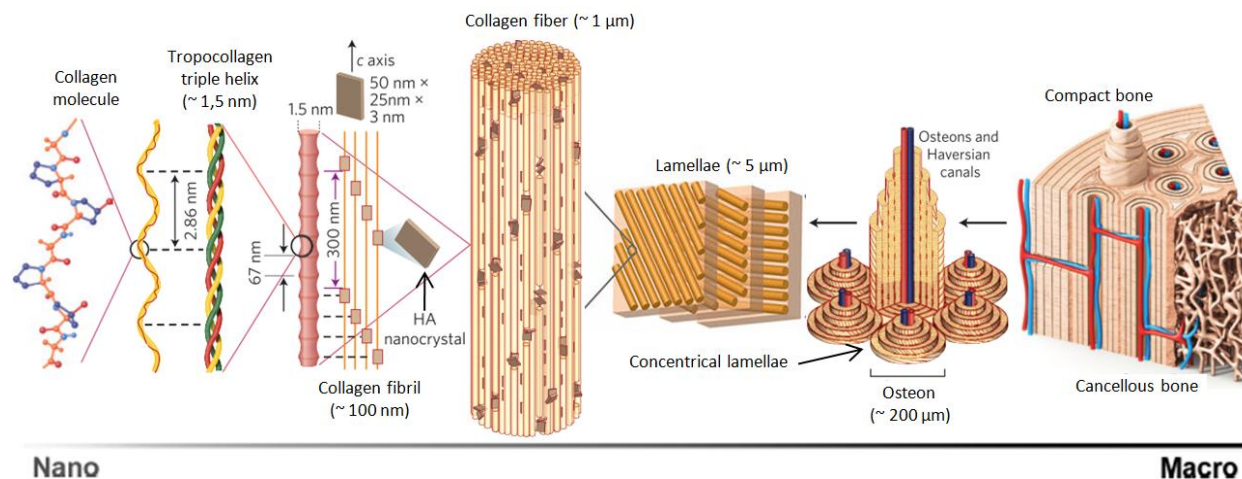
Figure 1.2. Hierarchical structure of bone.[20]

Recently, some studies revealed that besides the previously described ordered arrays of mineralized collagen fibrils, lamellar bone is also composed of a minor component being a relatively disordered material consistent of individual collagen fibrils with no preferred orientation, with crystals inside, and extensive ground mass, where the cellular components of bone are confined.[15]

This hierarchical structure is responsible for its high mechanical performance, and specifically for its inherent capacity to arrest crack propagation. Although bone is a relatively light weight material, the mineral phase provides it with strength under compressive loads. The collagen found in the organic matrix renders the bone with relatively high elastic modulus, which provides it with a significant degree of flexibility.[19] However, bone is still liable to fracture at high tensile loads, tensional forces or shear strengths.[1,21] The mechanical properties are dependent on the anatomic location and type of bone (**Fig. 1.3**),[22,23] and are influenced among others by the porosity and percentage of the mineral content.[24]

Finally, at a macrostructural level, we can differentiate between compact bone and cancellous bone, as depicted in **Fig. 1.3**. Compact bone, also known as cortical bone, is found in the hard outer layer of long and flat bones surrounding the marrow cavity and is organized in a lamellar cylindrical osteon system. It is a dense tissue with a total porosity around 5 to 10%. This porosity is constituted by Haversian canals, Volkmann's canals and resoprtion cavities.[9] Pore size in cortical bone ranges from 10 to 300 μm.[9] Compact bone possesses a high resistance to tensile and bending forces and it shows a low remodeling rate.[21]
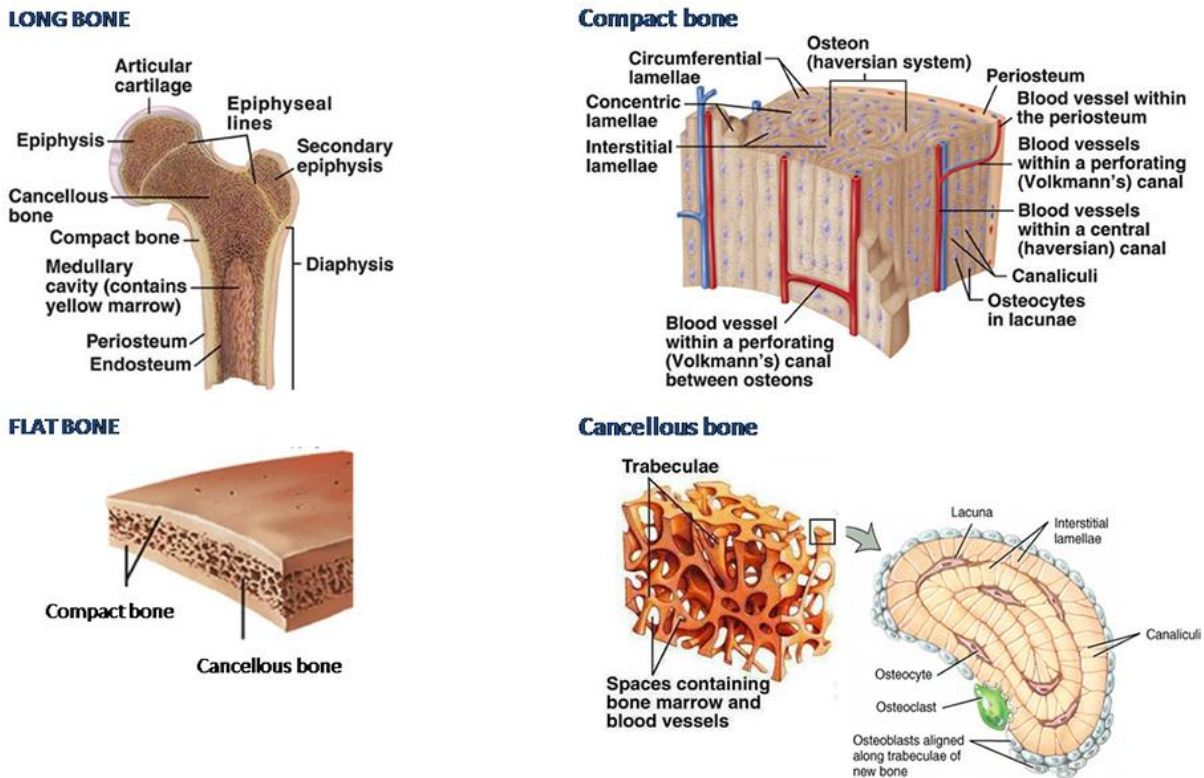
		Longitudinal plan	Transverse plan	Elastic modulus
Compact bone	Compression	131 – 224 MPa	106 – 133 MPa	13.7 GPa
	Tensile	79 – 151 MPa	51 – 56 MPa	
	Shear	53 – 70 MPa		
Cancellous bone	Compression	3 – 30 MPa	< 5 MPa	1.5 GPa
	Tensile	3 – 30 MPa	< 5 MPa	
	Shear	< 5 MPa	< 5 MPa	

Figure 1.3. Compact bone and cancellous bone in long and flat bones and their mechanical properties, adapted.[1,21]

Cancellous bone, also known as trabecular or spongy bone, is mainly found inside the epiphyseal areas of long bones and within flat and irregular bones. It presents a three-dimensional structure of longitudinally arranged lamellae irregularly interconnected, known as trabecuale (200 μm of thickness), with a total porosity between 75 and 95%. The interconnected pores in trabecular bone range from 200 to 600 μm and are filled with bone marrow. The size and interconnection of bone porosity is essential for vascularization, diffusion of nutrients and cells, and tissue ingrowth. It has a larger surface area than cortical bone to respond to metabolic demands, thus is more active and can remodel quicker. Moreover, this structure gives high compression resistance to the cancellous bone.[21] The human skeleton has a total of 213 bones, where 80% consist of cortical bone and 20% of trabecular bone. Moreover, based on the different mechanisms during embryonic development, bones can be classified in five families: long bones (i.e. femur, tibia), short bones (i.e. carpus, tarsus), flat bones (i.e. scapula, rib), irregular bones (i.e. vertebrae) and sesamoid bones (i.e. patella).[25]

The sophisticated architecture and composition of bone and the high organization level of the bone matrix not only account for its optimized mechanical performance, but also provide the adequate niche for bone cells migration, attachment, proliferation and differentiation, which allows for bone repair and regeneration.[26]

1.4 Bone biology

Bone is a dynamic tissue which is produced as a result of a series of complex events rigorously orchestrated by different types of bone cells interacting with each other and with the extracellular matrix. The cells constituting the bone tissue are mainly four subsets: osteoblasts, osteoclasts, osteocytes and bone-lining cells (**Fig. 1.4**). Osteoblasts, osteocytes and bone lining cells are originated from local stromal osteoprogenitor cells, whilst osteoclasts have an hematopoietic origin and derive from the fusion of mononuclear precursors, from the monocyte-macrophage lineage.[7,27]
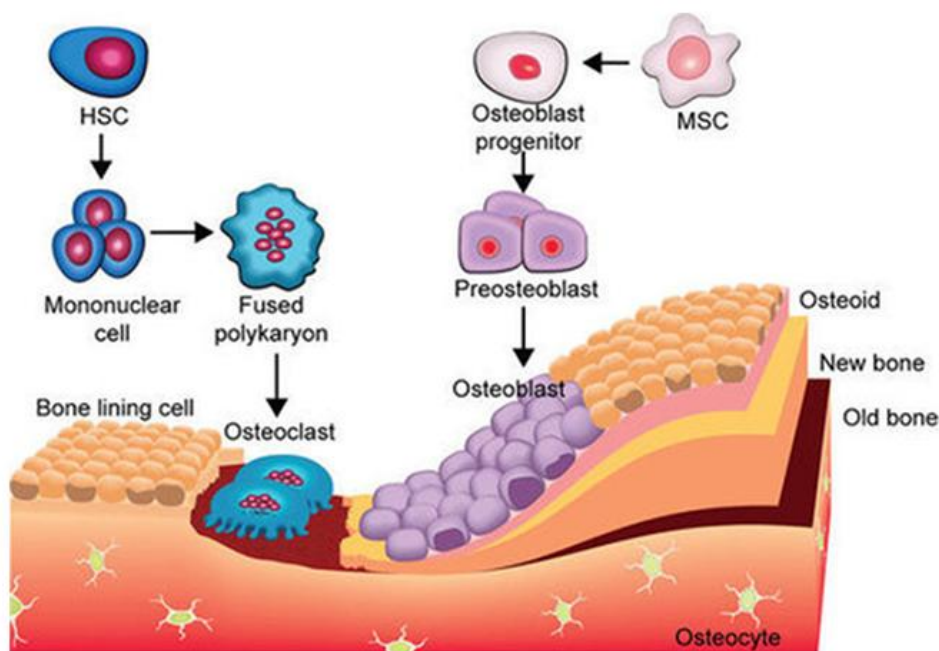
Figure 1.4. Bone cell types. Hematopoietic stem cells (HSC) and Mesenquimal stem cells (MSC).[28]

Bone lining cells have been suggested as a quiescent population of cells that cover inactive (non-remodeling) bone surfaces. They can be induced to proliferate and differentiate into osteogenic cells and represent a major source of mature osteoblasts during adulthood.[27,29]

Osteoblasts differentiate from the mesenchyme; i.e. from MSCs, as depicted in **Fig. 1.5**. The microenvironment of MSCs will dictate the differentiation into the bone lineage cells or alternatively, into chondrocytes, myioblasts or adipocytes. Osteoblasts differentiation can be activated by different pathways, being runt-related transcription factor 2 (Runx2), bone morphogenetic proteins (BMPs) and osterix (Osx) the main regulators. Osteoblasts are polarized, mononuclear, bone-forming cells. Their primary function is the synthesis and mineralization of the osteoid matrix. As such, they are always found lining the layer of bone matrix they are producing. They produce several substances such as GAGs (chondroitin sulfate and hyaluronic acid) and matrix proteins that include collagen (mostly collagen type-I, Col I), alkaline phosphatase (ALP), OPN, BSP, ONN, FN and OCN. Osteoblasts also secrete growth factors like transforming growth factors (TGFs), Runx2 or BMPs before mineral deposition. Mineralization of the organic matrix begins approximately 10 days after production. Once trapped inside mineralized matrix they become osteocytes, by down-regulation of ALP and Col I expression.[7,27]
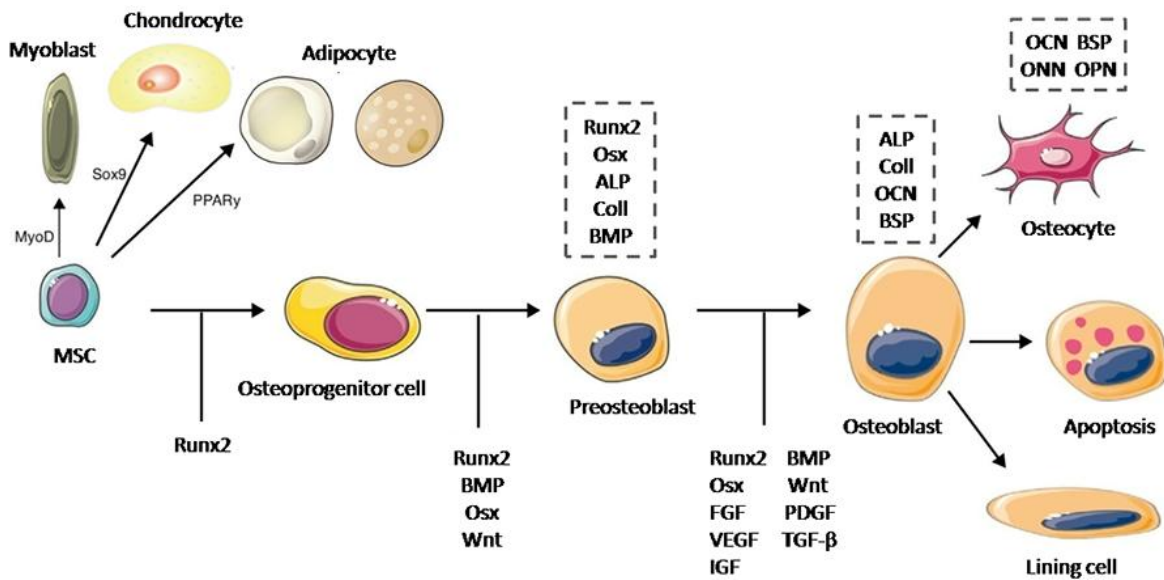
Figure 1.5. Model of osteoblast and osteocyte differentiation, adapted.[30]

Osteocytes are terminally differentiated osteoblasts, star-shaped cells (**Fig. 1.5**) that form the largest cellular constituent of bone, being ten times more numerous than osteoblasts. Osteocytes principally act as mechano-sensors and thus convert the stimulus of mechanical loading into biochemical signals by guiding both osteoblasts and osteoclasts activity during bone remodeling. These cells occupy lacunae (pits) embedded in the bone matrix and are interconnected via cytoplasmic extensions (filopodia) running through a canalicular network (canaliculi). Gap junctions between filopodia of different cells allow transfer of small intercellular signaling molecules, for example nitric oxide and prostaglandins.[27]

Osteoclasts are responsible for bone resorption. They are able to resorb the extracellular bone matrix by generating an acidic environment to dissolve the mineral phase of bone, and by secreting specific enzymes (matrix metalloproteinases-MMP and cathepsins) to degrade the organic components.[26] Osteoclasts are multinucleated cells formed by fusion of cells of the monocyte-macrophage lineage upon stimulation with proteins secreted by bone marrow stromal

cells or cells of the osteoblastic lineage. In fact, during maturation, osteoclasts resemble foreign body giant cells.[31]

Each type of cell exerts different functions during embryonic osteogenesis, bone remodeling and bone healing processes by a tight cross-talk, based on a complex protein-protein receptor network. These biological mechanisms will be described in the following sections.

1.4.1 Osteogenesis during skeletal development

Bone embryonic development occurs during determination of the dorsoventral axis through intramembranous and endochondral pathways, a complex multistep process of growth and development, which is completed only in adulthood.[32,33]

1.4.1.1 *Intramembranous ossification*

Intramembranous ossification generates flat bones and it entails direct differentiation of MSCs into osteoblasts. In the formation of the skeleton, MSCs from the neural crest (embryonic ectoderm cell layer) aggregate and form condensates of loose mesenchymal tissue, prefiguring the skeletal elements. Within these aggregates MSCs differentiate into the osteoblastic linage when in association with adequate vascularization and upon expression of Runx2, which induces another bone differentiation transcription factors (Osx, BMPs and Wnt). Runx2 is considered by many to be the 'master gene' for osteoblast differentiation, because it regulates the differentiation of MSCs to pre-osteoblasts and is required for the expression of non-collagenous proteins such as BSP and OCN. Subsequently, osteoblasts lay down new osteoid in a disorganized fashion, which is lately mineralized forming woven bone. Finally, woven bone is remodeled to well-organized lamellar bone resulting in either compact or cancellous bone.[32,33]

1.4.1.2 *Endochondral ossification*

Alternatively, in the endochondral ossification, condensates of MSCs can differentiate into chondrocytes in an avascular environment, producing a cartilage mold which is eventually replaced by bone. Endochondral ossification originates most of the bones of the body, such as the long bones. It begins when neural crest MSCs proliferate and condense, forming a cartilage mold surrounded by the perichondrium, a primary source of chondroblasts. Directed by transcription factors Sox9 and, then, Runx2, these cells differentiate into chondrocytes and begin to secrete extracellular matrix components that are rich in aggrecan and collagen IIa1 (hyaline cartilage). Runx2 expression in a specific chondrocyte population generates a hypertrophic zone. Hypertrophic chondrocytes secrete collagen X, promote direct mineralization of the cartilage, and induce the adjacent perichondrial cells to differentiate into osteoblasts, a key step in endochondral bone formation. Blood vessels producing vascular endothelial growth factor (VEGF) and other factors invade the mineralized cartilage mold, allowing for migration of osteoclasts to digest the calcified matrix synthesized by the hypertrophic chondrocytes. Then, osteoblast precursor cells deposit bone on the degraded matrix scaffold formed after death of the hypertrophic chondrocytes. In the perichondrium, important autocrine and paracrine factors, such as BMPs 2, 4, and 7, Indian hedgehog (Ihh), and parathormone related protein (PTHrP), are expressed to sustain differentiation and mature bone formation.[32-34]

1.4.2 <u>Bone remodeling</u>

Bone tissue shows the inherent capacity for continuous remodeling lifelong by removing old bone from the skeleton and forming new bone. It is a key process during which the newly formed bone grows adjusting to the mechanical demands and the activity of the person while maintaining the total bone volume, its structural integrity and metabolic functions. In the mature adult skeleton approximately 2 to 5% of cortical bone undergoes turnover annually, while trabecular bone is even more actively remodeled, up to 10% per year, due to the much larger specific surface area (SSA).[7,32]

The remodeling cycle of the corticocancellous bone requires the interaction of many cells which respond to mechanical stimuli and are tightly regulated by several bone-related proteins and paracrine and autocrine growth factors. The fundamental unit responsible for the remodeling process is called basic multicellular unit (BMU). It consists in a complex and unique structure made up of osteoblasts and osteoclasts organized into a cutting cone with osteoclastic resorption at the apex and osteoblasts laying down new osteoid at the base with blood vessels (endothelial cells) filling the cavity (**Fig. 1.6**). A BMU is an elongated cylindrical structure that burrows trough cortical bone, in a direction generally aligned with the long axis of the bone. It measures approximately 2 mm of length and 200 µm of diameter. The total number of these units and thus the rates of resorption and new bone formation are relatively constant at any given time.[7] In the cancellous bone, a BMU travels across the surface of a trabecuale excavating a trench rather than a tunnel with cross-sectional geometric cues of concavities after cyclic episodes of osteoclastogenesis (**Fig. 1.6**).[35]
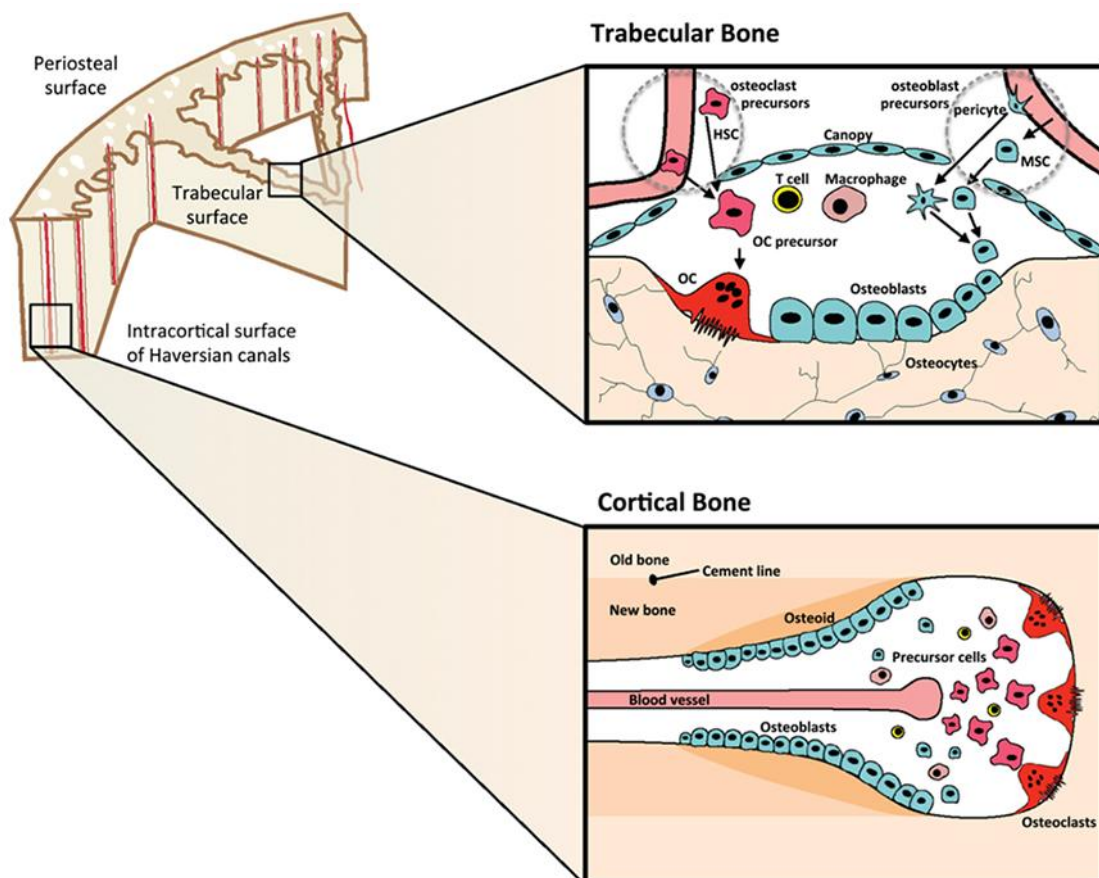
Figure 1.6. Schematic representation of a BMU, the fundamental unit of the remodeling cycle of the corticocancellous bone.[36]

The remodeling process entails five phases: quiescence, activation, resorption, formation, and mineralization, as shown in **Fig. 1.7**.
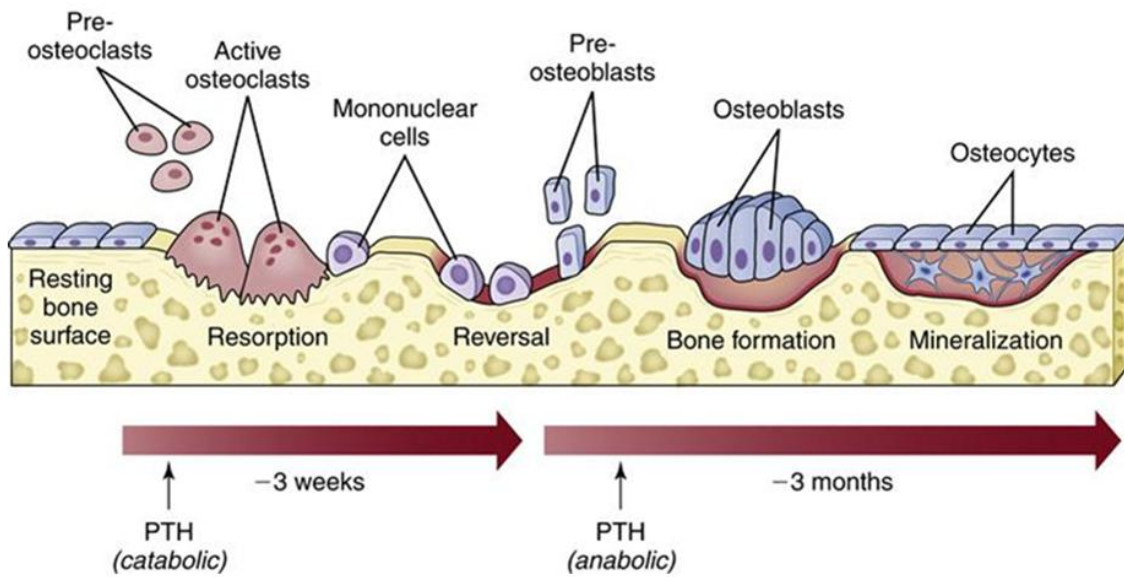
Figure 1.7. Schematic representation of the bone remodeling cycle.[37]

Quiescence/Activation

The quiescent bone (i.e not undergoing remodeling) starts the remodeling process usually activated by paracrinal signals such as parathyroid hormone (PTH). Remodeling is initiated at points beneath the canopy of cells lining trabecular bone and within cortical bone Haversian canals (**Fig. 1.6**). The first step is the separation of the lining cells to expose the bone surface and the recruitment of osteoclast precursor cells. Then, osteoclastogenesis is regulated by a host of factors such as osteoprotegerin (OPG), receptor activator of nuclear factor kappa B (RANK), RANK ligand (RANKL) and colony-stimulating factor (CSF) what is known as the RANK/RANKL/OPG pathway, illustrated in **Fig. 1.8**.
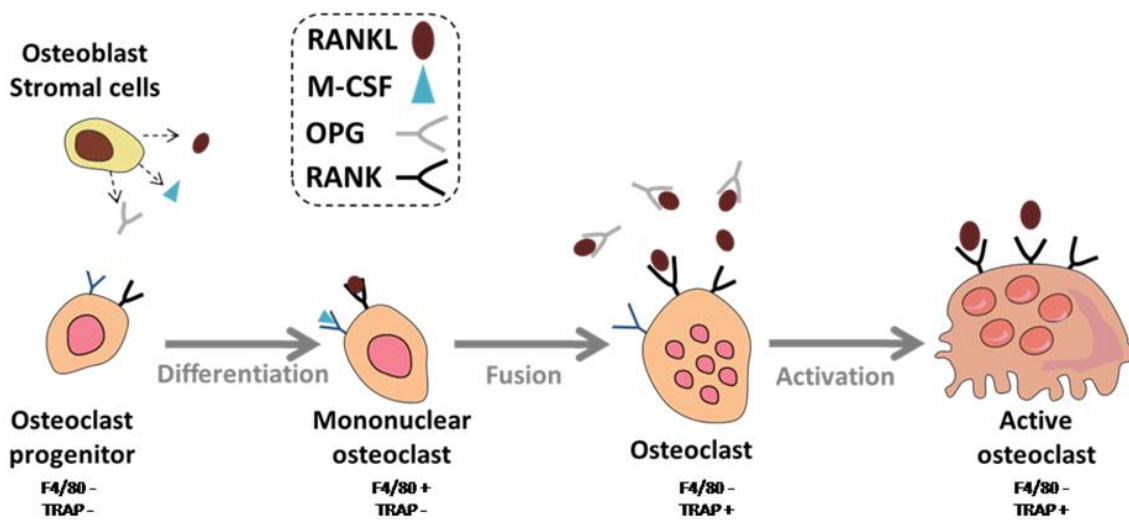
Figure 1.8. Model of osteoclast differentiation and activation, adapted.[27,38]

Specifically, RANK-RANKL interactions lead to osteoclast maturation, while OPG is a decoy receptor inhibiting RANK-RANKL interactions. Fusion of macrophages or mononuclear

osteoclasts under the stimulation with CSF and RANKL, among others, generates mature osteoclasts, which express high amounts of tartrate-resistant acid phosphatase (TRAP). Other environmental stimuli can regulate osteoclastic activity such as prostaglandin E2 (PGE$_2$), vitamin D, calcitonin, or cytokines such as interleukin 11 (IL-11), tumor necrosis factor stimulated gene-6 (TSG-6) and tumor necrosis factor alpha (TNF-α).[31,39,40]

Resorption

During the resorption phase, differentiated osteoclasts form a cutting cone and degrade the bone matrix. Osteoclasts attach to bone by polarizing their membrane forming a 'ruffled border' typical from this type of cells. Once attached and sealed by the ruffled membrane, osteoclasts release hydrogen ions and transport acidifying vesicles to degrade bone. Thus, bone resorption by osteoclasts takes places under acidic conditions, normally at pH around 4.5. Adenosintriphosphatase (ATPase) and carbonic anhydrase are some of the proteases mediating this acidification which degrades bone mineral matrix (low pH dissolves the crystal content of the matrix). Then, organic matrix is degraded via the release of lysosomal enzymes (cathepsin K and MMP) by osteoclasts and by the action of mononuclear cells, which clean the resorbed surfaces (reversal phase). The final step of this phase is the apoptosis of osteoclasts.[35]

Formation

Subsequently, the resulting pit cut by osteoclastogenesis, known as Howship's lacunae, is colonized by MSCs which differentiate to preosteoblasts and finally to mature osteoblasts. The stimulation and control of the osteoblastic differentiation process is governed by a complex pathway of interactions between transcriptional regulators, growth factors, hormones and signaling molecules. For instance, during osteoclastogenesis calcium and phosphate ions are released from bone matrix. This causes a local increase in the ion concentration to supra-physiological levels, which has a significant impact on the proliferation and differentiation of osteoblasts, as well as on the subsequent bone formation process.[35] High calcium concentrations have been shown to stimulate pre-osteoblast chemotaxis to the resorption site via the activation of calcium sensing receptors.[41,42] Besides the effect on cell chemotaxis, the release of extracellular calcium also plays an important role in controlling the proliferation (via c-fos transcription factor expression) and differentiation (via dephosphorylation of NFAT transcription factor) of osteoblasts near the Howship's lacunae, through the calcium/calmodulin signaling.[42] Moreover, the release of phosphate ions at the resorption site also plays a role in osteoblast proliferation and differentiation through different signal pathways such as Fos-related antigen-1 and extracellular signal-regulated kinase (matrix Gla protein).[43] On the other hand, the most important cytokines involved in the osteoblastic differentiation during this formation phase are osteoclastic BMPs, platelet derived growth factor (PDGF), TGF-β, VEGF, fibroblast growth factor (FGF), and insulin-like growth factors (IGF). The Wnt group of proteins has also been shown to have a role in increasing bone mass through a number of pathways including osteoblastogenesis and inhibition of osteoblast apoptosis. Once differentiated, osteoblasts start the new bone formation by producing the organic matrix (osteoid).[7,35]

Mineralization

Osteoblasts also control the mineralization process of the bone matrix which is the last step of the remodeling cycle.[7,35] The matrix mineralization process is also regulated by specific

cytokines. For instance, ALP is a periplasmic enzyme that hydrolyses pyrophosphate (a mineralization inhibitor), thereby providing phosphate ions to promote mineralization.[44] Thus, ALP is considered an early marker of osteoblast differentiation. PHOSPHO1 is another phosphatase highly expressed in bone, which plays a role in the initiation of mineral formation.[45] On the other hand, OCN and ONN regulate the size and speed of crystal formation,[46] BSP acts as a crystal nucleator, whereas OPN influences the type of crystal formed.[47] Moreover, BMP-2 is involved in the control of ALP expression and osteoblast mineralization via a Wnt autocrine loop,[48] as well as in the enhancement of phosphate ion transportation into cells for matrix mineralization.[49] Eventually, expression of molecules such as sclerostin bind to osteoblasts and bone formation ceases.[7,35]

The maintenance of bone mass across the cycles is achieved through the balance between bone resorption and formation. Indeed, osteoblast-osteoclast relationships are mediated through OPG/RANKL and Wnt/BMP signaling pathways. Specifically, osteoblasts are crucial in the osteoclastogenesis through a mechanism involving cell-to-cell contact with osteoclast progenitors. The rate of osteoclastic activity is reduced by OPG. Osteoblasts secrete OPG, which binds to RANKL to inhibit both osteoclast stimulation and the resultant rate of bone turnover.[50] In the opposite direction, it has been reported the secretion of BMPs and other osteogenic growth factors (Wnt, S1P, OSM, PDGF-BB and CTHRC1) by osteoclasts, which stimulated osteoblast differentiation of local precursors.[51-54] The discovery of these relationships has confirmed the idea that osteoblasts are involved in the processes of osteoclast pathways and viceversa. Moreover, the balance between bone resorption and formation is under control of several factors as genetic, vascular, nutritional, hormonal and mechanical. For example, BMU can be activated when an appropriate mechanical solicitation exists; a phenomenon called mechano-transduction and governed by the Wolff's law. This allows bones to adapt in both size and shape to the mechanical stresses suffered.[35,55]

1.4.3 Bone healing

It is known that bone is one of the few tissues that can heal without forming a fibrous scar. As such, the process of fracture healing recapitulates bone development and can be considered a form of tissue regeneration.[56] Bone healing is comprised of a well-organized series of biological process of bone induction and conduction that requires the synergistic action of cells, cytokines, and growth factors through a definite temporal and spatial sequence, in an effort for optimization of skeletal repair and restoration of skeletal function.[57] Whilst normal bone turnover and the mechanisms by which fractured bone is repaired are entirely separate processes, they share a number of common features.[7] Following the initial trauma and depending on both mechanical and biological microenvironments of the bone defect, it can be repaired by either direct or indirect fracture healing.

1.4.3.1 *Direct bone healing*

Direct or primary bone healing consists of intramembranous bone healing and it does not commonly occur in the natural process of fracture healing. It requires a correct anatomical reduction of the fracture ends, without any or minimal gap formation and a rigid fixation resulting in a substantial decrease in the interfragmentary strain. When these requirements are

achieved, direct bone healing can occur by direct remodeling of lamellar bone. Depending on the species, it usually takes from a few months to a few years, before complete healing is achieved. Primary healing of fractures can either occur through contact healing or gap healing, as depicted in **Fig. 1.9**. Both processes involve an attempt to directly re-establish an anatomically correct and biomechanically competent lamellar bone structure.[56]
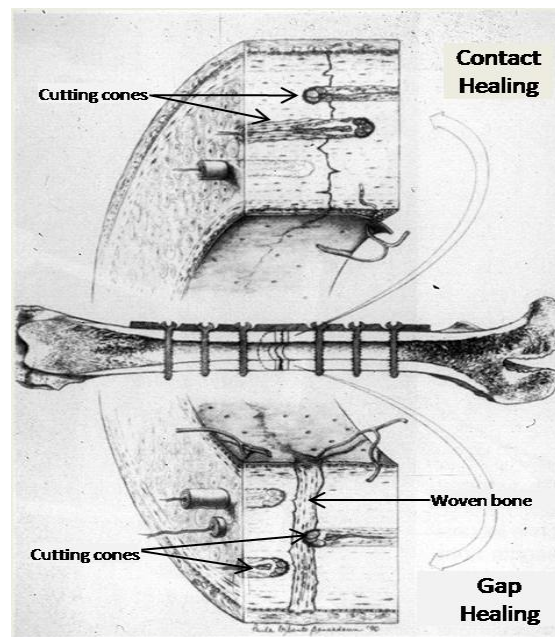
Figure 1.9. Primary healing of fractures can either occur through contact healing or gap healing.[57]

Contact healing

If the gap between bone ends is less than 0.01 mm and interfragmentary strain is less than 2%, the fracture unites by so-called contact healing. It occurs in the presence of perfect anatomical fracture reduction fixed with compression at the fracture site. Under these conditions, cutting cones are formed at the ends of the osteons closest to the fracture site. Osteoclasts cross the fracture line, generating longitudinal cavities at a rate of 50-100 μm/day, which are later filled by concentric lamellae produced by osteoblasts residing at the rear of the cutting cone (**Fig. 1.9**). This results in the simultaneous generation of a bony union and the restoration of Haversian systems formed in an axial direction. The re-established Haversian systems allow for penetration of blood vessels carrying osteoblastic precursors. The bridging osteons later mature by direct remodelling into lamellar bone resulting in fracture healing without the formation of periosteal callus.[56]

Gap healing

If the gap is between 0.01 mm to 1 mm, the fracture unites by so-called gap healing. In this process the fracture site is primarily filled by osteoid matrix elaborated by surrounding osteoblasts creating woven bone oriented perpendicular to the long axis. This initial process takes approximately 3 to 8 weeks, after which a secondary remodelling resembling the contact healing cascade with cutting cones takes place. Although not as extensive as endochondral remodelling, this second phase is necessary in order to fully restore the anatomical and biomechanical properties of the lamellar bone. Thus, gap healing differs from contact healing in that bony union and Haversian remodelling do not occur simultaneously.[56]

1.4.3.2 *Indirect bone healing*

Indirect or secondary bone healing is the most common form of fracture healing and it consists mainly of endochondral ossification. It does not require anatomical reduction or rigidly stable conditions. On the contrary, it is enhanced by axial micromotion and weight-bearing. However, too much motion and/or load is known to result in delayed healing or even non-union. Indirect bone healing typically occurs in non-operative fracture treatment and in certain operative treatments in which some motion occurs at the fracture site such as external fixation, intramedullary pinning, interlocking nailing or internal fixation of complicated comminuted fractures with locking plates.[56] Indirect bone healing process consists of three main phases: i) a primary acute inflammatory response with an hematoma formation surrounding the ridges of the fracture site, followed by ii) a repair phase where the hematoma is converted into a fibro-cartilage callus that evolves to woven bone callus, and finally iii) a remodeling phase where woven bone is converted into lamellar bone to meet mechanical demands (**Fig. 1.10**).[7]
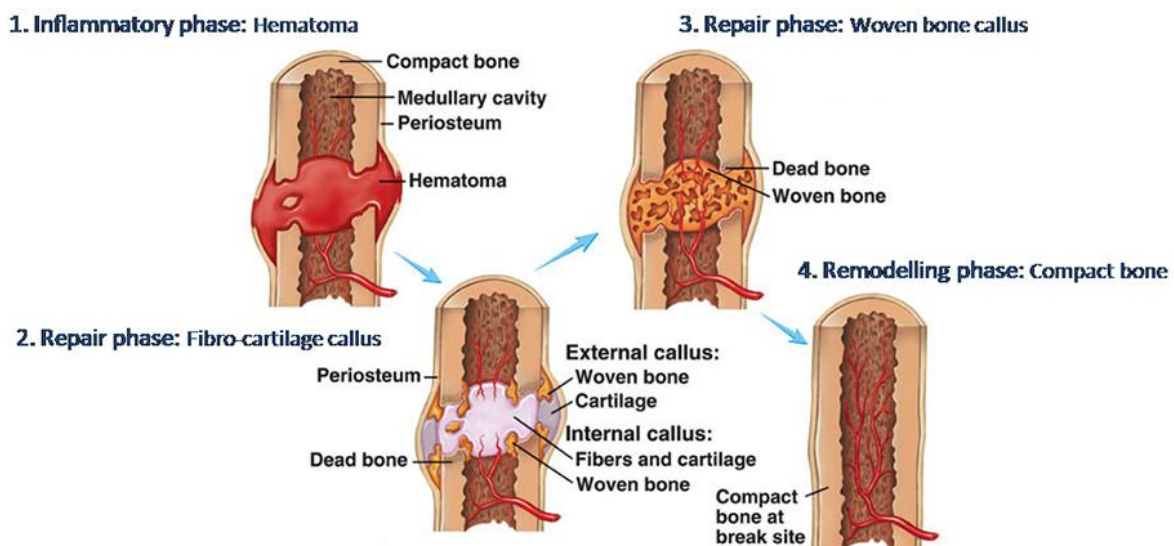
Figure 1.10. Schematic representation of the indirect bone healing process, adapted.[58]

Acute Inflammatory phase

Immediately after the trauma, disruption of periosteal and endosteal blood supply, and damage to peripheral vascularized tissues causes local necrosis, exudation of proteins, fluids and blood cells at the injured site leading to a clot formation.[59] The clot of platelets and blood cells initiates an inflammatory response with the recruitment of inflammatory cells from the immune system by means of several interleukins and specific cytokine-proteins (such as platelet factor 4 and PDGF), which are necessary for the healing to progress.[59-62] The acute inflammatory response peaks within the first 24 h and is complete after 7 days, when the clot is coagulated in between and around the fracture ends forming an hematoma, which will serve as a template for callus formation.[56]

Immune cells arriving at the injured site during the acute inflammatory reaction are responsible for degrading and phagocytizing any pathogen or injured tissue, as well as signaling the pathways for cells to resolve inflammation and restore tissue. Leukocytes, connective tissue cells and extracellular matrix components are the main factors regulating the chemical signaling to resolve inflammation. Initially, a provisional matrix is formed consisting mainly of fibrin which

furnishes structural and biochemical components to the process of wound healing. Neutrophils and monocytes arrive at this provisional network and release chemotactic factors over different time periods activating in turn, different cell functions. The first released chemical factors are reactive oxygen species (ROS) which generate oxidative stresses into the microenvironment. ROS levels dictate the effect on cellular mechanisms; high concentrations are deleterious to cells due to their oxidizing effect on cell proteins, lipids and DNA. Low ROS concentrations instead, function as signaling molecules for cell growth, adhesion, differentiation and apoptosis.[63] Neutrophils are short-life cells and undergo apoptosis within hours or few days. On the contrary, when monocytes adhere to tissue, they transform into different types of macrophages depending of the microenvironment stimuli. According to these stimuli, macrophages release cytokines to help address healing by signaling other cell types such as fibroblast, endothelial cells and mesenchymal cells.[64]

Macrophages assume diverse and context dependent profiles (known as macrophage polarization) between pro-inflammatory and anti-inflammatory phenotypes,[64] as summarized in **Fig. 1.11**. They are classified as M1 and M2, according to their pro- or anti-inflammatory phenotypes, respectively.[65] The early stage of the healing process is dominated by the pro-inflammatory M1 phenotype where cytokines such as TNF-α, IL-1β, IL-6, IL-11 and IL-18 are released. These factors recruit other necessary inflammatory cells and MSCs, stimulate the VEGF production and angiogenesis, promote the production of the primary cartilaginous callus and induce the differentiation of osteoblasts and osteoclasts.[56] In an ideal scenario after the first hours, M1 cytokines would be down-regulated by the release of anti-inflammatory cytokines such as IL-4, IL-10, IL-13 or TGF-β restraining inflammation and initiating tissue repair.[66]
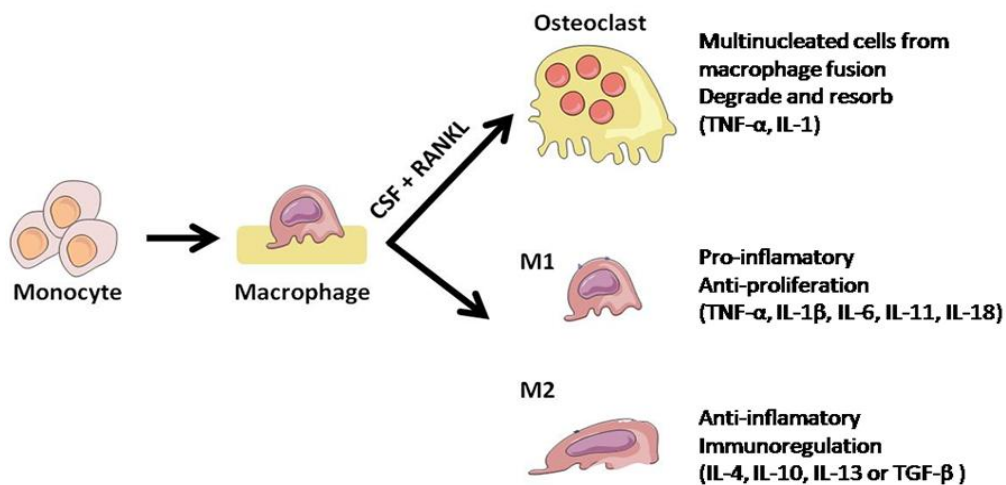
Figure 1.11. Macrophage polarization and their associated functions and cytokines released, adapted.[64]

This tight interrelation between the immune and the skeletal system has led to a new emerging field called osteoimmunology that seeks to understand and benefit from the tight crosstalk between both systems. Leukocytes and macrophages release proteins which can activate for instance osteoclast maturation, such as IL-1, IL-6, IL-11 and TNF-α, known as osteolytic cytokines, or promote osteogenesis by the regulation of BMPs.[67,68] Even though a brief and highly regulated secretion of proinflammatory molecules following the acute injury is critical to start bone repair, a chronic exposure to inflammatory cytokines can have a negative effect on bone healing (with or without bone grafting) leading to fibrotic tissue encapsulation and tissue granulation. Thus, a balance between pro-inflammatory and pro-healing cytokines is fundamental.[56]

Repair phase

Following the formation of the primary hematoma, a fibrin-rich granulation tissue is formed. Within this tissue, endochondral formation occurs in between the fracture ends and external to periosteal sites. These regions are also mechanically less stable and the cartilaginous tissue forms a soft callus which gives the fracture a stable structure. If the soft cartilaginous callus provides enough stability, it will be calcified, increasing thus the interfragmentary stability of the fracture. In order for bone regeneration to progress, the calcified cartilaginous callus needs to be resorbed and replaced by a hard woven bone callus. This step of fracture healing recapitulates embryological endochondral bone development,[69] described previously. The connection between bone regeneration and bone development has been further strengthened by a recent understanding of the role of the Wnt-family of molecules, which is of great importance in embryology and has also been shown to have an important role in bone healing. The Wnt-family is thought to regulate the differentiation of pluripotent MSCs into osteoblastic lineage (osteoinduction) and, at later stages of development, to positively regulate osteoblastic bone formation.[70] As the hard callus formation progresses and the calcified cartilage is replaced with woven bone, the callus becomes more solid and mechanically rigid.

At the same time and only under optimal vascular and mechanical conditions, an intramembranous ossification response could occur subperiostally directly adjacent to the distal and proximal ends of the fracture, generating a hard callus (**Fig. 1.10**).[7] This phenomenon has been controversial since some other authors disclaimed the presence of intramembranous ossification during the indirect bone healing process. In contrast, a short step consisting of the formation of chondroid tissue preceding the formation of woven bone was identified.[71,72] Extracellular matrix of chondroid tissue contains both type 1 and type II collagens simultaneously and possesses a higher rate of mineralization compared with cartilaginous tissues. It promotes the early formation of a calcified callus which acts as a support and thus permits the rapid apposition of woven bone.[71,72] The different calcified tissues in different locations of the fracture site can be explained by biological and mechanical factors. Proliferation of osteoprogenitor or chondroid cells occurs in areas of increased oxygen tension and decreased strain resulting in the early formation of woven bone, whereas areas of low oxygen tension or higher strain will result in cartilage production from differentiation of chondrocytes and the subsequent endochondral ossification process.[7]

The generation of these callus tissues is dependent on the recruitment of MSCs from the surrounding soft tissues, cortex, periosteum, bone marrow and the systemic mobilization of stem cells into the peripheral blood from remote hematopoetic sites. Moreover, pericytes, which are mural cells that lie on the albuminal side of blood vessels, have been shown to be a supplementary source of activated MSCs as osteoprogenitors in the periosteal osteogenesis.[73,74] The exact origin of MSCs is not fully understood. Although most data indicate that these MSCs are derived from surrounding soft tissues and bone marrow, some authors demonstrate that a systemic recruitment of circulating MSCs to the injured site might be of great importance for an optimal healing response.[75,76] Moreover, the precise molecular mechanisms that govern MSCs migration to sites of injury are also under debate.[77] In this regard, some authors reported that the release of pro-inflammatory cytokines such as TNF‑α, PDGF, IL‑1, and IL‑6 from inflammatory cells can enhance MSCs migration and proliferation,[33,59,78] whereas others found that an anti‑inflammatory effect through TGF‑β1 release is beneficial for MSC recruitment.[79]

Recent data suggested that stromal cell-derived factor-1(SDF-1) and its G-protein-coupled receptor CXCR-4 form an axis (SDF-1/CXCR-4) that is a key regulator of recruiting and homing specific MSCs to the site of trauma.[75,76] These reports show that SDF-1 expression is increased at the fracture site, and especially in the periosteum at the edges of the fracture, which demonstrates that SDF-1 has a specific role in recruiting CXCR-4 expressing MSCs to the injured site during endochondral fracture healing. Transplanted MSCs only home to the fracture site if they express CXCR-4, whereas CXCR-4 negative MSCs do not have this ability. The importance of this axis was further verified since the treatment with a SDF-1 antagonist or the genetic manipulation of SDF-1 and CXCR-4 impaired fracture healing.[75,76]

Once recruited, MSCs secrete autocrine and paracrine differentiation factors, such as Runx2, Osx, VEGF, FGF, Ihh, Wnt, and BMPs, inducing differentiation and maturation of these cells into active chondrocytes and osteoblasts and stimulating angiogenesis and vasculogenesis.[69] TGF-β superfamily members have been shown to be of great importance in this process. More specifically, TGF-β2, -β3 and Growth/differentiation factor 5 are involved in chondrogenesis and endochondral ossification, whereas BMP-5 and -6 have been suggested to induce cell proliferation in intramembranous ossification at periosteal sites.[80,81] In addition, BMP-2 has been shown to be crucial for initiation of the healing cascade.[82]

Remodeling phase

Although the hard callus is a rigid structure providing biomechanical stability, it does not fully restore the biomechanical properties of mature lamellar bone. In order to achieve this, the fracture healing cascade initiates a second resorptive phase, this time to remodel the woven bone callus into a lamellar bone structure with a central medullary cavity,[69] similar to the physiologic bone turnover described in a previous section. Collagen fibers of woven bone are structured in a disorganized fashion, making woven bone less resistant to deforming forces compared with lamellar bone, in which collagen fibers are arranged in parallel forming the typical longitudinal fibrils. This phase is biochemically orchestrated by IL-1 and TNF-α, which show high expression levels during this stage, as opposed to most members of the TGF-β family which have diminished in expression by this time. However, some BMPs such as BMP-2, are seemingly also involved in this phase with reasonably high expression levels.[59]

The remodelling process is carried out by a balance of hard callus resorption by osteoclasts, and lamellar bone deposition by osteoblasts. Although the process is initiated as early as 3-4 weeks in animal and human models, the remodelling may take years to be completed to achieve a fully regenerated bone structure. This process may occur faster in animals and younger patients.[56]

1.4.3.3 *Bone healing failure*

For bone healing to be successful, an adequate blood supply and a gradual increase in mechanical stability is crucial. In this respect, when the soft cartilaginous callus does not provide enough interfragmentary stability, it cannot be calcified and, hence, the physiologic bone healing cascade is interrupted. This scenario results in a hypertrophic non-union, also known as pseudoarthrosis. This is often due to inadequate fixation of the fracture, and treated with rigid immobilization. On the other hand, when the bone healing is impaired due to vascular (impaired blood supply to the bone fragments) or metabolic causes (e.g. diabetes), no callus is formed resulting in an atrophic non-union.[56]

On the other hand, the innate self-healing capacity of bone is significantly reduced as size of the bone defect increases. Several conditions such as trauma, infection, cyst or tumour resection, bone resorption around implants, corrective ostectomies, avascular necrosis, osteoporosis and some specific systemic diseases may produce large bone defects leading also to non-unions scenarios.[1,83] In such situations, the bone self-regeneration capacity is not sufficient and bone grafting surgical procedures are required in order to improve bone regeneration and to avoid the failure of bone repair.

1.5 Strategies for bone grafting

Bone grafting is a surgical procedure by which new bone or a replacement material is placed into spaces between or around broken bone to aid in healing.[84] The use of bone grafting dates back to the prehistoric period. The practice of cremation in many societies allowed only limited evidence for identifying substitute materials for replacement of missing bones and teeth. From the Fifth and Fourth centuries BC until the First or Second century AD, archeological findings showed that materials used then included ox teeth, shells, corals, ivory (elephant tusk), wood, human teeth from corpses, and metals (gold or silver).[26] Nowadays, the progressive increase of life expectancy has lead to a higher incidence of pathologic bone fractures due to osteoporosis and other degenerative bone diseases, becoming a significant public health issue.[85] The number of bone-grafting procedures has increased consequently placing a larger demand on the healthcare system to replace and restore lost bone.[86] Approximately, 2.2 million bone graft procedures are performed worldwide annually at an estimated global cost approaching $ 2.5 billion yearly.[3] Moreover, impaired bone healing situations are still associated with significant patient morbidity, psychological stress, functional disability, decreased life expectancy and a remarkable economic cost to society, which is predicted to increase significantly over the coming years.[4] Therefore, the treatment of these large bone defects remains an important clinical challenge in orthopedics.

The following sections will provide an overview of the most commonly used bone grafting strategies for the surgical treatment of critical-seized bone defects.

1.5.1 Autografts

In fresh autologous bone grafting, cortical or trabecular bone or a combination of both, are transplanted from one site in the body, such as the iliac crest, to the bone defect within the same patient. Since bone is taken from the same patient, it is both histocompatible and non-immunogenic.[87] Autologous bone grafting or autograft is still considered the gold standard clinical treatment and the most effective method for bone regeneration due to its outstanding biological performance in terms of osteoconduction, osteoinduction and osteogenesis.[3]

Osteoconduction

Autografts provide a three dimensional network that promotes cell migration and vascular infiltration through its macroporous internal structure leading to new bone formation by direct bone bonding, process known as osteoconduction.[5,88]

Osteoinduction

Autografts also induce local MSCs differentiation towards mature osteoblastic cell lineage thanks to its microstructure and due to the presence of endogenous growth factors (i.e BMPs), phenomena called osteoinduction.[5,89]

Osteogenesis

Finally, fresh autologous bone grafts are also considered to have a significant osteogenic potential since they are a source of undifferentiated MSCs and mature bone forming cells.[5,88]

However, the use of autografts is associated with important drawbacks such as limited availability of bone volume (particularly in children and elderly patients), higher risk of side effects associated with an additional invasive surgical procedure (increased intra-operative blood loss, infections, transfer of cancer cells to donor site, bone fracture, nerve/vascular injury, donor site morbidity, hypersensitivity and chronic pain), high volumetric change due to a too rapid resorption and higher operative time and cost.[4,5,90,91]

1.5.2 Allografts and xenografts

Some of the main disadvantages showed by autografting (associated with the harvesting surgery) can be overcome by using allografts or xenografts.

The allograft consists in cortical or trabecular bone harvested from a donor subject of the same species. Allografts are usually harvested from sections of the pelvis from cadavers or from removed femoral heads at primary total hip replacements. Then, allogenic bone grafts have to undergo processing techniques such as lyophilization, irradiation or freeze-drying to remove all immunogenic proteins, in order to avoid any risk of immunogenic reaction. In turn, these processing techniques have a negative impact on the osteoinductive potential and decrease their biological performance as compared with autografts. Thus, allografts possess only osteoconductive properties, since they preserve the original mineral interconnected macroporosity and when used as fresh frozen they also present limited osteoinductivity.[92]

The use of demineralized bone matrix (DBM) is a further alternative. DBM is made from allograft bone in which the inorganic mineral has been removed, leaving behind the organic matrix (collagen, non-collagenous proteins and growth factors). Therefore, DBM preserves certain degree of osteoinductivity, but with limited osteoconductive properties due the lack of a three-dimensional mineral network.[92]

The xenograft is based on bone harvesting from other animal species, generally corals, bovine, porcine or equine. Because of the high probability of immune rejection or contamination by viral proteins, the material extracted is treated either chemically or at high temperature to keep exclusively the mineral part of bone. The final result is equivalent to an allograft, meaning that it provides an osteoconductive framework for bone ingrowths with a negligible osteoinductive capacity.[9]

In addition to limited supply and high processing costs, other complications associated with allogenic and xenogenic bone grafts such as viral disease transmission or bacterial infections are of serious concern.[9] Furthermore, differences in graft preparation techniques lead to varying levels of immune response (donor incompatibility and graft rejection) and impaired healing

situations (fractures and non-unions) due to differences in the bone quality between the donor and the patient. Moreover, implanting human- or animal-derived grafts may generate ethical or religious concerns depending on both culture and religion of the patients.[92]

1.5.3 Synthetic bone grafts

The above-mentioned drawbacks of natural bone grafts have driven research efforts to focus on developing alternative bone repair strategies. A large number of synthetic bone substitutes have been developed presenting attractive features like unlimited availability, avoidance of second surgery, absence of risk of disease transmission and injectability or freedom of conformation.

Based on their chemical composition, synthetic bone grafts can be divided into four main groups: i) metallic implants, such as titanium and its alloys, stainless steel and cobalt-chromium alloys; ii) ceramics, such as calcium phosphate, alumina, carbon and glass ceramics; iii) polymers, such as poly(methyl-methacrylate), poly(urethane), ultra-high molecular weight polyethylene, silicon, polylactide and poly(lactic-co-glycolic acid), and iv) composites of the first three groups, such as calcium phosphate–ceramic coatings on metallic implants and polymer–ceramic composites.[5,9,84] Regardless of the strategy taken, it is obvious that the bone regenerative capacity of new bone graft substitutes needs to match that of the natural grafts, in order to be fully accepted as a comprehensive alternative.

A synthetic bone graft should fulfill the following requirements:[84,93]

- To provide an osteoconductive matrix by presenting a three-dimensional network with open and interconnected macropores that serves as a scaffold or template to guide and direct cell migration, cell attachment and cell proliferation along material's surface.

- To enhance angiogenesis and capillary infiltration, with the corresponding oxygen and nutrient supply, and the easy access of cells (inflammatory cells, stem cells) and soluble proteins, including signaling molecules and osteogenic growth factors.

- To be biomechanically stable when needed but biodegradable after bone substitution and within an appropriate time frame to avoid a second surgery to remove the implant. It is critical to show a tight synchronization between graft resorption and new bone deposition to allow a gradual and entire replacement of the material by the newly formed autologous bone tissue, avoiding a mechanically weakened stage during the bone defect healing process.

- To be non-immunogenic, free of transmission diseases and biocompatible.

- To possess easy clinical manageability, be amenable to contouring for optimal adaptation to the various shapes of bone defects and/or be suitable for minimally invasive surgery applications.

- To be an affordable product, in order to meet an ever-growing need without presenting a heavy burden on our health care system.

However, the biological performance of synthetic bone grafts developed so far are inferior to those of autologous bone grafts in terms of initiation and support of bone growth.[2] In this context, endowing osteoinductive properties to a synthetic bone substitute, i.e. the ability to induce MSCs differentiation into mature bone-forming cells, is one of the most challenging and,

at the same time, promising tasks for the development of an ideal bone graft substitute that can replace autografts. Strategies towards this aim are diverse, varying from addition of osteoinductive growth factors or MSCs/osteogenic cells to appropriate carrier materials (engineered osteoinductive biomaterials), to the development of smart synthetic biomaterials capable of triggering *de novo* bone formation *in vivo*, by tuning their physico-chemical and structural properties (intrinsic osteoinductive biomaterials).[2] In summary, it is evident that continuing research efforts in the field of biomaterials and tissue engineered constructs for bone regeneration are urgently needed to find more effective bone-healing therapeutic modalities.[2]

1.6 Osteoinductive biomaterials

Osteoinduction, initially defined by Friedenstein as the process of the "induction of undifferentiated inducible osteoprogenitor cells that are not yet committed to the osteogenic lineage to form osteoprogenitor cells"[94] is often considered the most critical property in order for the clinical performance of bone substitutes to match that of natural bone grafts.[2] Osteoinduction is a basic biological mechanism that occurs regularly as part of natural bone healing and is responsible for the majority of newly formed bone during fracture repair. Even if pre-existing osteoblasts may help to form new bone, it is generally agreed that such pre-existing cells only contribute a minor portion of the new bone needed in a fracture-healing situation.[84,95] In fact, it is difficult to differentiate between bone induction and bone conduction in an orthotopic site. Thus, the safest way to demonstrate the osteoinductive capacity of a biomaterial is by its ability to stimulate new bone formation when implanted ectopically (subcutaneously/intramuscularly) in a host animal.[96] Alternatively, the osteoinductive potential of a biomaterial can be assessed *in vitro* by studying the osteogenic differentiation of undifferentiated MSCs in contact with candidate bone graft substitutes. However, it has been demonstrated that while such *in vitro* tests give an indication of the potential osteoinductivity of a given material, confirmation of *in vivo* bone formation in ectopic sites is absolutely necessary before a material is classified as osteoinductive.[96]

The earliest proof of osteoinduction was observed in auto-implantation of transitional epithelium of the urinary bladder to the abdominal wall muscles in dogs as early as the beginning of the twentieth century.[97] The osteoinductive phenomenon was then reported by other authors after implantation of devitalized tissue and tissue extracts in heterotopic sites (muscles or the anterior chamber of the eye).[98-101] At that time, however, consistent results were rarely obtained and little was known about the elements involved in this process. Urist et al. set a landmark in the research on osteoinduction by publishing a report in which ectopic bone formation by hydrochloric acid-decalcified diaphyseal bone was consistently shown in the muscles of rabbits, rats, mice and guinea pigs.[89] Later work by Urist and Strates led to the conclusion that a discrete, soluble, low-molecular-weight glycoprotein, named bone morphogenetic protein (BMP), was involved in the cascade of chemotaxis, mitosis, differentiation, callus formation and finally bone formation.[102] BMP was then purified in 1984[103] and cloned in 1988 by using the recombinant gene technology, based on its potential to be used as therapeutic molecules for bone formation.[104]

Since Urist's discovery, at least 20 different BMPs have been identified in humans; however, not all of them are truly osteogenic molecules.[105,106] Apart from BMP-1 (a metalloprotease which modulate BMPs activities), BMPs are multifunctional cytokines belonging to the TGF-β

superfamily, comprised of approximately 50 genes. While BMP-2, BMP-4, BMP-5, BMP-6, BMP-7 (also called osteogenic protein-1 or OP-1), BMP-8 (OP-2), BMP-9, and BMP-10 contribute to bone formation, BMP-3 and BMP-13 act as BMP inhibitors. They are secreted by chondrocytes, osteoblasts and osteoclasts playing pivotal roles throughout embryonic skeletogenesis and in postnatal bone formation and endogenous repair mechanisms, as described in the previous sections. The rest of BMP members are involved in developmental activities of not only the musculoskeletal tissue (bone, cartilage, and tendon) but also of many other tissues such as teeth, nervous system, eye, lung, heart, pancreas, liver, kidney, ovary, and testis.[106]

1.6.1 Engineered osteoinductive biomaterials

The emergence field known as tissue engineering combines engineering and life sciences technologies toward the development of biological substitutes that restore, maintain, or improve tissue function.[107] Particularly, bone tissue engineering is an interdisciplinary research field that applies principles of materials engineering and biology to create a favorable osteoinductive environment that promotes local bone repair and aims to offer a better solution for the healing of large bone defects and non-unions,[1] as described in the following sections.

1.6.1.1 Osteoinductive biomaterials by adding exogenous BMPs

In the last decades, BMPs have been extensively studied within the field of bone tissue engineering in order to be used as therapeutic molecules for bone regeneration. Among the different identified BMPs, BMP-2 and BMP-7 seemed to be the strongest inducers of *novo* bone formation via the endochondral pathway when implanted in ectopic sites in different animal models, as a recapitulation of embryonic development.[106,108,109] A great number of experimental preclinical research projects involving these two types of BMPs were conducted confirming the expected potential to regenerate bone, which led to their investigation in human clinical trials.[106,108,109,110] The impressive reported outcomes of the clinical studies resulted in the FDA-approval of two recombinant human BMPs (rhBMPs), rhBMP-7 and rhBMP-2 for clinical use with restrictions. They were delivered specifically for spinal fusion, open tibial fractures, non-unions and oral maxillofacial applications via bone-derived collagen particles or an absorbable collagen sponge.[106,108,111]

Unfortunately, with the increased use of these commercial available rhBMPs in the different surgical procedures some dose-related complications showed up. Basically, the impressive and convincing results seen in animal models were difficult to reproduce in humans when using equivalent doses. While *in vitro* effects were evident at concentrations at femtomolar and nanomolar ranges, and histologically discernible bone formed in several mammalian species at microgram ranges, clinically significant induction of bone in humans was only achieved at doses in the milligram range. The extrapolation of data from animal models was unreliable, as dose seems to be species specific. Therefore, the result was that predicted BMPs doses in animal models were ineffective in clinical contexts. The clinical effective doses resulted to be several folds higher than those suggested by the results in animal models and at the same time exceeded one million times the physiological protein amount, produced in nanograms under normal bone repair conditions. These clinical, supraphysiological doses suggested ineffective or limited

biological activity of BMPs after the recombination process in DNA. Alternatively, some authors also related it to rhBMPs' short biological half life (7-16 min) *in vivo*.[106,111,112]

Moreover, with the application of these rhBMPs supraphysiological doses in human patients, reports started to emerge regarding a series of safety concerns and undesirable side effects that were not published in the early clinical trials. Due to these problems and because of the high proportion of surgical procedures performed with BMPs deviating from the original approved indications, the FDA released them for orthopedic treatments, keeping the FDA-approval only for lumbar interbody fusion procedures.[33] The most frequently reported side effects were exaggerated inflammatory response in surrounding soft tissues (local edema, erythema and generalized hematomas), inflammatory vessel fibrosis, compartment syndrome, local bone resorption, pseudoarthrosis, osteolysis, unicameral bone cysts, ectopic bone formation, dysphagia and dyspnea in cervical spinal fusions (due to mechanical or inflammatory pressure on the esophagus or trachea), postoperative radiculitis and nerve root compression, male sterility, retrograde ejaculation (due to mechanical or inflammatory injury to the superior hypogastric plexus), cancerogenicity (when using a BMP-high dose product, Amplify™: rhBMP-2, 40 mg) and brain injury, resulting some of them in life threatening injuries.[113-115]

These adverse events were associated with the receptor saturation due to the supraphysiological doses used or the limited availability of responding cells, leading the stimulation by these BMPs at undesirable locations.[113] Some other authors suggested that the collagen-based delivery system used for BMPs clinical applications caused a too rapid release, which besides inducing bone formation at the target site, also caused these critical side effects. Basically, the main drawback of the absorbable bovine collagen sponge carrier was the little affinity of BMPs for collagen and its too fast degradation during the initial days after surgery, as a consequence of the inflammatory response caused by the surgical procedure.[113,114]

The concept that optimal induction of bone formation is dependent on the combinatorial action of an osteogenic-soluble molecular signal (e.g. BMPs), and a complementary substratum (carrier) is of paramount importance for future therapeutic applications.[116] Thus, an attractive approach in order to improve the current uncontrollable release kinetics of BMPs and decrease their effective dose in humans, avoiding systemic diffusion and, therefore, the risk of the above-mentioned side effects, would be to investigate carriers that may favor spatio-temporal physiological protein release; i.e maintain a critical threshold concentration of BMP at the implantation site (spatial distribution: local effect) for the required period of time (temporal distribution).[106]

The ideal carrier, apart from providing a controlled and localized sustained release of the incorporated growth factor, should maintain its biological properties during the releasing period, possess certain affinity for growth factor binding, adapt easily to the bone defect, provide immediate structural support to the reconstructed bone (adequate mechanical properties), possess a macroporous matrix of interconnected pores in order to allow first the infiltration of cells and then vascular in-growth (osteoconductive) and elicit a suitable and commensurate immunological response.[1,109] It should be also biodegradable with a resorption kinetics closely connected with the advancing osteogenetic front. By this way, it may protect BMPs from degradation for a sufficient period of time.[106]

Overall, the prevalence of the reported adverse events and complications related to the use of rhBMPs has raised many ethical and legal concerns for surgeons.[117] Therefore, the attempt for an

alternative treatment strategy is still required. MSCs that have the potential to differentiate into bone-forming cells and secrete a wide range of growth factors can be considered as an attractive option to fabricate a promising tissue-engineered construct with the aiming to improve its osteoinductivity and accelerate healing of bone defects.[118]

1.6.1.2 *Osteoinductive biomaterials by adding MSCs*

One of the above-mentioned reasons for the low clinical efficiency of the current commercial available BMP devices relate to the lack of sufficient numbers of responding cells at the site of implantation in the host.[119] Therefore, MSCs-based therapy has been postulated as a promising option to explore in the bone tissue engineering field.

Over 40 years ago, Friedenstein first reported evidence of multipotential MSCs that were isolated from bone marrow and formed fibroblast-like colonies with potential to differentiate into adipocytes, chondrocytes, osteoblasts, and myocytes.[120] Originally, MSCs were believed to derive from the mesodermal germ layer and to build up the major part of the skeleton during embryogenesis.[121] Then, they were also identified in various adult tissues as local self-renewing cells that had the ability to serve as long-lasting progenitor cells maintaining and restoring tissues like bone. Since then, research focused on stem cells has gathered tremendous momentum for bone tissue engineering strategies.

MSCs have now been identified not only in mesodermal tissues (bone marrow, trabecular bone, synovium, cartilage, fat, muscle, and tonsil) but also in endoderm (thymus, liver)- and ectoderm (skin, hair follicle, duramater, and dental pulp)- derived tissues.[122] In fact, MSCs are a heterogeneous population of pluripotent progenitor cells capable of differentiating into osteoblasts, chondrocytes, adipocytes, myocytes, cardiomyocytes, fibroblasts, myofibroblasts, epithelial cells, and neurons.[23] Since MSCs do not have any specific and unique surface markers that would simplify their enrichment and characterization, the International Society for Cellular Therapy have proposed minimal criteria to define these cells: i) the ability to adhere to plastic in culture, ii) the expression and coincident absence of a variety of clusters of differentiation (positive for: CD105, CD73, CD90; negative for: CD34, CD45, CD14 or CD11b, CD79a or CD19, HLA-DR) and iii) the capability to differentiate into osteoblasts, chondrocytes and adipocytes in vitro.[124]

However, to determine if cultured MSCs are also able to form bone *in vivo*, they have to be combined with a suitable three dimensional scaffold, which promotes cell adhesion and differentiation, and transferred into an orthotopic or ectopic environment. Human MSCs seeded on different carriers have been shown to induce bone formation when implanted ectopically into immunocompromized animals, as well as, to enhance the repair of experimentally induced large bony defects in different experimental animal models.[118] Beside their multipotency, MSCs have been shown to exhibit immunomodulatory properties and to act in a trophic way by secreting bioactive factors, which make them additionally attractive for possible bone therapeutic applications.[125]

For their clinical therapeutic application, MSCs can be isolated from organs and tissues including adult bone marrow, trabecular bone, synovial membrane, periosteum, adipose tissue, fetal bone marrow, the umbilical cord and umbilical cord blood.[86,118] However, there is no consensus as to which source is optimal. More recently, several studies have demonstrated that

isolated MSCs exhibit characteristic features of perivascular cells, which encircle small blood vessels within diverse tissues, leading to the assumption that the perivascular niche is now believed to be a common stem cell microenvironment for MSCs populations.[126,127]

To date, there are still few clinical trials describing the transplantation of human autologous MSCs for bone regeneration procedures[128-136]. These preliminary clinical studies demonstrate the potential use of human autologous MSCs for cell-based bone tissue engineering strategies. However, due to existing discrepancies in the way human MSCs are harvested, isolated and cultured *ex vivo*, in addition to donor-dependent variability regarding the bone forming potency; further investigations are needed to standardize the production and quality of these rare progenitor cells for therapeutic applications.[137-141]

1.6.1.3 *Alternative bone tissue-engineering strategies*

Other commonly used strategies grouped within the bone tissue engineering techniques in order to enhance the osteoinductive capabilities of biomaterials include the use of platelet rich plasma (PRP). PRP has been considered as an easily derivable alternative to BMPs since it contains TGF-β1, FGF, IGF, VEGF and PDGF among other growth factors. However, its efficacy in bone regeneration is not yet established beyond doubt and comprehensive comparative analyses between clinical performance of BMPs and PRPs are still awaited.[142,143]

In addition, icariin flavonoid, a flavonol glycoside extracted from Herba Epimedii, has been postulated as a potential candidate to substitute BMPs, since it is cheaper and safer than BMPs and other osteogenic growth factors, as well as, it has demonstrated a remarkable osteoinductive and angiogenic potential.[144,145]

Another option to increase osteoinductive capabilities of biomaterials is the addition of simvastatin. As a member of statins it has been shown to increase the expression of BMP-2 and VEGF and by these mechanisms it has been shown to endow biomaterials with significant osteoinductive properties.[146,147]

Finally, gene therapy-based strategies have been also introduced to improve BMPs and other growth factors delivery and their effectiveness at the target site.[148,149] Research into genetic manipulation of bone healing is based on the hypothesis that gene transfer could achieve more satisfactory osteoinductive and osteogenic promotion. The advantages of gene delivery include the ability to establish a local and constant endogenous synthesis of proteins at the site of deterioration or injury, whereby therapeutic substances are produced directly by local cells.[150] The concept is to transfer genes encoding osteogenic factors to cells in the location of osseous lesions. Unlike the recombinant protein, the growth factor synthesized *in situ* as a result of gene transfer undergoes authentic post-translational processing and is presented to the surrounding tissues in a natural, cell-based manner. Unfortunately, cells do not spontaneously take up and express exogenous genes. Moreover, delivery of foreign genes to recipient cells is limited by normal extracellular and intracellular protective mechanisms.[151] For this reason, successful gene transfer requires vectors, which can be viral or non-viral. Gene transfer with viral vectors is known as transduction, whereas gene transfer with non-viral vectors is known as transfection.[152,153]

However, all of the above-mentioned tissue-engineering approaches have been associated with critical drawbacks for their clinical application. The production of recombinant growth factors,

the high or repeated dose injections of BMPs required to be effective, the undesirable side effects and variable efficacy of the exogenous applied bioactive molecules, the collection and transport of the biopsies and culture of autologous MSCs are some of the factors that make tissue engineering time-, money- and labour consuming. Moreover, they are often subject to increased regulatory scrutiny due to safety and ethical concerns which limits their clinical applicability. Therefore, it is a general agreement that these high costs and safety drawbacks must be decreased or prevented by finding a viable alternative strategy in the challenging field of osteoinductive materials, for its clinical application.

1.6.2 Intrinsic osteoinductive biomaterials

At the time of Urist's discovery of BMPs as osteoinductive factors, the phenomenon of osteoinduction triggered by a completely synthetic biomaterial, by no means resembling the composition of implants used in Urist's studies, was also reported. In 1960, Selye and coworkers implanted Pyrex® glass tubes subcutaneously in rats. Histological analysis of tissue formed inside the glass tubes 60 days after implantation, revealed the presence of bone, cartilage and hemopoietic tissue.[154] In 1968, Winter and Simpson reported an observation of bone induction by a sponge made of polyhydroxyethyl methacrylate (poly-HEMA) in the soft tissue of pigs, which was at that time used, for example, for breast augmentations.[155] The authors observed that the implanted sponge became calcified prior to bone formation. The observed phenomenon of bone induction by the glass tubes or by the polymeric sponge could not be explained by Urist's theory, as these materials neither contained nor produced BMPs. The first reports on heterotopic bone formation triggered by a synthetic biomaterial that did not contain BMPs or any other osteogenic factors caused both disbelief and excitement, considering important advantages of synthetics versus biologics, such as generally lower cost of production and better stability. However, it was not until 1990s that researchers actively started searching for synthetic biomaterials with intrinsic osteoinductive potential.[4]

Indeed, in the past three decades, some CaP ceramics have been found to exhibit an intrinsic osteoinductive capacity when implanted ectopically in various animal models.[96] Besides CaP biomaterials, osteoinduction has been also observed in alumina ceramic[156] and glass ceramics.[157] In the family of metals, porous titanium have shown osteoinductivity, alone,[158,159] coated with a thin layer of CaP[160] or in a construct with CaP ceramic.[161] Finally, composites, consisting of polylactide and HA particles have shown to be osteoinductive too.[162,163]

To date, however, scientists still lack fundamental understanding of the biological mechanism underlying the phenomenon of osteoinduction by biomaterials. Initially, some authors proposed that these smart materials act as solid substrata for the adsorption of BMPs, for which probably a concentration threshold has to be reached in order to induce bone formation.[96] These ideas were shared by De Groot, who proposed the rational design and development of BMP concentrators that, after implantation in the patient, were capable of concentrating and immobilizing the endogenous BMP complex.[164] Instead, other theories concentrate on the material's ability to trigger cellular secretion of factors leading to bone formation, rather than to their ability to accumulate them on the surface. For instance, the expression of BMP-2, BMP-4 and BMP-7 has been shown to be markedly upregulated in response to inflammatory stresses,[75,165,166] just like caused by surgical implantation of a biomaterial.[167] In this regard, some authors have suggested that first, inflammatory cell-mediated resorption of the osteoinductive substrate occurs,

accompanied with the release of growth factors, that in turn stimulate angiogenesis and osteogenic differentiation of stem cells. Upon osteogenic differentiation, stem cells are then suggested to express and secrete more BMPs which are incorporated into the biomaterial surface to eventually induce heterotopic bone formation.[168]

It is furthermore unknown whether the mechanisms of engineered osteoinduction by BMPs and intrinsic osteoinduction by biomaterials are related and, if so, to which extent. The four apparent differences in osteoinduction by BMPs or by biomaterials are that: i) bone induced by biomaterials is mainly intramembraneous, while BMP-induced bone is mostly formed via the endochondral pathway; ii) in small animals such as rodents, bone is very rarely induced by biomaterials but easily by BMPs; iii) bone induction by BMPs takes place as early as 2-3 weeks upon heterotopic implantation whereas osteoinduction by biomaterials is rather slow, requiring weeks to months after their ectopic implantation; and iv) while bone is never observed on the periphery of the biomaterials and it is always formed inside their pores, bone formation by BMPs is regularly seen on the outside of the carrier and even in the soft tissue distant from the carrier surface.[5,96]

Given the disadvantages associated with exogenous application of BMPs or MSCs, further improvement of biomaterials is needed in order to make tissue engineering more successful and, ideally, even unnecessary.[5] Hence, the future design of new osteoinductive biomaterials should aim to erect synthetic matrices that instruct the endogenous expression of the osteogenic-soluble molecular signals of the TGF-β superfamily.[116] Thus, the implanted patients would provide their own locally expressed and secreted osteogenic gene products to be embedded into these smart scaffolds instead of adding expensive megadoses of exogenous growth factors with the above-mentioned associated complications. Although the exact underlying phenomenon is not known, it has been suggested that CaPs might play an important role in the process of intrinsic osteoinduction of biomaterials.[96] Therefore, CaP-based biomaterials constitute an ideal platform to reach this goal being the most promising avenue for the future research in this field. Moreover, CaPs can be produced in large quantities, their production and storage are inexpensive as compared to growth factors or cells-based strategies and they are stable and therefore readily available off-the-shelf, all together simplifying the regulatory path towards their clinical application.[4,169]

1.7 Intrinsic osteoinduction of calcium phosphates biomaterials

Following the rationale that damaged tissue can be best repaired by something with close resemblance, CaP-based biomaterials were already proposed for fracture treatment in 1920.[170] However, CaP biomedical research did not soar until the 1970s and it was only in the late 1990s that their clinical use spread out as a consequence of the appearance of diseases such as acquired immune deficiency syndrome (AIDS),[171] and bovine spongiform encephalopathy (BSE)[172] and, hence, a stricter regulation for nature-derived products (xeno- and allografts).[4] Since then, CaP biomaterials have traditionally been used for a broad range of orthopedic and dental applications due to its strong resemblance to the inorganic phase of bone tissue.[26]

Nowadays, CaP-based bone substitutes are the most widely applied synthetic biomaterials for repair and regeneration of damaged and diseased bone, and their use is expected to further increase. Synthetic CaP biomaterials are commercially-available in different physical forms such

as particulates/granules, blocks, cements, coatings on metal implants and composites with polymers.[26] As previously mentioned, an increasing need exists for effective and affordable bone graft substitutes, and CaPs have the potential to play a pivotal role in a socially responsible bone tissue engineering.[169] This is justified by their outstanding biocompatibility and bioactivity, which means that they are easily recognized by the body due to their biomimetic features, and they are able to elicit or modulate specific biological processes of paramount importance for bone healing. The bioactivity of CaPs encompasses their biodegradability (various CaPs are resorbed by a cell-mediated process), bone-bonding capacity (thus forming a uniquely direct, adherent and strong interface with the bone tissue), osteoconductivity, and in some cases, intrinsic osteoinductivity, constituting all of them ideal properties for an optimal bone graft substitute.[1,169]

However, their use is also associated with drawbacks, with poor mechanical properties being probably the most relevant one for application in orthopedics and dentistry. Therefore, CaP biomaterials are not suitable for load-bearing areas, unless being coupled with an appropriate complementary bone fixation system.[173] In this respect, a paradigm shift occurred at the turn of the millennium: instead of designing load-bearing bone graft substitutes, researchers aimed for CaP bone graft substitutes providing a fast healing response, that is a fast turnover from a bone defect to mature bone and, hence, mechanically competent. Strategies have included a change in composition and an improvement of the material architecture and textural properties, as discussed in the following sections.[4]

Some distinct clinical successes have been achieved with CaPs,[1,4] and in a few studies, the bone regenerative potential *in vivo* has been shown even comparable to that of autologous bone.[174,175] However, it is worth mentioning that the combination of all the desirable properties into one material requires a tight control on the processing techniques and a thorough understanding of the necessary physicochemical properties of the material that effectively trigger cellular cascades towards bone regeneration. Still now, this control is not easy and efficient enough.[4,169]

In this context, improvement of the intrinsic osteoinductivity of CaP biomaterials is probably one of the most promising landmarks in the bone regeneration field. The underlying mechanisms influencing this intrinsic osteoinductive capacity are still largely unknown. While it may seem straightforward that their chemical composition is one of the key factors for their osteoinductive capacity, it should be emphasized that CaPs are complex functional biomaterials, with a set of largely intertwined physico-chemical and structural properties, many of which are believed to play a role in the intrinsic osteoinduction of these materials.[169] The next section will provide an overview of the key factors that have been reported to affect the intrinsic osteoinduction of CaP biomaterials.

1.7.1 Parameters affecting the intrinsic osteoinduction of CaP biomaterials

In contrast to the limited number of reports on osteoinduction by polymers and metals, a large number of publications have illustrated intrinsic osteoinduction by diverse CaP-based biomaterials: HA,[168,176-190] β-tricalcium phosphate (β-TCP),[190-196] biphasic calcium phosphate (BCP), that designates the mixture of HA and β-TCP,[185,186,189,190,197-202] carbonated apatite,[186,201,203] dicalcium phosphate anhydrous (DCPA),[204] dicalcium phosphate dihydrate

(DCPD),[204] calcium deficient HA (CDHA),[205] calcium pyrophosphates[206] and HA/calcium carbonate (CC) mixtures.[168,181]

These studies suggested that CaP biomaterials can show intrinsic osteoinductive properties when they exhibit specific chemical and structural characteristics, since this osteoinductive capacity was observed only in some CaP materials but not in others of similar compositions. However, the exact processes involved in the mechanism of osteoinduction by CaP biomaterials are still incompletely understood. Various attempts have been made to describe the biological mechanisms behind the phenomenon of intrinsic osteoinduction by CaPs, as well as to understand which material properties are essential for rendering a ceramic osteoinductive.[4] The most critical material properties which so far have been suggested to play a role in osteoinduction are: the chemical composition, the macropore architecture (total porosity, size and geometry of macropores) and the microstructural properties (microporosity, surface roughness/topography, SSA and crystallinity), as summarized in **Fig. 1.12**.[5,96,116]
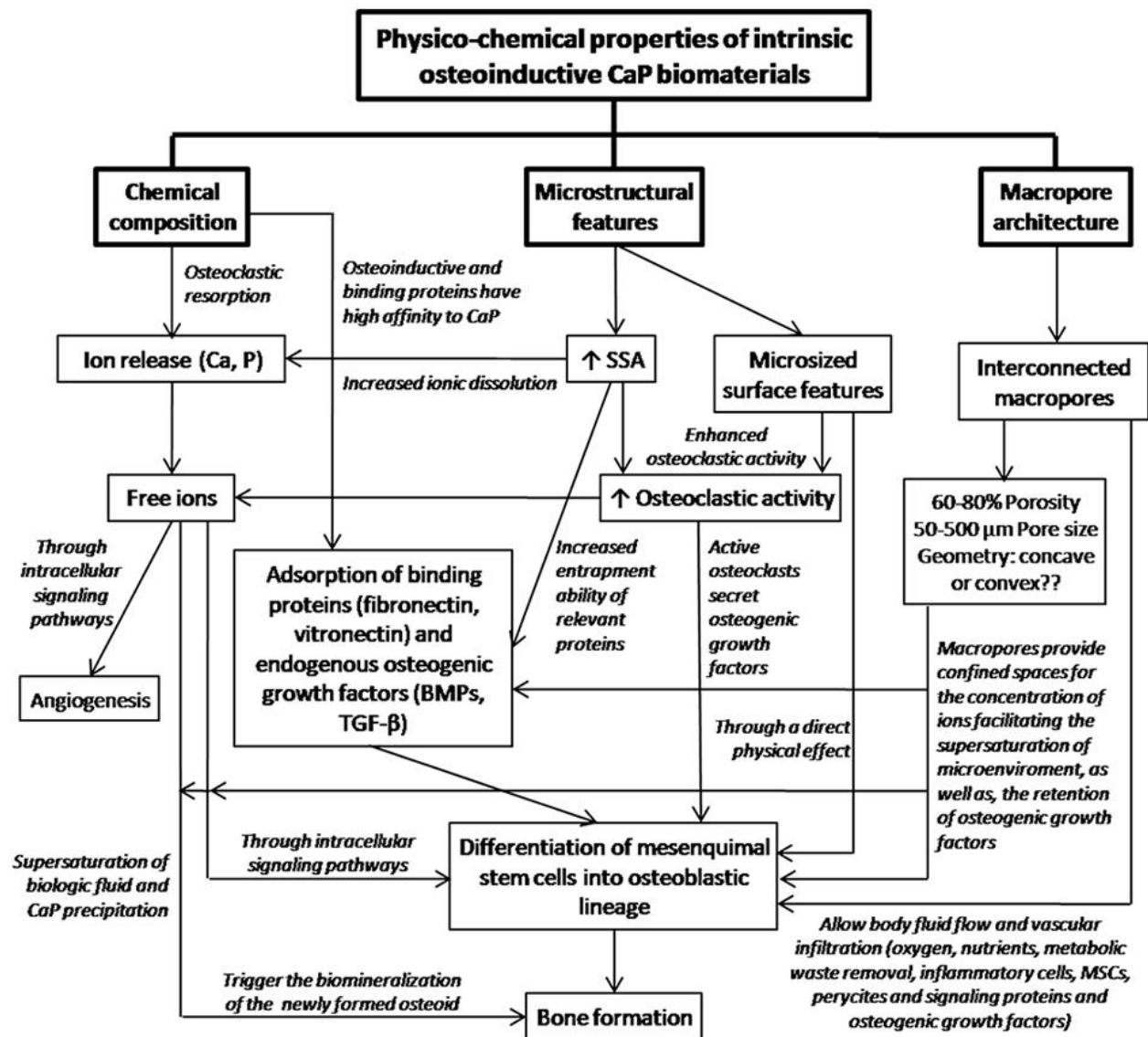
Figure 1.12. Schematic diagram summarizing the physico-chemical properties of CaP biomaterials and the associated mechanisms which so far have been suggested to play a role in their intrinsic osteoinduction, adapted.[96]

1.7.1.1 *Influence of chemical composition*

The majority of synthetic biomaterials so far shown intrinsic osteoinduction contained CaP. Moreover, the rest of synthetic materials reported as osteoinductive that do not contain CaP, such as titanium[158,159] or poly-HEMA[155] have been shown to calcify when exposed to body fluid, before heterotopic bone formation occurred. These data suggest the importance of calcium and phosphate ions in the process of osteoinduction by biomaterials.[96]

On the one hand, osteoinductive proteins such as BMPs and TGF-β are known to have a high affinity to CaP.[103,190] Therefore, it has been hypothesized that CaP-based biomaterials may act as an *in vivo* affinity column/concentrator of the endogenous osteoinductive molecules upon implantation, which then renders the biomaterial osteoinductive.[1] Moreover, it has been shown that, apart from osteogenic growth factors, CaP-based biomaterials are sensitive to absorb binding proteins such as FN and vitronectin, which provide an optimal matrix for MSCs attachment, proliferation and osteogenic differentiation via mechanotransduction trough a focal adhesion process.[110,190,207,208] Once differentiated into bone forming cells, they produce extracellular matrix, which is biomineralized leading eventually to the new bone formation.[5,26]

On the other hand, CaP biomaterials elicit an inflammatory response after implantation that attracts the infiltration of mono- and multinucleated cells (macrophages and osteoclasts), which results in the partial dissolution of the CaP ceramics due to the acidic environment associated with this cellular activity. The effect of the cellular degradation by mineral-resorbing cells has been also suggested to be critical in the process of heterotopic bone formation by CaP biomaterials.[209,210] Osteoclastic activity triggers a direct effect onto MSCs inducing their proliferation and differentiation into bone-forming cells through intracellular signalling pathways.[209] Specifically, the osteoclastic inference on the osteogenic differentiation of MSCs has been ascribed to the secretion of osteogenic growth factors by active osteoclasts,[51-54] [196,202,210-212] as well as due to the high concentration of calcium and phosphate ions resulting from the osteoclastic resorption of CaP materials.[41-43,193,213-215] Moreover, the liberated ions increase the supersaturation condition of the biologic fluid, which causes their precipitation triggering the biomineralization of the newly formed organic bone matrix. In addition to the calcium and phosphate ions, other ions (carbonate, magnesium, sodium) from the biologic fluid become incorporated in the mineralized bone matrix. Accordingly, it has been reported a reduced ectopic bone formation and a decreased BMP expression in osteoinductive CaP biomaterials when treated with bisphosphonate, an osteoclast inhibitor.[209,210,215]

Indeed, the osteoinductive potential of CaP biomaterials has been directly related to the solubility of the material.[26] It is well known that dissolution properties of CaPs are phase-dependent,[216] and in some studies, a direct comparison was made between implants with varying chemical composition. For instance, for synthetic sintered ceramics, the extent of dissolution in acidic buffers is the greatest for, tetracalcium phosphate, followed by α-TCP, β-TCP, and is the least for HA. For unsintered CaPs the solubility decreases in the order: amorphous calcium phosphate (ACP) > DCPD > octacalcium phosphate (OCP) > CDHA.[9,216] However, the role of CaP phase composition and the associated degradation behavior in osteoinduction is still controversial. In this regard, it is generally agreed that certain degree of degradation is desirable, since it provides the calcium and phosphate ions needed for the collagen biomineralization, as well as to stimulate angiogenesis[217,218] and osteogenic differentiation of MSCs through intracellular signaling pathways.[41-43,193,213-215] However, a too high degradation may impair

osteoinduction due to the lack of a stable surface where the new bone has to be deposited.[201] In this context, a few studies comparing HA and β-TCP or HA and BCP with similar macro- and microstructures demonstrated that the presence of a more soluble phase (β-TCP) is beneficial for the amount of induced bone.[185,190,199] Instead, other studies showed that the addition of β-TCP negatively affected bone induction.[198]

Since both, a high solubility and a high osteoclastic resorption have been associated with an enhanced osteoinductivity of CaPs,[96] a promising strategy to foster osteoinductive biological cascade would be ionic substitution.[219] CaPs admit the substitution of a portion of calcium and phosphate ions in the crystal lattice by other ions with therapeutic potential, usually called bioinorganics (carbonate, magnesium, strontium, silicate, cobalt, fluoride, copper and zinc).[169] In fact, the incorporation of ions such as carbonate or magnesium into the crystal structure of synthetic apatites does not only impart chemical similarity to natural bone but also decreases their crystallinity (reduction in crystal size) which increases their chemical reactivity.[26]

In this respect, *in vitro* studies have demonstrated that doping the crystal lattice of HA with carbonate ions enhances its solubility[220-224] and promotes the osteoclastic resorption,[225-227] which could potentially enhance the osteoinduction properties of carbonated apatites. In addition, carbonated hydroxyapatite-based biomaterials have already been reported as more bioactive and soluble when evaluated in orthotopic implantation models than stoichiometric sintered HA.[228-230] However, in some *in vivo* ectopic implantation studies the osteoinductive capacity of sintered carbonated apatites were shown to be negatively affected by a too fast resorption rate and, hence, by the loss of a stable three-dimensional macrostructure, which is required for the onset of bone formation.[186,201,203]

Finally, it is worth mentioning that by substituting a calcium, a phosphate, or, in the case of HA, a hydroxide ion by a guest ion, it does not only change the chemical composition of the ceramic, but it also modifies many other physico-chemical properties, such as the micro/nanostructure. Consequently, when investigating the behavior of cells or tissues on such ceramics, it is difficult to attribute an effect solely to the change in chemistry, i.e. the addition of a new ion.[169]

1.7.1.2 *Influence of macropore architecture*

Macropore architecture has been also suggested to be a key factor for the osteoinductive capacity of synthetic CaP bone grafts.[5,9,26,96]

It is generally agreed that macroporous scaffolds with open-interconnected macropores ranging from 50 to 500 μm in size and a total porosity around 70% are beneficial for the intrinsic osteoinductive properties of CaP biomaterials.[169,199,231] This is associated to the need of body fluid flow and vascular infiltration (angiogenesis), with the corresponding oxygen and nutrient supply, metabolic waste removal and the easy access of cells (inflammatory cells, MSCs, perycites) and soluble proteins, including signaling molecules and osteogenic growth factors.[199-231-233]

In the above-mentioned osteoinductive CaP biomaterials, ectopic bone formation was always observed within the macropores and never on the implant periphery. This emphasizes the importance of a porous structure that provides protective areas required to reach an optimal microenviroment for the differentiation of MSCs to osteoblasts. In other words, macroporous scaffolds provide confined spaces for the concentration of calcium and phosphate ions

facilitating the supersaturation of microenviroment, as well as the retention of osteogenic growth factors. These confined spaces within macropores are protected from high body fluid flows and mechanical forces due to implant movements, which enhance the angiogenic and osteoinductive capabilities of these materials.[96,116]

Besides the presence of interconnected macropores with suitable dimensions, geometry of the macroporosity has been also shown to be a driving cue for MSCs differentiation into osteogenic cells, but there is still controversy in this matter.[187,231,234-236] Some authors suggested that concave surfaces of macropores are required to promote the expression of the osteogenic phenotype[199,231] since they biomimetize the nature's structural geometries involved in the bone remodelling phenomena.[231] Instead, other authors reported a better osteoinductive potential for HA-based biomaterials with channel-like architectures with convex surfaces when compared to scaffolds with honeycomb-like architectures with concave surfaces.[187]

In this context, there are several conventional methods to introduce interconnected macropores similar to that of bone, to CaP scaffolds. These include particulate (fibers and meshes) leaching, freeze drying, gas/chemical foaming, emulsion and polymeric foaming (positive replica) amongst others.[237] However, by these methods it is challenging to have a precise control on the pore shape (geometry), pore size, pore interconnectivity, pore distribution and pore volume fraction. Moreover, they have poor reproducibility and offer a lack of variety of pore structures.[237]

To overcome these limitations, rapid prototyping (RP) techniques, also known as solid free form fabrication, have attracted a great deal of attention in the last years. RP is an emerging tool that allows a fast fabrication of individual complex geometrical scaffolds with high precision on the internal architecture and on the outer shape with a high reproducibility.[232,237,238] Different strategies have been explored within the RP technology field to create scaffolding materials with controlled macroporosity including direct and indirect extrusion free forming, selective laser sintering, stereolithohraphy, fused deposition modelling, multiphase jet solidification and microextrusion.[232,238] This last technique, also known as 3D-printing or robocasting, has several advantages over the rest like a high resolution and a high degree of control over complex geometry.[239-241]

1.7.1.3 *Influence of microstructural properties*

In addition to chemical composition and macropore architecture, microstructural properties have been also shown to play a determining role in osteoinduction of CaP biomaterials.[5,96]

Recent publications pointed to microporosity and SSA as essential elements for the CaPs-associated osteoinduction.[186,195,196,199-202,210,242] Several *in vivo* studies have evaluated CaP biomaterials with different microstructures, consistently showing the best results in terms of osteoinduction in the CaPs with higher levels of microporosity and higher SSA.[186,195,196,199-202,210,242] The results obtained in these studies suggested that some mechanisms relevant for intrinsic osteoinduction, such as the dissolution/reprecipitation events occurring on the ceramic surface, as well as, mineral deposition from the body fluids, in combination with the adsorption, and retention of binding proteins and osteogenic growth factors are promoted in microstructured materials with increased SSAs.[243] It is worth mentioning, however, that some authors have

hypothesized that there is a limit in the increase of SSA of biomaterials that positively influences osteoinduction, adducing that materials with a SSA above the optimum might degrade too fast.[201]

Furthermore, some researchers have proposed that the induction of bone formation by microporous ceramics may be related with the inflammatory response.[200] It has been hypothesized that particles smaller than 5 μm are released from the ceramics and provoke an inflammatory reaction, with the consequent promotion of macrophagic activity and release of cytokines that trigger the chemotaxis of MSCs and their differentiation into osteoblasts.[200] For instance, it has been reported an increased release of PGE_2, a factor that is produced by macrophages, in response to micro-rough surfaced HA as compared to cells cultured on smooth HA surfaces.[244] PGE_2 has shown to be chemotactic for MSCs and to stimulate their osteogenic differentiation.[244] Similarly, it has been observed the promotion of osteoclastic activity by submicrometric microstructures of CaP biomaterials and, thus, the enhancement of their osteoinductive potential.[196,202,210] Based on these findings, it has been suggested that the enhanced heterotopic bone formation by microstructured ceramics lies in a specific inflammatory reaction upon implantation which triggers the invasion of the material by macrophages and osteoclasts-like cells, which in turn cause chemotaxis of MSCs, their osteogenic differentiation and eventually new bone formation, as described previously.

Apart from this indirect effect of microstructure and large SSA in osteoinduction related to the increased ionic dissolution kinetics, the increased entrapment ability of relevant proteins, as well as the enhanced macrophagic/osteoclastic activity; the size and shape of crystals have been shown to exert a direct physical effect on cells involved in osteoinduction. In this regard, the osteogenic differentiation of MSCs *in vitro* has been reported to be fostered by micro and nanosized surface features of CaPs.[245-252] Moreover, it has been also observed that nanostructured surfaces facilitate cell attachment and proliferation,[246,248,253,254] as well as protein adsorption (particularly low molecular weight proteins such as osteogenic growth factors) and longer protein retention times.[255-257]

However, the main limitation in this matter is that most *in vivo* studies evaluating the intrinsic osteoinduction of CaPs have been performed with sintered ceramics (including HA, β-TCP, and the mixtures of the two, BCP), in which the high temperature (1000-1300ºC) processing precludes the introduction of nanoporosity, as shown in **Fig. 1.13**. Consequently, low SSAs are obtained, normally in the range of 0.2-2 m^2/g.[96]
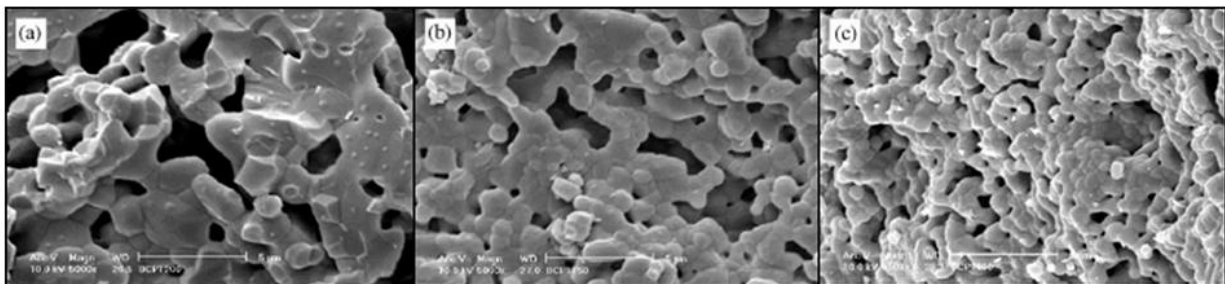
Figure 1.13. SEM images of a BCP scaffold obtained at different sintering temperatures: A:1200ºC; B: 1150ºC, and C:1100ºC. Lower sintering temperature results in an increase of micropores and a decrease in the crystal size, but the high temperature of sintering processing precludes the introduction of nanoporosity in all three cases.[199]

Although different strategies have been explored to overcome this limitation, such as reducing the sintering temperature (**Fig. 1.13**),[195,196,199] using spark plasma sintering to avoid grain

coarsening,[246,254] or covering the surface of sintered ceramics with nano-hydroxyapatite coatings obtained by hydrothermal routes,[248] these strategies did not manage to increase substantially the SSA of the materials, reaching values only around 6-10 m^2/g. The discovery of biomimetic routes based on the self-setting reaction of CaP cements (CPCs) at physiological temperature opened up new possibilities in this respect, since they allow obtaining nanostructured CaP scaffolds with significantly higher SSAs,[237] which is, in fact, the objective of the present thesis, as described in more detail in the last section of this chapter.

1.7.1.4 *Influence of animal model*

Besides the intrinsic physicochemical properties of CaPs, there are other important factors that can determine their osteoinductive potential when evaluated *in vivo*.

It has been reported that ectopic bone formation is a species-dependent phenomenon, being more significant and frequent in large animals (dog, sheep, goat and pig) than in small species (mouse, rat and rabbit).[183,185,197,211] Trying to explain these interspecies variations would be at best speculative as long as the exact mechanism behind osteoinduction by biomaterials is incompletely understood, but physiological and genetic differences are expected to play a role,[96] such as differences in the osteoclastic activity between species.[211]

Large animal models are generally considered of first choice when testing bone grafts materials for orthopedic applications since they closely represent the biomechanics and physiology of human bone[258-260] and they allow the implantation of large scaffolds. In fact, this is another factor that has been shown to stimulate the new ectopic bone formation compared to smaller constructs, probably due to the larger tissue-implant.[201] However, the use of large species is one of the delaying factors in the fully comprehension at the molecular and cellular levels of the mechanism behind biomaterials-associated osteoinduction since essential biological research tools, such as antibodies, are far less available than for smaller species.[96] On the other hand, despite the better adapted research tools and the high reproducibility of small animal models, rodents and rabbits possess significant dissimilarities in terms of bone tissue macro/microstructure (structure) and metabolic rate compared with human bone tissue, as well as important limitations of size.[259,260]

Among large animal models, differences are also present since studies involving dogs were in general more successful than those performed in the rest of large species, with the exception of non-human primates.[96,183] Although being a rough comparison as no other factors regarding the material or animal model were considered, this suggests that a material tested in a dog has higher chances of inducing ectopic bone formation than in a goat, for instance.[197] Moreover, dogs have been described as having the most similar characteristics (bone composition, microstructure, density) to human bone tissue.[259-262] On the other hand, working with other large species such as sheep, goats and pigs represents important handling, housing, and economic issues, although it does not have such ethical implications as experimenting with dogs.[259,260]

Apart from inter-species variation, large differences among individuals of the same species have been observed when evaluating the osteoinductive potential of a given material.[186,199,201,204,263] Whereas mice, rats, rabbits and sometimes minipigs can be obtained with similar or identical genetic make ups, larger animals (dogs, sheep and goats) are relatively heterogeneous with respect to strain, age and body weight.[96,260] Therefore, osteoinduction experiments should be

performed with animals of similar characteristics in order to limit the effect of age, sex and weight. However, it has been reported large variations in the amount and timing of bone induction in different individuals, despite keeping as many parameters of the animal model constant as possible.[201] It could be explained due to intra-specific different basal levels of endogenous growth factors,[26] and especially due to genetic factors that origins different responses to BMPs,[264] as happens in humans.[199,265]

Finally, several authors have also investigated the osteoinductive capacity of a material, depending on the implantation site.[197,201] These studies suggested that at intramuscular locations, ectopic bone formation occurs more frequently or, at least, at a higher rate than subcutaneous implantations. The higher vascularisation of muscle compared to subcutaneous tissue is probably the reason why subcutis has been shown to be a less inductive implantation site than muscle.[201]

Based on the above-mentioned considerations, the intrinsic osteoinductive potential of biomaterials should be assessed by means of their intramuscular implantation in a large animal model, using an homogenous group of animals (with controlled sex, age, weight and breed) and applying a block design (one sample of each biomaterial per animal) with paired comparisons in order to reduce the noise of the large intra-specific variations.

1.7.2 Correlation of CaPs osteoinduction with the bone healing capacity

Overall, while a growing number of studies confirmed that osteoinductivity can be an intrinsic property of some CaP ceramics, the clinically relevant question remained whether such ceramics would also result in an improved healing capacity of challenging bone defects for their clinical application.[4] The real interest in intrinsically osteoinductive biomaterials, therefore, lies in the hypothesis that a material that is able to induce bone ectopically will also perform better at orthotopic sites than those that are merely osteoconductive.[5]

Due to the lack of understanding of the biological mechanism behind osteoinduction by CaPs, many studies still focus on ectopic implantations, as this is the only way to give real evidence of osteoinductivity.[5] Thus, the number of studies in which osteoinductive potential of a material is directly linked to its performance in clinically relevant orthotopic defects is very limited.[175,203,266,267] The few published reports so far, proved that materials showing a better intrinsic osteoinductive potential when implanted ectopically were also able to increase the amount of bone at clinically more relevant orthotopic sites.[175,203,266,267] While the depth of bone penetration within the porous spaces via osteoconduction was confined to the peripheral regions of the bone defect in the non-osteoinductive ceramics, newly generated bone was also detected in the central areas of bone defects treated with osteoinductive ceramics. Therefore, these studies suggested that osteoinductive ceramics possess a higher bone healing capacity than non-osteoinductive CaPs.

1.7.3 Biomimetic CaPs as potential osteoinductive biomaterials

The use of biomimetic routes based on the self-setting reaction of CPCs allows obtaining nanostructured CaP scaffolds, with controlled micro and nanoporosity, and, hence, with high SSAs.[237] CPCs are made of one or more calcium orthophosphate powders, which upon mixing with a liquid phase, usually water or an aqueous solution, form a paste able to harden and set

through a dissolution and precipitation process in physiological conditions. Monocalcium phosphate monohydrate, monocalcium phosphate anhydrous, OCP, DCPD (brushite), DCPA (monetite), ACP, and CDHA can all be produced through biomimetic dissolution-precipitations reactions at or close to room temperature, this resulting in SSAs up to two orders of magnitude higher than the values exhibited by sintered ceramics.[4]

By far, the most interesting low temperature biomimetic CaP is CDHA, which can be obtained by hydrolysis of α-TCP **(Fig. 1.14).** As a result of the setting reaction, an entangled network of CDHA nanocrystals can be obtained at physiological temperature (37ºC), which not only mimic the composition and morphology of the natural bone apatite better than sintered HA (non-stoichiometric, calcium-deficient - Ca/P molar ratio lower than 1.67 and poor crystallinity) but also consist of a porous network of crystals with high nano/micro porosity, and consequently, high SSAs (20-40 m^2/g) (**Fig. 1.14**). Since cementitious reactions involve mixing a powder with a liquid phase, this simple reaction offers a wide range of tunable parameters such as the particle size of the reactants, the liquid phase composition, the liquid to powder ratio (L/P) or the setting environment.

Specifically, the total porosity increases when the L/P ratio is increased due to the higher distance between particles (**Fig. 1.14**). Moreover, by changing the starting size of the α-TCP powder size from fine to coarse, a change in the morphology of the precipitated nanocrystals from needles to plates occurs with a consequent change in the SSA. The use of starting powders with larger particle sizes (coarse) makes them less reactive and this favors the formation of a few nuclei leading to the precipitation of a lower number of larger crystals (plates) (**Fig. 1.14**).[268]

A) Setting reaction

$3\alpha\text{-}Ca_3(PO_4)_2 + H_2O \rightarrow Ca_9(HPO_4)(PO_4)_5OH$

α-TCP → CDHA

B) Liquid to powder ratio

Low L/P — Low inter-aggregate distance

High L/P — High inter-aggregate distance

C) Particle size

Fine Particles — Needle-like crystals

Coarse Particles — Plate-like crystals
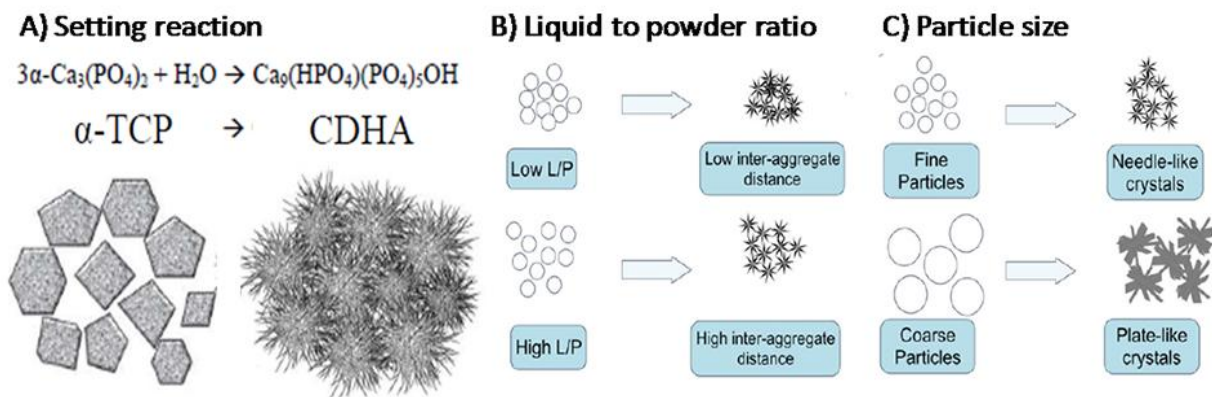
Figure 1.14. (A) Hydrolysis reaction of α-TCP to CDHA. **(B)** By changing the initial L/P ratio the total porosity can be modified. **(C)** By changing the starting α-TCP powder size from fine to coarse, a change in the morphology of the precipitated nanocrystals from needles to plates occurred, adapted.[268]

The nanoporosity (pores > 0.1 μm) of CDHA is ascribed to the voids generated within the precipitated entangled nanocrystals while the microporosity (1-10 μm) is assigned to the voids formed between crystal aggregates (**Fig. 1.15**). Moreover, in addition to the intrinsiccally porous nature of this biomimetic CaPs with pores in the nano- and micrometric ranges, another property that can be modulated is the macroporosity. Recently, our group has optimized the 3D-microextrusion technology,[269,270] as well as the foaming method[271,272] to make them compatible with the low-temperature biomimetic routes. This allowed fabricating scaffolds with different macropore geometries and dimensions in a controlled way, while preserving the specific

nanostructure typical of biomimetic ceramics and hence, high SSAs. The multiscale porosity levels achievable with these biomimetic CaPs are depicted in **Fig. 1.15**.
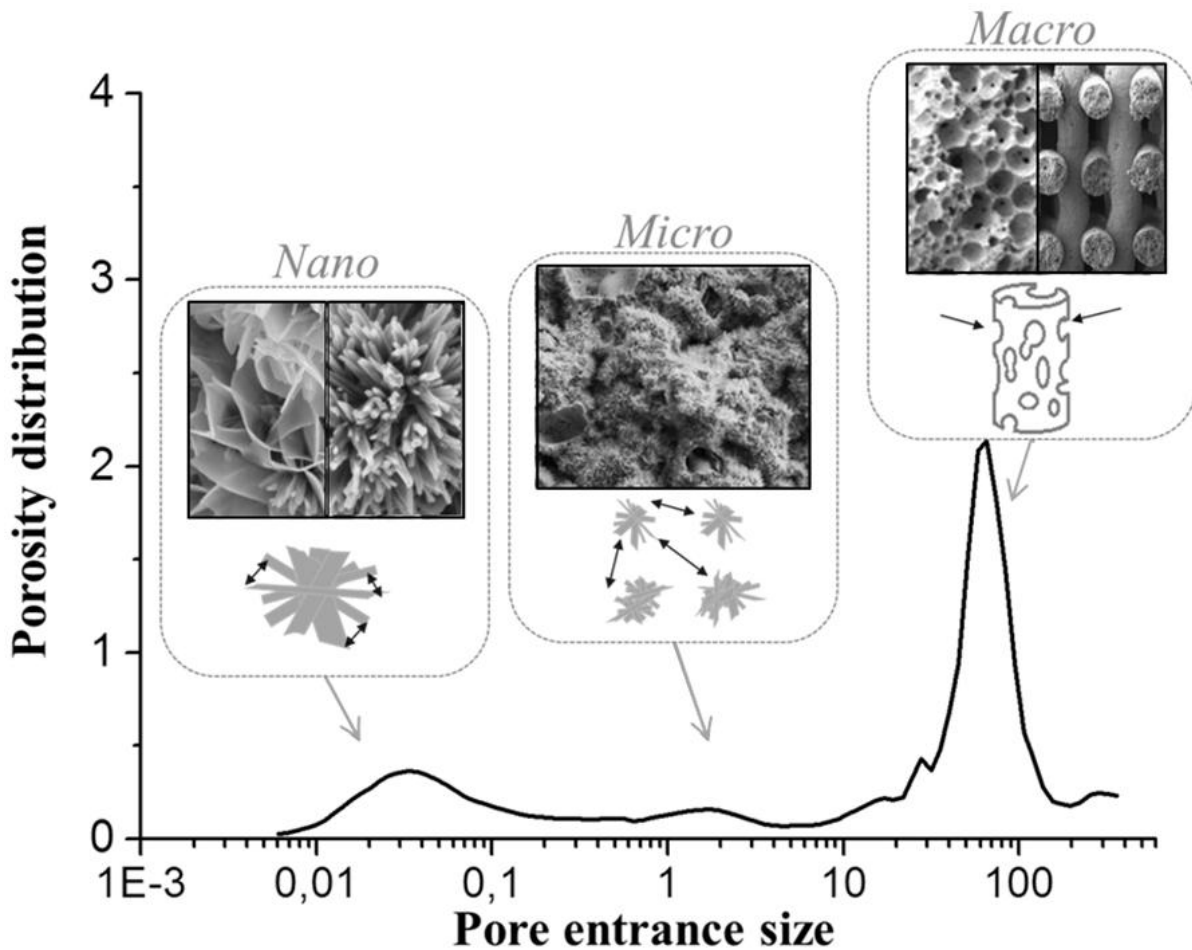
Figure 1.15. Pore entrance size distribution associated to the nano-, micro- and macrostructure in CDHA scaffolds. Nanoporosity: voids generated within the precipitated entangled plate/needle-like nanocrystals due to setting reaction. Microporosity: voids formed between crystal aggregates due to L/P ratio. Macroporosity: macropores generated due to foaming and 3D-microextrusion processes, adapted.[273]

Moreover, in order to further mimic biological apatite, CDHA can be synthesized incorporating ionic substitutions present in bone, such as carbonate, magnesium or strontium.[268]

The biomimetic chemical composition and nanostructured morphology of these low temperature CaPs in conjunction with their associated high SSAs are expected to stimulate protein adsorption, osteoclastic resorption, ionic dissolution and osteogenic differentiation of MSCs, as summarized in **Fig. 1.16**. Therefore, we hypothesize that this novel family of biomimetic CaPs will present superior biological properties compared with sintered CaP ceramics.

Although nowadays it is possible to produce almost any type of CaP in almost any shape, *in vivo* studies proving the superior biological behavior of CaP phases obtained at body temperature are still missing.[4]
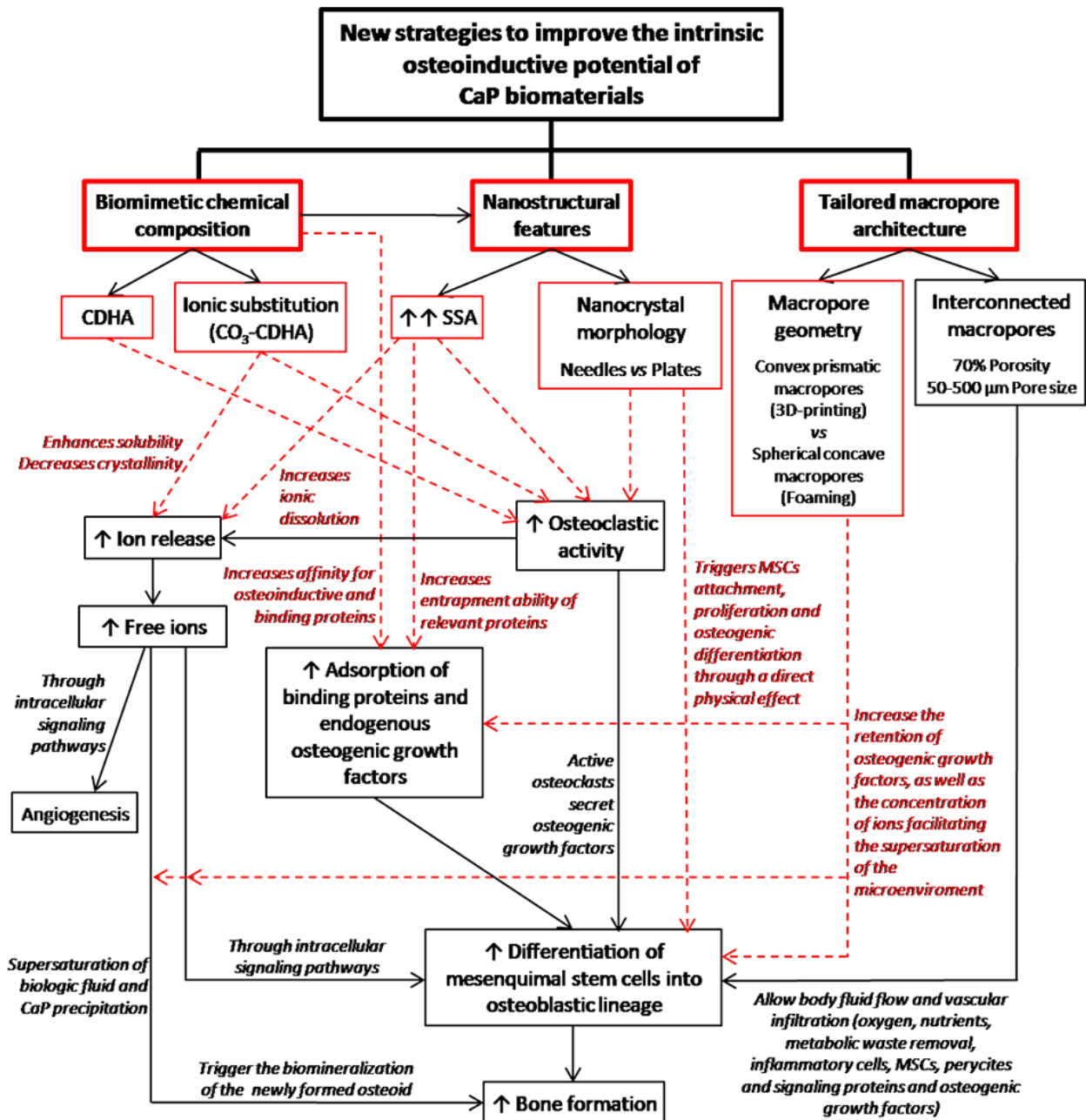
Figure 1.16. Schematic diagram summarizing the new strategies (red frames) proposed in the present thesis in order to enhance the intrinsic osteoinductive potential of CaP biomaterials and the hypothesized associated mechanisms (red arrows and text) and the expected consequences.

1.8 References

[1]   Chai YC, Carlier A, Bolander J, Roberts SJ, Geris L, Schrooten J, Van Oosterwyck H, Luyten FP. Current views on calcium phosphate osteogenicity and the translation into effective bone regeneration strategies. Acta Biomater 2012;8:3876-87.

[2]   Habibovic P. Strategic Directions in Osteoinduction and Biomimetics. Tissue Eng Part A 2017;23:1295-96.

[3]   Giannoudis PV, Dinopoulos H, Tsiridis E. Bone substitutes: an update. Injury 2005;36:20-7.

[4]   Habraken W, Habibovic P, Epple M, Bohner M. Calcium phosphates in biomedical applications: materials for the future? Mater Today 2016;19:69-87.

[5]   Habibovic P, de Groot K. Osteoinductive biomaterials-properties and relevance in bone repair. J Tissue Eng Regen Med 2007;1:25-32.

[6]   Patterson J, Martino MM, Hubbell JA. Biomimetic materials in tissue engineering. Mater Today 2010;13:14-22.

[7]   Bayliss L, Mahoney DJ, Monk P. Normal bone physiology, remodelling and its hormonal regulation. Surgery (Oxford) 2012;30:47-53.

[8]   Florencio-Silva R, Sasso GR, Sasso-Cerri E, Simões MJ, Cerri PS. Biology of Bone Tissue: Structure, Function, and Factors That Influence Bone Cells. Biomed Res Int 2015;2015:421746.

[9]   LeGeros RZ. Properties of osteoconductive biomaterials: calcium phosphates. Clin Orthop Relat Res 2002;395:81-98.

[10]   Wopenka B, Pasteris JD. A mineralogical perspective on the apatite in bone. Mater Sci Eng C 2005;25:131-43.

[11]   Termine JD, Eanes ED, Greenfield DJ, Nylen MU, Harper RA. Hydrazine-deproteinated bone mineral. Physical and chemical properties. Calcif Tissue Res 1973;12:73-90.

[12]   Bigi A, Cojazzi G, Panzavolta S, Ripamonti A, Roveri N, Romanello M, Noris Suarez K, Moro L. Chemical and structural characterization of the mineral phase from cortical and trabecular bone. J Inorg Biochem 1997;68:45-51.

[13]   Rey C, Renugopalakrishnan V, Collins B, Glimcher MJ. Fourier transform infrared spectroscopic study of the carbonate ions in bone mineral during aging. Calcif Tissue Int 1991;49:251-258.

[14]   Vallet-Regi M. Calcium phosphates as substitution of bone tissues. Prog Solid State Chem 2004:32:1-31.

[15]   Reznikov N, Shahar R, Weiner S. Bone hierarchical structure in three dimensions. Acta Biomater. 2014;10:3815-26.

[16]   Hohenester E, Engel J. Domain structure and organisation in extracellular matrix proteins. Matrix Biol 2002;21:115-28.

[17]   Theocharis AD, Skandalis SS, Gialeli C, Karamanos NK. Extracellular matrix structure. Adv Drug Deliv Rev 2016;97:4-27.

[18]   Weiner S, Wagner HD. The material bone: Structure-mechanical function relations. Annu Rev Mater Sci 1998;28:271-98.

[19]   Rho JY, Kuhn-Spearing L, Zioupos P, Mechanical properties and the hierarchical structure of bone. Med Eng Phys 1998;20:92-102.

[20]   Wegst UGK, Bai H, Saiz E, Tomsia AP, Ritchie RO, Ortiz C, Boyce M. Bioinspired structural materials. Nat Mater 2015;14:23-36.

[21]   Athanasiou KA, Zhu C, Lanctot DR, Agrawal CM, Wang X. Fundamentals of biomechanics in tissue engineering of bone. Tissue eng 2000;6:361-81.

[22]   Goldstein SA. The mechanical properties of trabecular bone: dependence on anatomic location and function. J Biomech 1987;20:1055-61.

[23]   Keaveny TM, Morgan EF, Niebur GL, Yeh OC. Biomechanics of trabecular bone. Annu Rev Biomed Eng 2001;3:307-33.

[24] Minns RJ, Atkinson A, Steven FS. The role of calcium in the mechanical behaviour of bone. Phys Med Biol 1983;28:1057-66.

[25] Clarke B. Normal bone anatomy and physiology. Clin J Am Soc Nephrol 2008;3:S131-9.

[26] LeGeros RZ. Calcium phosphate-based osteoinductive materials. Chem Rev 2008;108:4742-53.

[27] Bilezikian J, Raisz L, Martin T. Principles of bone biology. Third edition. Amsterdam: Elsevier/Academic Press;2008.

[28] Rahman MS, Akhtar N, Jamil HM, Banik RS, Asaduzzaman SM. TGF-β/BMP signaling and other molecular events: regulation of osteoblastogenesis and bone formation. Bone Res 2015;3:15005.

[29] Matic I, Matthews BG, Wang X, Dyment NA, Worthley DL, Rowe DW, Grcevic D, Kalajzic I. Quiescent Bone Lining Cells Are a Major Source of Osteoblasts During Adulthood. Stem Cells 2016;34:2930-42.

[30] Arboleya L, Castañeda S. Osteoimmunology: the study of the relationship between the immune system and bone tissue. Reumatol Clin 2013;9:303-15.

[31] Udagawa N, Takahashi N, Akatsu T, Tanaka H, Sasaki T, Nishihara T, Koga T, Martin TJ, Suda T. Origin of osteoclasts: mature monocytes and macrophages are capable of differentiating into osteoclasts under a suitable microenvironment prepared by bone marrow-derived stromal cells. Proc Natl Acad Sci USA 1990;87:7260-64.

[32] Little N, Rogers B, Flannery M. Bone formation, remodelling and healing. Surgery (Oxford) 2011;29:141-5.

[33] Carreira AC, Lojudice FH, Halcsik E, Navarro RD, Sogayar MC, Granjeiro JM. Bone morphogenetic proteins: facts, challenges, and future perspectives. J Dent Res 2014;93:335-45.

[34] Mackie EJ, Ahmed YA, Tatarczuch L, Chen KS, Mirams M. Endochondral ossification: How cartilage is converted into bone in the developing skeleton. Int J Biochem Cell Biol 2008;40:46-62.

[35] Raggatt LJ, Partridge NC. Cellular and molecular mechanisms of bone remodeling. J Biol Chem 2010;285: 25103-8.

[36] Sims NA, Martin TJ. Coupling the activities of bone formation and resorption: a multitude of signals within the basic multicellular unit. Bonekey Rep 2014;3:481.

[37] Garg AK. Implant dentistry: a practical approach. Second edition. Mosby: Elsevier;2009.

[38] Boyle WJ, Simonet WS, Lacey DL. Osteoclast differentiation and activation. Nature 2003;423:337-42.

[39] Teitelbaum SL. Bone Resorption by Osteoclasts, Science 2000;289:1504-8.

[40] Väänänen HK, Zhao H, Mulari M, Halleen JM. The cell biology of osteoclast function. J Cell Sci 2000;113:377-81.

[41] Dvorak MM, Riccardi D. Ca^{2+} as an extracellular signal in bone. Cell Calcium 2004;35:249-55.

[42] Zayzafoon M. Calcium/calmodulin signaling controls osteoblast growth and differentiation. J Cell Biochem 2006;97:56-70.

[43] Beck Jr GR. Inorganic phosphate as a signaling molecule in osteoblast differentiation. J Cell Biochem 2003;90:234-43.

[44] Orimo H. The mechanism of mineralization and the role of alkaline phosphatase in health and disease. J Nihon Med Sch 2010;77:4-12.

[45] Roberts S, Narisawa S, Harmey D, Millan JL, Farquharson C. Functional involvement of PHOSPHO1 in matrix vesicle-mediated skeletal mineralization. J Bone Miner Res 2007;22:617-27.

[46] Meyer U, Meyer T, Vosshans J, Joos U. Decreased expression of osteocalcin and osteonectin in relation to high strains and decreased mineralization in mandibular distraction osteogenesis. J Craniomaxillofac Surg 1999;27:222-7.

[47] Roach HI. Why does bone matrix contain non-collagenous proteins? The possible roles of osteocalcin, osteonectin, osteopontin and bone sialoprotein in bone mineralisation and resorption. Cell Biol Int 1994;18:617-28.

[48] Rawadi G, Vayssiere B, Dunn F, Baron R, Roman-Roman S. BMP-2 controls alkaline phosphatase expression and osteoblast mineralization by a Wnt autocrine loop. J Bone Miner Res 2003;18:1842-53.

[49] Suzuki A, Ghayor C, Guicheux J, Magne D, Quillard S, Kakita A, Ono Y, Miura Y, Oiso Y, Itoh M, Caverzasio J. Enhanced expression of the inorganic phosphate transporter Pit-1 is involved in BMP-2- induced matrix mineralization in osteoblast-like cells. J Bone Miner Res 2006;21:674-83.

[50] Suda T, Takahashi N, Udagawa N, Jimi E, Gillespie MT, Martin TJ. Modulation of osteoclast differentiation and function by the new members of the tumor necrosis factor receptor and ligand families. Endocr Rev 1999;20:345-57.

[51] Garimella R, Tague SE, Zhang J, Belibi F, Nahar N, Sun BH, Insogna K, Wang J, Anderson HC. Expression and synthesis of bone morphogenetic proteins by osteoclasts: a possible path to anabolic bone remodeling. J Histochem Cytochem 2008;56:569-77.

[52] Pederson L, Ruan M, Westendorf JJ, Khosla S, Oursler MJ. Regulation of bone formation by osteoclasts involves Wnt/BMP signaling and the chemokine sphingosine-1-phosphate. Proc Natl Acad Sci USA 2008;105:20764-69.

[53] Kreja L, Brenner RE, Tautzenberger A, Liedert A, Friemert B, Ehrnthaller C, Huber-Lang M, Ignatius A. Non-resorbing osteoclasts induce migration and osteogenic differentiation of mesenchymal stem cells. J Cell Biochem 2010;109:347-55.

[54] Takeshita S, Fumoto T, Matsuoka K, Park K, Aburatani H, Kato S, Ito M, Ikeda K. Osteoclast-secreted CTHRC1 in the coupling of bone resorption to formation. J Clin Invest 2013;123:3914-24.

[55] Hadjidakis DJ, Androulakis II. Bone remodeling. Ann N Y Acad Sci 2006;1092:385-96.

[56] Marsell R, Einhorn TA. The biology of fracture healing. Injury 2011;42:551-5.

[57] Rahn BA. Bone healing: histologic and physiologic concepts. In: Fackelman, GE, ed. Bone in clinical orthopedics. Second edition. Stuttgart: Thieme;2002.

[58] Gerstenfeld LC, Alkhiary YM, Krall EA, Nicholls FH, Stapleton SN, Fitch JL, Bauer M, Kayal R, Graves DT, Jepsen KJ, Einhorn TA. Three-dimensional reconstruction of fracture callus morphogenesis. J Histochem Cytochem 2006;54:1215-28.

[59] Ai-Aql ZS, Alagl AS, Graves DT, Gerstenfeld LC, Einhorn TA. Molecular mechanisms controlling bone formation during fracture healing and distraction osteogenesis. Journal of Dental Research 2008;87:107-18.

[60] Ronnstrand L, Heldin CH. Mechanisms of platelet-derived growth factor-induced chemotaxis. Int J Cancer 2001;9:757-62.

[61] Alvarez RH, Kantarjian HM, Cortes JE. Biology of platelet-derived growth factor and its involvement in disease. Mayo Clin Proc 2006;8:1241-57.

[62] Kaigler D, Avila G, Wisner-Lynch L, Nevins ML, Nevins M, Rasperini G, Lynch SE, Giannobile WV. Platelet-derived growth factor applications in periodontal and peri-implant bone regeneration. Expert Opin Biol Ther 2011;1:375-85.

[63] Mittal M, Siddiqui MR, Tran K, Reddy SP, Malik AB. Reactive oxygen species in inflammation and tissue injury. Antioxid Redox Signal 2014;20:1126-67.

[64] Mantovani A, Biswas SK, Galdiero MR, Sica A, Locati M. Macrophage plasticity and polarization in tissue repair and remodelling. J Pathol 2013;229:176-85.

[65] Mosser DM, Edwards JP. Exploring the full spectrum of macrophage activation. Nat Rev Immunol 2008;8:958-69.

[66] Chen Z, Klein T, Murray RZ, Crawford R, Chang J, Wu C, Xiao Y. Osteoimmunomodulation for the development of advanced bone biomaterials. Mater Today 2016;19:304-21.

[67] Takayanagi H. Osteoimmunology: shared mechanisms and crosstalk between the immune and bone systems. Nat Rev Immunol 2007;7:292-304.

[68] Chen Z, Wu C, Gu W, Klein T, Crawford R, Xiao Y. Osteogenic differentiation of bone marrow MSCs by β-tricalcium phosphate stimulating macrophages via BMP2 signalling pathway. Biomaterials 2014;35:1507-18.

[69] Gerstenfeld LC, Cullinane DM, Barnes GL, Graves DT, Einhorn TA. Fracture healing as a post-natal developmental process: molecular, spatial, and temporal aspects of its regulation. J Cell Biochem 2003;88:873-84.

[70] Chen Y, Alman BA. Wnt pathway, an essential role in bone regeneration. J Cell Biochem 2009;106:353-62.

[71] Goret-Nicaise M, Dhem A. Comparison of calcium content of different tissues present in the human mandible. Acta Anal 1995;124:167-72.

[72] Franch J, Garcia F, Camon J, Manzanares MC. Backscattered Electron Imaging of the Calcified Tissues Present in Bone Healing. VCOT 1998;11:105-11.

[73] Diaz-Flores L, Gutierrez R, Lopez-Alonso A, Gonzalez R, Varela H. Pericytes as a supplementary source of osteoblasts in periosteal osteogenesis. Clin Orthop Relat Res 1992;275:280-6.

[74] Collett GD, Canfield AE. Angiogenesis and pericytes in the initiation of ectopic calcification. Circ Res 2005;96:930-38.

[75] Granero-Moltó F, Weis JA, Miga MI, Landis B, Myers TJ, O'Rear L, Longobardi L, Jansen ED, Mortlock DP, Spagnoli A. Regenerative effects of transplanted mesenchymal stem cells in fracture healing. Stem Cells 2009;27:1887-98.

[76] Kitaori T, Ito H, Schwarz EM, Tsutsumi R, Yoshitomi H, Oishi S, Nakano M, Fujii N, Nagasawa T, Nakamura T. Stromal cell-derived factor 1/CXCR4 signaling is critical for the recruitment of mesenchymal stem cells to the fracture site during skeletal repair in a mouse model. Arthritis Rheum 2009;60:813-23.

[77] Méndez-Ferrer S, Michurina TV, Ferraro F, Mazloom AR, Macarthur BD, Lira SA, Scadden DT, Ma'ayan A, Enikolopov GN, Frenette PS. Mesenchymal and haematopoietic stem cells form a unique bone marrow niche. Nature 2010;466:829-34.

[78] Sundelacruz S, Kaplan DL. Stem cell‑and scaffold‑based tissue engineering approaches to osteochondral regenerative medicine. Semin Cell Dev Biol 2009;20:646-55.

[79] Forostyak S, Jendelova P, Sykova E. The role of mesenchymal stromal cells in spinal cord injury, regenerative medicine and possible clinical applications. Biochimie 2013;95:2257-70.

[80] Cho TJ, Gerstenfeld LC, Einhorn TA. Differential temporal expression of members of the transforming growth factor beta superfamily during murine fracture healing. J Bone Miner Res 2002;17:513-20.

[81] Marsell R, Einhorn TA. The role of endogenous bone morphogenetic proteins in normal skeletal repair. Injury 2009;40:S4-7.

[82] Tsuji K, Bandyopadhyay A, Harfe BD, Cox K, Kakar S, Gerstenfeld L, Einhorn T, Tabin CJ, Rosen V. BMP2 activity, although dispensable for bone formation, is required for the initiation of fracture healing. Nat Genet. 2006;38:1424-9.

[83] Dimitriou R, Jones E, McGonagle D, Giannoudis PV. Bone regeneration: current concepts and future directions. BMC Med 2011;9:66.

[84] Daculsi G, Fellah BH, Miramond T, Durand M. Osteoconduction, Osteogenicity, Osteoinduction, what are the fundamental properties for a smart bone substitutes. IRBM 2013;34:346-8.

[85] Ensrud KE. Epidemiology of fracture risk with advancing age. J Gerontol A Biol Sci Med Sci 2013;68:1236-42.

[86] Miron RJ, Zhang YF. Osteoinduction: a review of old concepts with new standards. J Dent Res 2012;91:736-44.

[87] Brown KL, Cruess RL. Bone and cartilage transplantationin orthopaedic surgery. A review. J Bone Joint Surg Am 1982;64:270-9.

[88] Lane JM, Tomin E, Bostrom MP. Biosynthetic bone grafting. Clin Orthop 1999;367:S107-17.

[89] Urist MR. Bone: formation by autoinduction. Science 1965;150:893-9.

[90] Younger EM, Chapman MW. Morbidity at bone graft donor sites. J Orthop Trauma 1989;3:92-5.

[91] Goulet JA, Senunas LE, DeSilva GL, Greenfield ML. Autogenous iliac crest bone graft: Complications and functional assessment. Clinical Orthopaedics & Related Research 1997;339:76-81.

[92] Delloye C, Cornu O, Druez V, Barbier O. Bone allografts: what they can offer and what they cannot. J Bone Joint Surge 2007;89:574-80.

[93] Lichte P, Pape HC, Pufe T, Kobbe P, Fischer H. Scaffolds for bone healing: Concepts, materials and evidence. Injury 2011;42:569-73.

[94] Friedenstein AY. Induction of bone tissue by transitional epithelium. Clin Orthop Relat Res 1968;59:21-37.

[95] Albrektsson T, Johansson C. Osteoinduction, osteoconduction and osseointegration. Eur Spine J 2001;10:S96-101.

[96] Barradas AM, Yuan H, van Blitterswijk CA, Habibovic P. Osteoinductive biomaterials: current knowledge of properties, experimental models and biological mechanisms. Eur Cell Mater 2011;21:407-29.

[97] Huggins C. The formation of bone under the influence of epithelium of the urinary tract. Arch Surg 1931;22:377-408.

[98]   Levander G. On the formation of new bone in bone transplantation. Acta Chir Scand 1934;74:425-6.

[99]   Bertelsen A. Experimental investigations into post-foetal osteogenesis. Acta Orthop Scand 1944;15:139-81.

[100] Urist MR, McLean FC. Osteogenetic potency and new-bone formation by induction in transplants to the anterior chamber of the eye. J Bone Joint Surg Am 1952;34A:443-76.

[101] Urist MR, Grant TT, Lindholm TS, Mirra JM, Hirano H, Finerman GA. Induction of new-bone formation in the host bed by human bone-tumour transplants in athymic nude mice. J Bone Joint Surg Am 1979;61:1207-16.

[102] Urist MR, Strates BS. Bone morphogenetic protein. J Dent Res 1971;50:1392-406.

[103] Urist MR, Huo YK, Brownell AG, Hohl WM, Buyske J, Lietze A, Tempst P, Hunkapiller M, DeLange RJ. Purification of bovine bone morphogenetic protein by hydroxyapatite chromatography. Proc Natl Acad Sci U S A 1984;81:371-5.

[104] Wozney JM, Rosen V, Celeste AJ, Mitsock LM, Whitters MJ, Kriz RW, Hewick RM, Wang EA. Novel regulators of bone formation: molecular clones and activities. Science. 1988;242:1528-34.

[105] Kang Q, Sun MH, Cheng H, Peng Y, Montag AG, Deyrup AT, Jiang W, Luu HH, Luo J, Szatkowski JP, Vanichakarn P, Park JY, Li Y, Haydon RC, He TC. Characterization of the distinct orthotopic bone-forming activity of 14 BMPs using recombinant adenovirus-mediated gene delivery. Gene Ther 2004;11:1312-20.

[106] Bialy IE, Jiskoot W, Nejadnik MR. Formulation, Delivery and Stability of Bone Morphogenetic Proteins for Effective Bone Regeneration. Pharm Res 2017;34:1152-70.

[107] Langer R, Vacanti JP. Tissue engineering. Science 1993;260:920-6.

[108] Bessa PC, Casal M, Reis RL. Bone morphogenetic proteins in tissue engineering: the road from the laboratory to the clinic, part I (basic concepts). J Tissue Eng Regen Med. 2008;2:1-13.

[109] Calori GM, Donati D, Di Bella C, Tagliabue L. Bone morphogenetic proteins and tissue engineering: future directions. Injury 2009;40:S67-76.

[110] Reddi AH. Morphogenesis and tissue engineering of bone and cartilage: Inductive signals, stem cells and biomimetic biomaterials. Tissue Eng 2000;6:351-9.

[111] Garrison KR, Donell S, Ryder J, Shemilt I, Mugford M, Harvey I, Song F. Clinical effectiveness and cost-effectiveness of bone morphogenetic proteins in the non-healing of fractures and spinal fusion: a systematic review. Health Technol Assess 2007;11:1-150.

[112] Ferretti C, Ripamonti U, Tsiridis E, Kerawala CJ, Mantalaris A, Heliotis M. Osteoinduction: translating preclinical promise into clinical reality. Br J Oral Maxillofac Surg 2010;48:536-9.

[113] Carragee EJ, Ghanayem AJ, Weiner BK, Rothman DJ, Bono CM. A challenge to integrity in spine publications: years of living dangerously with the promotion of bone growth factors. Spine J 2011;11:463-8.

[114] Tannoury CA, An HS. Complications with the use of bone morphogenetic protein 2 (BMP-2) in spine surgery. Spine J 2014;14:552-9.

[115] Faundez A, Tournier C, Garcia M, Aunoble S, Le Huec JC. Bone morphogenetic protein use in spine surgery-complications and outcomes: a systematic review. Int Orthop 2016;40:1309-19.

[116] Ripamonti U, Roden LC, Ferretti C, Klar RM. Biomimetic matrices self-initiating the induction of bone formation. J Craniofac Surg 2011;22:1859-70.

[117] Roh JS, Yeung CA, Field JS, McClellan RT. Allogeneic morphogenetic protein vs recombinant human bone morphogenetic protein-2 in lumbar interbody fusion procedures: a radiographic and economic analysis. J Orthop Surg Res 2013;8:49.

[118] Janicki P, Schmidmaier G. What should be the characteristics of the ideal bone graft substitute? Combining scaffolds with growth factors and/or stem cells. Injury 2011;42:S77-81.

[119] Gautschi OP, Frey SP, Zellweger R. Bone morphogenetic proteins in clinical applications. ANZ J Surg 2007;77:626-31.

[120] Friedenstein AJ, Chailakhjan RK, Lalykina KS. The development of fibroblast colonies in monolayer cultures of guinea-pig bone marrow and spleen cells. Cell Tissue Kinet 1970;3:393-403.

[121] Caplan AI. Mesenchymal stem cells. J Orthop Res 1991;9:641-50.

[122] Phinney DG, Prockop DJ. Concise review: mesenchymal stem/multipotent stromal cells: the state of transdifferentiation and modes of tissue repair-current views. Stem Cells 2007;25:2896-902.

[123] Liu ZJ, Zhuge Y, Velazquez OC. Trafficking and differentiation of mesenchymal stem cells. J Cell Biochem 2009;106:984-91.

[124] Horwitz EM, Le Blanc K, Dominici M, Mueller I, Slaper-Cortenbach I, Marini FC, Deans RJ, Krause DS, Keating A. Clarification of the nomenclature for MSC: The International Society for Cellular Therapy position statement. Cytotherapy 2005;7:393-5.

[125] Le Blanc K. Mesenchymal stromal cells: tissue repair and immune modulation. Cytotherapy 2006;8:559-61.

[126] Crisan M, Yap S, Casteilla L, Chen CW, Corselli M, Park TS, Andriolo G, Sun B, Zheng B, Zhang L, Norotte C, Teng PN, Traas J, Schugar R, Deasy BM, Badylak S, Buhring HJ, Giacobino JP, Lazzari L, Huard J, Péault B. A perivascular origin for mesenchymal stem cells in multiple human organs. Cell Stem Cell 2008;3:301-13.

[127] Zannettino AC, Paton S, Arthur A, Khor F, Itescu S, Gimble JM, Gronthos S. Multipotential human adipose-derived stromal stem cells exhibit a perivascular phenotype in vitro and in vivo. J Cell Physiol 2008;214:413-21.

[128] Castillo-Cardiel G, López-Echaury AC, Saucedo-Ortiz JA, Fuentes-Orozco C, Michel-Espinoza LR, Irusteta-Jiménez L, Salazar-Parra M, González-Ojeda A. Bone regeneration in mandibular fractures after the application of autologous mesenchymal stem cells, a randomized clinical trial. Dent Traumatol 2017;33:38-44.

[129] Prins HJ, Schulten EA, Ten Bruggenkate CM, Klein-Nulend J, Helder MN. Bone regeneration using the freshly isolated autologous stromal vascular fraction of adipose tissue in combination with calcium phosphate ceramics. Stem Cells Transl Med 2016;5:1362-74.

[130] Chen FM, Gao LN, Tian BM, Zhang XY, Zhang YJ, Dong GY, Lu H, Chu Q, Xu J, Yu Y, Wu RX, Yin Y, Shi S, Jin Y. Treatment of periodontal intrabony defects using autologous periodontal ligament stem cells: a randomized clinical trial. Stem Cell Res Ther 2016;7:33.

[131] Rajan A, Eubanks E, Edwards S, Aronovich S, Travan S, Rudek I, Wang F, Lanis A, Kaigler D. Optimized cell survival and seeding efficiency for craniofacial tissue engineering using clinical stem cell therapy. Stem Cells Transl Med 2014;3:1495-503.

[132] Wildburger A, Payer M, Jakse N, Strunk D, Etchard-Liechtenstein N, Sauerbier S. Impact of autogenous concentrated bone marrow aspirate on bone regeneration after sinus floor augmentation with a bovine bone substitute--a split-mouth pilot study. Clin Oral Implants Res 2014;251175-81.

[133] Marx RE, Harrell DB. Translational research: The CD34+ cell is crucial for large-volume bone regeneration from the milieu of bone marrow progenitor cells in craniomandibular reconstruction. Int J Oral Maxillofac Implants 2014;29:e201-9.

[134] Sauerbier S, Stricker A, Kuschnierz J, Bühler F, Oshima T, Xavier SP, Schmelzeisen R, Gutwald R. In vivo comparison of hard tissue regeneration with human mesenchymal stem cells processed with either the FICOLL method or the BMAC method. Tissue Eng Part C Methods 2010;16:215-23.

[135] Gan Y, Dai K, Zhang P, Tang T, Zhu Z, Lu J. The clinical use of enriched bone marrow stem cells combined with porous beta-tricalcium phosphate in posterior spinal fusion. Biomaterials 2008;29:3973-82.

[136] Marcacci M, Kon E, Moukhachev V, Lavroukov A, Kutepov S, Quarto R, Mastrogiacomo M, Cancedda R. Stem cells associated with macroporous bioceramics for long bone repair: 6- to 7-year outcome of a pilot clinical study. Tissue Eng 2007;13:947-55.

[137] Watson L, Elliman SJ, Coleman CM. From isolation to implantation: a concise review of mesenchymal stem cell therapy in bone fracture repair. Stem Cell Res Ther 2014;5:51.

[138] Sponer P, Kučera T, Diaz-Garcia D, Filip S. The role of mesenchymal stem cells in bone repair and regeneration. Eur J Orthop Surg Traumatol 2014;24:257-62.

[139] Singh J, Onimowo JO, Khan WS. Bone marrow derived stem cells in trauma and orthopaedics: a review of the current trend. Curr Stem Cell Res Ther 2015;10:37-42.

[140] Stanovici J, Le Nail LR, Brennan MA, Vidal L, Trichet V, Rosset P, Layrolle P. Bone regeneration strategies with bone marrow stromal cells in orthopaedic surgery. Curr Res Transl Med 2016;64:83-90.

[141] Brozek R, Kurpisz M, Koczorowski R. Application of stem cells in denstistry for bone regeneration. J Physiol Pharmacol 2018;69:23-33.

[142] Marques LF, Stessuk T, Camargo IC, Sabeh Junior N, dos Santos L, Ribeiro-Paes JT. Platelet-rich plasma (PRP): methodological aspects and clinical applications. Platelets 2015;26:101-13.

[143] Begam H, Nandi SK, Kundu B, Chanda A. Strategies for delivering bone morphogenetic protein for bone healing. Mater Sci Eng C Mater Biol Appl. 2017;70:856-69.

[144] Zhao J, Ohba S, Komiyama Y, Shinkai M, Chung UI, Nagamune T. Icariin: a potential osteoinductive compound for bone tissue engineering. Tissue Eng Part A 2010;16:233-43.

[145] Zhang X, Liu T, Huang Y, Wismeijer D, Liu Y. Icariin: does it have an osteoinductive potential for bone tissue engineering? Phytother Res 2014;28:498-509.

[146] Fukui T, Ii M, Shoji T, Matsumoto T, Mifune Y, Kawakami Y, Akimaru H, Kawamoto A, Kuroda T, Saito T, Tabata Y, Kuroda R, Kurosaka M, Asahara T. Therapeutic effect of local administration of low-dose simvastatin-conjugated gelatin hydrogel for fracture healing. J Bone Miner Res 2012;27:1118-31.

[147] Moshiri A, Sharifi AM, Oryan A. Role of Simvastatin on fracture healing and osteoporosis: a systematic review on in vivo investigations. Clin Exp Pharmacol Physiol 2016;43:659-84.

[148] Menendez MI, Clark DJ, Carlton M, Flanigan DC, Jia G, Sammet S, Weisbrode SE, Knopp MV, Bertone AL. Direct delayed human adenoviral BMP-2 or BMP-6 gene therapy for bone and cartilage regeneration in a pony osteochondral model. Osteoarthritis Cartilage 2011;19:1066-75.

[149] Wilson CG, Martın-Saavedra FM, Vilaboa N, Franceschi RT. Advanced BMP gene therapies for temporal and spatial control of bone regeneration. J Dent Res 2013;9:409-17.

[150] Parikh SN. Gene therapy: principles and clinical applications in orthopedics. Orthopedics 2004;27:294-303.

[151] Elangovan S, D'Mello SR, Hong L, Ross RD, Allamargot C, Dawson DV, Stanford CM, Johnson GK, Sumner DR, Salem AK. The enhancement of bone regeneration by gene activated matrix encoding for platelet derived growth factor. Biomaterials 2014;35:737-47.

[152] Franceschi RT. Biological approaches to bone regeneration by gene therapy. J Dent Res 2005;84:1093-103.

[153] Nixon AJ, Goodrich LR, Scimeca MS, Witte TH, Schnabel LV, Watts AE, Robbins PD. Gene therapy in musculoskeletal repair. Ann N Y Acad Sci 2007;1117:310-27.

[154] Selye H, Lemire Y, Bajusz E. Induction of bone, cartilage and hemopoietic tissue by subcutaneously implanted tissue diaphragms. Wilhelm Roux Arch Entwickl Mech Org 1960;151:572-585.

[155] Winter GD, Simpson BJ. Heterotopic bone formed in a synthetic sponge in the skin of young pigs. Nature 1969;223:88-90.

[156] Yuan H, de Bruijn JD, Zhang X, van Blitterswijk CA, de Groot K. Osteoinduction by porous alumina ceramic. European Conference on Biomaterials 2001, London, UK.

[157] Yuan H, de Bruijn JD, Zhang X, van Blitterswijk CA, de Groot K. Bone induction by porous glass ceramic made from Bioglass (45S5). J Biomed Mater Res 2001;58:270-6.

[158] Fujibayashi S, Neo M, Kim HM, Kokubo T, Nakamura T. Osteoinduction of porous bioactive titanium metal. Biomaterials 2004;25: 443-50.

[159] Takemoto M, Fujibayashi S, Matsushita T, Suzuki J, Kokubo T, Nakamura T. Osteoinductive ability of porous titanium implants following three types of surface treatment. Proc 51st Ann Meet Orthopaed Res Soc 2005,Washington DC, USA.

[160] Barrère F, van der Valk CM, Dalmeijer RA, Meijer G, van Blitterswijk CA, de Groot K, Layrolle P. Osteogenecity of octacalcium phosphate coatings applied on porous metal implants. J Biomed Mater Res A 2003;66:779-88.

[161] Li J, Habibovic P, Yuan H, van den Doel M, Wilson CE, de Wijn JR, van Blitterswijk CA, de Groot K. Biological performance in goats of a porous titanium alloy biphasic calcium phosphate composite. Biomaterials 2007;28:4209-18.

[162] Hasegawa S, Neo M, Tamura J, Fujibayashi S, Takemoto M, Shikinami Y, Okazaki K, Nakamura T. In vivo evaluation of a porous hydroxyapatite/poly-DLlactide composite for bone tissue engineering. J Biomed Mater Res A 2007;81:930-938.

[163] Barbieri D, Renard AJ, de Bruijn JD, Yuan H. Heterotopic bone formation by nano-apatite containing poly(D,L-lactide) composites. Eur Cell Mater 2010;19:252-61.

[164] de Groot J. Carriers that concentrate native bone morphogenetic protein in vivo. Tissue Eng 1998;4:337-41.

[165] Cola C, Almeida M, Li D, Romeo F, Mehta JL. Regulatory role of endothelium in the expression of genes affecting arterial calcification. Biochem Biophys Res Commun 2004;320:424-7.

[166] Sorescu GP, Song H, Tressel SL, Hwang J, Dikalov S, Smith DA, Boyd NL, Platt MO, Lassegue B, Griendling KK, Jo H . Bone morphogenic protein 4 produced in endothelial cells by oscillatory shear stress induces monocyte adhesion by stimulating reactive oxygen species production from a Nox1-based NADPH oxidase. Circ Res 2004;95:773-9.

[167] Le Nihouannen D, Saffarzadeh A, Gauthier O, Moreau F, Pilet P, Spaethe R, Layrolle P, Daculsi G. Bone tissue formation in sheep muscles induced by a biphasic calcium phosphate ceramic and fibrin glue composite. J Mater Sci Mater Med 2008;19:667-75.

[168] Ripamonti U, Crooks J, Khoali L, Roden L. The induction of bone formation by coral-derived calcium carbonate/hydroxyapatite constructs. Biomaterials 2009;30:1428-39.

[169] Galván-Chacón VP, Habibovic P. Deconvoluting the Bioactivity of Calcium Phosphate-Based Bone Graft Substitutes: Strategies to Understand the Role of Individual Material Properties. Adv Healthc Mater 2017;6:1601478.

[170] Albee H, Morrison SJ. Studies in bone growth: triple calcium phosphate as a stimulus to osteogenesis. Ann Surg 1920;71:32-9.

[171] Hofmann GO, Kirschner MH, Wangemann T, Falk C, Mempel W, Hammer C. Infections and immunological hazards of allogeneic bone transplantation. Arch Orthop Trauma Surg 1995;114:159-66.

[172] Wenz B, Oesch B, Horst M. Analysis of the risk of transmitting bovine spongiform encephalopathy through bone grafts derived from bovine bone. Biomaterials 2001;22:1599-606.

[173] Garrido CA, Lobo SE, Turibio FM, Legeros RZ. Biphasic calcium phosphate bioceramics for orthopaedic reconstructions: clinical outcomes. Int J Biomater 2011;2011:129727.

[174] Russell TA, Leighton RK. Comparison of autogenous bone graft and endothermic calcium phosphate cement for defect augmentation in tibial plateau fractures. A multicenter, prospective, randomized study. J Bone Joint Surg Am 2008;90:2057-61.

[175] Yuan H, Fernandes H, Habibovic P, de Boer J, Barradas AMC, de Ruiter A, Walsh WR, van Blitterswijk C, de Bruijn JD. Osteoinductive ceramics as a synthetic alternative to autologous bone grafting. Proc Natl Acad Sci USA 2010;107:13614-19.

[176] Yamasaki H. Heterotopic bone formation around porous hydroxyapatite ceramics in the subcutis of dogs. Japan J Oral Biol 1990;32:190-2.

[177] Ripamonti U. The morphogenesis of bone in replicas of porous hydroxyapatite obtained from conversion of calcium carbonate exoskeletons of coral. J Bone Joint Surg Am 1991;73:692-703.

[178] Yamasaki H, Sakai H. Osteogenic Response to Porous Hydroxyapatite Ceramics under the Skin of Dogs. Biomaterials 1992;13:308-12.

[179] Van Eeden SP, Ripamonti U. Bone differentiation in porous hydroxyapatite in baboons is regulated by the geometry of the substratum: Implications for reconstructive craniofacial surgery. Plast Reconstr Surg 1994;93:959-66.

[180] Klein C, de Groot K, Chen W, Li Y, Zhang X. Osseous substance formation induced in porous calcium phosphate ceramics in soft tissues. Biomaterials 1994;15:31-4.

[181] Pollick S, Shors EC, Holmes RE, Kraut RA. Bone formation and implant degradation of coralline porous ceramics placed in bone and ectopic sites. J Oral Maxillofac Surg 1995;53:915-23.

[182] Magan A, Ripamonti U. Geometry of porous hydroxyapatite implants influences osteogenesis in baboons (Papio ursinus). J Craniofac Surg 1996;7:71-8.

[183] Ripamonti U. Osteoinduction in porous hydroxyapatite implanted in heterotopic sites of different animal models. Biomaterials 1996;17:31-5.

[184] Yuan H, Kurashina K, de Bruijn JD, Li Y, de Groot K, Zhang X. A preliminary study on osteoinduction of two kinds of calcium phosphate ceramics. Biomaterials 1999;20:1799-806.

[185] Yuan H, van Blitterswijk CA, de Groot K, de Bruijn JD. Crossspecies comparison of ectopic bone formation in biphasic calcium phosphate (BCP) and hydroxyapatite (HA) scaffolds. Tissue Eng 2006;12:1607-15.

[186] Habibovic P, Kruyt MC, Juhl MV, Clyens S, Martinetti R, Dolcini L, Theilgaard N, van Blitterswijk CA. Comparative in vivo study of six hydroxyapatite-based bone graft substitutes. J Orthop Res 2008;26:1363-70.

[187] Wang H, Zhi W, Lu X, Li X, Duan K, Duan R, Mu Y, Weng J. Comparative studies on ectopic bone formation in porous hydroxyapatite scaffolds with complementary pore structures. Acta Biomater 2013;9:8413-21.

[188] Lee HR, Kim HJ, Ko JS, Choi YS, Ahn MW, Kim S, Do SH. Comparative characteristics of porous bioceramics for an osteogenic response in vitro and in vivo. PLoS One 2013;8:e84272.

[189] Wang L, Zhang B, Bao C, Habibovic P, Hu J, Zhang X. Ectopic osteoid and bone formation by three calcium-phosphate ceramics in rats, rabbits and dogs. PLoS One 2014;9:e107044.

[190] Wang J, Chen Y, Zhu X, Yuan T, Tan Y, Fan Y, Zhang X. Effect of phase composition on protein adsorption and osteoinduction of porous calcium phosphate ceramics in mice. J Biomed Mater Res A 2014;102:4234-43.

[191] Yuan H, de Bruijn JD, Li Y, Feng Z, Yang K, de Groot K, Zhang X. Bone formation induced by calcium phosphate ceramics in soft tissue of dogs: A comparative study between Alpha-TCP and Beta-TCP. J Mater Sci Mater Med 2001;12:7-13.

[192] Yuan H, Yang Z, de Bruijn JD, de Groot K, Zhang X. Material-dependent bone induction by calcium phosphate ceramics: A 2.5-year study in dog. Biomaterials 2001;22:2617-23.

[193] Kondo N, Ogose A, Tokunaga K, Umezu H, Arai K, Kudo N, Hoshino M, Inoue H, Irie H, Kuroda K, Mera H, Endo N. Osteoinduction with highly purified beta-tricalcium phosphate in dog dorsal muscles and the proliferation of osteoclasts before heterotopic bone formation. Biomaterials 2006;27:4419-27.

[194] Davison NL, Yuan H, de Bruijn JD, Barrere-de Groot F. In vivo performance of microstructured calcium phosphate formulated in novel water-free carriers. Acta Biomater 2012;8:2759-69.

[195] Zhang J, Luo X, Barbieri D, Barradas AM, de Bruijn JD, van Blitterswijk CA, Yuan H. The size of surface microstructures as an osteogenic factor in calcium phosphate ceramics. Acta Biomater 2014;10:3254-63.

[196] Davison NL, Luo X, Schoenmaker T, Everts V, Yuan H, Barrère-de Groot F, de Bruijn JD. Submicron-scale surface architecture of tricalcium phosphate directs osteogenesis in vitro and in vivo. Eur Cell Mater 2014;27:281-97.

[197] Yang Z, Yuan H, Tong W, Zou P, Chen W, Zhang X. Osteogenesis in extraskeletally implanted porous calcium phosphate ceramics: Variability among different kinds of animals. Biomaterials 1996;17:2131-7.

[198] Kurashina K, Kurita H, Wu Q, Ohtsuka A, Kobayashi H. Ectopic osteogenesis with biphasic ceramics of hydroxyapatite and tricalcium phosphate in rabbits. Biomaterials 2002;23:407-12.

[199] Habibovic P, Yuan H, van der Valk CM, Meijer G, van Blitterswijk CA, de Groot K. 3D microenvironment as essential element for osteoinduction by biomaterials. Biomaterials 2005;26:3565-75.

[200] Le Nihouannen D, Daculsi G, Saffarzadeh A, Gauthier O, Delplace S, Pilet P, Layrolle P. Ectopic bone formation by microporous calcium phosphate ceramic particles in sheep muscles. Bone 2005;36:1086-93.

[201] Habibovic P, Sees TM, van den Doel MA, van Blitterswijk CA, de Groot K. Osteoinduction by biomaterials-physicochemical and structural influences. J Biomed Mater Res A 2006;77:747-62.

[202] Davison NL, Su J, Yuan H, van den Beucken JJ, de Bruijn JD, Barrère-de Groot F. Influence of surface microstructure and chemistry on osteoinduction and osteoclastogenesis by biphasic calcium phosphate discs. Eur Cell Mater 2015;29:314-29.

[203] Habibovic P, Juhl MV, Clyens S, Martinetti R, Dolcini L, Theilgaard N, van Blitterswijk CA. Comparison of two carbonated apatite ceramics in vivo. Acta Biomater 2010;6:2219-26.

[204] Habibovic P, Gbureck U, Doillon CJ, Bassett DC, van Blitterswijk CA, Barralet JE. Osteoconduction and osteoinduction of low-temperature 3D printed bioceramic implants. Biomaterials 2008;29:944-53.

[205] Yuan H, Li Y, de Bruijn JD, de Groot K, Zhang X. Tissue responses of calcium phosphate cement: a study in dogs. Biomaterials 2000;21:1283-90.

[206] Toth J, Lynch K, Hackbarth D. Ceramic-induced osteogenesis following subcutaneous implantation of calcium phosphates. Bioceramics 1993;6:9-13.

[207] Puleo DA, Nanci A. Understanding and controlling the bone implant interface. Biomaterials 1999;20:2311-21.

[208] Sawyer AA, Hennessy KM, Bellis SL. Regulation of mesenchymal stem cell attachment and spreading on hydroxyapatite by RGD peptides and adsorbed serum proteins. Biomaterials 2005;26:1467-75.

[209] Ripamonti U, Klar RM, Renton LF, Ferretti C. Synergistic induction of bone formation by hOP-1, hTGF-beta3 and inhibition by zoledronate in macroporous coral-derived hydroxyapatites. Biomaterials 2010;31:6400-10.

[210] Davison NL, Gamblin A-L, Layrolle P, Yuan H, de Bruijn JD, Barrère-de Groot F. Liposomal clodronate inhibition of osteoclastogenesis and osteoinduction by submicrostructured beta-tricalcium phosphate. Biomaterials 2014;35:5088-97.

[211] Akiyama N, Takemoto M, Fujibayashi S, Neo M, Hirano M, Nakamura T. Difference between dogs and rats with regard to osteoclast-like cells in calcium-deficient hydroxyapatite-induced osteoinduction. J Biomed Mater Res A 2011;96:402-12.

[212] Guihard P, Danger Y, Brounais B, David E, Brion R, Delecrin J, Richards CD, Chevalier S, Rédini F, Heymann D, Gascan H, Blanchard F. Induction of osteogenesis in mesenchymal stem cells by activated monocytes/macrophages depends on oncostatin M signaling. Stem Cells 2012;30:762-72.

[213] Barradas AM, Fernandes HA, Groen N, Chai YC, Schrooten J, van de Peppel J, van Leeuwen JP, van Blitterswijk CA, de Boer J. A calcium-induced signaling cascade leading

to osteogenic differentiation of human bone marrow-derived mesenchymal stromal cells. Biomaterials 2012;33:3205-15.

[214] Habibovic P, Bassett DC, Doillon CJ, Gerard C, McKee MD, Barralet JE. Collagen biomineralization in vivo by sustained release of inorganic phosphate ions. Adv Mater 2010;22:1858-62.

[215] Klar RM, Duarte R, Dix-Peek T, Dickens C, Ferretti C, Ripamonti U. Calcium ions and osteoclastogenesis initiate the induction of bone formation by coral-derived macroporous constructs. J Cell Mol Med 2013;17:1444-57.

[216] Dorozhkin SV. Bioceramics of calcium orthophosphates. Biomaterials 2010;31:1465-85.

[217] Kohn EC, Alessandro R, Spoonster J, Wersto RP, Liotta LA. Angiogenesis: role of calcium-mediated signal transduction. Proc Natl Acad Sci USA. 1995;92:1307-11.

[218] Wu Q, Shao H, Darwin ED, Li J, Li J, Yang B, Webster KA, Yu H. Extracellular calcium increases CXCR4 expression on bone marrow-derived cells and enhances pro-angiogenesis therapy. J Cell Mol Med 2009;13:3764-73.

[219] Boanini E, Gazzano M, Bigi A. Ionic substitutions in calcium phosphates synthesized at low temperature. Acta Biomater 2010;6:1882-94.

[220] LeGeros RZ. Effect of Carbonate on the Lattice Parameters of Apatite. Nature 1965;206:403-04.

[221] Legeros RZ, Trautz OR, Legeros JP, Klein E, Shirra WP. Apatite crystallites: effects of carbonate on morphology. Science 1967;155:1409-11.

[222] Okazaki M, Moriwaki Y, Aoba T, Doi Y, Takahashi J. Solubility behavior of CO3Apatites in relation to crystallinity. Caries Res 1981;15:477-83.

[223] Nelson DG, Featherstone JD, Duncan JF, Cutress TW. Paracrystalline disorder of biological and synthetic carbonate-substituted apatites. J Dent Res 1982;61:1274-81.

[224] Gibson IR, Bonfield W. Novel synthesis and characterization of an AB-type carbonate substituted hydroxyapatite. J Biomed Mater Res 2001;59:697-708.

[225] Doi Y, Shibutani T, Moriwaki Y, Kajimoto T, Iwayama Y. Sintered carbonate apatites as bioresorbable bone substitutes. J Biomed Mater Res 1998;39:603-10.

[226] Doi Y, Iwanaga K, Shibutani T, Moriwaki Y, Iwayama Y. Osteoclastic responses to various calcium phosphates in cell cultures. J Biomed Mater Res 1999;47:424-33.

[227] Spence G, Patel N, Brooks R, Bonfield W, Rushton N. Osteoclastogenesis on hydroxyapatite ceramics: the effect of carbonate substitution. J Biomed Mater Res A 2010;92:1292-300.

[228] Landi E, Celotti G, Logroscino G, Tampieri A. Carbonated hydroxyapatite as bone substitute. J Eur Ceram Soc 2003;23:2931-7.

[229] Hasegawa M, Doi Y, Uchida A. Cell-mediated bioresorption of sintered carbonate apatite in rabbits. J Bone Joint Surg Br 2003;85:142-7.

[230] Porter A, Patel N, Brooks R, Best S, Rushton N, Bonfield W. Effect of carbonate substitution on the ultrastructural characteristics of hydroxyapatite implants. J Mater Sci Mat Med 2005;16:899-907.

[231] Ripamonti U, Richter PW, Thomas ME. Self-inducing shape memory geometric cues embedded within smart hydroxyapatite-based biomimetic matrices. Plast Reconstr Surg 2007;120:1796-807.

[232] Hollister SJ. Porous scaffold design for tissue engineering. Nat Mater 2005;4:518-24.

[233] Karageorgiou V, Kaplan D. Porosity of 3D biomaterial scaffolds and osteogenesis. Biomaterials 2005;26:5474-91.

[234] Rumpler M, Woesz A, Dunlop JW, van Dongen JT, Fratzl P. The effect of geometry on three-dimensional tissue growth. J R Soc Interface 2008;5:1173-80.

[235] Bidan CM, Kommareddy KP, Rumpler M, Kollmannsberger P, Bréchet YJ, Fratzl P, et al. How linear tension converts to curvature: geometric control of bone tissue growth. PLoS One 2012;7:e36336.

[236] Bidan CM, Kommareddy KP, Rumpler M, Kollmannsberger P, Fratzl P, Dunlop JW. Geometry as a factor for tissue growth: towards shape optimization of tissue engineering scaffolds. Adv Healthc Mater 2013;2:186-94.

[237] Ginebra MP, Espanol M, Montufar EB, Perez RA, Mestres G. New processing approaches in calcium phosphate cements and their applications in regenerative medicine. Acta Biomater 2010;6:2863-73.

[238] O'Brien CM, Holmes B, Faucett S, Zhang LG. Three-dimensional printing of nanomaterial scaffolds for complex tissue regeneration. Tissue Eng Part B Rev 2015;21:103-14.

[239] Fielding G, Bose S. SiO2 and ZnO dopants in three-dimensionally printed tricalcium phosphate bone tissue engineering scaffolds enhance osteogenesis and angiogenesis in vivo. Acta Biomater 2013;9:9137-48.

[240] Franco J, Hunger P, Launey ME, Tomsia AP, Saiz E. Direct write assembly of calcium phosphate scaffolds using a water-based hydrogel. Acta Biomater 2010;6:218-28.

[241] Vorndran E, Klarner M, Klammert U, Grover LM, Patel S, Barralet JE, Gbureck U. 3D powder printing of β-tricalcium phosphate ceramics using different strategies. Adv Eng Mater 2008;10:B67-71.

[242] Chan O, Coathup MJ, Nesbitt A, Ho CY, Hing KA, Buckland T, Campion C, Blunn GW. The effects of microporosity on osteoinduction of calcium phosphate bone graft substitute biomaterials. Acta Biomater 2012;8:2788-94.

[243] Li X, van Blitterswijk CA, Feng Q, Cui F, Watari F. The effect of calcium phosphate microstructure on bone-related cells in vitro. Biomaterials 2008;29:3306-16.

[244] de Bruijn J, Shankar K, Yuan H, Habibovic P. Osteoinduction and its evaluation. In: Kokubo T, ed. Bioceramics and Their Clinical Applications. First edition. Cambridge: Woodhead Publishing Ltd;2008. pp 199-219.

[245] Dalby MJ, Gadegaard N, Tare R, Andar A, Riehle MO, Herzyk P, Wilkinson CD, Oreffo RO. The control of human mesenchymal cell differentiation using nanoscale symmetry and disorder. Nat Mater 2007;6:997-1003.

[246] Li B, Chen XN, Guo B, Wang XL, Fan HS, Zhang XD. Fabrication and cellular biocompatibility of porous carbonated biphasic calcium phosphate ceramics with a nanostructure. Acta Biomater 2009;5:134-43.

[247] Hesaraki S, Nazarian H, Pourbaghi-Masouleh M, Borhan S. Comparative study of mesenchymal stem cells osteogenic differentiation on low-temperature biomineralized nanocrystalline carbonated hydroxyapatite and sintered hydroxyapatite. J Biomed Mater Res B Appl Biomater 2014;102:108-18.

[248] Hu J, Zhou Y, Huang L, Liu J, Lu H. Effect of nano-hydroxyapatite coating on the osteoinductivity of porous biphasic calcium phosphate ceramics. BMC Musculoskelet Disord 2014;15:114.

[249] Nagai H, Kobayashi-Fujioka M, Fujisawa K, Ohe G, Takamaru N, Hara K, Uchida D, Tamatani T, Ishikawa K, Miyamoto Y. Effects of low crystalline carbonate apatite on

proliferation and osteoblastic differentiation of human bone marrow cells. J Mater Sci Mater Med 2015;26:99.

[250] Danoux C, Pereira D, Döbelin N, Stähli C, Barralet J, van Blitterswijk C, Habibovic P. The Effects of Crystal Phase and Particle Morphology of Calcium Phosphates on Proliferation and Differentiation of Human Mesenchymal Stromal Cells. Adv Healthc Mater 2016;5:1775-85.

[251] Dobbenga S, Fratila-Apachitei LE, Zadpoor AA. Nanopattern-induced osteogenic differentiation of stem cells - A systematic review. Acta Biomater 2016;46:3-14.

[252] Sadowska JM, Guillem-Marti J, Montufar EB, Espanol M, Ginebra MP. Biomimetic Versus Sintered Calcium Phosphates: The in Vitro Behavior of Osteoblasts and Mesenchymal Stem Cells. Tissue Eng Part A 2017;23:1297-309.

[253] Kasten P, Luginbühl R, van Griensven M, Barkhausen T, Krettek C, Bohner M, Bosch U. Comparison of human bone marrow stromal cells seeded on calcium-deficient hydroxyapatite, beta-tricalcium phosphate and demineralized bone matrix. Biomaterials 2003;24:2593-603.

[254] Guo XY, Gough JE, Xiao P, Liu J, Shen ZJ. Fabrication of nanostructured hydroxyapatite and analysis of human osteoblastic cellular response. J Biomed Mater Res A 2007;82:1022-32.

[255] Scopelliti PE, Borgonovo A, Indrieri M, Giorgetti L, Bongiorno G, Carbone R, Podestà A, Milani P. The effect of surface nanometre-scale morphology on protein adsorption. Plos One 2010;5:e11862.

[256] Espanol M, Casals I, Lamtahri S, Valderas MT, Ginebra MP. Assessment of protein entrapment in hydroxyapatite scaffolds by size exclusion chromatography. Biointerphases 2012;7:37.

[257] Zhu XD, Zhang HJ, Li DX, Fan HS, Zhang XD. Study on the enhanced protein adsorption of microwave sintered hydroxyapatite nanoceramic particles: Role of microstructure. J Biomed Mater Res B: Appl Biomater 2012;100:516-23.

[258] Muschler GF, Raut VP, Patterson TE, Wenke JC, Hollinger JO. The design and use of animal models for translational research in bone tissue engineering and regenerative medicine. Tissue Eng Part B Rev 2010;16:123-45.

[259] Pearce AI, Richards RG, Milz S, Schneider E, Pearce SG. Animal models for implant biomaterial research in bone: a review. Eur Cell Mater 2007;13:1-10.

[260] An YH, Friedman RJ. Animal models of bone defect repair. In: An YH, Friedman RJ, eds. Animals Models in Orthopaedic Research. First edition. Boca Raton: CRC Press LLC;1998. pp 241-60.

[261] Aerssens J, Boonen S, Lowet G, Dequeker J. Interspecies differences in bone composition, density, and quality: potential implications for in vivo bone research. Endocrinology 1998;139:663-70.

[262] Wang X, Mabrey JD, Agrawal CM. An interspecies comparison of bone fracture properties. Biomed Mater Eng 1998;8:1-9.

[263] Barradas AM, Yuan H, van der Stok J, Le Quang B, Fernandes H, Chaterjea A, Hogenes MC, Shultz K, Donahue LR, van Blitterswijk C, de Boer J. The influence of genetic factors on the osteoinductive potential of calcium phosphate ceramics in mice. Biomaterials 2012;33:5696-705.

[264] Marusic A, Katavic V, Grcevic D, Lukic IK. Genetic variability of new bone induction in mice. Bone 1999;25:25-32.

[265] Geesink RGT, Hoefnagels NHM, Bulstra SK. Osteogenic activity of OP-1 bone morphogenetic protein (BMP-7) in a human fibular defect. J Bone Joint Surg (Br) 1999;81:710-18.

[266] Yuan H, van Blitterswijk CA, de Groot K, de Bruijn J D. A comparison of bone formation in biphasic calcium phosphate (BCP) and hydroxyapatite (HA) implanted in muscle and bone of dogs at different time periods. J Biomed Mater Res Part A 2006;78:139-47.

[267] Habibovic P, Yuan H, van den Doel M, Sees TM, van Blitterswijk CA, de Groot K. Relevance of osteoinductive biomaterials in critical-sized orthotopic defect. J Orthop Res 2006;24:867-76.

[268] Ginebra MP, Canal C, Espanol M, Pastorino D, Montufar EB. Calcium phosphate cements as drug delivery materials. Adv Drug Deliv Rev 2012;64:1090-110.

[269] Maazouz Y, Montufar EB, Guillem-Marti J, Fleps I, Öhman C, Persson C, Ginebra MP. Robocasting of biomimetic hydroxyapatite scaffolds using self-setting inks. J Mater Chem B 2014;2:5378-86.

[270] Maazouz Y, Montufar EB, Malbert J, Espanol M, Ginebra MP. Self-hardening and thermoresponsive alpha tricalcium phosphate/pluronic pastes. Acta Biomater 2017;49:563-74.

[271] Montufar EB, Traykova T, Gil C, Harr I, Almirall A, Aguirre A, Engel E, Planell JA, Ginebra MP. Foamed surfactant solution as a template for self-setting injectable hydroxyapatite scaffolds for bone regeneration. Acta Biomater 2010;6:876-85.

[272] Pastorino D, Canal C, Ginebra MP. Drug delivery from injectable calcium phosphate foams by tailoring the macroporosity-drug interaction. Acta Biomater 2015;12:250-9.

[273] Diez-Escudero A (2017). Tuning the biological performance of calcium phosphates through microstructural and chemical modifications. PhD Thesis. Doctoral Program of Material Science and Engineering. Universitat Politècnica de Catalunya. Barcelona. Spain.

Chapter 2

OSTEOINDUCTION BY FOAMED AND 3D-PRINTED CALCIUM PHOSPHATE SCAFFOLDS: EFFECT OF NANOSTRUCTURE AND PORE ARCHITECTURE

2.1 Introduction

Some biomaterials are able to instruct cells and by driving cell fate, they are able to modulate the regenerative potential of specific tissues. A good example is what has been called material-associated osteoinduction, i.e., the capacity of some biomaterials to induce the differentiation of MSCs into the osteoblastic lineage, even in absence of exogenously applied BMPs. This property, which was discovered in the early 1990s in CaPs,[1,2] is of paramount importance when designing synthetic bone grafts. Intrinsic osteoinduction can bestow the biomaterial with the capacity to regenerate bone even in compromised clinical situations, avoiding the detrimental side effects associated with the use of BMPs.[3,4] The relevance of this topic is linked to the high incidence of bone grafting procedures, around 2.2 million worldwide annually.[5] In this context, the development of synthetic bone substitutes with enhanced performance, which are able to outperform autologous bone grafts and to avoid their intrinsic drawbacks (e.g., limited availability, donor site pain and risk of infection or disease transmission)[6] is an urgent challenge.

Great attention has been paid in the last years to the parameters leading to biomaterial-associated osteoinduction. Some CaP ceramics have been found to exhibit an intrinsic osteoinductive capacity when implanted ectopically in several animal models.[7] This capacity is associated with a higher bone healing capacity when implanted orthotopically, compared with nonosteoinductive ceramics.[8] It has also been reported that osteoinductive ceramics perform similarly to both autologous bone grafts and rhBMP2-impregnated collagen sponges in repairing critical-size bone defects.[9] Although the mechanism underlying bone induction is still not fully understood, the textural properties of the material are believed to play a key role.[10-13] However, most studies on osteoinduction of CaPs have been performed with sintered ceramics, in which the high-temperature processing precludes the introduction of nanoporosity. Consequently, low SSAs are obtained, normally in the range of 0.2-2 m^2/g. This leaves the hypothesis about the role of textural properties without a complete verification and establishes the need to provide a full picture of the situation, by assessing the osteoinductive properties of CaP biomaterials with nanostructured features and higher SSA.

The recent biomimetic routes, based on the self-setting reaction of CPCs, have opened up new possibilities in this respect, because they allow the obtaining of nanostructured CaP scaffolds, with controlled micro- and nanoporosity, together with a tailored architecture.[14] As a result of the setting reaction, an entangled network of hydroxyapatite nanocrystals is obtained at physiological temperature. This does not simply mimic the composition and morphology of the bone mineral phase better than sintered CaP biomaterials, but it also generates a porous structure with specific nano- and microporosities, and consequently generates much higher SSAs than sintered ceramics.

One additional advantage of CPCs is their simplicity in processing, which makes them extremely versatile and compatible with many techniques. Nanostructured hydroxyapatite foams with open

interconnected macropores can be obtained by adding small amounts of a surfactant to the liquid phase of the CPC and applying mechanical stirring.[15,16] Moreover, biomimetic processing of hydroxyapatite is compatible with additive manufacturing strategies. Self-setting CaP inks have been designed[17] that allow the fabrication of nanostructured hydroxyapatite scaffolds with controlled pore architecture, using 3D-microextrusion techniques, also known as robocasting.[18]

Taking advantage of these technologies, scaffolds with diverse pore architectures can be obtained that preserve the specific textural properties typical of biomimetic ceramics. The possibility to tailor porosity at different levels, from the nano- to the macroscale, significantly extends the range of the textures analyzed so far and allows scientists to address more in-depth the effect of the nanostructure on the osteoinductive properties of CaPs. The aim of this study was to assess the relative importance of nanostructural features and scaffold architecture to the osteoinduction of CaP-based biomaterials in a canine ectopic model. Biomimetic CDHA scaffolds with different pore architectures were compared to two sintered CaP ceramics, i.e., BCP and β-TCP.

2.2 Materials and Methods

2.2.1 Calcium phosphate materials

2.2.1.1 *Synthesis of alpha-tricalcium phosphate*

Alpha-tricalcium phosphate (α-Ca$_3$(PO$_4$)$_2$) was the solid phase of the cement used for the fabrication of the scaffolds. Briefly, α-TCP was obtained by heating calcium hydrogen phosphate (CaHPO$_4$, Sigma-Aldrich, St. Louis, MO) and calcium carbonate (CaCO$_3$, Sigma-Aldrich, St. Louis, MO) at a 2:1 molar ratio for 15 h at 1400°C, followed by quenching in air. Subsequently, the powder was milled in an agate ball mill (Pulverisette 6, Fritsch GmbB, Markt Einersheim, Germany) with 10 balls (d = 30 mm) for 60 min at 450 rpm, followed by a second milling for 40 min at 500 rpm with 10 balls (d = 30 mm) and a third one for 60 min at 500 rpm with 100 balls (d = 10 mm), in order to attain a mean powder particle size of 2.8 μm.

2.2.1.2 *Preparation of foamed scaffolds*

To obtain the CDHA foams (CDHA-Foam), a solid phase consisting of 98 wt% α-TCP and 2 wt% precipitated hydroxyapatite (PHA, Merck KGaA, Darmstadt, Germany) was mixed with an aqueous solution of 1 wt% Polysorbate 80 (Tween 80, Sigma-Aldrich, St. Louis, MO) at a liquid to powder ratio of 0.65 mL/g. The mixture was foamed with a domestic food mixer for 30 s at 7000 rpm and then transferred to Teflon cylindrical molds (5 mm diameter and 10 mm height). After keeping the samples in 100% relative humidity for 8 h to ensure cohesion, they were immersed in deionized water at 37°C for 10 days, to allow for the hydrolysis reaction of α-TCP to CDHA to take place, according to the following reaction:

$$3 \ Ca_3(PO_4)_2 + H_2O \rightarrow Ca_9(PO_4)_5(HPO_4)OH$$
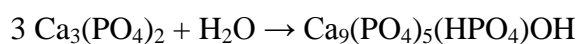
To obtain the biphasic HA/β-TCP foams (BCP-Foam), instead of immersing the foams in water at 37ºC, they were unmolded, immersed in a 1 wt% sodium bicarbonate solution (NaHCO$_3$, Sigma-Aldrich, St. Louis, MO) and autoclaved at 120ºC and 1 atm for 30 min. Subsequently, they were sintered at 1100°C for 9 h to obtain a BCP with a 80:20 HA:β-TCP ratio. Additional information on this protocol is provided in the Appendix (**Fig. A2.1**). The β-TCP foams (β-TCP-Foam) were obtained by sintering the CDHA foams at 1100°C for 9 h.

For the *in vitro* studies, discs (5 mm diameter x 0.3 mm height) of CDHA (CDHA-disc), β-TCP (β-TCP-disc) and BCP (BCP-disc) were prepared following the procedures described above for the foamed scaffolds, except for the foaming step, which was substituted with a mortar mixing for 1 min.

2.2.1.3 *Preparation of robocast scaffolds*

To prepare the CDHA self-setting ink, a 30 wt% aqueous solution of poloxamer 407 (P2443 - Pluronic F-127, Sigma-Aldrich, St. Louis, MO) was mixed with the α-TCP powder at a liquid to powder ratio of 0.65 g/g. A cylindrical CAD model of the scaffolds (5 mm diameter and 10 mm height) was designed (Solidworks 2014, Dassault Systèmes SolidWorks Corp., Waltham, MA) and converted to an STL 3D mesh, with a rectilinear pattern and an infill of 0.45. Nozzles with inner diameters of 450 and 250 μm were used for CDHA-Rob-450 and CDHA-Rob-250, respectively. To print the scaffolds, the self-setting ink was introduced immediately after mixing into the cartridge of the robocasting device (Pastecaster, BCN3D Technologies, Barcelona, Spain). The scaffolds were left overnight in an incubator at 100% relative humidity at 37ºC and subsequently immersed in deionized water at 37ºC for a 10 day hardening period.

2.2.1.4 *Materials characterization*

The scaffolds were characterized in terms of phase composition, microstructure, SSA and porosity. Phase characterization was performed by X-ray diffraction using a diffractometer (D8 Advance, Bruker, Billerica, MA) equipped with a Cu Kα anode operated at 40 kV and 40 mA. Data were collected in 0.02° steps over the 2θ range of 10°-80° with a counting time of 2 s per step. Phase identification was accomplished by comparing the experimental patterns to those of HA (JCPDS 09-0432), α-TCP (JCPDS 09-0348) and β-TCP (JCPDS 09-0169). Quantitative phase-composition analyses were carried out using DIFFRAC.EVA software, (Bruker, Billerica, MA). The morphology of the scaffolds was assessed by microcomputed tomography (micro-CT, SkyScan 1172, Bruker microCT, Kontich, Belgium) at a voltage of 90 kV and a current of 112 μA and with a Cu-Al filter. Images were acquired using an isotropic pixel size of 5 μm. Reconstruction of cross sections was done using software package NRecon (Bruker microCT, Kontich, Belgium). Calculations of macroporosity were performed with CTAn (Bruker microCT, Kontich, Belgium). The microstructure was characterized by scanning electron microscopy (Zeiss Neon40 EsBCrossBeam, Zeiss, Oberkochen, Germany). Prior to imaging, samples were coated with carbon to enhance conductivity. The SSA was determined by nitrogen adsorption using the Brunauer-Emmett-Teller (BET) method (ASAP 2020, Micrometrics Instrument Corp., Norcross, GA). Porosity and pore-entrance-size distribution were measured by mercury-intrusion porosimetry (MIP, AutoPore IV, Micrometrics Instrument Corp., Norcross, USA). All samples were dried at 100°C for 2 h prior to measurement.

2.2.2 In vivo study

2.2.2.1 *Animal model and intramuscular implantation*

The capacity of the scaffolds to form ectopic bone was evaluated in a standardized, intramuscular implantation canine model. Twelve adult beagle dogs (body weight 14-17 kg) were purchased from a professional stock breeder (Isoquimen S.L., Barcelona, Spain). All animal procedures were in compliance with the Guide for Care and Use of Laboratory Animals[19] and the European Community Guidelines (Directive 2010/63/EU) for the protection of animals used for scientific purposes.[20] Ethical approval for the procedures was obtained from the local ethic committee (CEAAH 2338). On reception, animals were randomly divided into two groups of six dogs each, corresponding to two different sacrificial times (6 weeks or 12 weeks). Afterward, the animals were acclimatized to their local environment for 2 weeks prior to surgery.

For the surgical procedure, dogs were preanesthetized using an intramuscular injection of medetomidine and methadone. Anesthesia was induced by intravenous injection of propofol and diazepam and maintained with inhaled isoflorane in an oxygen carrier. During surgery, the animals received an intravenous saline isotonic solution and intravenous injection of cefazolin. For the intramuscular implantation, animals were placed in sternal recumbency and the lumbar areas were shaved and scrubbed with a chlorhexidine gluconate solution for an aseptic preparation of the surgical field. Subsequently, one skin incision was performed on the lumbar region and fascia incisions were created in the paraspinal muscles bilaterally by scalpel. Using blunt dissection, intramuscular pockets were created in a cranio-caudal direction 4 cm lateral to the spinal axis. Each intramuscular pocket was filled with one of the above-mentioned cylindrical scaffolds (5 mm diameter x 10 mm height): CDHA-Foam, CDHA-Rob-450, CDHA-Rob-250, BCP-Foam or β-TCP-Foam. Implant position was assigned according to a rotatory allocation system using a block designed. Therefore, one construct of each material was implanted in each dog, resulting in five scaffolds implanted per animal, leaving a distance of 5 cm between implants. All scaffolds had been previously sterilized by Gamma irradiation at a dose of 25 kG. **Table 2.1** shows the list of implanted materials. Finally, muscular fasciae were closed with monofilament synthetic nonresorbable sutures for identification at harvest and subcutaneous tissue and skin incisions were closed layer by layer with monofilament, synthetic, absorbable sutures. Immediately after surgery, the animals received a prophylactic long-acting antibiotic (cefovecin) and pain relievers (methadone and meloxicam).

Table 2.1. Summary of implanted samples

Architecture	Composition	Codes	Intramuscular implantation	
			6 weeks	12 weeks
Foams	Calcium-deficient hydroxyapatite	CDHA-Foam	6	6
	80:20 Hydroxyapatite:β-TCP	BCP-Foam	6	6
	β-TCP	β-TCP-Foam	6	6
Robocast	Calcium-deficient hydroxyapatite	CDHA-Rob-450	6	6
	Calcium-deficient hydroxyapatite	CDHA-Rob-250	6	6

During the postoperative period, a nonsteroidal anti-inflammatory drug (NSAID) was given subcutaneously to the animals for 7 days to prevent pain and inflammation. The animals were euthanized at 6 and 12 weeks postimplantation, by an intravenous injection of an overdose of pentobarbital sodium. A pre-euthanasia sedation of medetomidine was used for animal welfare reasons.

2.2.2.2 *Sample harvest and histological processing*

Immediately after euthanasia, the samples were harvested with their surrounding muscular tissue and fixed in 4% neutral buffered formalin solution for 72 h. After fixation, they were dehydrated in an increasing series of ethanol solutions and embedded in four different graded mixtures of ethanol and methyl methacrylate resin (Technovit 7200, HeraeusKulzer GmbH, Hanau, Germany) under vacuum conditions. The specimens were subsequently photopolymerized with 2 h of white light and 4 h of ultraviolet light, resulting in blocks that were scanned by X-ray micro-CT. After micro-CT scanning, each block was divided transversally, perpendicular to the long axis of the implant, into two equal pieces. One piece was sectioned and polished (EXAKT Cutting and Grinding System, EXAKT Advanced Technologies GmbH, Norderstedt, Germany) prior to the sputtering of the surface with carbon to enhance conductivity for backscattered scanning electron microscopy analysis (BS-SEM). The other piece was sliced into 500 μm thick sections, followed by a subsequent thinning to 50 μm by grinding (Cutting and Grinding System, EXAKT Advanced Technologies GmbH, Norderstedt, Germany). The sections were then stained with Goldner-Masson trichrome and toluidine blue for histological observation using light microscopy.

2.2.2.3 *Histology and histomorphometry*

The micro-CT analysis (SkyScan 1172, Bruker microCT, Kontich, Belgium) of the tissue samples was performed using the same settings as those for the scaffold scanning described above. The 3D quantification of new bone formation and scaffold degradation was performed following a previously established protocol,[21] in which the BS-SEM images were used as a reference in the determination of the gray-scale intensity thresholds, which were used to differentiate bone and CaP biomaterial in the micro-CT images. The following parameters were quantified:

a) Percentage of newly formed bone within the available macropore space:

% newly formed bone = (bone volume / available macropore volume) * 100

b) Percentage of scaffold degradation, calculated by subtracting the remaining scaffold volume from the initial scaffold volume prior to implantation:

% scaffold degradation = [(initial scaffold volume – final scaffold volume) / initial scaffold volume] * 100

Moreover, the radius of each implanted scaffold was divided into five equal segments, which define five concentric volumes of interest (VOIs). The percentage of newly formed bone was calculated in each VOI to assess the distribution of the new ectopic bone formation.

The BS-SEM observations (Zeiss Neon40 EsBCrossBeam, Zeiss, Oberkochen, Germany) were made at 20 kV to assess the presence, localization and maturity of the newly formed bone tissue

and to assess the scaffold degradation based on its morphology and the different contrast levels. The number of samples that showed any bone formation per the total number of samples implanted (bone incidence rate) was recorded.

Stained histological sections were scanned using a light microscope (Nikon Eclipse E800, Nikon Corp.,Tokyo, Japan) fitted with a digital camera (ProgRes, Jenoptik AG, Jena, Germany) for a qualitative evaluation, which focused on fibrous tissue infiltration, the presence of bone cells (osteoblasts, osteocytes and osteoclasts), the grade of neovascularization and the grade of the peri-implant inflammatory reaction. Digital images were captured using an image analysis software (ProgRes CapturePro, Jenoptik AG, Jena, Germany).

2.2.3 In vitro study

2.2.3.1 *Cell culture*

To better understand the mechanisms leading to osteoinduction, rat mesenchymal stem cells (rMSCs) were cultured in direct contact with the different materials used in the *in vivo* study. rMSCs were isolated from tibias and femurs of Lewis rats and characterized by flow cytometry as described elsewhere.[22] Cells were expanded in Advanced Dulbecco's Modified Eagle Medium (AdvDMEM) supplemented with 10% fetal bovine serum (FBS), 20 mM4-(2-hydroxyethyl)piperazine-1-ethanesulfonic acid (HEPES) buffer, 2 mM L-glutamine (50 U/mL) and penicillin/streptomycin (50 µg/mL), all from Thermo Fisher Scientific Inc. (Waltham, MA). Cells at passages 3-4 were used in all experiments.

Discs were sterilized by immersion in 70% ethanol and rinsed three times with phosphate buffered saline (PBS, Gibco, Thermo Fisher Scientific Inc., Waltham, MA). Afterward, samples were placed in 24-well plates and incubated with 2.5 mL medium/well overnight.

2.2.3.2 *Cell differentiation: Real-time quantitative PCR*

Cells were seeded on the samples (300 cells/mm^2) and incubated for different time periods. The differentiation to osteoblastic phenotype was assessed by measuring gene expression of osteogenic markers (**Table 2.2**) by real-time quantitative polymerase chain reaction (RT-qPCR). Total RNA was extracted at 6 h and 1 and 3 days using an RNeasy Mini Kit (Qiagen GmbH, Hilden, Germany), according to the recommendations of the manufacturer. For OCN, a late osteogenic marker, RNA at 7 and 14 days was also monitored. Prior to RNA extraction, samples were transferred into new well plates and rinsed with PBS (Gibco, Thermo Fisher Scientific Inc., Waltham, MA). Total RNA was quantified by NanoDrop ND-1000 spectrophotometer (NanoDrop Products, Thermo Fisher Scientific Inc., Waltham, MA), and 120 µg were used for synthesis of complementary DNA (cDNA) using the QuantiTect Reverse Transcription Kit (Qiagen GmbH, Hilden, Germany). cDNA templates were amplified using specific primers (**Table 2.2**) in SYBR Green RT-qPCR analyses using the QuantiTect SYBR Green RT-PCR Kit (Qiagen GmbH, Hilden, Germany) in an RT-PCR StepOnePlus (Applied Biosystems, Thermo Fisher Scientific Inc., Waltham, MA). The specificity of primers was ensured by melt-curves analysis in all RT-qPCR runs. To verify the absence of contamination and genomic DNA, a no-RNA control and a no-RT-enzyme control were evaluated in parallel. The expression of the studied genes was normalized to expression of β-actin (a housekeeping gene), and relative fold

changes (FC) were related to tissue-culture polystyrene (TCPS) at 6 h of culture. The following formula was used: $FC = E_{target}^{\Delta Cq\ target\ (TCPS\ 6\ h\ -\ sample)} / E_{housekeeping}^{\Delta Cq\ housekeeping\ (TCPS\ 6\ h\ -\ sample)}$, where C_q is the median value of the quantification cycle of the triplicate of each sample, and E corresponds to the efficiency of amplification and is determined from the slope of the log-linear portion of the calibration curve, as $E=10^{(-1/slope)}$. The experiment was performed in two independent runs.

Table 2.2. Primers' sequences used for RT-qPCR

Gene	Gene symbol	Forward primer sequence (5' to 3')	Reverse primer sequence (5' to 3')
β-actin	ACTB	CCCGCGAGTACAACCTTCT	CGTCATCCATGGCGAACT
Bone morphogenetic protein-2	BMP-2	CCCCTATATGCTCGACCTGT	AAAGTTCCTCGATGGCTTCTT
Alkaline phosphatase	ALP	GCACAACATCAAGGACATCG	TCAGTTCTGTTCTTGGGGTACAT
Collagen I	Col I	CATGTTCAGCTTTGTGGACCT	GCAGCTGACTTCAGGGATGT
Osteonectin	ONN	GTTTGAAGAAGGTGCAGAGGA	GGTTCTGGCAGGGGTTTT
Osteopontin	OPN	CGGTGAAAGTGGCTGAGTTT	GGCTACAGCATCTGAGTGTTTG
Osteocalcin	OCN	ATAGACTCCGGCGCTACCTC	CCAGGGGATCTGGGTAGG

2.2.4 Statistical analysis

The histomorphometric and *in vitro* results are presented as mean values ± standard error. All analyzed data were normally distributed according to Anderson-Darling and Kolmogorov-Smirnov tests and showed homogeneity of variances according to Levenne's and Barralet's tests. Statistical comparisons among experimental groups were performed using One-way repeated measures ANOVA followed by Tukey's post hoc test in GraphPad Prism software (GraphPad Software Inc., La Jolla, CA). A pairwise comparison result of $p<0.05$ was considered statistically significant.

2.3 Results

2.3.1 Materials characterization

The textural properties of the different scaffolds, including total porosity, macroporosity and SSA are summarized in **Table 2.3**. The architecture of the foamed and 3D-printed scaffolds, as well as the microstructure of the different materials can be seen in the SEM images in **Fig. 2.1A** and the pore size distribution, measured by MIP, is shown in **Fig. 2.1B**. Similar microstructures were observed for CDHA-Foam, CDHA-Rob-450 and CDHA-Rob-250, with the typical entangled network of needle-like CDHA nanocrystals (**Fig. 2.1A**), which resulted in a high SSA, around 35 m^2/g (**Table 2.3**). As a consequence, the three CDHA groups presented nanosized pores (**Fig. 2.1B**). Whereas the robocast samples displayed a nanopore size distribution ranging from 0.006 to 0.1 µm, the CDHA-Foam group showed a wider and more continuous distribution, covering both the nano- and the microscale. In contrast, the two sintered ceramics (BCP-Foam and β-TCP-Foam) consisted of polyhedral crystals with smooth faces (**Fig. 2.1A**), displayed low SSA values (**Table 2.3**), had an absence of nanoporosity, and instead had micropores centered around 1 µm for the β-TCP-Foam group and at 1.2 µm for the BCP-Foam group.
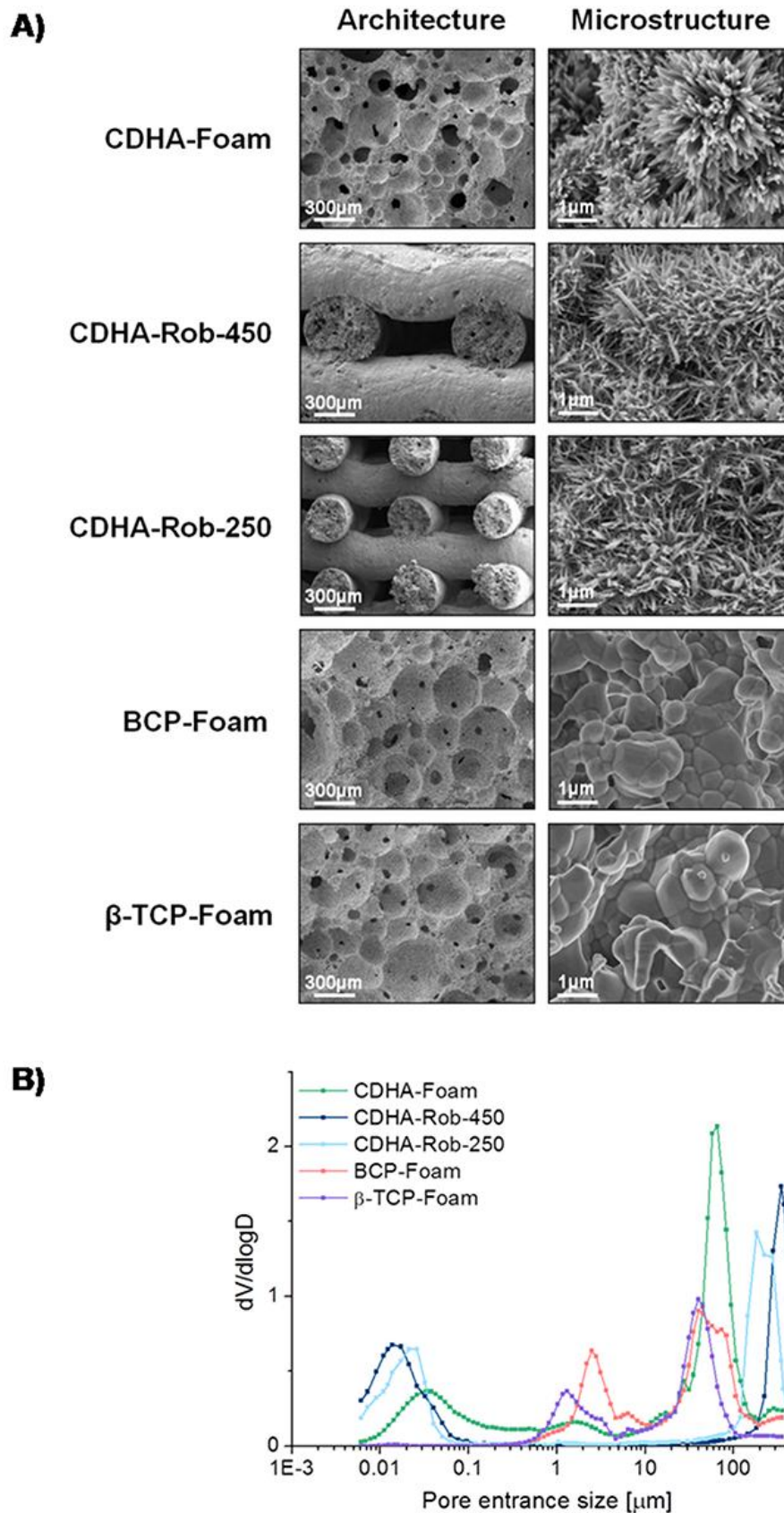
Figure 2.1. (A) Scanning electron micrographs of the five implanted materials: CDHA-Foam, BCP-Foam and β-TCP-Foam groups showed similar architecture, consisting of open and interconnected, spherical, concave macropores, whereas the robocast scaffolds presented open and interconnected, prismatic, convex macropores. The microstructure of the CDHA scaffolds consisted of the typical network of entangled, needle-like nanocrystals, whereas the sintered ceramics showed polyhedral smooth crystals. **(B)** Pore entrance size distribution of the five implanted materials as determined by MIP.

Table 2.3. Porosity and SSA of the different scaffolds

Materials	Porosity					SSA (m^2/g)
	% Total Porosity by MIP	% Macroporosity by MIP (>10 μm)	% Macroporosity by micro-CT	Macropore entrance size by MIP (μm)*	Macropore size by micro-CT (μm)*	
CDHA-Foam	76.5	49.5	52.3	70	227.0	38.49
CDHA-Rob-450	64.8	46.5	47.4	350	409.7	32.02
CDHA-Rob-250	65.4	48.7	54.1	200	288.7	32.35
BCP-Foam	71.8	47.2	47.4	50	214.8	0.42
β-TCP-Foam	64.6	43.2	48.9	40	232.0	0.46

*Whereas the value measured by MIP provided the average entrance size of the macropores, the value measured by micro-CT corresponds to the average pore size itself.

All scaffolds presented similar amounts of macroporosity and total porosity, as shown in **Table 2.3**, but different pore sizes and, more markedly, different pore entrance sizes (**Fig. 2.1**, **Table 2.3**), which were larger for the robocast scaffolds. Moreover, as observed in **Fig. 2.1A**, the foamed scaffolds presented very similar architecture of interconnected spherical macropores, irrespective of their biomimetic or sintered nature.

As shown by the X-ray diffraction (XRD) patterns (Appendix, **Fig. A2.2**), the CDHA-Foam and the CDHA-Rob scaffolds consisted of poorly crystalline apatitic phases, as indicated by the broad peaks, typical of biomimetic apatites. Small amounts of unreacted α-TCP were detected, and quantified to be 2 and 3% for CDHA-Foam and CDHA-Rob scaffolds, respectively. The sintered scaffolds exhibited sharper peaks, typical of highly crystalline materials. β-TCP-Foam scaffolds consisted of phase-pure β-TCP, and BCP-Foam consisted of a mixture of 82.7% HA and 17.3% β-TCP.

2.3.2 Intramuscular implantation

All surgeries were uneventful, all animals had normal recoveries after surgery, and their postoperative courses proceeded without any complications. No clinical evidence of inflammatory responses or adverse tissue reactions around implants were observed during the experimental period or at retrieval. Histology showed low-grade peri-implant inflammatory reactions at both time points for all scaffolds, which were surrounded by well-vascularized muscle tissue. A small number of inflammatory cells, mainly limphoplasmocitary cells, were found and no fibrous-capsule formation was observed, indicating the good biocompatibility of the different scaffolds. At 6 weeks, fibrous tissue infiltration with abundant neovascularization was observed within the interconnected macropores, both in the foamed and in the robocast scaffolds. Collagen fibers appeared to be oriented following the walls of the macropores (**Fig. 2.2**).

The results for new ectopic bone formation in the different scaffolds are summarized in **Fig. 2.3**. At 6 weeks, new bone was detected only in the CDHA-Foam group, in 4 out of 6 animals, while no signs of bone formation were found either in the sintered ceramic foams or in the biomimetic robocast scaffolds. In the CDHA-Foam group, although no statistically significant differences among the five concentric VOIs were noted, the ectopic bone was mainly found in the outer and middle regions (Appendix, **Fig. A2.3**). No ectopic bone was observed on the outside surfaces of the cylinders.
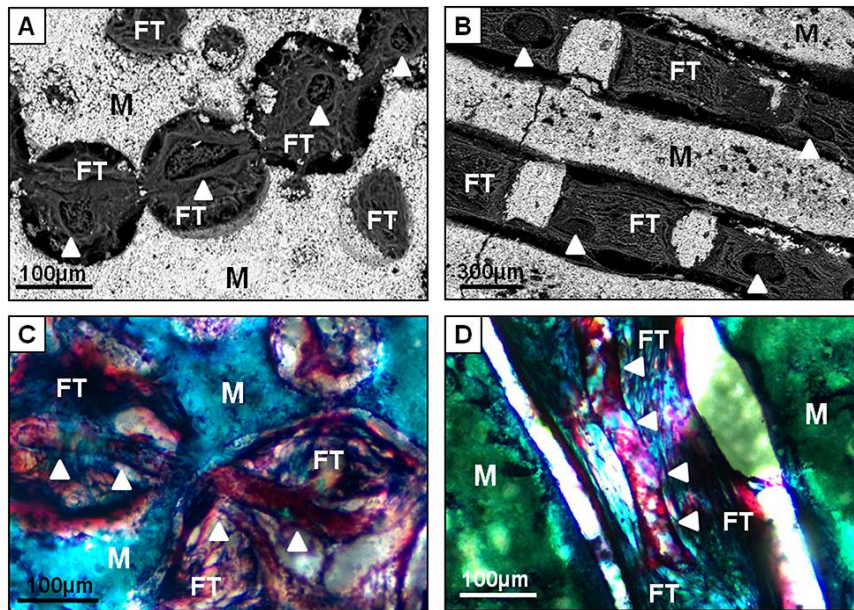
Figure 2.2. Backscattered scanning electron micrographs **(A,B)** and micrographs of undecalcified Goldner-Masson trichrome stained sections **(C,D)** of a representative foam scaffold **(A,C)** and of a robocast scaffold **(B,D)**, 6 weeks after implantation. All foams and robocast materials showed fibrous tissue infiltration and blood vessels (arrow heads) within the interconnected macropores at 6 weeks. M=Material, FT=Fibrous Tissue.
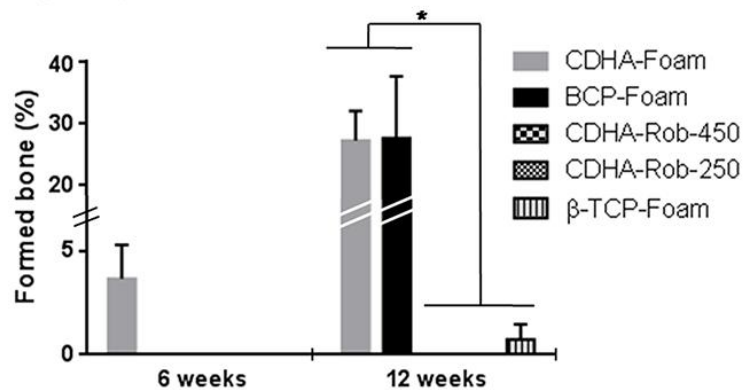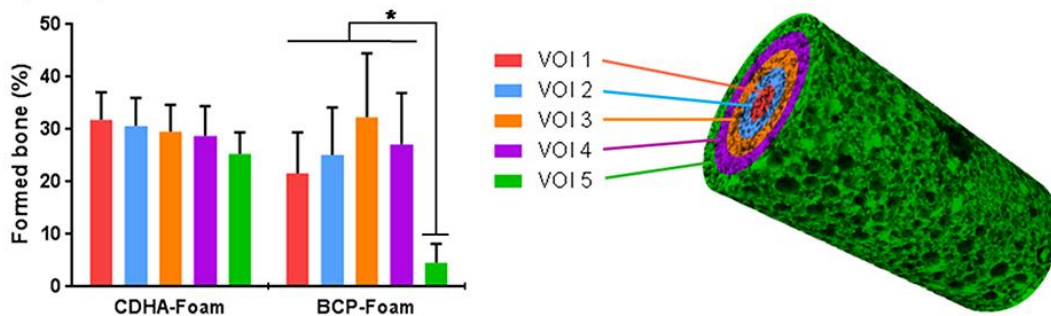
Figure 2.3. (A) Bone incidence 6 and 12 weeks after implantation. **(B)** Histomorphometrical results: percentage of newly formed bone within the available macropore spaces at 6 and 12 weeks postimplantation, as measured by μ-CT. The mean value for the CDHA-Rob-450 group is 0.01 ± 0.01%, which is not appreciable in the graphic. (*) denotes groups with statistically significant differences ($p < 0.05$). **(C)** Histomorphometrical results: percentage of newly formed bone in the available macropore spaces within the five VOIs, 12 weeks after implantation in CDHA-Foam and BCP-Foam scaffolds. The bone was uniformly distributed over the entire implant in the CDHA-Foams, whereas in the BCP-Foams, there was very little bone in the outer VOI and it was concentrated mostly in the middle VOIs. (*) denotes groups with statistically significant differences ($p < 0.05$).

The newly formed bone was predominately located in the concavities of the macropores and in direct contact with the biomaterial, as shown in **Fig. 2.4B**, and consisted of a mineralized bone matrix, with osteocytes inside lacunae and aligned osteoblasts laying down new osteoid (**Fig. 2.4D**). The newly deposited bone was basically woven bone, with some areas of lamellar bone and a few Haversian structures (**Fig. 2.4C**). No endochondral ossification was detected during the ectopic bone formation process.
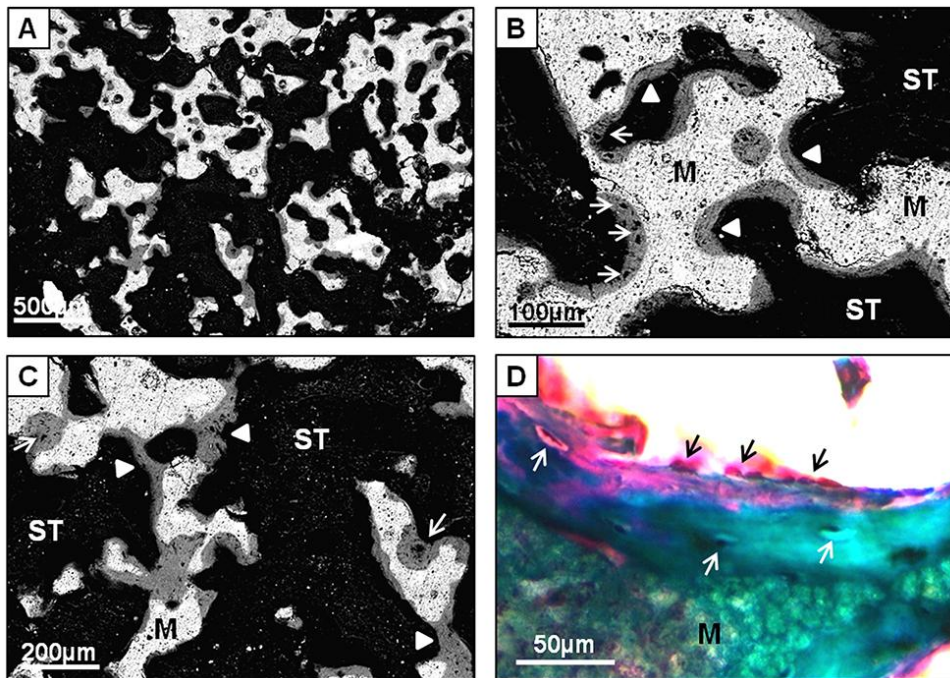
Figure 2.4. (A,B,C) Backscattered scanning electron micrographs of undecalcified section of a CDHA-Foam scaffold 6 weeks after implantation. **(B)** The newly formed bone (white arrow heads) was arranged concentrically to the concave surface of the scaffold macropores and was always in direct contact with the material. Note the formation of a well-mineralized bone matrix with some lacunae (white arrows). **(C)** The new ectopic bone (white arrow heads) was basically woven bone with some osteon-like structures (white arrows). M=Material, ST=Soft tissue (in black). **(D)** Micrograph of an undecalcified Goldner-Masson trichrome stained section of a CDHA-Foam scaffold after 6 weeks of implantation showing a well-mineralized bone matrix (in green), with osteocytes inside the lacunae (white arrows) and aligned osteoblasts (black arrows) laying down new osteoid (in pink). M=Material.

At 12 weeks, a significant amount of new ectopic bone was observed in the macropores of the CDHA-Foam scaffolds in 6 out of 6 animals (27.98 ± 4.80% ectopic bone) and in the macropores of the BCP-Foam scaffolds, in 4 out of 6 animals (28.30 ± 10.11% ectopic bone) (**Fig. 2.3A/B**). The bone was uniformly distributed over the entire implant in CDHA-Foams, and no significant differences among the five concentric VOIs at this time point were observed (**Fig. 2.3C** and **Fig. 2.5A**). However, BCP-Foams exhibited a repetitive pattern: almost no bone formation was in the outer VOI (VOI 5), and most of the bone was concentrated in the middle VOI (VOI 3) (**Fig. 2.3C** and **Fig. 2.5B**). Moreover, distinctive bone formation patterns were observed in these two groups, as shown in **Fig. 2.5**. Whereas in the BCP-Foam group, the new bone was deposited on top of the surface of the scaffold and was filling the macropore space (**Fig. 2.5B**), in the CDHA-Foam group, the bone seemed to replace the scaffold (**Fig. 2.5A**). This observation was confirmed when the amounts of pore volume before and after implantation in these two groups were compared. Thus, even if both groups showed a similar amount of new ectopic bone formation, the fraction of total pore volume at 12 weeks decreased to 4.56% in the BCP-Foam group and it increased to 4.77% in the CDHA-Foam group, when compared with the original scaffolds.
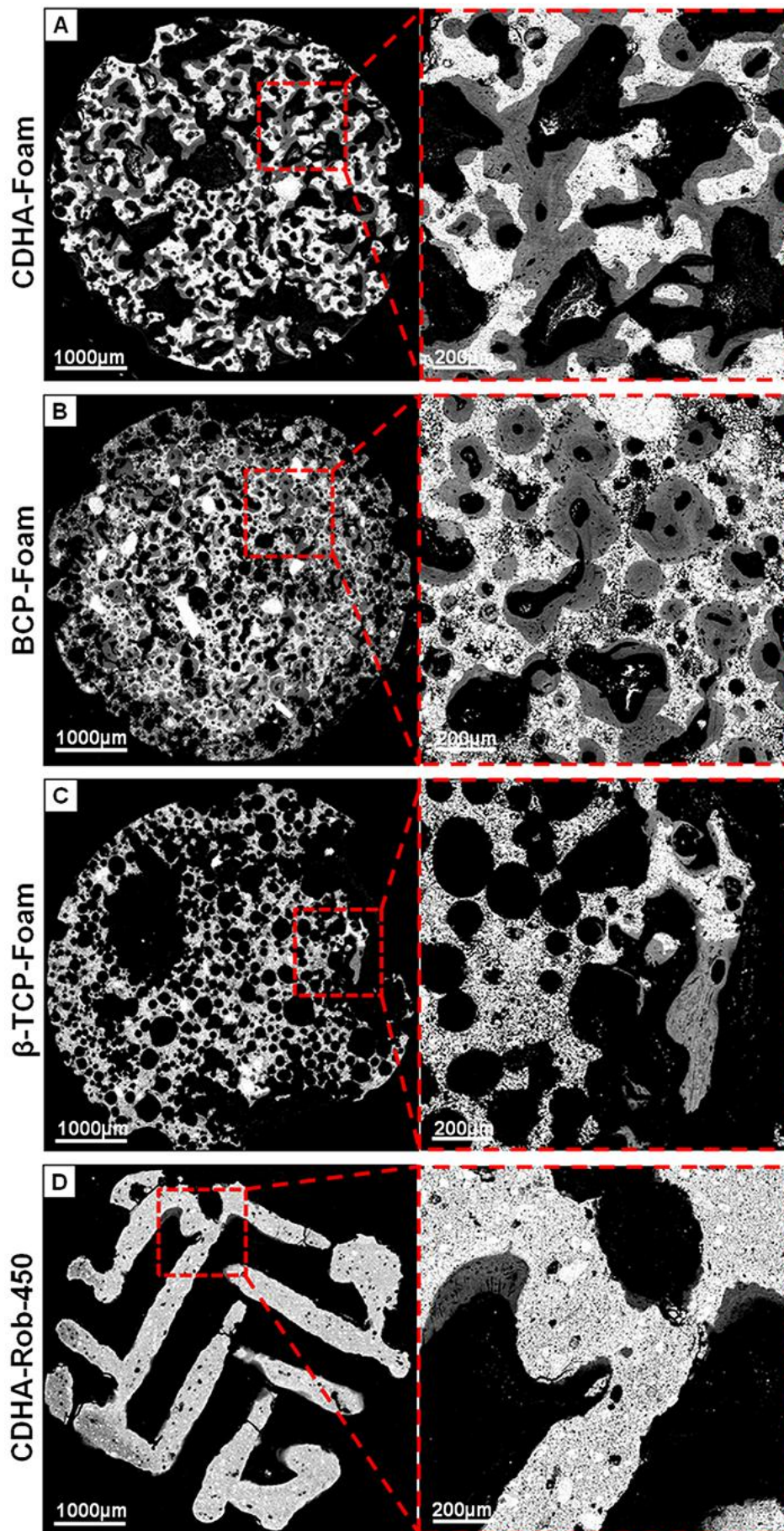
Figure 2.5. Backscattered scanning electron micrographs 12 weeks after implantation of studied scaffolds: **(A)** CDHA-Foam, **(B)** BCP-Foam, **(C)** β-TCP-Foam and **(D)** CDHA-Rob-450 robocast scaffold.

The new ectopic bone was observed within macropores from 10 to 300 μm in diameter in both groups, and it consisted of mature lamellar bone with some areas of osteonal bone following a Haversian pattern (**Fig. 2.5A/B** and **Fig. 2.6A/B/D/E**). Moreover, abundant extracellular calcified bone matrix was observed within the micropores (<10 μm) of these two groups, as shown in **Fig. 2.6G/H**.
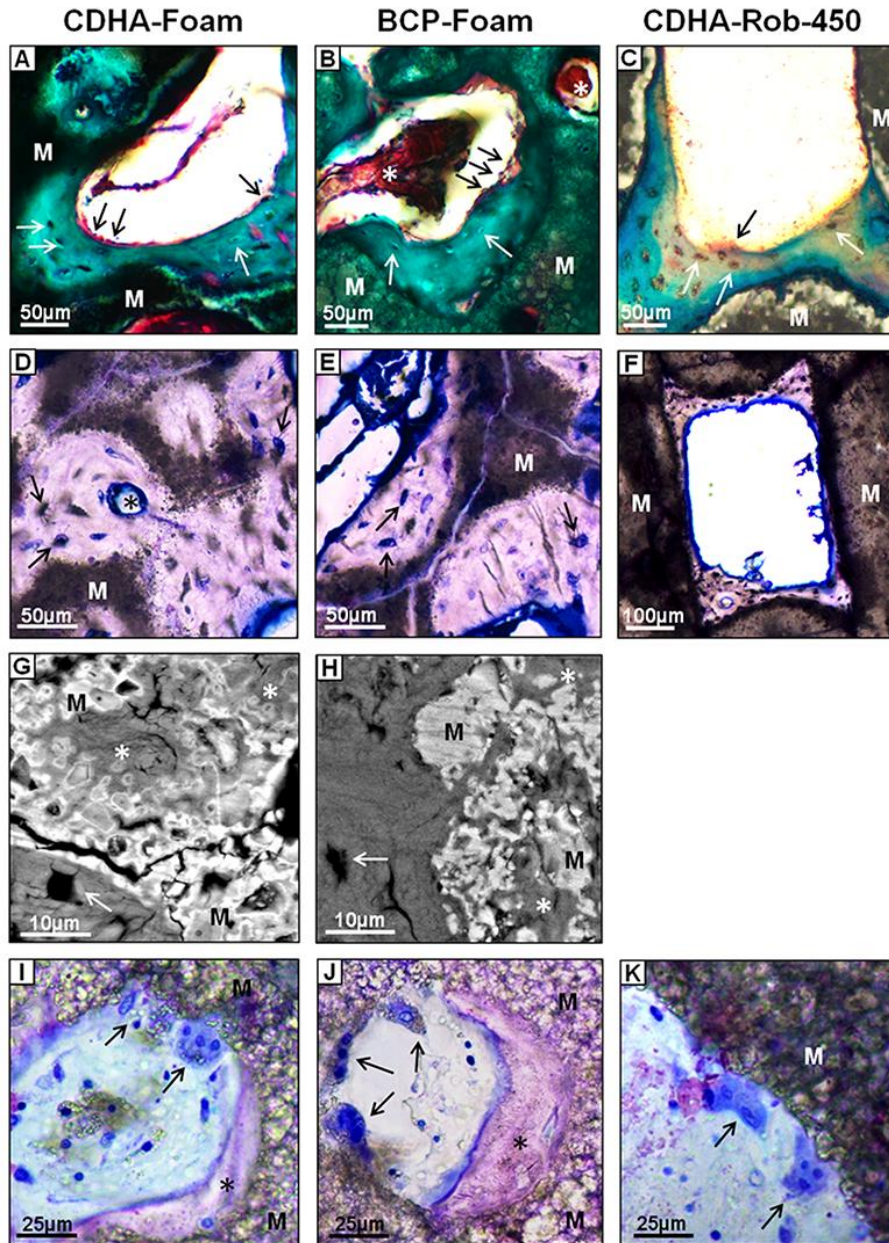
Figure 2.6. (A,B,C) Micrographs of undecalcified Goldner-Masson trichrome stained sections of the CDHA-Foam, BCP-Foam and CDHA-Rob-450 scaffolds 12 weeks after implantation, showing well-mineralized bone matrix (in green), osteocytes inside lacunae (white arrows), and aligned osteoblasts (black arrows) laying down new osteoid (pink). M=Material, Asterisk=blood vessel. **(D,E,F)** Micrographs of undecalcified toludine blue stained sections of the CDHA-Foam, BCP-Foam and CDHA-Rob-450 scaffolds 12 weeks after implantation, showing well-mineralized bone matrix (in purple), osteocytes inside lacunae (black arrows) and bone canaliculi. In the CDHA-Rob-450, bone is mostly found in the corners, which are the only parts of the robocast samples with concave-like regions. M=Material, Asterisk=blood vessel. **(G,H)** Backscattered scanning electron micrographs of the CDHA-Foam and BCP-Foam scaffolds 12 weeks after implantation, showing calcified bone matrix (asterisk) within micropores and an osteocyte (white arrow) located within a nearby macropore. M=Material. **(I,J,K)** Micrographs of undecalcified toluidine blue stained sections of the CDHA-Foam, BCP-Foam and CDHA-Rob-450 scaffolds 12 weeks after implantation, showing multinucleated osteoclast-like cells (black arrows) resorbing the material and displaying intracellular scaffold particles. M=Material, Asterisk=Bone matrix.

In the CDHA-Rob-450 and β-TCP-Foam groups, new ectopic bone was found in just 1 animal out of 6 and in small amounts (**Fig. 2.3A/B** and **Fig. 2.5C/D**). In CDHA-Rob-450, bone was mostly found in the corners, which are the only parts of robocast samples with concavities (**Fig. 2.5D** and **Fig. 2.6C/F**). CDHA-Rob-250 scaffolds did not show any ectopic bone formation at 12 weeks (**Fig. 2.3A/B** and Appendix, **Fig. A2.4**).

Some multinucleated osteoclast-like cells were consistently observed resorbing the materials in all scaffolds. However, a qualitative histological assessment identified a greater number of osteoclast-like cells in the CDHA-Foam and BCP-Foam scaffolds (**Fig. 2.6I/J**, respectively) than in the CDHA-Rob and β-TCP-Foam samples at both time points.

The results concerning scaffold resorption in the different groups are summarized in **Fig. 2.7A**. Higher degradation was observed for the CDHA-Foam scaffolds compared with the other groups at 6 weeks, whereas at 12 weeks, CDHA-Foam and β-TCP-Foam showed similar degradation, both significantly higher than that in CDHA-Rob-450 and 250, and the BCP-Foam groups (**Fig. 2.7A**). Importantly, the degradation of the CDHA-Foam scaffolds was progressive and homogeneous, whereas that showed by the β-TCP-Foam scaffolds was more heterogeneous, leaving big holes within the constructs, as revealed by the micro-CT images (**Fig. 2.7B**).
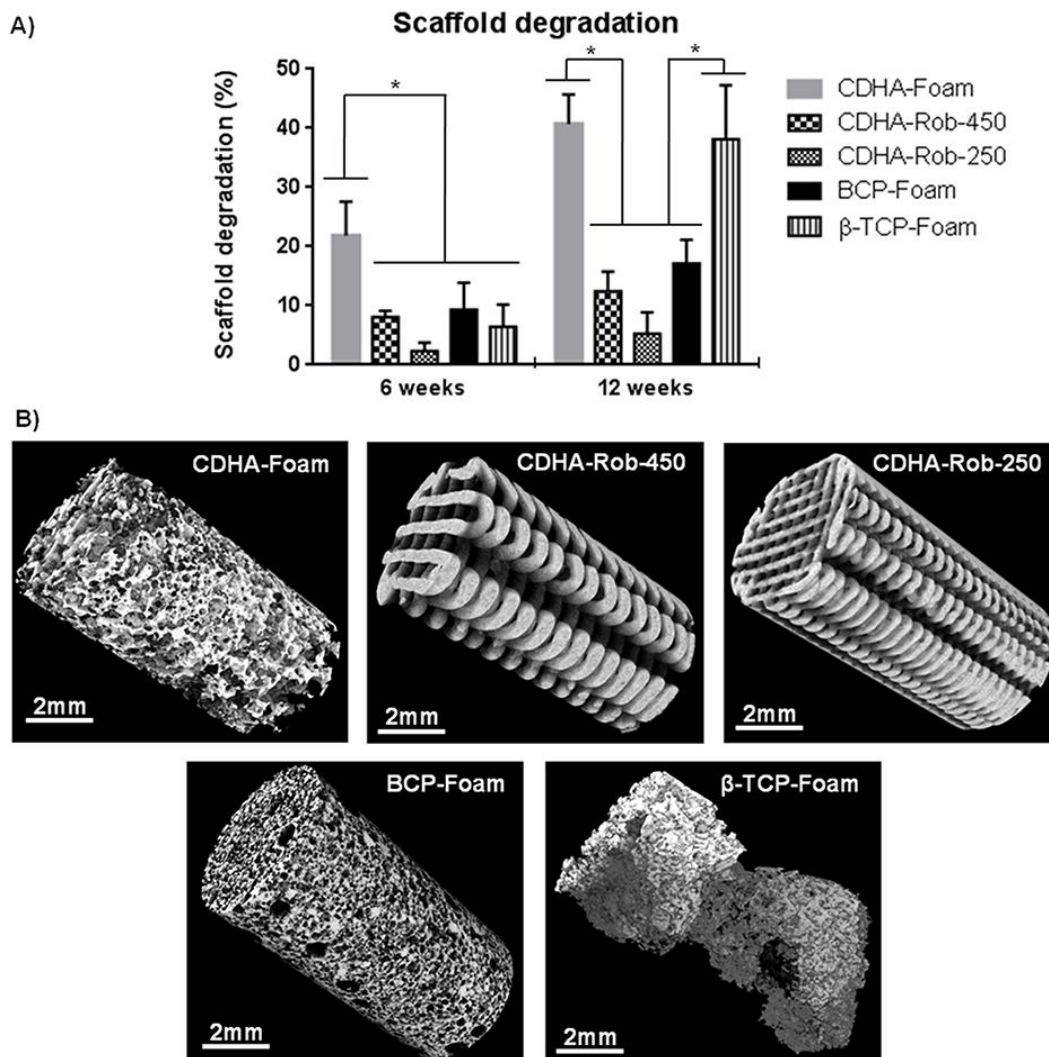
Figure 2.7. (A) Histomorphometry results: percentage of scaffold degradation 6 and 12 weeks after implantation. (*) denote groups with statistically significant differences (p < 0.05). **(B)** Micro-CT 3D reconstructions of implanted scaffolds 12 weeks after implantation.

2.3.3 In vitro study: cell differentiation (RT-qPCR)

The expression profiles of the osteogenic markers of rMSCs were analysed in planar discs of the different materials used to fabricate the scaffolds, namely, CDHA, BCP and β-TCP. The physicochemical properties of the discs are summarized in the Appendix (**Fig. A2.5**). The results obtained by RT-qPCR analysis are displayed in **Fig. 2.8**.
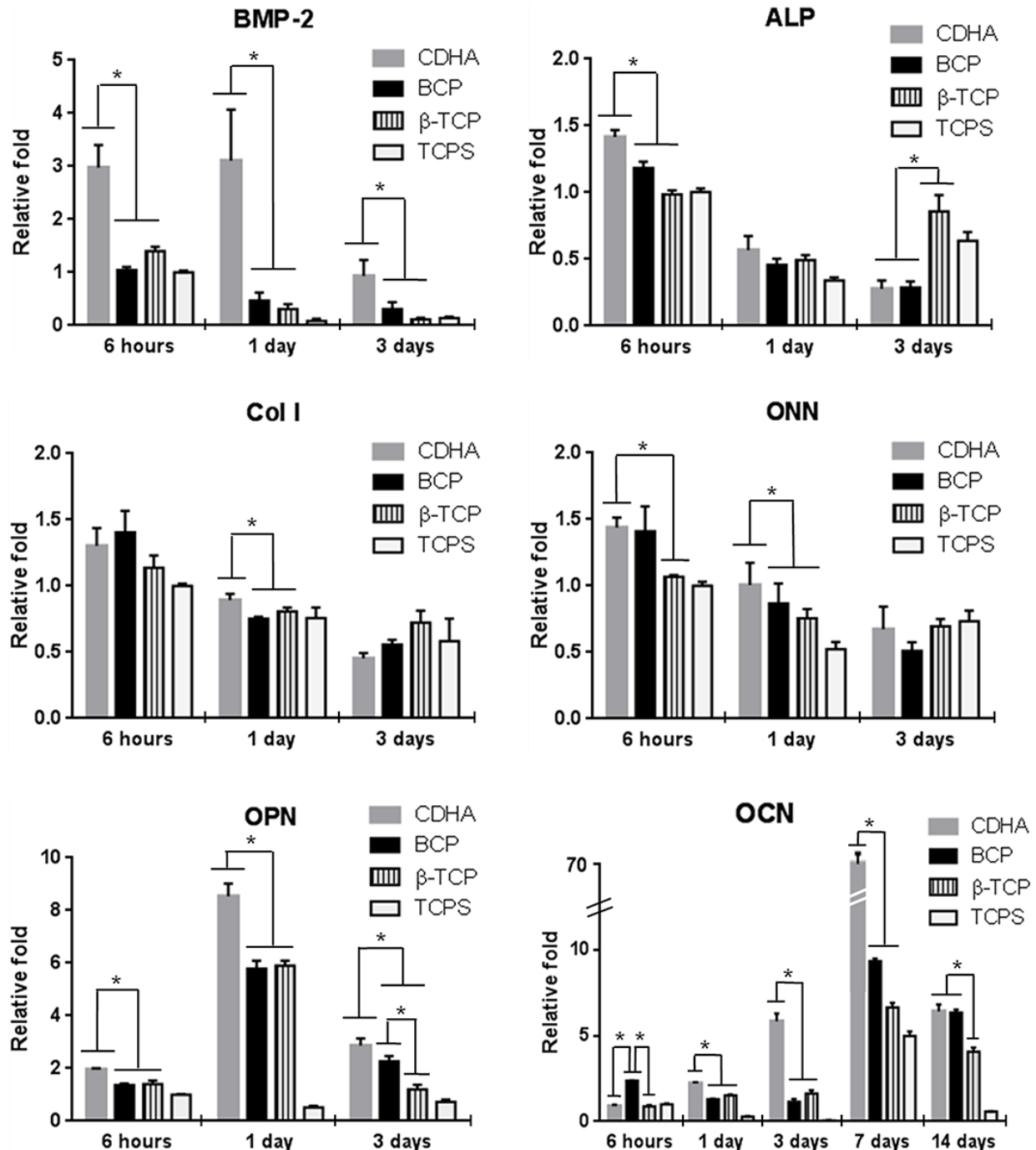
Figure 2.8. Gene expression, measured by RT-qPCR, of osteogenic markers of rMSCs cultured on planar discs of the different materials used to fabricate the scaffolds (CDHA, BCP and β-TCP). TCPS was used as a reference. Cells were cultured in a basic medium. Statistical comparisons were performed between CaP materials. (*) denote groups with statistically significant differences (p < 0.05).

The expression profiles of BMP-2, OPN and OCN were significantly higher at all time points for cells cultured on CDHA compared with those of sintered ceramics with the exception of OCN at 6 h. ALP, Col I and ONN expression followed similar trends, presenting the highest values at 6 h and decreasing over time. Specifically, the expression of ALP at 6 h in cells cultured on CDHA was significantly higher than that of sintered ceramics, whereas cells cultured on β-TCP showed significantly higher levels at 3 days compared with those on CDHA and BCP. Col I gene expression at day 1 was significantly higher for cells cultured on CDHA compared with that on BCP. The expression of ONN at 6 h by cells cultured on CDHA was significantly higher than that on β-TCP and also significantly higher than that on the two sintered ceramics at day 1. Finally, for OCN, a late osteogenic marker, the analysis was prolonged until 7 and 14 days, resulting in a higher overexpression of OCN when the cells were cultured on CDHA compared with that on the sintered ceramics at 7 days. At 14 days, similar values were found on CDHA and BCP, and both were higher than on β-TCP.

2.4 Discussion

The main goal of the present study was to obtain a better understanding of the role of textural properties and macropore architecture in osteoinduction, aiming to shed light on the behavior of biomimetic nanostructured materials as compared with conventional sintered ceramics. Previous results pointed to microporosity and SSA as critical factors for the material-associated osteoinduction, although only a limited range of porosities and SSA had been analyzed up to this moment. In this work, we have been able to extend this range to nanoscale porosities, in combination with different macropore architectures. The results showed that both parameters are relevant, as foams induced ectopic bone formation to a much higher extent than robocast scaffolds, and among the foams, biomimetic nanostructured CDHA produced a higher incidence and accelerated bone formation when compared with microstructured sintered CaPs. Moreover, different patterns of bone formation were observed, as discussed below.

2.4.1 Animal model and surgical protocol

The intrinsic osteoinductive potential of a biomaterial, i.e., its capacity to trigger the differentiation of MSCs to the osteoblastic lineage, can be proved by its ability to stimulate new bone formation when implanted ectopically in a host animal. In the present study, intramuscular implantation in a canine model was chosen, because ectopic bone formation is a species-dependent phenomenon, being more frequent in large animals (dogs, sheep and goats) than in small animals (mice, rats and rabbits).[23-26] The higher vascularization of muscle compared with that of subcutaneous tissue was the reason for choosing this implantation site.[24,26]

Concerning the surgical protocol, it is worth mentioning that in our study a NSAID was administered to the animals postoperatively. This was done both for ethical reasons and in an attempt to be close to real clinical situations, in which NSAIDs, combined with opioid drugs, are routinely used for 7 to 10 days after orthopedic surgeries to control pain and inflammation. This is relevant because it is well-known that NSAIDs inhibit cyclooxygenase-2 function, thereby impairing bone formation at early stages.[27] Moreover, it has been suggested that a certain degree of inflammation might foster osteoinduction, through the local release of inflammatory cytokines

produced by monocytes and macrophages; the cytokines may then stimulate circulating stem cells to differentiate into the osteoblastic lineage.[28-31] For this reason, most studies on biomaterial-associated osteoinduction just used opioid drugs postoperatively[12,13,26,32,33] or no pain relievers or analgesic drugs.[9,11,34-38]

Interestingly, the use of NSAIDs did not impair nor reduce the incidence of ectopic bone formation compared with its use in other studies. Although it is difficult to make direct comparisons because of the various animal models and different characteristics of the materials (granules, cement pastes, blocks, etc.), we found similar or even larger amounts of ectopic bone that found in previous studies with analogous designs (i.e., intramuscular implantations in large species).[9,11,12,23,26,32-34,36,38-42]

2.4.2 Effect of macropore geometry on osteoinduction

The presence of interconnected macropores is considered to be a prerequisite for osteoinduction by biomaterials.[1,12,35,43] This is associated with the need for body fluid flow and vascular infiltration, which corresponds with oxygen and nutrient supply and the easy access of cells (inflammatory cells, stem cells) and soluble proteins, including signaling molecules and osteogenic growth factors.[1,11]

However, the results obtained in this work showed that the interconnected macroporosity is necessary but not sufficient. Instead, the shape of the macropores seems to be critical for osteoinduction. Three groups of CDHA scaffolds with the same chemical composition, similar percentages of interconnected macroporosity and similar nanostructures and SSAs but with different macropore architectures were analyzed. It was decided to keep constant the total porosity of the foamed and robocast scaffolds, and this resulted in different pore entrance sizes (**Table 2.3**). CDHA-Foam exhibited concave macropores with bottleneck morphologies, pore diameters between 10 and 300 μm and pore entrance sizes around 70 μm. In contrast, the robocast scaffolds presented prismatic, convex macropores with pore dimensions around 350 μm for CDHA-Rob-450 and 200 μm for CDHA-Rob-250 (**Fig. 2.1** and **Table 2.3**). Ectopic bone was formed in the CDHA-Foam in 4 out of 6 animals at 6 weeks and in all animals at 12 weeks, whereas in the CDHA-Rob-450 group, bone was formed in a very small amount in just 1 out of the 6 animals at 12 weeks, and no signs of bone formation were observed in the CDHA-Rob-250 at both time points (**Fig. 2.3A/B**). Remarkably, ectopic bone in the CDHA-Rob-450 group was found only in the corners, where robocast scaffolds show concave-like regions (**Fig. 2.5D** and **Fig. 2.6C/F**). It is worth mentioning that no correlation was found between angiogenesis and ectopic bone formation, because abundant neovascularization, homogeneously distributed throughout the constructs, was observed both in the foams and in the robocast scaffolds (**Fig. 2.2**).

Although most authors recognize the positive effect of concave porosity on osteoinduction,[12,43] there is still controversy. Wang et al.[41] reported a better osteoinductive potential for HA-based biomaterials with channel-like architectures and convex surfaces compared with that for scaffolds with honeycomb-like architectures and concave surfaces. However, in our case the results pointed quite categorically to the need of concave macropores to trigger osteoinduction. This suggests that the spherical macropores provide confined spaces, which acted as niches with the adequate microenvironment for the differentiation of MSCs to osteoblasts. This

microenvironment includes the adequate concentration of calcium and phosphate in the vicinity of the scaffold and the presence and retention of osteoinductive growth factors. This microenvironment is not preserved in the more open structure of the robocast scaffolds, where both ions and proteins easily diffuse instead of being retained locally.

Moreover, recent studies have shown that, in addition to triggering osteoinduction, geometry is a factor that contributes to the control of the kinetics of tissue deposition by osteoblastic cells.[44-46] Specifically, these authors demonstrated that bone matrix deposition by osteoblasts happened in concave surfaces rather than on convex or flat surfaces, and moreover, the local growth rate of tissue formed in a concave space was proportional to the concave curvature. This is in good agreement with the higher amount of bone found in the foamed scaffolds and with the localization of bone in the corners of the robocast scaffolds (**Fig. 2.5D** and **Fig. 2.6C/F**).

2.4.3 Effect of micro- and nanostructural parameters on osteoinduction

Foamed scaffolds with similar percentages of spherical concave macroporosity but different chemical compositions, microstructures and SSAs were compared. The analysis of the micro-CT images, together with the BS-SEM images, allowed us to precisely calculate the volume of newly formed bone in each scaffold.[21] CDHA-Foam was the only group that showed ectopic bone formation at 6 weeks, whereas no signs of bone formation were observed in the sintered ceramics (BCP and β-TCP foams) at this time point. Moreover, CDHA-Foam was the only group showing a significant amount of ectopic bone formation in all animals at 12 weeks, whilst at this time point, bone formation was observed in only 4 out of the 6 animals in the BCP-Foam group and in 1 out of the 6 animals in the β-TCP-Foam group.

These results point in the same direction as previous studies that clearly showed that the microstructure of CaP-based biomaterials plays a determinant role in stimulating osteoinduction.[2,10-13,33,42,47-49] Several *in vivo* studies have evaluated CaP-based biomaterials with different microstructures, consistently showing the best results in terms of osteoinduction in the CaPs that have higher levels of microporosity and higher SSAs.[12,13,26,32,33,42,48,49] However, only sintered ceramics, which have the limitation of lacking nanoporosity, have been analyzed in this respect so far. Although different strategies have been explored to overcome this limitation, such as reducing the sintering temperature,[26,33,42] using spark plasma sintering to avoid grain coarsening,[50,51] or covering the surface of sintered ceramics with nanohydroxyapatite coatings obtained by hydrothermal routes,[52] these strategies do not manage to increase substantially the SSA of the materials, reaching values only around 6-10 m^2/g. In contrast, the biomimetic processing used in this work allowed the obtaining of foamed CDHA scaffolds which exhibited interconnected macropores, porosity on the micro- and nanoscale, and a SSA as high as 38 m^2/g.

The results obtained suggest that some mechanisms relevant for osteoinduction, such as the release of calcium and phosphate ions and the entrapment or attraction of relevant proteins and growth factors (e.g., BMPs)[7,12] are promoted in nanostructured biomimetic materials.

It is worth mentioning that poor results in terms of ectopic bone formation were obtained in previous studies of CPCs with similar compositions to the CDHA used in the present work.[36,53] However, this could be attributed to the lack of interconnected macroporosity in the cement pastes and prehardened scaffolds. In contrast, the foaming and 3D-printing techniques used in

the present study allowed the combination of the required interconnected macroporosity and the micro- and nanoporosities relevant for the osteoinductive processes.

Besides the acceleration and promotion of the process of osteoinduction, clear differences were observed in the pattern of bone formation when comparing CDHA and BCP Foams (**Fig. 2.5A/B**). Whereas bone was deposited on the surface of the scaffold in the BCP-Foam, resulting in the progressive filling of the macropores, in the CDHA-Foam bone replaced the pre-existing scaffold structure, meaning that bone formation was preceded by the resorption of the scaffold. This trend was confirmed by the higher degradation rate measured for the CDHA-Foams (**Fig. 2.7**), as discussed below.

To better understand the role that nanostructure and phase composition played in the differentiation of MSCs, rMSC were cultured on the surfaces of the discs of the different materials used in the *in vivo* study, without adding osteogenic factors in the culture medium. Overexpression of some osteogenic genes, namely, BMP-2, ONN, OPN and OCN was found to be more pronounced on CDHA discs than on the sintered BCP and β-TCP groups, indicating that biomimetic CDHA triggered the osteogenic differentiation of rMSCs (**Fig. 2.8**). The calcium and phosphate fluctuations registered in the cell culture medium in contact with the different materials during the cell culture study were not statistically significant (Appendix, **Fig. A2.5E**). Therefore, the osteogenic differentiation produced was mostly attributed to the topographical features, which had been identified as a parameter controlling differentiation of MSCs.[54,55] This, in fact, was in agreement with previous studies in which osteogenic differentiation of rMSC cultured on CDHA or in other nanostructured substrates like octacalcium phosphate was observed.[56,57] Similarly, other authors reported higher osteogenic differentiation of MSCs on low-temperature nanocrystalline HA compared with that on sintered HA, suggesting that nanoporosity, surface roughness and nanocrystal morphology are responsible for osteoinduction of MSCs.[58,59]

In this study, besides the bone formed within concave macropores from 10 to 300 μm in diameter in CDHA-Foam and BCP-Foam (**Fig. 2.6A/B**), abundant extracellular calcified bone matrix was observed within the micropores (<10 μm) of both groups (**Fig. 2.6G/H**). Other authors previously reported the presence of calcified bone matrix within micropores. In some cases, it had been associated with the osteoid produced by nearby cells being able to flow and penetrate into small micropores.[49,60,61] In contrast, other authors claimed that this calcified tissue might be produced by the invasion of the micropores by bone cells,[62,63] through pore interconnections smaller than their diameter (4-12 μm).[64] Although in our case no cells were seen within the micropores, immuno-histochemical staining using, for example, an osteocyte marker like sclerostin[63] would have been needed to conclusively exclude the presence of cells. Unfortunately, this was not possible since the samples were embedded in resin, which did not allow this type of immuno-histochemical investigation.

Regarding spatial distribution, bone was found only inside the foamed constructs but not on the external surface of the cylinders. As displayed in **Fig. 2.5A**, bone was uniformly distributed within the CDHA-Foam scaffolds with no significant differences between the five concentric VOIs (**Fig. 2.3C**). However, BCP-Foams consistently showed minimal bone formation in the outer VOI (VOI 5), and most of the new bone concentrated in the middle VOI (VOI 3) (**Fig. 2.3C** and **Fig. 2.5B**). This pattern for the BCP-Foams agreed with previous studies in which bone

induction was observed only in the center of the implant and not in the implant periphery. This was attributed to the fast diffusion of the released calcium and phosphate ions at the peripheral regions of the scaffolds, which prevented the attainment of the supersaturation required for ectopic bone formation and, also to the shear stresses on the outer regions of the ceramic blocks, which might have prevented bone tissue formation.[12] However, in the case of CDHA-Foams, the presence of bone uniformly distributed within the entire construct, including the periphery, can be explained by the higher reactivity of the substrate, associated with both its chemical composition and its textural properties, which led to higher implant degradation, resulting in higher levels of calcium and phosphate released in the whole volume of the construct.

2.4.4 Degradation patterns and osteoinduction

The role of CaP-based materials degradation in osteoinduction is still unknown. Some authors claim that whereas certain degree of degradation is desirable because it provides the calcium and phosphate ions needed to stimulate MSC differentiation and foster mineralization, too much degradation may impair osteoinduction because of the lack of stable surfaces where the new bone can be deposited.[7] This is the argument used to explain the higher osteoinduction found in BCP ceramics compared to both the hardly soluble sintered stoichiometric HA and the more soluble β-TCP.[12,26,32,35,37,47] The analysis of the micro-CT data obtained in this work allowed the quantification in 3D of the resorption of the different scaffolds, showing different patterns when looking at sintered ceramics and biomimetic CDHA.

When comparing the foamed scaffolds, the results showed that the material presenting the highest osteoinduction, CDHA-Foam, was also the one showing the highest degradation, which was above that of the sintered foams (BCP and β-TCP) at 6 weeks and above that of the BCP-Foam but was similar to that of the β-TCP-Foam at 12 weeks (**Fig. 2.7**). The high degradation rate of CDHA, compared particularly with the more soluble β-TCP, agrees with previous studies[65] and can be explained by its specific features, i.e., its nanosized crystals and consequently high SSA, its low crystallinity and its lack of stoichiometry. The degradation rate of the BCP-Foam, which presented a high amount of ectopic bone formation at 12 weeks, was significantly smaller. This can be associated with the low solubility of sintered HA together with its low SSA and can be the reason for its delayed ectopic bone formation compared with that of the CDHA-Foam. In the BCP-Foam, a longer time is probably required to achieve the supersaturation of the local environment with calcium and phosphate ions, which precedes new ectopic bone formation. On the other hand, the bone formation pattern described in the previous section is in good agreement with this lower degradation of the BCP-Foam, as bone was deposited on the surface of the scaffold instead of replacing the biomaterial (**Fig. 2.5**).

The results obtained demonstrate that the high resorption rate of CDHA-Foam, far from being an obstacle for osteoinduction, clearly promote it. Considering that the physiological fluid is supersaturated with respect to CDHA, the homogeneous and progressive degradation of the CDHA-Foam scaffolds suggest that the high degradation profile of the CDHA-Foam scaffolds was mainly due to the activity of multinucleated osteoclast-like cells (**Fig. 2.6G**), as also reported by Yuan et al.[36] These results are in good agreement with previous studies, which emphasized the promotion of osteoclastic activity by submicrometric microstructures of CaP and its close relation with osteoinduction.[13,25,33,48,66] The secretion of BMPs and other osteogenic

growth factors by osteoclasts is able to trigger MSC differentiation toward the osteogenic lineage, leading eventually to bone formation through intramembranous ossification,[7,34,66-69] as observed in the present study. It is noteworthy, however, that previous studies reported a lack of osteoinductive properties in carbonated hydroxyapatites with a SSA between 7 and 10 m^2/g.[26,70] Therefore, it was hypothesized that there was a limit in the increase of SSA of biomaterials that positively influences osteoinduction, deducing that a material with a SSA above the optimum might degrade too fast.[26] In contrast, the present results demonstrate that it is possible to couple degradation and bone formation in an ectopic site.

The situation with the β-TCP foams was different. Although the degradation percentage at 12 weeks was similar to those of CDHA foams, the degradation pattern was very heterogeneous, leaving big holes within the constructs (**Fig. 2.7B**). The loss of a stable, three-dimensional macrostructure, which is required to facilitate new bone growth, was probably the main reason why this group did not show significant ectopic bone formation (**Fig. 2.3A/B** and **Fig. 2.5C**), despite having the same macroporosity, microstructure and SSA as the BCP-Foam group (**Fig. 2.1** and **Table 2.2**).

Remarkably, pore architecture also had a significant effect on the degradation of the scaffolds. CDHA-Foam scaffolds showed higher degradation than the biomimetic robocast scaffolds at both time points (**Fig. 2.7**), in spite of having identical chemical compositions, and very similar nanostructures and SSAs, which should entail similar dissolution rates. Importantly, a higher number of osteoclast-like cells were identified in the concave macropores of the CDHA-Foam compared with in the convex, prismatic macropores of the robocast scaffolds. These findings suggested that osteoclast-like cell activity and consequently cell-mediated degradation were enhanced by the microenvironment created inside the concave macropores. Likewise, the lack of osteoinduction by the robocast scaffolds confirmed in turn the close relation between osteoclastic activity and osteoinduction.

Overall, besides providing additional information about the role of structural parameters in osteoinduction and the biological mechanisms behind it, the enhanced osteoinduction of the biomimetic CDHA-Foams may have a direct clinical application in the repair of large bone defects. Some studies have demonstrated the clinical utility of osteoinductive bone substitutes for the treatment of critical-sized bone defects, showing that these materials are better bone-void fillers than those that are merely osteoconductive.[8,9,37,70] Thus, the next step will be to confirm this hypothesis by evaluating these novel biomimetic CaP scaffolds in an orthotopic model.

2.5 Conclusions

The results obtained in this study show that both pore architecture and reactivity of the substrate play a crucial role in osteoinduction. The high reactivity of biomimetic CDHA, which resulted from its poor crystallinity, nanostructured nature and high SSA combined with the concave macroporosity produced by a foaming process, resulted in accelerated osteoinduction when compared with conventional sintered BCP ceramics with the same macropore architecture. Different bone formation patterns were exhibited by sintered and biomimetic scaffolds. Whereas CDHA scaffolds were progressively resorbed and replaced by new ectopic bone, in the BCP scaffolds, bone was deposited on the surface of the material, progressively filling the pore space.

Conversely, very limited osteoinduction was found in the 3D robocast scaffolds with prismatic pore geometries. In conclusion, we have shown that tailoring both the nanostructure and the macropore geometry of biomimetic CDHA obtained by a low-temperature self-setting reaction allows us to push the osteoinduction potential beyond the limits obtained for the microstructured CaP ceramics.

2.6 Appendix

Further characterization of materials, such as XRD patterns of implanted scaffolds and BCP foams, as well as complete physicochemical characterization of planar discs used in the *in vitro* study are provided in this section. Moreover, additional results of the *in vivo* study, such as ectopic bone distribution in CDHA-Foam scaffolds at 6 weeks and backscattered electron micrographs of CDHA-Rob-250 scaffolds at 12 weeks of implantation are also included.

2.6.1 XRD patterns of BCP foams

The biphasic hydroxyapatite/β-TCP foams (BCP-Foam) were obtained by immersing the as-prepared α-TCP foams in a sodium bicarbonate solution (NaHCO3, Sigma-Aldrich, St. Louis, USA), autoclaving them at 120ºC and 1 atm for 30 min and subsequently sintering them at 1100°C for 9 h. The HA:β-TCP ratio can be tuned by adjusting the concentration of the sodium bicarbonate solution, as shown in the **Fig. A2.1**.

NaHCO₃ concentration (wt%)	β-TCP (wt%)	HA (wt%)
0.1	84.9	15.1
0.5	59	41
1	17.3	82.7
1.25	10.5	89.5
1.5	7.5	92.5
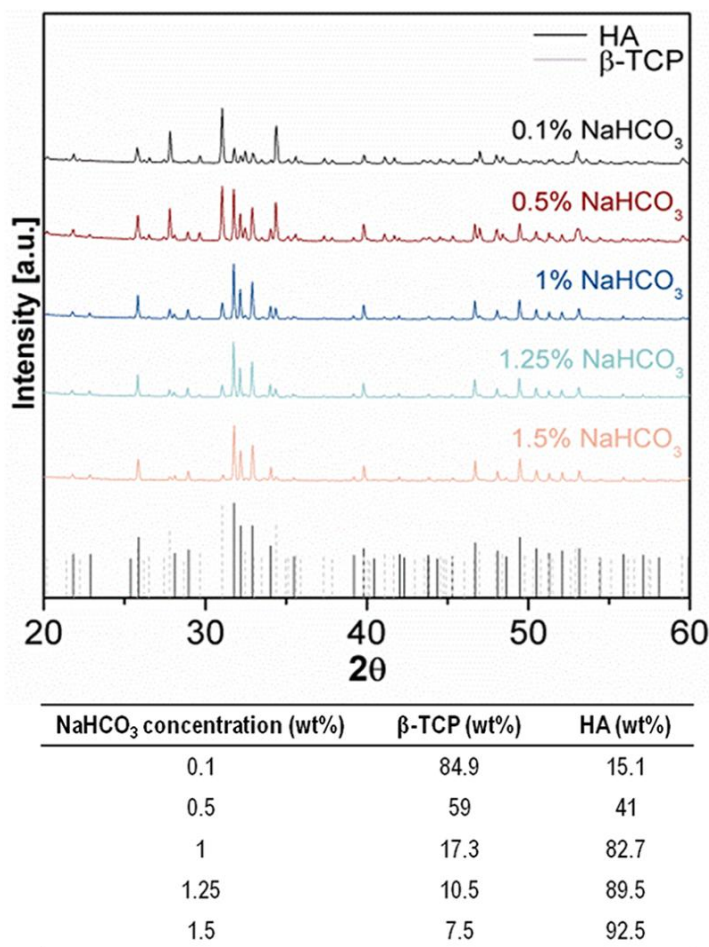
Figure A2.1. XRD patterns of the biphasic materials obtained after immersing the α-TCP foams in solutions with different concentrations of NaHCO₃, followed by autoclaving and subsequent sintering at 1100ºC for 9h.

2.6.2 XRD patterns of implanted scaffolds
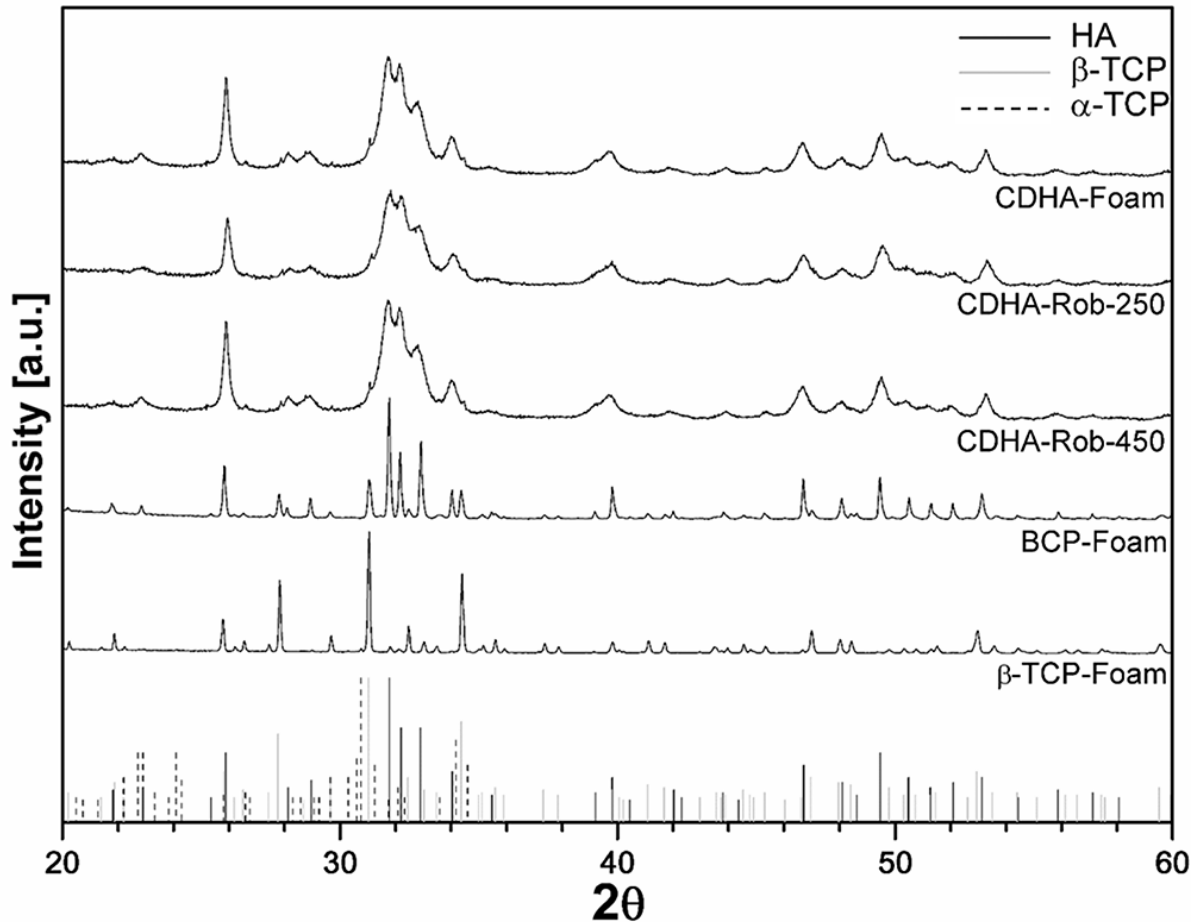
Figure A2.2. XRD patterns of implanted scaffolds: the CDHA-Foam and the CDHA-Rob scaffolds consisted of a poorly crystalline apatitic phases, as indicated by the broad peaks, typical of biomimetic apatites. Small amounts of unreacted α-TCP were detected, and quantified to be 2 and 3% for CDHA-Foam and CDHA-Rob scaffolds, respectively. The sintered scaffolds exhibited the sharp XRD peaks, typical of highly crystalline materials. β-TCP-Foam scaffolds consisted of phase-pure β-TCP and BCP-Foam consisted of a mixture of 82.7% HA and 17.3% β-TCP.

2.6.3 Ectopic bone distribution of CDHA-Foam scaffolds at 6 weeks
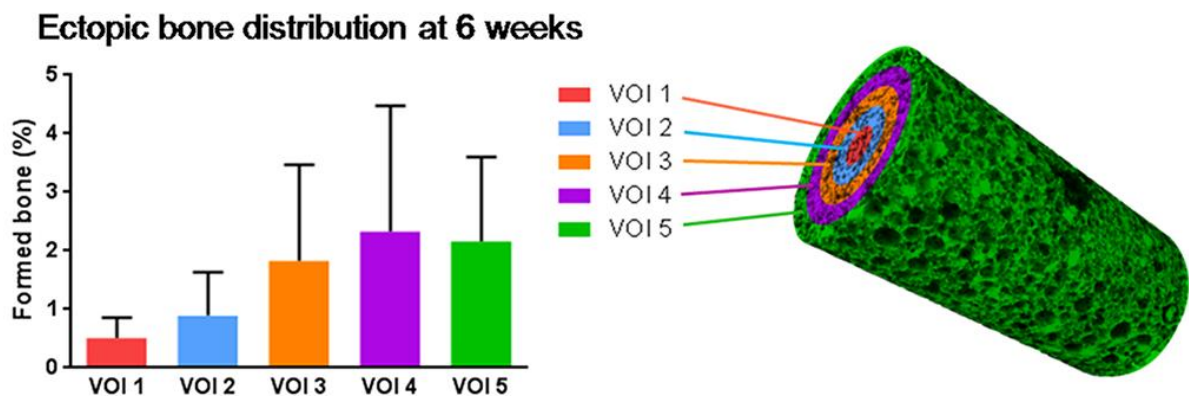
Figure A2.3. Histomorphometrical results: percentage of newly formed bone in the available macropore spaces within the five volumes of interest (VOIs), 6 weeks after implantation in the CDHA-Foam scaffolds. Although no significant differences among the five concentric VOIs were noted, the ectopic bone was mainly found in the outer and middle regions.

2.6.4 Backscattered electron micrographs of CDHA-Rob-250 scaffolds at 12 weeks
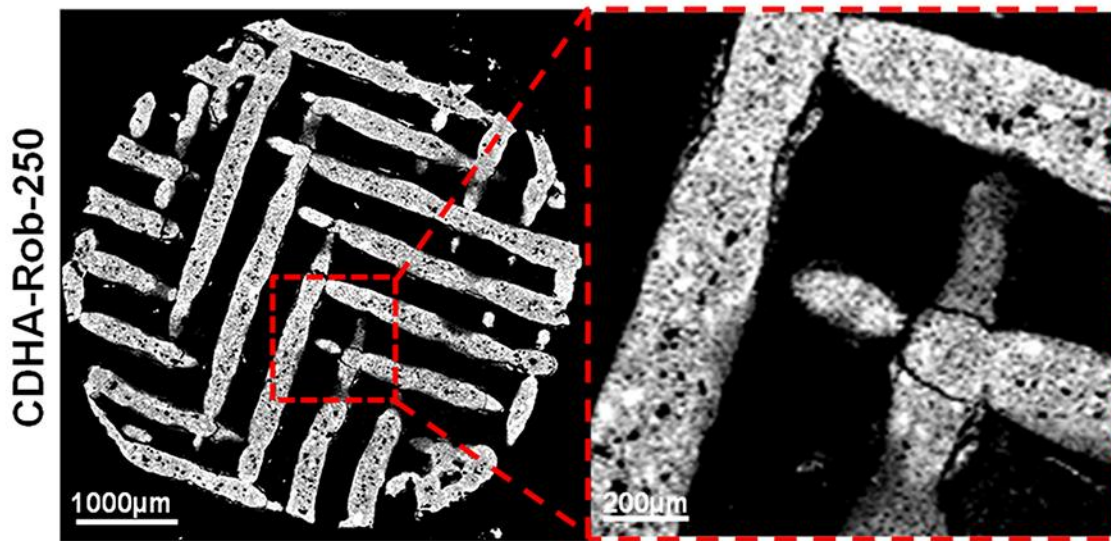
Figure A2.4. Backscattered electron micrographs of CDHA-Rob-250 scaffolds 12 weeks after implantation. CDHA-Rob-250 scaffolds did not show ectopic bone formation in any animal.

2.6.5 Physicochemical characterization of planar discs used in the in vitro study

The planar discs were characterized in terms of phase composition, microstructure, SSA and porosity using the same techniques as described for the scaffolds characterization. In order to analyse ionic exchanges on cell culture medium after incubation of materials in presence of rMSCs, Ca^{2+} levels were quantified by O-cresolphtaleincomplexone method,[71,72] whereas P_i levels were quantified using Phosphate Colorimetric Kit (Sigma-Aldrich, St. Louis, USA). In both cases, a calibration curve with decreasing concentration of either calcium or phosphate was prepared to express the results. The absorbance was read spectrophotometrically at 570 nm and 650 nm, respectively.
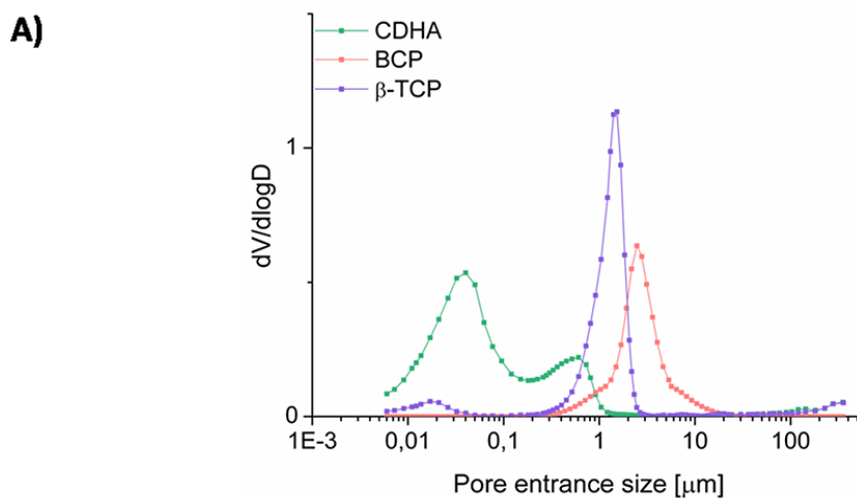
Figure A2.5. Physicochemical characterization of the planar discs used in the in vitro study. **(A)** Pore entrance size distribution of the three samples determined by MIP: CDHA discs exhibited a clear bimodal pore size distribution, intra aggregate pores (10-200 nm range) and inter aggregate pores (centered around 0.6-0.8 μm). Thermal treatment removed the nanoscale porosity and, as a result, the microscale porosity increased leading to a sharp monomodal pore size distribution in β-TCP and BCP samples, centered at 1.5 and 2.5 μm, respectively.
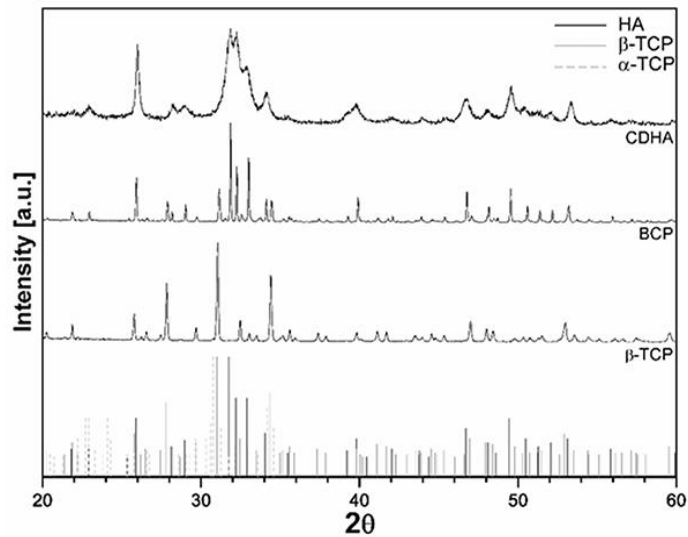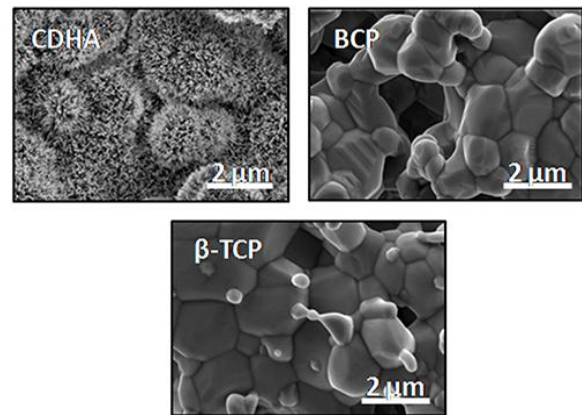
Figure A2.5 (cont.). (B) XRD patterns of the three CaP materials: the CDHA discs consisted of a poorly crystalline apatitic phases, as indicated by the broad peaks, typical of biomimetic apatites. The sintered ceramics exhibited the sharp XRD peaks, typical of highly crystalline materials. The β-TCP discs consisted of phase-pure β-TCP, and the BCP discs consisted of a mixture of 82.7% HA and 17.3% β-TCP. **(C)** Total porosity (%) and SSA (m^2/g) of the three samples: although all materials presented similar values of total porosity, the CDHA discs presented a high SSA value, whereas sintered materials showed lower SSA values (<1 m^2/g). **(D)** Scanning electron micrographs of the three materials: the microstructure of the CDHA discs consisted of the typical network of entangled needle-like nanocrystals, while the sintered ceramics showed polyhedral smooth crystals.
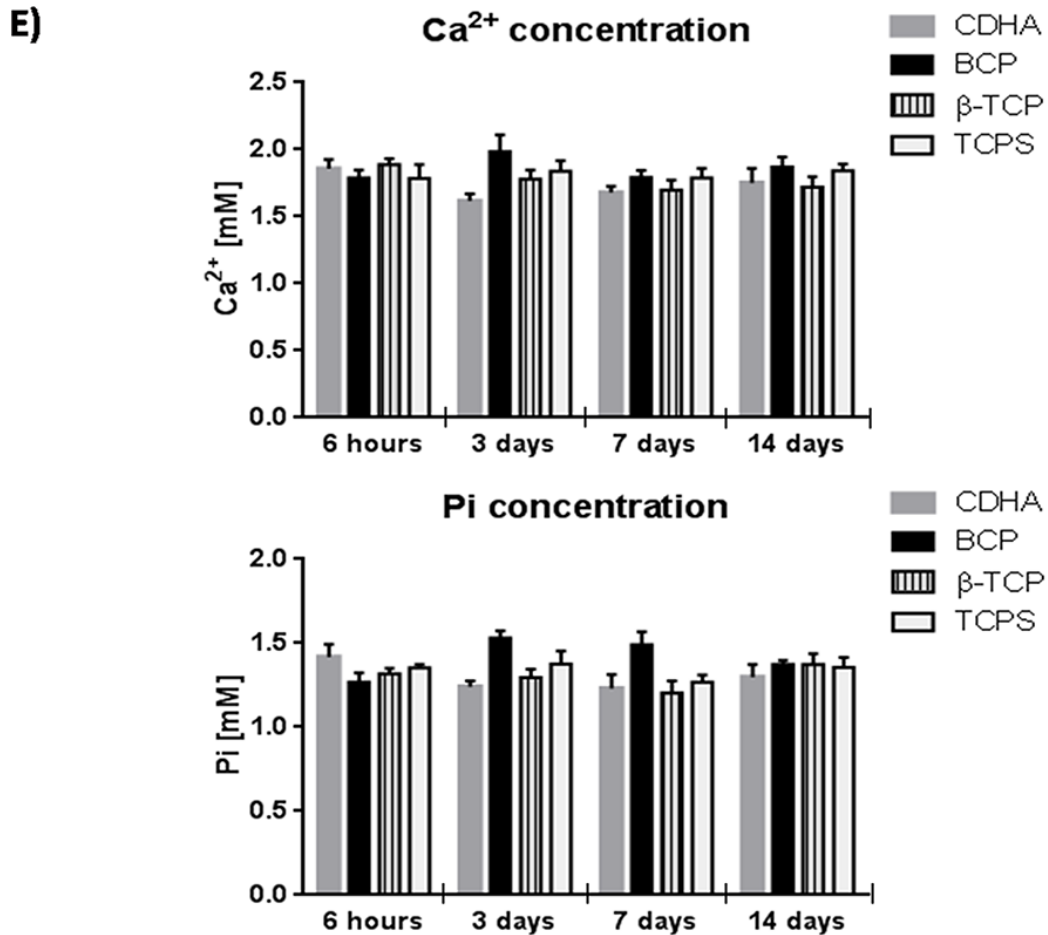
Figure A2.5 (cont.). (E) Ca^{2+} and P_i levels of cell culture medium after incubation of the three materials in presence of rMSCs in advDMEM for 6 h, 3 days, 7 days and 14 days: all materials kept Ca^{2+} and P_i concentrations in tested culture medium constant and followed similar behaviour at each time compared to TCPS. No significant differences were noted among groups at any time. Experimental concentrations of Ca^{2+} and P_i for advanced DMEM are 1.87 mM and 1.16 mM, respectively.

2.7 References

[1]   Ripamonti U. The morphogenesis of bone in replicas of porous hydroxyapatite obtained from conversion of calcium carbonate exoskeletons of coral. J Bone Joint Surg Am 1991;73:692-703.

[2]   Yamasaki H, Saki H. Osteogenic response to porous hydroxyapatite ceramics under the skin of dogs. Biomaterials 1992;13:308-12.

[3]   Shields LB, Raque GH, Glassman SD, Campbell M, Vitaz T, Harpring J, Shields CB. Adverse effects associated with high-dose recombinant human bone morphogenetic protein-2 use in anterior cervical spine fusion. Spine (Phila Pa 1976) 2006;31:542-7.

[4]   Zara JN, Siu RK, Zhang X, Shen J, Ngo R, Lee M, Li W, Chiang M, Chung J, Kwak J, Wu BM, Ting K, Soo C. High doses of bone morphogenetic protein 2 induce structurally abnormal bone and inflammation in vivo. Tissue Eng Part A 2011;17:1389-99.

[5]   Giannoudis PV, Dinopoulos H, Tsiridis E. Bone substitutes: an update. Injury 2005;36:20-7.

[6]   Younger EM, Chapman MW. Morbidity at bone graft donor sites. J Orthop Trauma 1989;3:92-5.

[7]   Barradas AMC, Yuan H, van Blitterswijk CA, Habibovic P. Osteoinductive biomaterials: current knowledge of properties, experimental models and biological mechanisms. Eur Cell Mater 2011;21:407-29.

[8]   Habibovic P, Yuan H, van den Doel M, Sees TM, van Blitterswijk CA, de Groot K. Relevance of osteoinductive biomaterials in critical-sized orthotopic defect. J Orthop Res 2006;24:867-76.

[9]   Yuan H, Fernandes H, Habibovic P, de Boer J, Barradas AMC, de Ruiter A, Walsh WR, van Blitterswijk CA, de Bruijn JD. Osteoinductive ceramics as a synthetic alternative to autologous bone grafting. Proc Natl Acad Sci USA 2010;107:13614-19.

[10]   Yuan H, Kurashina K, de Bruijn JD, Li Y, de Groot K, Zhang X. A preliminary study on osteoinduction of two kinds of calcium phosphate ceramics. Biomaterials 1999;20:1799-806.

[11]   Le Nihouannen D, Daculsi G, Saffarzadeh A, Gauthier O, Delplace S, Pilet P, Layrolle P. Ectopic bone formation by microporous calcium phosphate ceramic particles in sheep muscles. Bone 2005;36:1086-93.

[12]   Habibovic P, Yuan H, van der Valk CM, Meijer G, van Blitterswijk CA, de Groot K. 3D microenvironment as essential element for osteoinduction by biomaterials. Biomaterials 2005;26:3565-75.

[13]   Davison NL, Su J, Yuan H, van den Beucken JJ, de Bruijn JD, Barrère-de Groot F. Influence of surface microstructure and chemistry on osteoinduction and osteoclastogenesis by biphasic calcium phosphate discs. Eur Cell Mater 2015;29:314-29.

[14]   Ginebra MP, Espanol M, Montufar EB, Perez RA, Mestres G. New processing approaches in calcium phosphate cements and their applications in regenerative medicine. Acta Biomater 2010;6:2863-73.

[15]   Montufar EB, Traykova T, Gil C, Harr I, Almirall A, Aguirre A, Engel E, Planell JA, Ginebra MP. Foamed surfactant solution as a template for self-setting injectable hydroxyapatite scaffolds for bone regeneration. Acta Biomater 2010;6:876-85.

[16]   Pastorino D, Canal C, Ginebra MP. Drug delivery from injectable calcium phosphate foams by tailoring the macroporosity-drug interaction. Acta Biomater 2015;12:250-9.

[17]   Maazouz Y, Montufar EB, Malbert J, Espanol M, Ginebra MP. Self-hardening and thermoresponsive alpha tricalcium phosphate/pluronic pastes. Acta Biomater 2017;49:563-74.

[18]   Maazouz Y, Montufar EB, Guillem-Marti J, Fleps I, Öhman C, Persson C, Ginebra MP. Robocasting of biomimetic hydroxyapatite scaffolds using self-setting inks. J Mater Chem B 2014;2:5378-86.

[19]   National Research Council. Guide for the Care and Use of Laboratory Animals; National Academy Press: Washington, DC, 1996; pp 41-194.

[20]   Directive 2010/63/EU of the European Parliament and of the Council of 22 September 2010 on the Protection of Animals Used for Scientific Purposes. Available at http://data.europa.eu/eli/dir/2010/63/oj.

[21]   Lewin S, Barba A, Persson C, Franch J, Ginebra MP, Öhman-Mägi C. Evaluation of bone formation in calcium phosphate scaffolds with μCT – method validation using SEM. Biomed Mater 2017;12:65005.

[22] González-Vázquez A, Planel, JA, Engel E. Extracellular calcium and CaSR drive osteoinduction in mesenchymal stromal cells. Acta Biomater 2014;6:2824-33.

[23] Ripamonti U. Osteoinduction in porous hydroxyapatite implanted in heterotopic sites of different animal models. Biomaterials 1996;17:31-5.

[24] Yang Z, Yuan H, Tong W, Zou P, Chen W, Zhang X. Osteogenesis in extraskeletally implanted porous calcium phosphate ceramics: variability among different kinds of animals. Biomaterials 1996;17:2131-7.

[25] Akiyama N, Takemoto M, Fujibayashi S, Neo M, Hirano M, Nakamura T. Difference between dogs and rats with regard to osteoclast-like cells in calcium-deficient hydroxyapatite-induced osteoinduction. J Biomed Mater Res A 2011;96:402-12.

[26] Habibovic P, Sees TM, van den Doel MA, van Blitterswijk CA, de Groot K. Osteoinduction by biomaterials--physicochemical and structural influences. J Biomed Mater Res A 2006;77:747-762.

[27] Simon AM, O'Connor JP. Dose and time-dependent effects of cyclooxygenase-2 inhibition on fracture-healing. J Bone Joint Surg Am 2007;89:500-11.

[28] Brown BN, Ratner BD, Goodman SB, Amar S, Badylak SF. Macrophage polarization: an opportunity for improved outcomes in biomaterials and regenerative medicine. Biomaterials 2012;33:3792-802.

[29] Mountziaris PM, Spicer PP, Kasper FK, Mikos AG. Harnessing and modulating inflammation in strategies for bone regeneration. Tissue Eng Part B Rev 2011;17:393-402.

[30] Almeida CR, Vasconcelos DP, Gonçalves RM, Barbosa MA. Enhanced mesenchymal stromal cell recruitment via natural killer cells by incorporation of inflammatory signals in biomaterials. J R Soc Interface 2012;9:261-71.

[31] Fellah B, Josselin N, Chappard D, Weiss P, Layrolle P. Inflammatory reaction in rats muscle after implantation of biphasic calcium phosphate micro particles. J Mater Sci: Mater Med 2007;18:287-94.

[32] Habibovic P, Kruyt MC, Juhl MV, Clyens S, Martinetti R, Dolcini L, Theilgaard N, Van Blitterswijk CA. Comparative in vivo study of six hydroxyapatite-based bone graft substitutes. J Orthop Res 2008;26:1363-70.

[33] Davison NL, Luo X, Schoenmaker T, Everts V, Yuan H, Barrère-de Groot F, de Bruijn JD. Submicron-scale surface architecture of tricalcium phosphate directs osteogenesis in vitro and in vivo. Eur Cell Mater 2014;27:281-97.

[34] Kondo N, Ogose A, Tokunaga K, Umezu H, Arai K, Kudo N, Hoshino M, Inoue H, Irie H, Kuroda K, Mera H, Endo N. Osteoinduction with highly purified beta-tricalcium phosphate in dog dorsal muscles and the proliferation of osteoclasts before heterotopic bone formation. Biomaterials 2006;27:4419-27.

[35] Kurashina K, Kurita H, Wu Q, Ohtsuka A, Kobayashi H. Ectopic osteogenesis with biphasic ceramics of hydroxyapatite and tricalcium phosphate in rabbits. Biomaterials 2002;23:407-12.

[36] Yuan H, Li Y, de Bruijn JD, de Groot K, Zhang X. Tissue responses of calcium phosphate cement: a study in dogs. Biomaterials 2000;21:1283-90.

[37] Yuan H, van Blitterswijk CA, de Groot K, de Bruijn JD. A comparison of bone formation in biphasic calcium phosphate (BCP) and hydroxyapatite (HA) implanted in muscle and bone of dogs at different time periods. J Biomed Mater Res A 2006;78:139-47.

[38] Wang L, Zhang B, Bao C, Habibovic P, Hu J, Zhang X. Ectopic osteoid and bone formation by three calcium-phosphate ceramics in rats, rabbits and dogs. PLoS One 2014;9:e107044.

[39] Davison NL, Yuan H, de Bruijn JD, Barrere-de Groot F. In vivo performance of microstructured calcium phosphate formulated in novel water-free carriers. Acta Biomater 2012;8:2759-69.

[40] Habibovic P, Gbureck U, Doillon CJ, Bassett DC, van Blitterswijk CA, Barralet JE. Osteoconduction and osteoinduction of low-temperature 3D printed bioceramic implants. Biomaterials 2008;29:944-53.

[41] Wang H, Zhi W, Lu X, Li X, Duan K, Duan R, Mu Y, Weng J. Comparative studies on ectopic bone formation in porous hydroxyapatite scaffolds with complementary pore structures. Acta Biomater 2013;9:8413-21.

[42] Zhang J, Luo X, Barbieri D, Barradas AMC, de Bruijn JD, van Blitterswijk CA, Yuan H. The size of surface microstructures as an osteogenic factor in calcium phosphate ceramics. Acta Biomater 2014;10:3254-63.

[43] Ripamonti U, Richter PW, Thomas ME. Self-inducing shape memory geometric cues embedded within smart hydroxyapatite-based biomimetic matrices. Plast Reconstr Surg 2007;120:1796-807.

[44] Rumpler M, Woesz A, Dunlop JW, van Dongen JT, Fratzl P. The effect of geometry on three-dimensional tissue growth. J R Soc Interface 2008;5:1173-80.

[45] Bidan CM, Kommareddy KP, Rumpler M, Kollmannsberger P, Bréchet YJ, Fratzl P, Dunlop JW. How linear tension converts to curvature: geometric control of bone tissue growth. PLoS One 2012;7:e36336.

[46] Bidan CM, Kommareddy KP, Rumpler M, Kollmannsberger P, Fratzl P, Dunlop JW. Geometry as a factor for tissue growth: towards shape optimization of tissue engineering scaffolds. Adv Healthc Mater 2013;2:186-94.

[47] Yuan H, van den Doel M, Li S, Van Blitterswijk CA, De Groot K, De Bruijn JD. A comparison of the osteoinductive potential of two calcium phosphate ceramics implanted intramuscularly in goats. J Mater Sci: Mater Med 2002;13:1271-5.

[48] Davison NL, Gamblin A-L, Layrolle P, Yuan H, de Bruijn JD, Barrère-de Groot F. Liposomal clodronate inhibition of osteoclastogenesis and osteoinduction by submicrostructured beta-tricalcium phosphate. Biomaterials 2014;35:5088-97.

[49] Chan O, Coathup MJ, Nesbitt A, Ho CY, Hing KA, Buckland T, Campion C, Blunn GW. The effects of microporosity on osteoinduction of calcium phosphate bone graft substitute biomaterials. Acta Biomater 2012;8:2788-94.

[50] Guo XY, Gough JE, Xiao P, Liu J, Shen ZJ. Fabrication of nanostructured hydroxyapatite and analysis of human osteoblastic cellular response. J Biomed Mater Res A 2007;82:1022-32.

[51] Li B, Chen XN, Guo B, Wang XL, Fan HS, Zhang XD. Fabrication and cellular biocompatibility of porous carbonated biphasic calcium phosphate ceramics with a nanostructure. Acta Biomater 2009;5:134-43.

[52] Hu J, Zhou Y, Huang L, Liu J, Lu H. Effect of nano-hydroxyapatite coating on the osteoinductivity of porous biphasic calcium phosphate ceramics. BMC Musculoskelet Disord 2014;15:114.

[53] Gosain AK, Song L, Riordan P, Amarante MT, Nagy PG, Wilson CR, Toth JM, Ricci JL. A 1-year study of osteoinduction in hydroxyapatite-derived biomaterials in an adult sheep model: part I. Plast Reconstr Surg 2002;109:619-30.

[54] McBeath R, Pirone DM, Nelson CM, Bhadriraju K, Chen CS. Cell shape, cytoskeletal tension, and RhoA regulate stem cell lineage commitment. Dev Cell 2004;6:483-95.

[55] Kilian KA, Bugarija B, Lahn BT, Mrksich M. Geometric cues for directing the differentiation of mesenchymal stem cells. Proc Natl Acad Sci U S A 2010;107:4872-7.

[56] Sadowska JM, Guillem-Marti J, Montufar EB, Espanol M, Ginebra MP. Biomimetic Versus Sintered Calcium Phosphates: The In Vitro Behavior of Osteoblasts and Mesenchymal Stem Cells. Tissue Eng Part A 2017; 23:1297-309.

[57] Danoux C, Pereira D, Döbelin N, Stähli C, Barralet J, van Blitterswijk C, Habibovic P. The Effects of Crystal Phase and Particle Morphology of Calcium Phosphates on Proliferation and Differentiation of Human Mesenchymal Stromal Cells. Adv Healthc Mater 2016;5:1775-85.

[58] Hesaraki S, Nazarian H, Pourbaghi-Masouleh M, Borhan S. Comparative study of mesenchymal stem cells osteogenic differentiation on low-temperature biomineralized nanocrystalline carbonated hydroxyapatite and sintered hydroxyapatite. J Biomed Mater Res B Appl Biomater 2014;102:108-18.

[59] Nagai H, Kobayashi-Fujioka M, Fujisawa K, Ohe G, Takamaru N, Hara K, Uchida D, Tamatani T, Ishikawa K, Miyamoto Y. Effects of low crystalline carbonate apatite on proliferation and osteoblastic differentiation of human bone marrow cells. J Mater Sci Mater Med 2015;26:99.

[60] Dellinger JG, Eurell JAC, Jamison RD. Bone response to 3D periodic hydroxyapatite scaffolds with and without tailored microporosity to deliver bone morphogenetic protein 2 J. Biomed Mater Res A 2005;76:366-37.

[61] Simon JL, Michna S, Lewis JA, Rekow ED, Thompson VP, Smay JE, Yampolsky A, Parsons JR, Ricci JL. In vivo bone response to 3D periodic hydroxyapatite scaffolds assembled by direct ink writing. J Biomed Mater Res A 2007;83:747-58.

[62] Lapczyna H, Galea L, Wüst S, Bohner M, Jerban S, Sweedy A, Doebelin N, van Garderen N, Hofmann S, Baroud G, Müller R, von Rechenberg B. Effect of grain size and microporosity on the in vivo behaviour of β-tricalcium phosphate scaffolds. Eur Cell Mater 2014;28:299-319.

[63] Bohner M, Baroud G, Bernstein A, Döbelin N, Galea L, Hesse B, Heuberger R, Meille S, Pascal M, von Rechenberg B, Sague J, Seeherman H. Characterization and distribution of mechanically competent mineralized tissue in micropores of β-tricalcium phosphate bone substitutes. Mater Today 2017;20:106-15.

[64] Polak SJ, Rustom LE, Genin GM, Talcott M, Wagoner Johnson AJ. A mechanism for effective cell-seeding in rigid, microporous substrates. Acta Biomater 2013;9:7977-86.

[65] Díez-Escudero A, Espanol M, Beats S, Ginebra MP. In vitro degradation of calcium phosphates: effect of multiscale porosity, textural properties and composition. Acta Biomater 2017;60:81-92.

[66] Ripamonti U, Klar RM, Renton LF, Ferretti C. Synergistic induction of bone formation by hOP-1, hTGF-beta3 and inhibition by zoledronate in macroporous coral-derived hydroxyapatites. Biomaterials 2010;31:6400-10.

[67] Garimella R, Tague SE, Zhang J, Belibi F, Nahar N, Sun BH, Insogna K, Wang J, Anderson HC. Expression and synthesis of bone morphogenetic proteins by osteoclasts: a possible path to anabolic bone remodeling. J Histochem Cytochem 2008;56:569-77.

[68] Pederson L, Ruan M, Westendorf JJ, Khosla S, Oursler MJ. Regulation of bone formation by osteoclasts involves Wnt/BMP signaling and the chemokine sphingosine-1-phosphate. Proc Natl Acad Sci USA 2008;105:20764-69.

[69] Klar RM, Duarte R, Dix-Peek T, Dickens C, Ferretti C, Ripamonti U. Calcium ions and osteoclastogenesis initiate the induction of bone formation by coral-derived macroporous constructs. J Cell Mol Med 2013;17:1444-57.

[70] Habibovic P, Juhl MV, Clyens S, Martinetti R, Dolcini L, Theilgaard N, van Blitterswijk CA. Comparison of two carbonated apatite ceramics in vivo. Acta Biomater 2010;6:2219-26.

[71] Stern J, Lewis WH. The colorimetric estimation of calcium in serum with ocresolphthalein complexone. Clin Chim Acta 1957;2:576-80.

[72] Gitelman JH. An improved automated procedure for the determination of calcium in biological specimens. Anal Biochem 1967;18:521-31.

Chapter 3

OSTEOGENESIS BY FOAMED AND 3D-PRINTED NANOSTRUCTURED CALCIUM PHOSPHATE SCAFFOLDS: EFFECT OF PORE ARCHITECTURE

3.1 Introduction

Bone has a high capacity for regeneration that is not, however, unlimited. When a bone defect exceeds a critical size, bone is not able to regenerate itself, it requires the use of a substrate, which can be natural or synthetic, to serve as a support and guide the action of bone regenerating cells.[1] While autograft is still the gold standard, the serious drawbacks associated with the need of a second surgery to harvest it and the limited availability,[2] has prompted the search for alternatives within synthetic materials. CaPs have been used since the 1970s for this application. They are osteoconductive materials and perform well in many situations. However, in very demanding situations they do not promote osteogenesis sufficiently. The combination of scaffolds with cells or growth factors has attracted much attention lately, although it raises ethical, logistic and economic concerns, besides suffering from poor reproducibility and patient variability.[3] An attractive alternative lies in having a deeper knowledge of the material-tissue interaction, which allows designing cell instructive biomaterials, capable of triggering the biological mechanisms behind the bone healing process.

In this context, endowing intrinsic osteoinductive properties to a synthetic bone substitute by tuning its physico-chemical and structural properties is one of the most challenging and, at the same time, promising tasks for the development of an ideal bone graft substitute that can replace autografts.[4] The design of new osteoinductive biomaterials should aim to develop biomimetic matrices that trigger the endogenous expression of osteogenic growth factors instead of adding expensive doses of exogenous growth factors[5] with the well-known associated risks.[6-9]

Although sintered CaP ceramics, including HA, β-TCP and BCP, have traditionally been the most widely used synthetic bone substitutes, their biological performance is still inferior to autografts, especially in terms of initiation of bone growth and simultaneous, synchronized material resorption.[4,10] This is probably associated with the high crystallinity and lack of nanostructure of sintered ceramics, which significantly differ from the non-stoichiometric, calcium-deficient (Ca/P molar ratio lower than 1.67) and low-crystalline form of the natural bone apatite.[11,12]

To overcome these limitations, biomimetic routes based on the self-setting reaction of CPCs constitute an ideal platform to mimic the composition and morphology of the bone mineral phase much better than sintered ceramics, obtaining low-crystalline, non-stoichiometric and nanostructured CDHA.[13] Moreover, our group has developed processing methods to obtain scaffolds with defined macroporous architectures while preserving the biomimetic nanostructure of the CDHA, such as 3D-printing by robocasting[14,15] or foaming.[16,17]

In the previous chapter (Chapter 2), we demonstrated in an *in vivo* canine study that both nanostructure and macropore geometry play a critical role in osteoinduction of CaPs.[18] Bone formation was significantly accelerated and stimulated when the scaffolds were implanted

intramuscularly in the shape of nanostructured biomimetic foams compared with the high-temperature microstructured counterparts. Moreover, in agreement with other studies that have highlighted the importance of geometrical factors like curvature in bone tissue regeneration,[19-21] we demonstrated that foamed scaffolds, with concave pores, induced a significantly higher amount of ectopic bone than 3D-printed scaffolds with orthogonal-shaped struts and therefore prismatic pores.[18]

The present study moves one step forward, since it aims at analyzing the effect of the geometrical features of nanostructured CaPs on their osteogenic potential and resorption behaviour in a bony environment. To this end, biomimetic CDHA scaffolds, with identical chemical composition and nanostructure but different macropore geometries and dimensions were evaluated in a canine orthotopic model. We hypothesized that the high osteoinductive, spherical, concave, macroporous, foamed scaffolds (CDHA-Foam) would have a superior bone healing capacity compared with the poorly osteoinductive prismatic, convex, macroporous, robocast scaffolds (CDHA-Rob).

3.2 Materials and Methods

3.2.1 Calcium deficient hydroxyapatite scaffolds

CDHA scaffolds were prepared according to previously described methods (Chapetr 2), based on the hydrolysis of α-TCP (α-$Ca_3(PO_4)_2$).[18]

Briefly, α-TCP was obtained by heating calcium hydrogen phosphate ($CaHPO_4$, Sigma-Aldrich, St. Louis, MO) and calcium carbonate ($CaCO_3$, Sigma-Aldrich, St. Louis, MO) at a 2:1 molar ratio for 15 h at 1400°C followed by quenching in air. Subsequently, the powder was milled in an agate ball mill (Pulverisette 6, Fritsch GmbB, Markt Einersheim, Germany) to a mean particle size of 2.8 μm.

The CDHA-Foams were obtained by foaming a mixture of a solid phase, consisting of 98 wt% α-TCP and 2 wt% of precipitated hydroxyapatite (PHA, Merck KGaA, Darmstadt, Germany), and an aqueous solution of 1 wt% Polysorbate 80 (Tween 80®,Sigma-Aldrich, St. Louis, MO) at a liquid to powder ratio of 0.65 mL/g using a customized hand mixer. The foam was transferred to Teflon cylindrical moulds (5 mm diameter and 10 mm height).

To obtain the robocast scaffolds, a CDHA self-setting ink was prepared containing a 30 wt% aqueous solution of poloxamer 407 (P2443 - Pluronic® F-127, Sigma-Aldrich, St. Louis, MO) and α-TCP powder, at a liquid to powder ratio of 0.65 g/g. A cylindrical CAD model of the scaffolds (5 mm diameter and 10 mm height) was designed (Solidworks 2014, Dassault Systèmes SolidWorks Corp., Waltham, MA) and converted to a STL 3D mesh, with a rectilinear pattern and an infill of 0.45. Scaffolds were printed using a robocasting device (Pastecaster, BCN3D Technologies, Barcelona, Spain) with two different nozzle diameters, 450 and 250 μm for the CDHA-Rob-450 and CDHA-Rob-250, respectively.

The transformation to CDHA, which results in the hardening of the scaffolds, was achieved by immersion of both the foams and the robocast scaffolds in deionized water at 37°C for 10 days, to allow for the hydrolysis reaction of α-TCP, according to the following reaction:

$$3\,Ca_3(PO_4)_2 + H_2O \rightarrow Ca_9(PO_4)_5(HPO_4)OH$$
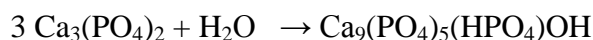
The architecture of the foamed and 3D-printed scaffolds was determined by micro-CT (SkyScan 1172, Bruker microCT, Kontich, Belgium) at a voltage of 90 kV and a current of 112 μA and with a Cu−Al filter. Images were acquired using an isotropic pixel size of 5 μm. Reconstruction of cross sections was done using software package NRecon (Bruker microCT, Kontich, Belgium). Calculations of macroporosity were performed with CTAn software (Bruker microCT, Kontich, Belgium). The microstructure was characterized by scanning electron microscopy (Zeiss Neon40 EsBCrossBeam, Zeiss, Oberkochen, Germany).

The compressive strength of the different scaffolds (n = 6 specimens per group) was measured using a Universal Testing Machine (Instron 8511, Instron, Norwood, MA) at a cross-head speed of 1 mm/min until fracture.

3.2.2 In vivo study

3.2.2.1 Animal model

All animal procedures in this study were performed in compliance with the Guide for Care and Use of Laboratory Animals[22] and the European Community Guidelines (Directive 2010/63/EU) for the protection of animals used for scientific purposes[23], and under the permission of the local animal ethics committee (CEAAH 2338). The study was performed on 12 adult beagle dogs (body weight 14-17 kg) purchased from a professional stock breeder (Isoquimen S.L., Barcelona, Spain). Animals were randomly divided into 2 groups of 6 dogs each, corresponding to two different experimental times (6 or 12 weeks), and acclimatized for 2 weeks prior to surgery.

Surgical procedures were carried out under standard anesthetic and analgesic protocols, as described in the previous chapter (Chapter 2).[18] For the orthotopic implantation, animals were placed in lateral recumbence and the left hind limb was clipped, scrubbed and draped for an aseptic surgery. Subsequently, the lateral aspect of the femur was approached by blunt dissection. Three round monocortical bone defects (5 mm diameter) were drilled under continuous irrigation of physiological saline and one of the above-mentioned scaffolds (5 mm diameter x 10 mm height) was inserted in each defect by press-fit. All scaffolds had previously been sterilized by gamma irradiation at a dose of 25 kG. One scaffold of each series was implanted in each dog (**Table 3.1**), the implant position being assigned according to a rotatory allocation system using a block design. The surgical wound was finally closed in layers.

Table 3.1. Summary of implanted scaffolds

Architecture	Codes	6 weeks	12 weeks
Foams	CDHA-Foam	6	6
Robocast	CDHA-Rob-450	6	6
	CDHA-Rob-250	6	6

Animals were allowed to full weight bearing and received a normal diet immediately after surgery. During the postoperative period, a NSAID, routinely used after orthopedic surgeries, was given to the animals for 7 days to prevent pain and inflammation. The animals were euthanized at 6 and 12 weeks postimplantation by an overdose of pentobarbital sodium, after sedation with medetomidine.

3.2.2.2 *Sample harvest and histological processing*

After explantation, samples were fixed in 4% neutral buffered formalin solution for 72 h and analyzed by micro-CT. After micro-CT scanning, tissue samples were dehydrated in an increasing series of ethanol solutions and embedded in four different graded mixtures of ethanol and methyl methacrylate resin (Technovit 7200, HeraeusKulzer GmbH, Hanau, Germany) under vacuum conditions. The specimens were subsequently photopolymerized resulting in blocks, which were divided along the longitudinal axis of the implant, and transverse to the femur in order to evaluate the full thickness of the cortical bone defect. One piece was sectioned and polished (EXAKT Cutting & Grinding System, EXAKT Advanced Technologies GmbH, Norderstedt, Germany) prior to sputtering the surface with carbon for BS-SEM analysis. The other piece was sliced and ground (Cutting & Grinding System, EXAKT Advanced Technologies GmbH, Norderstedt, Germany) to obtain histological sections (50 μm), which were stained with Goldner-Masson trichrome and toluidine blue for histological evaluation using light microscopy.

3.2.2.3 *Histology and histomorphometry*

Micro-CT analysis (SkyScan 1172, Bruker microCT, Kontich, Belgium) of bone-tissue samples was performed as described above with the exception of an isotropic pixel size of 10 μm. The micro-CT 3D quantification of new bone formation and scaffold degradation was performed following a previously established protocol,[24] using BS-SEM images as a reference for establishing the gray-scale intensity thresholds to differentiate bone and calcium phosphate biomaterials. The following parameters were quantified:

c) Percentage of newly formed bone within the monocortical bone defect:

% newly formed bone = (bone volume / initial available macropore volume) * 100

d) Percentage of scaffold degradation within the monocortical bone defect:

% scaffold degradation = [(initial scaffold volume – final scaffold volume) / initial scaffold volume] * 100

Both parameters were quantified only in the monocortical bone defect volume, without considering the intramedullarly portion of the scaffold. Moreover, the radius of each scaffold was divided into three equal segments, which define three concentric VOIs: outer, middle and inner VOI. The percentage of newly formed bone was calculated in each VOI, to assess the distribution of the new bone formation.

The BS-SEM observations (Zeiss Neon40 EsBCrossBeam, Zeiss, Oberkochen, Germany) were made at 20 kV to assess the localization and maturity of the newly formed bone based on morphology and the different contrast levels.

Stained histological sections were observed using a light microscope (Nikon Eclipse E800, Nikon Corp., Tokyo, Japan) fitted with a digital camera (ProgRes, Jenoptik AG, Jena, Germany) for a qualitative histological evaluation focused on the grade of peri-implant inflammatory reaction, fibrous-tissue infiltration and angiogenesis, as well as on the search for cell-mediated scaffold resorption evidences. Digital images were analyzed using an image analysis software (ProgResCapturePro, Jenoptik AG, Jena, Germany).

3.2.3 Statistical analysis

Histomorphometric results are presented as mean values ± standard error. All analyzed data were normally distributed according to Anderson-Darling and Kolmogorov-Smirnov tests and showed homogeneity of variances according to Levenne's and Barralet's tests. Statistical comparisons among experimental groups at each time point were performed using one-way repeated measures ANOVA followed by Tukey's post hoc test in GraphPad Prism software (GraphPad Software Inc., La Jolla, CA). A pair-wise comparison result of $p < 0.05$ was considered statistically significant.

3.3 Results

3.3.1 Materials characterization

The micro-CT reconstructions of the different scaffolds, as well as the nanostructures observed by SEM are shown in **Fig. 3.1A**. Similar nanostructures were observed for the CDHA-Foam, CDHA-Rob-450 and CDHA-Rob-250 with the typical entangled network of needle-like CDHA nanocrystals, which resulted in high SSA (**Fig. 3.1B**). All scaffolds presented similar macroporosity and total porosity, determined by MIP and micro-CT, although different pore sizes and, more markedly, different pore entrance sizes, which were larger for the robocast scaffolds, as determined in the previous study (Chapter 2) and summarized in **Fig. 3.1B**.[18] Moreover, similar compression strength values (around 5 MPa) were found for all scaffolds irrespective of their architecture (foamed vs. robocast) and the strand diameter in the robocast constructs (**Fig. 3.1C**).

3.3.2 In vivo results

Surgeries were uneventful and all animals completed a normal postoperative period without any clinical complication. All implanted scaffolds were retrieved and processed for histological evaluation. Histology showed mild peri-implant inflammatory reactions at both time points for all scaffolds. The cortical bone tissue became closely connected to all three types of scaffolds and no fibrous capsules were observed at the host cortical bone-material interfaces (**Fig. 3.2A/B/C**). All scaffolds showed a certain degree of loose fibrous-tissue infiltration within interconnected macropores, minimal in the foams and more pronounced in the robocast scaffolds, especially in the central areas of the defects (**Figure 3.2D/E/F**). A rich widespread blood vessel network was found in the macropores of all three groups, from small capillaries to medium size vessels, as shown in the Goldner-Masson trichrome stained sections (**Fig. 3.2G/H/I**).

A)

	Architecture	Nanostructure
CDHA-Foam	A1 2 mm	A4 1μm
CDHA-Rob-450	A2 2 mm	A5 1μm
CDHA-Rob-250	A3 2 mm	A6 1μm
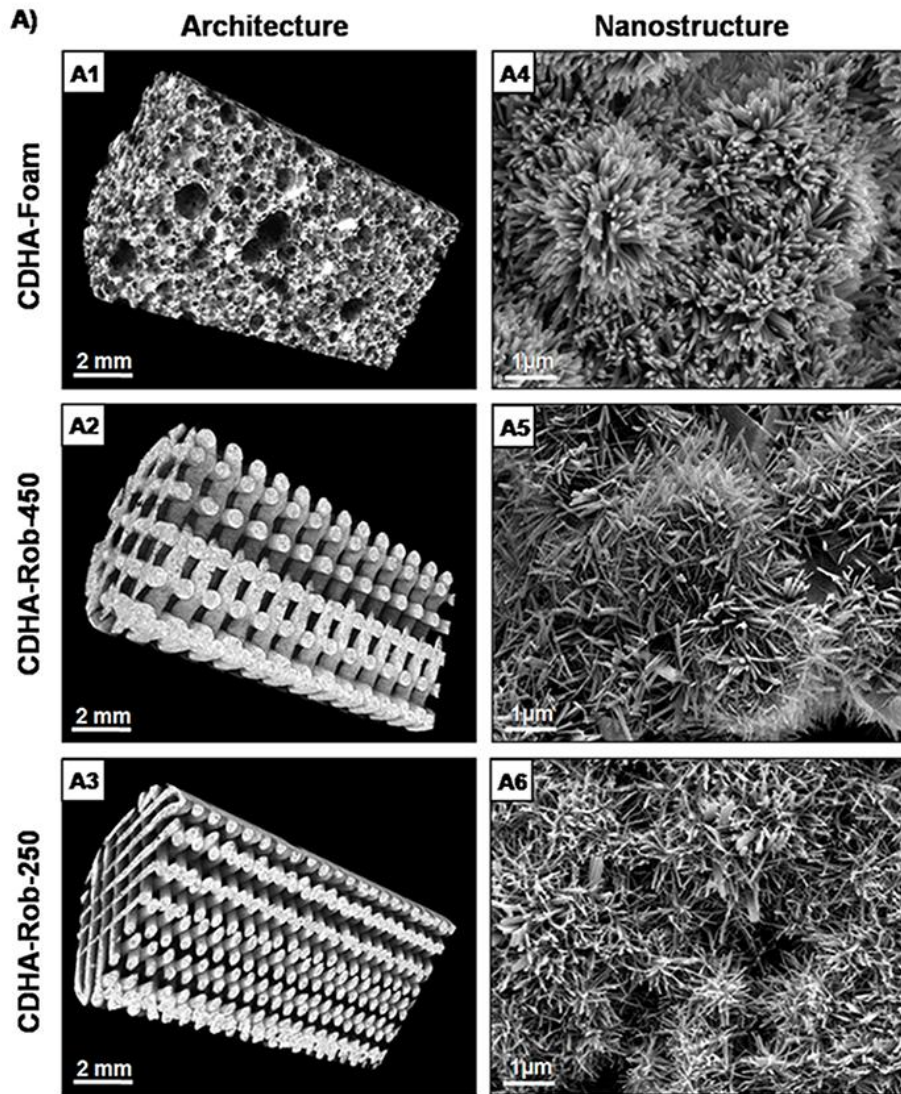
B) Porosity and SSA of the different scaffolds [Barba *et al* 2017]

Materials	Porosity					SSA (m²/g)
	% Total Porosity by MIP	% Macroporosity by MIP	% Macroporosity by micro-CT	Macropore entrance size by MIP (µm)	Macropore size by micro-CT (µm)	
CDHA-Foam	76.5	49.5	52.3	70	227.0	38.49
CDHA-Rob-450	64.8	46.5	47.4	350	409.7	32.02
CDHA-Rob-250	65.4	48.7	54.1	200	288.7	32.35

C) Compression Test

Figure 3.1. (A1,A2,A3) Micro-CT 3D reconstructions of the three implanted materials showing the different macropore shapes and sizes. Note the open and interconnected, spherical, concave macropores of different sizes in the CDHA-Foam group, whereas both robocast scaffolds present open and interconnected, prismatic, convex macropores with different strand diameters between groups and, hence, different pore sizes. **(A4,A5,A6)** Scanning electron micrographs of the three implanted materials showing similar nanostructures for all groups with the typical entangled network of needle-like CDHA nanocrystals. **(B)** Textural properties of the three implanted scaffolds: total porosity and macroporosity determined by mercury intrusion porosimetry (MIP), macroporosity measured by micro-CT, average entrance size of the macropores by MIP, average macropore size measured by micro-CT and specific surface area (SSA) determined by nitrogen adsorption.[18] **(C)** Compressive strength of the studied scaffolds.
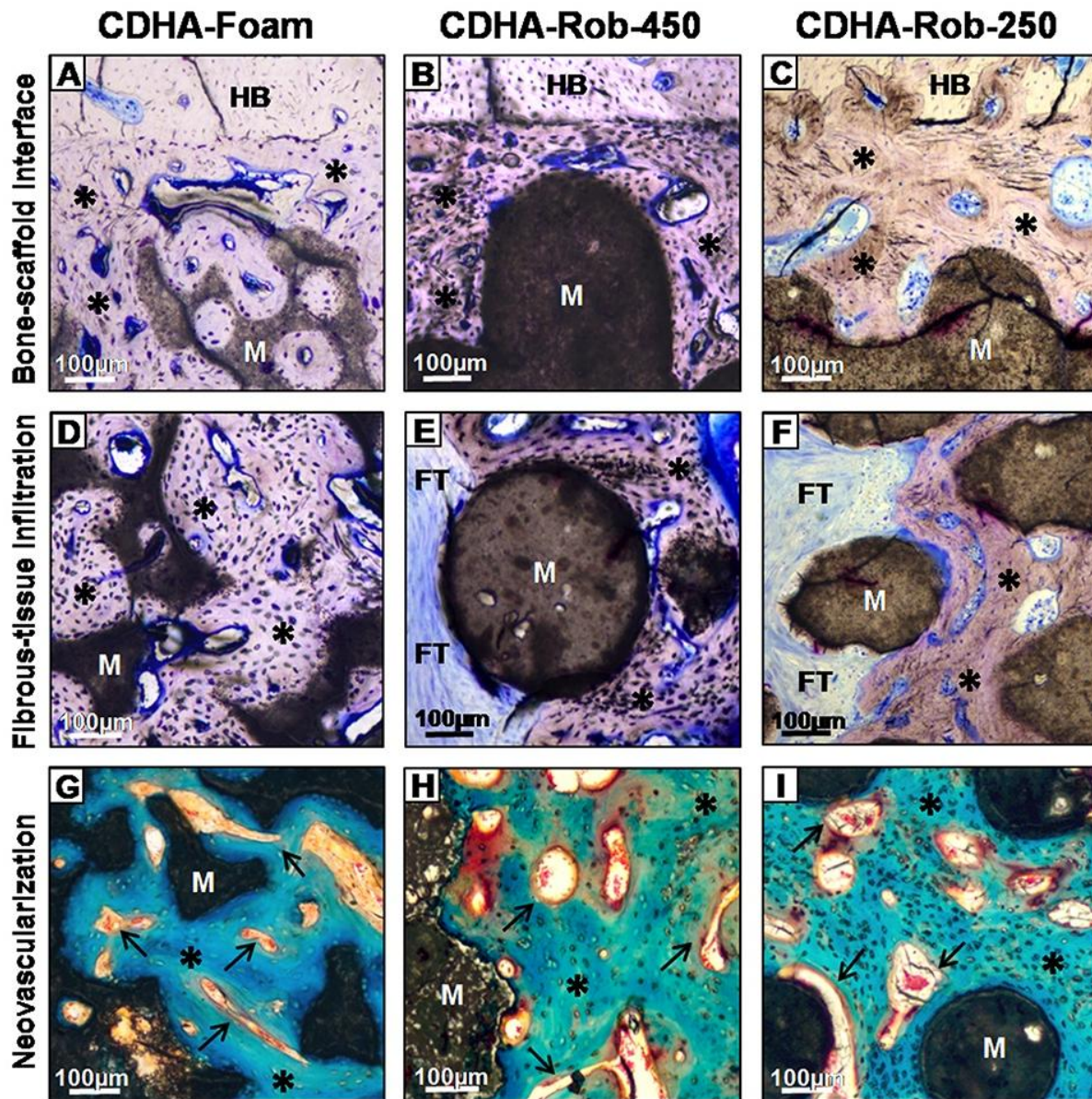
Figure 3.2. Micrographs of undecalcified sections of CDHA-Foam, CDHA-Rob-450 and CDHA-Rob-250 scaffolds after 6 weeks of implantation. **(A,B,C)** Toluidine blue stained sections showing the absence of fibrous-tissue interposition between the host cortical bone (HB) and material (M) in all three groups. Note the formation of well-mineralized bone matrix (asterisks) in close contact to all three materials. **(D,E,F)** Toluidine blue stained sections showing loose fibrous-tissue (FT) infiltration in the central regions of both robocast scaffolds, whereas no fibrous-tissue was detected within the macropores of the same region in the foams. M is material, and asterisks denote calcified bone matrix. **(G,H,I)** Goldner-Masson trichrome stained sections showing a rich widespread blood vessel (black arrows) network within the macropores of all three scaffolds. M is material, and asterisks denote calcified bone matrix.

The morphology of newly deposited bone, which consisted of a mix of woven bone with some areas of well organized lamellar bone following a Haversian pattern, was also similar for all groups (**Fig. 3.2** and **Fig. 3.3**). The main finding, however, was that CDHA-Foams promoted a higher penetration of the cortical bone, with new bone present in the centre of the scaffold already at 6 weeks, in contrast to the robocast scaffolds in which at this time point the new bone was penetrating into the scaffold only from the margin of the defect (**Fig. 3.3**).

Figure 3.3. Micro-CT 3D images and BS-SEM micrographs of the different scaffolds after 6 weeks of implantation. **(A)** Micro-CT 3D reconstruction, **(B)** Micro-CT section and **(C)** BS-SEM micrograph of a CDHA-Foam scaffold. Note the presence of newly formed bone in direct contact to the concave surfaces of spherical macropores in the centre of the defect aside from the centripetal new bone formation coming from the margins of the cortical defect. **(D)** Micro-CT 3D reconstruction, **(E)** Micro-CT section and **(F)** BS-SEM micrograph of a CDHA-Rob-450 scaffold. **(G)** Micro-CT 3D reconstruction, **(H)** Micro-CT section, and **(I)** BS-SEM micrograph of a CDHA-Rob-250 scaffold. Note the absence of new bone in the central region of the defect in the two robocast scaffolds, in which the newly formed bone is restricted to the peripheral areas of the scaffold, in the edges of the cortical defect.

These histological findings were confirmed by the histomorphometric results, summarized in **Fig. 3.4**. At 6 weeks the percentage of newly formed bone was significantly higher in the CDHA-Foam group than in the robocast groups (**Fig. 3.4A**). Regarding bone distribution within the scaffolds (**Fig. 3.4B**), the percentage of newly formed bone at 6 weeks was superior in all three VOIs for the foamed scaffolds compared with the robocast counterparts (**Fig. 3.4C**). The main difference was that small amounts of bone were detected in the robocast scaffolds within the middle and, especially, within the inner VOIs, whereas in the foamed scaffolds bone distribution was more homogeneous (**Fig. 3.4C**).
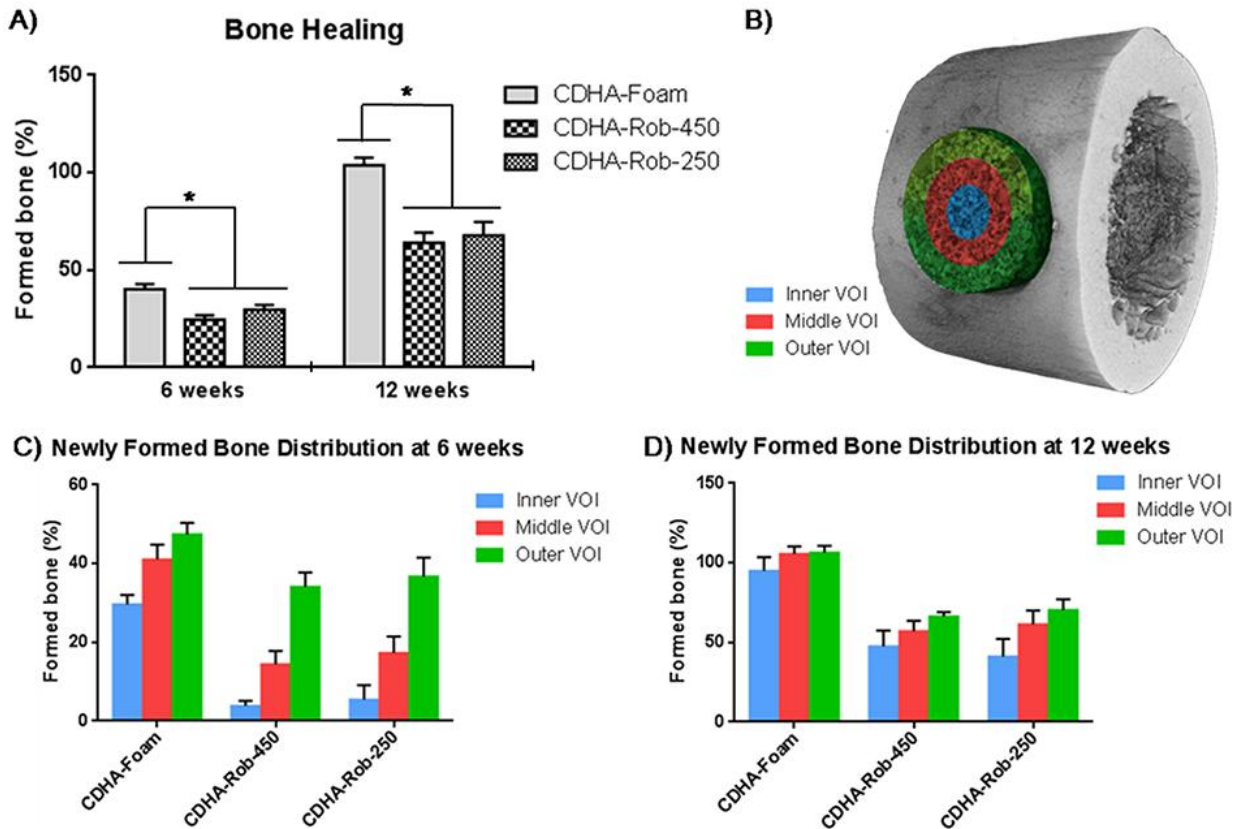
Figure 3.4. (A) Histomorphometrical results: percentage of newly formed bone within the monocortical bone defect at 6 and 12 weeks postimplantation, as measured by micro-CT. (*) denotes groups with statistically significant differences at the same time points (p < 0.05). **(B)** Diagram of the three volumes of interest (VOIs). The radius of each implanted scaffold was divided into three equal segments, which define three concentric VOIs: outer, middle and inner VOI. **(C)** Histomorphometrical results: percentage of newly formed bone within the three VOIs 6 weeks after implantation. Small amounts of bone were detected in the middle and inner VOIs in both robocast scaffolds, whereas in the foamed scaffolds bone distribution was more homogeneous, regardless of the VOIs. **(D)** Histomorphometrical results: percentage of newly formed bone within the three VOIs after 12 weeks of implantation.

The same trend was observed at 12 weeks, with newly formed bone increasing both in quantity and maturity for all groups (**Fig. 3.4A** and **Fig. 3.5**). CDHA-Foams showed a full-thickness cortical bone bridging while some gaps were still observed in the central regions of the bone defects in most robocast scaffolds (**Fig. 3.5**). The histomorphometrical results showed a significantly larger amount of newly formed bone in the CDHA-Foam group than in CDHA-Rob-450 and CDHA-Rob-250 groups (**Fig. 3.4A**). No significant differences were found between the two robocast groups despite the different macropore sizes, similarly to what happened at 6 weeks. Bone distribution between the inner, middle and outer VOIs was more homogeneous than it was at 6 weeks for all scaffolds, including the robocast ones (**Fig. 4D**).
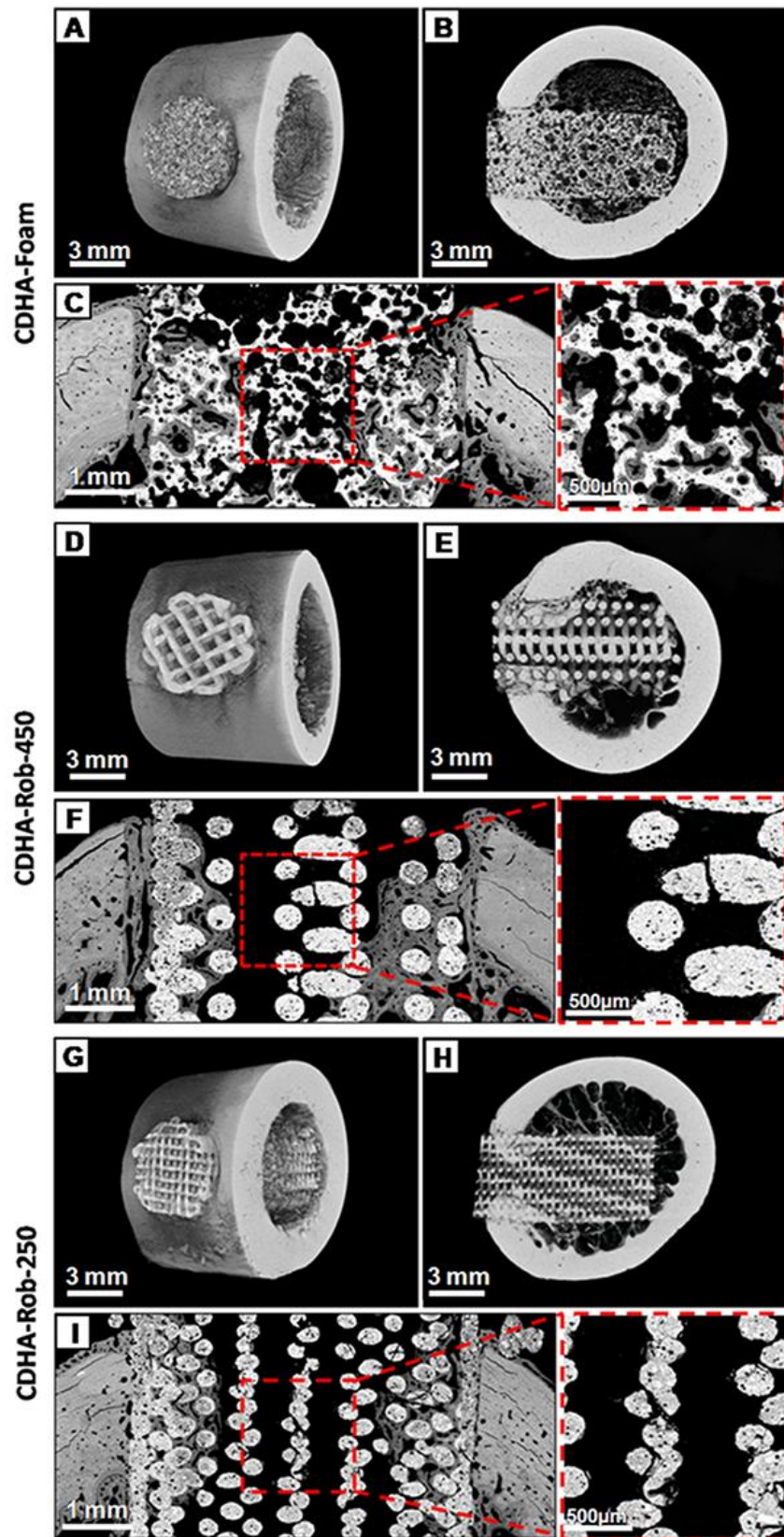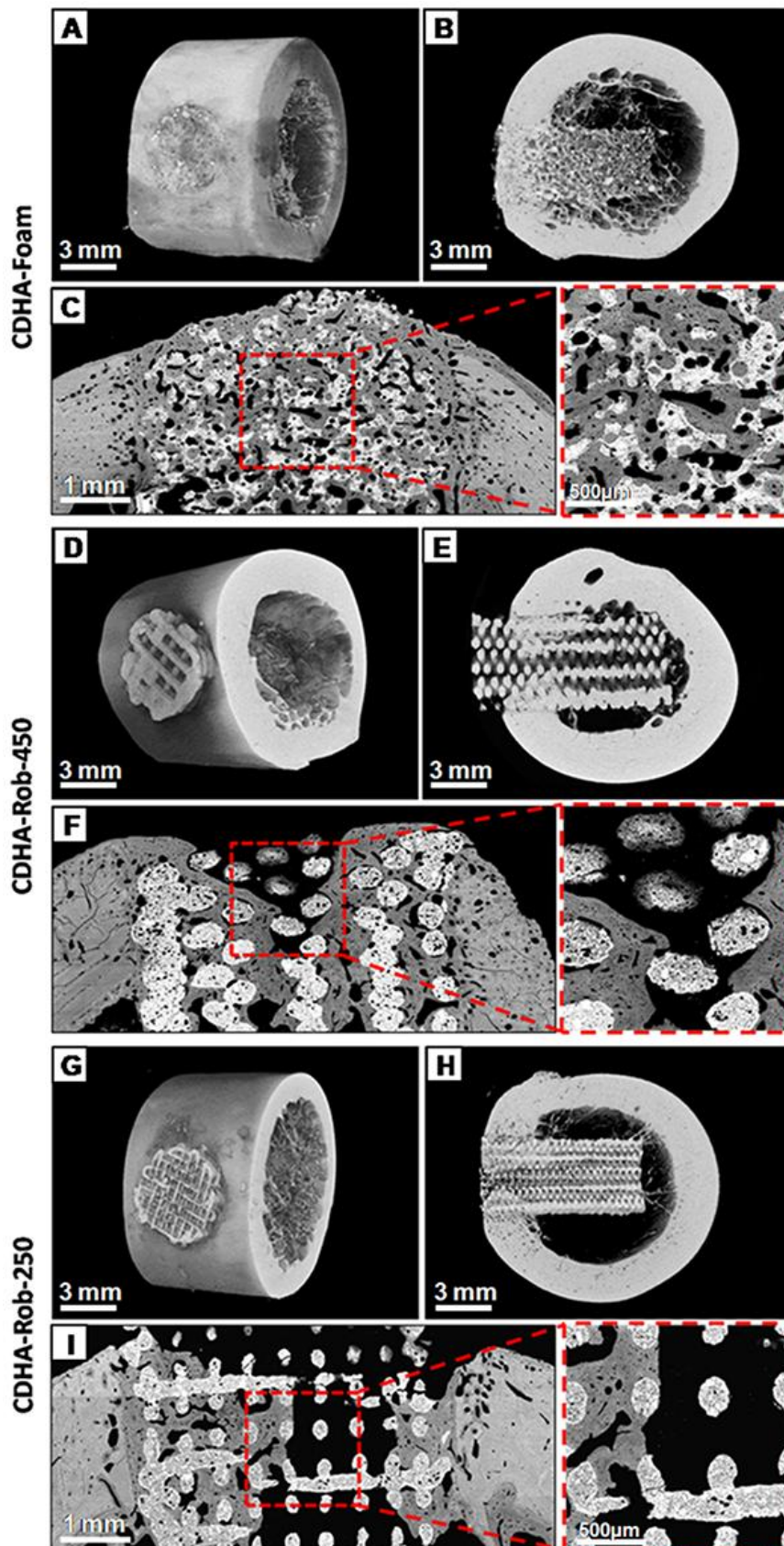
Figure 3.5. Micro-CT 3D images and BS-SEM micrographs of the different scaffolds after 12 weeks of implantation. **(A)** Micro-CT 3D reconstruction, **(B)** Micro-CT section and **(C)** BS-SEM micrograph of a CDHA-Foam scaffold showing a full-thickness cortical bone bridging and a significant resorption of the scaffold. **(D)** Micro-CT 3D reconstruction, **(E)** Micro-CT section and **(F)** BS-SEM micrograph of a CDHA-Rob-450 scaffold. Note the gap in the central region of the cortical defect. **(G)** Micro-CT 3D reconstruction, **(H)** Micro-CT section and **(I)** BS-SEM micrograph of a CDHA-Rob-250 scaffold showing the incomplete bone bridging after 12 weeks of implantation.

Additionally, new bone formation was observed also in the intramedullary portion of the scaffold in the case of CDHA-Foam, while no bone was observed in the robocast scaffolds, as shown in **Fig. 3.6**.
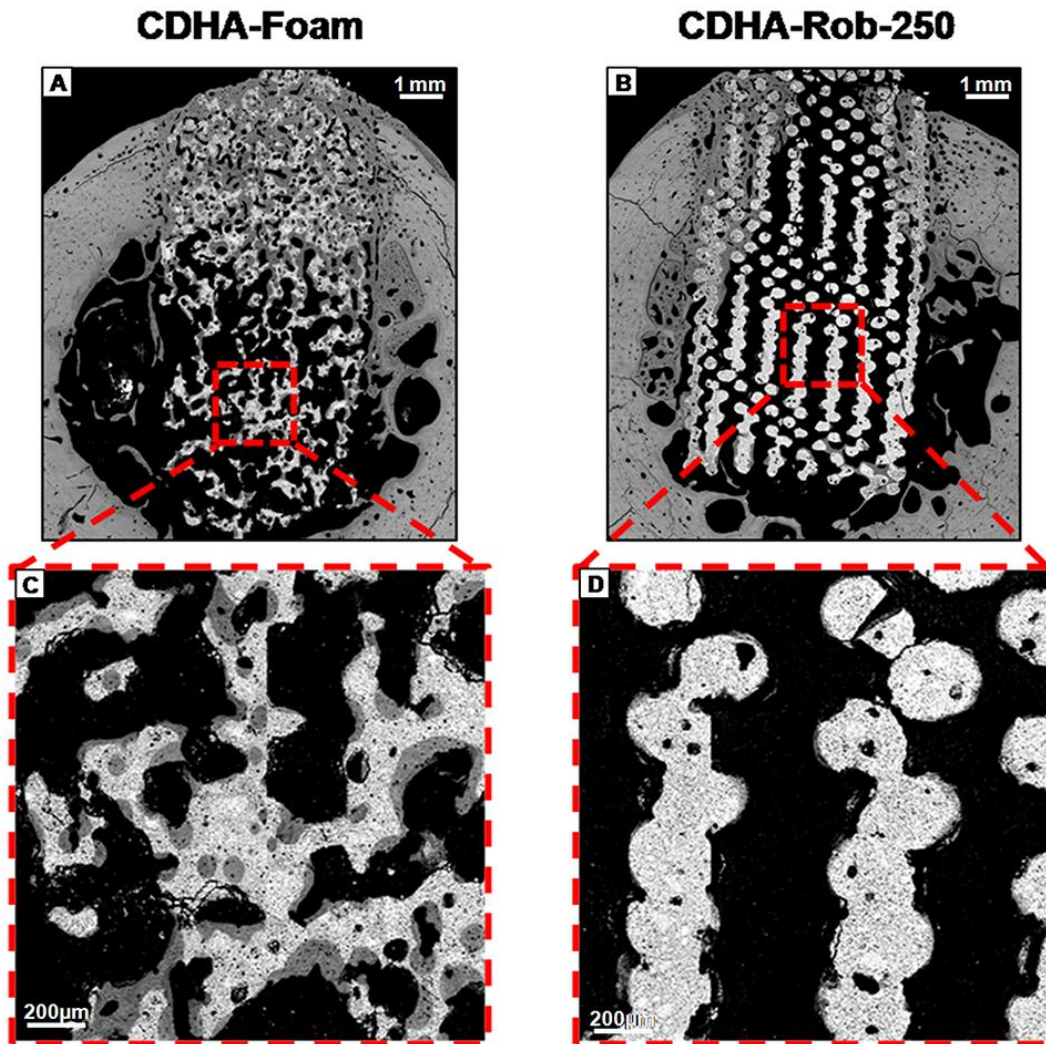
Figure 3.6. BS-SEM micrographs of a CDHA-Foam scaffold **(A)** and of a CDHA-Rob-250 **(B)** after 12 weeks of implantation. Note the presence of new bone formation in close contact to the concave surfaces of the central macropores in the intramedullary portion of the foamed scaffold **(C)**, whereas no bone is observed within the central macropores of the same region in the robocast scaffold **(D)**.

The micro-CT quantitative analysis of scaffold degradation is summarized in **Fig. 3.7A**. A significantly higher degradation was found for the CDHA-Foams compared with the robocast scaffolds at 12 weeks postimplantation, while no significant differences were found at 6 weeks. The resorption of robocast scaffolds did not progress among the 6 and 12 week time point (**Fig. 3.7A**). Histological images showed that both foamed and robocast scaffolds sustained cell-mediated degradation as revealed by the presence of cutting cones in close contact with the materials and the consistent observation of multinucleated osteoclast-like cells eroding the materials in all groups (**Fig. 3.7B**). Morphologies compatible with typical Howship's Lacunae were clearly observed in the three scaffolds, as shown in **Fig. 3.7B**. A greater amount of osteoclast-like cells were observed in the CDHA-Foams than in the robocast samples, especially 12 weeks after implantation.
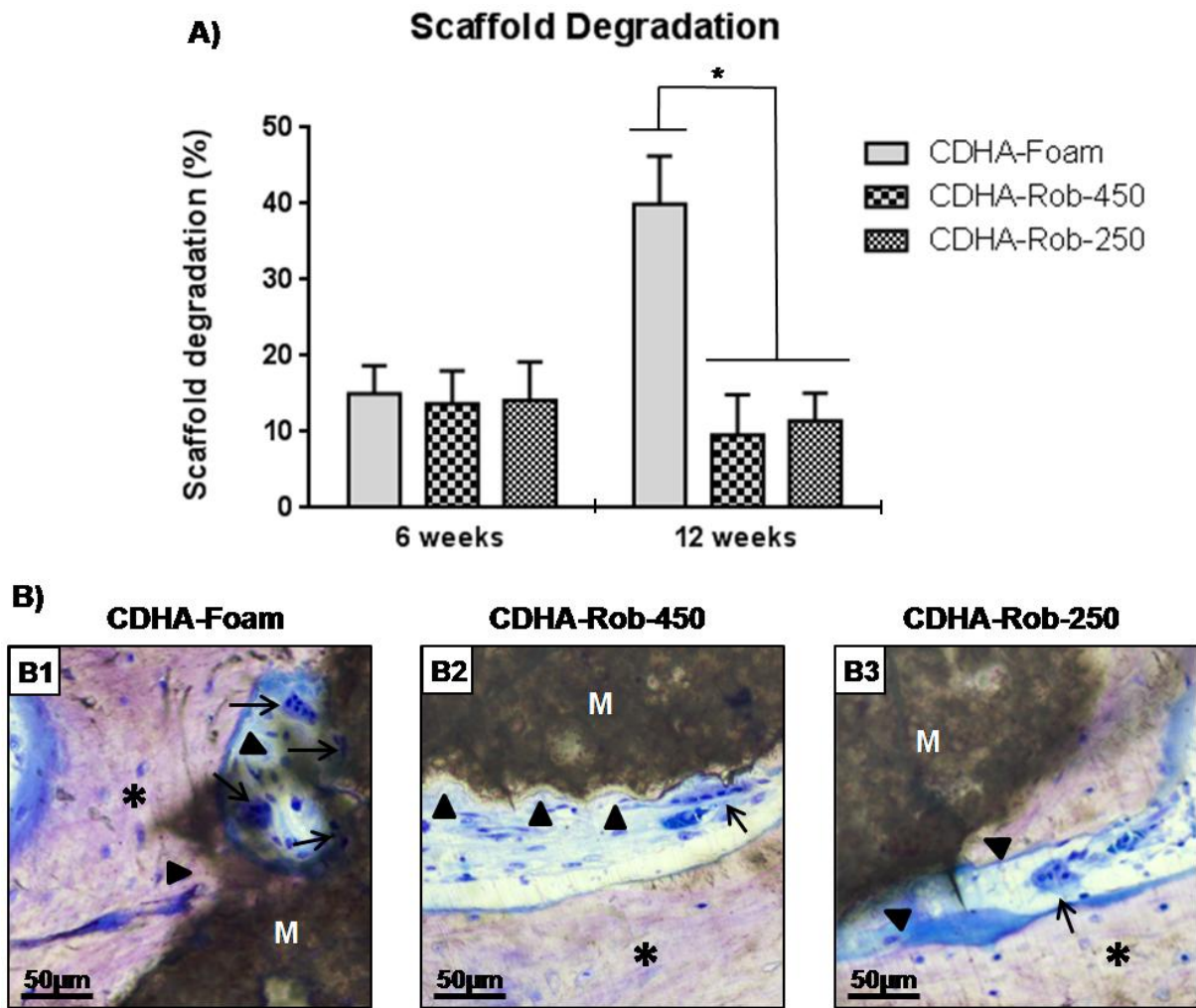
Figure 3.7. Scaffold degradation. **(A)** Histomorphometry results: percentage of scaffold degradation after 6 and 12 weeks of implantation. (*) denotes groups with statistically significant differences at the same time point (p < 0.05). **(B)** Micrographs of undecalcified toluidine blue stained sections after 12 weeks of implantation of studied scaffolds: (B1) CDHA-Foam, (B2) CDHA-Rob-450, (B3) CDHA-Rob-250. Note the presence of the typical resorption pits (black arrow heads) in the material surfaces, known as Howship's Lacunae, eroded by active multinucleated osteoclast-like cells (black arrows) in all three groups, being more numerous in the CDHA-Foam. M is material, and asterisks denote calcified bone matrix.

3.4 Discussion

The aim of the present study was to assess the relevance of macropore geometry in the osteogenic potential and degradation of nanostructured biomimetic CaP scaffolds. The interest of these materials was highlighted in the previous study (Chapter 2),[18] in which we demonstrated a synergistic effect between nanostructure and pore architecture with regards to osteoinduction, i.e., the capacity to produce bone in a non-osseous environment, which is associated with the differentiation of progenitor cells to the osteogenic lineage. Therein, nanostructured CDHA-Foams, with concave macropores, exhibited an accelerated and enhanced osteoinduction when compared with nanostructured 3D-printed CDHA scaffolds (CDHA-Rob).[18] The correlation between the intrinsic osteoinduction and the osteogenic potential in an osseous environment was also the subject of the present study.

3.4.1 Biocompatibility and angiogenesis

The histological evaluation of the samples showed the host cortical bone directly connected to all scaffolds with no evidence of fibrous encapsulation neither foreign body reaction (**Fig. 3.2A/B/C**), which confirmed the good biocompatibility of the CDHA-based biomaterials, as observed in previous ectopic[18,25] and orthotopic[12,25-31] studies.

However, a certain degree of loose fibrous-tissue infiltration, coming from the soft tissues in contact with the external surface of the scaffold was observed in all groups since guided bone regeneration membranes were not used to protect the bone defect from soft tissue invasion. It is worth mentioning, however, that fibrous-tissue infiltration was significantly more extensive within the central macropores of the robocast samples than that observed in the foams (**Fig. 3.2D/E/F**). This finding can probably be associated with the linear geometry and larger macropore entrance size of these scaffolds (**Fig. 3.1B**) compared with the foamed scaffolds, and suggests that the smaller pore entrance size of the CDHA-Foam scaffolds (70 μm) together with their more tortuous morphology prevent fibrous tissue colonization into the bone defect guiding the bone healing more effectively. This could partly explain the lower values of newly formed bone and, especially, the lack of new bone formation in the central regions of the robocast scaffolds compared with the CDHA-Foam group at 6 weeks.

Abundant neovascularization was found, homogeneously distributed within the macropores of all three scaffolds (**Fig. 3.2G/H/I**), enabled by the open and highly interconnected macroporosity both in the foamed and the robocast scaffolds. Angiogenesis is in fact one of the top priorities in bone tissue engineering, since it provides oxygen and nutrient supply to the bone forming cells, it represents the main access pathway of cells (inflammatory cells, stem cells) and soluble proteins (signalling molecules and osteogenic growth factors), and it is a source of undifferentiated cells called vascular pericytes, that can potentially differentiate into osteogenic lineage cells.[5,10]

3.4.2 Effect of macropore architecture on osteoinduction and osteoconduction

The histomorphometrical results showed a significantly higher percentage of new bone formation in the CDHA-Foams than in the robocast scaffolds at both time points (**Fig. 3.4A**). Considering that the foamed and the robocast scaffolds shared the same chemical composition (CDHA), a similar percentage of total porosity (around 70%), a similar nanostructure (needle-like crystals) and a similar SSA (around 35 m^2/g) (**Fig. 3.1**), the differences observed in their bone healing capacity can be attributed to the different macropore architectures (**Fig. 3.1A**).

It is worth noting that, while abundant bone ingrowth was observed in the outer VOI in all three groups, proving excellent osteoconductive properties, very small amounts of bone were detected in the central macropores of the robocast scaffolds at 6 weeks (**Fig. 3.3** and **Fig. 3.4C**). However, a significant amount of new bone was observed in the central areas of the CDHA-Foams at this time point (**Fig. 3.3** and **Fig. 3.4C**). Likewise, new bone was found within the central macropores of the intramedullary portion of CDHA-Foams (**Fig. 3.6A**), far from the host cortical bone regeneration front, whereas no bone was observed within the prismatic macropores of the intramedullary portion of robocast scaffolds (**Fig. 3.6B**). Although, it cannot be ruled out that the better performance of foamed scaffolds could derive from an increased osteoconductive capacity, the higher osteoinductive potential demonstrated previously[18] (Chapter 2) for the foamed

scaffolds compared with the robocast scaffolds suggest that osteoinduction could be the underlying mechanism of bone formation in these specific sites. The osteoinductive phenomena, thus, would contribute directly to the higher osteogenesis of the CDHA-Foams when implanted in a bony site. A similar correlation between osteoinduction and osteogenic capacity was previously reported by other authors evaluating sintered ceramics.[32-35]

Although the same trend was observed at 12 weeks, the differences among the outer VOI versus the middle and inner VOIs in the robocast scaffolds were less pronounced than those observed at 6 weeks (**Fig. 3.4C/D**), probably because the high osteoconductivity of the robocast scaffolds compensated for the lack of osteoinductive capacity, highlighting the contribution of both osteoconduction and osteoinduction in the total bone formation.

Regarding the role of pore geometry on bone formation, our results seem to be in contradiction with previous studies that reported better bone healing capacities for scaffolds with prismatic macropores with convex[36] or flat[37] surfaces, obtained by rapid prototyping techniques (robocasting and microstereolithography) than for constructs with spherical macropores with concave surfaces obtained by conventional processing methods like salt leaching or gas foaming processes.[36,37] However, in both orthotopic studies the authors attributed the lower bone healing capacity of the scaffolds with concave macropores to their limited interconnectivity, and consequently their lower osteoconductive potential. Therefore, the different macropore interconnectivity and the lack of characterization of other parameters such as microstructure and the surface topography in those studies prevented the identification of the real role of macropore geometry on the osteogenic capacity of these scaffolds.

Regarding the role of pore size on bone healing capacity, it is difficult to compare foamed and robocast scaffolds due to the different pore geometry. Whereas in the foams pore entrance size is much smaller than pore size (bottle neck effect), this is not the case in robocast scaffolds. When comparing CDHA-Rob-450 and CDHA-Rob-250, which had different pore sizes, no differences were found in terms of the amount and distribution of newly formed bone. In accordance to these findings, some authors reported bone ingrowth in 3D-printed scaffolds with pore sizes in the same range to the ones tested in the present study to be largely independent of the rod diameter[38,39] and the distance between rods.[38]

3.4.3 Effect of macropore architecture on scaffold resorption and osteoclastogenesis

Pore architecture also had a significant effect on the degradation of the biomimetic scaffolds. CDHA-Foams underwent a four times greater degradation than the biomimetic robocast scaffolds after 12 weeks of implantation (**Fig. 3.7A**), which was in line with the previous study where the same scaffolds were implanted intramuscularly (Chapter 2).[18] Interestingly, this high degradation rate was coupled with the high osteogenic potential of the CDHA-Foams, allowing a synchronization that led to the progressive replacement of the scaffold by new bone (**Fig. 3.5** and **Fig. 3.6**). This explains why at 12 weeks the percentage of newly formed bone within the initial macropore volume was over a hundred per cent (**Fig. 3.4A**), since the final macropore volume was larger than the initial macropore volume and it was almost completely filled with new bone. In contrast, the new bone in the robocast scaffolds was deposited on the surface of the scaffold struts, with limited degradation, which did not increase between 6 and 12 weeks (**Fig. 3.5**).

The fact that the physiological fluid is supersaturated with respect to CDHA, together with the presence of cutting cones in close contact with the scaffolds and the consistent observation of multinucleated osteoclast-like cells eroding the materials in all groups point to a cell-mediated degradation rather than a passive degradation (chemical physiologic dissolution), which is in agreement with previous *in vivo* studies with CDHA-based biomaterials.[18,25-28,31] Moreover, it is worth highlighting that the histological assessment identified a higher number of osteoclast-like cells in the concavities of the CDHA-Foams compared to the prismatic convex macropores of the robocast scaffolds. These results are again in agreement with the previous ectopic implantation study[18] (Chapter 2) and demonstrate that osteoclast-like cells activity and consequently, the degradation rate, are strongly influenced by the geometry of the macropores.

The superior osteoclast activity observed in the CDHA-Foams could also be an explanation for their superior osteoinductive potential and, hence, the superior bone healing capacity compared with the robocast scaffolds. The active involvement of osteoclasts in osteoinduction has been demonstrated in previous studies by the reduced ectopic bone formation and a decreased BMP expression by osteoinductive CaP biomaterials when treated with bisphosphonate, an osteoclast inhibitor.[40-42]

The fostering of bone formation by CDHA-Foams can, therefore, be associated with the concave macropores, with small entrance sizes and nanostructured walls, which provide the adequate microenvironment that may act as a powerful attractant for macrophages and trigger osteoclastogenesis. In turn, the retention within this volume of both osteogenic growth factors secreted by active osteoclasts (BMPS, Wnts, S1P, OSM, PDGF-BB and CTHRC1)[42-48] and calcium and phosphate ions resulting from the osteoclastic resorption of CaP materials[49-54] are known to trigger not only the activity of osteoblasts but also the differentiation of MSCs into bone-forming cells, leading eventually to *de novo* bone formation.

The results obtained in this study, far from going against 3D-printing, a technology that enables the fast fabrication of patient-specific complex bone grafts, stress the importance of pushing the enormous possibilities of this technique in the right direction. Its great versatility allows exerting a superior control of the architecture of the constructs that are obtained. It is important to take advantage of this feature to design the right pore geometry, looking for concave surfaces that allow having the optimum microenvironment to trigger the bone healing mechanisms. While in the present work we chose the simplest pattern with orthogonal struts, the osteogenic potential of other patterns, with more complex internal geometries should be assessed in future studies.

3.5 Conclusions

Pore geometry plays a crucial role in the *in vivo* performance of biomimetic CDHA-based bone substitutes. Both bone formation and material degradation of chemically identical materials with the same nanostructure and similar pore volumes were drastically affected by the macropore architecture of the scaffolds. Whereas CDHA was highly osteoconductive both in the robocast and foamed scaffolds, the superior bone healing capacity of the foamed scaffolds with spherical concave macropores correlated well with their higher intrinsic osteoinductive potential. The contribution of both osteoconduction and osteoinduction accelerated the complete healing of the bone defects. Moreover, the foamed scaffolds showed a superior resorption to the robocast

constructs, triggering the simultaneous and progressive scaffold replacement by new bone. The different macropore size between the two robocast scaffolds did not have a significant effect neither on new bone formation nor on degradation. Overall, the high osteogenic potential of this new family of biomimetic nanostructured CDHA foams makes them a very attractive alternative, safer and more affordable than the use of exogenous growth factors and cell-based therapies. The next step towards the clinical application would be to test its efficacy in a large segmental bone defect.

3.6 References

[1]   Giannoudis PV, Dinopoulos H, Tsiridis E. Bone substitutes: an update. Injury 2005;36:20-7.

[2]   Younger EM, Chapman MW. Morbidity at bone graft donor sites. J Orthop Trauma 1989;3:92-5.

[3]   Habraken W, Habibovic P, Epple M, Bohner M. Calcium phosphates in biomedical applications: materials for the future? Mater Today 2016;19:69-87.

[4]   Habibovic P. Strategic Directions in Osteoinduction and Biomimetics. Tissue Eng Part A 2017;23:1295-96.

[5]   Ripamonti U, Roden LC, Ferretti C, Klar RM. Biomimetic matrices self-initiating the induction of bone formation. J Craniofac Surg 2011;22:1859-70.

[6]   Garrison KR, Donell S, Ryder J, Shemilt I, Mugford M, Harvey I, Song F. Clinical effectiveness and cost-effectiveness of bone morphogenetic proteins in the non-healing of fractures and spinal fusion: a systematic review. Health Technol Assess 2007;11:1-150.

[7]   Shields LB, Raque GH, Glassman SD, Campbell M, Vitaz T, Harpring J, Shields CB. Adverse effects associated with high-dose recombinant human bone morphogenetic protein-2 use in anterior cervical spine fusion. Spine (Phila Pa 1976) 2006;31:542-7.

[8]   Argintar E, Edwards S, Delah, J. Bone morphogenetic proteins in orthopaedic trauma surgery. Injury 2011;42:730-4.

[9]   Zara JN, Siu RK, Zhang X, Shen J, Ngo R, Lee M, Li W, Chiang M, Chung J, Kwak J, Wu BM, Ting K, Soo C. High doses of bone morphogenetic protein 2 induce structurally abnormal bone and inflammation in vivo. Tissue Eng Part A 2011;17:1389-99.

[10]   Barradas AMC, Yuan H, van Blitterswijk CA, Habibovic P. Osteoinductive biomaterials: current knowledge of properties, experimental models and biological mechanisms. Eur Cell Mater 2011;21:407-29.

[11]   Wopenka B, Pasteris JD. A mineralogical perspective on the apatite in bone. Mater Sci Eng C 2005;25:131-43.

[12]   Sponer P, Strnadová M, Urban K. In Vivo Behaviour of Low-temperature calcium-deficient hydroxyapatite: comparison with deproteinised bovine bone. Int Orthop 2011;35:1553-60.

[13]   Ginebra MP, Espanol M, Montufar EB, Perez RA, Mestres G. New processing approaches in calcium phosphate cements and their applications in regenerative medicine. Acta Biomater 2010;6:2863-73.

[14]   Maazouz Y, Montufar EB, Malbert J, Espanol M, Ginebra MP. Self-hardening and thermoresponsive alpha tricalcium phosphate/pluronic pastes. Acta Biomater 2017;49:563-74.

[15]   Maazouz Y, Montufar EB, Guillem-Marti J, Fleps I, Öhman C, Persson C, Ginebra MP. Robocasting of biomimetic hydroxyapatite scaffolds using self-setting inks. J Mater Chem B 2014;2:5378-86.

[16]   Montufar EB, Traykova T, Gil C, Harr I, Almirall A, Aguirre A, Engel E, Planell JA, Ginebra MP. Foamed surfactant solution as a template for self-setting injectable hydroxyapatite scaffolds for bone regeneration. Acta Biomater 2010;6:876-85.

[17]   Pastorino D, Canal C, Ginebra MP. Drug delivery from injectable calcium phosphate foams by tailoring the macroporosity-drug interaction. Acta Biomater 2015;12:250-9.

[18]   Barba A, Diez-Escudero A, Maazouz Y, Rappe K, Espanol M, Montufar EB, Bonany M, Sadowska JM, Guillem-Marti J, Öhman-Mägi C, Persson C, Manzanares MC, Franch J, Ginebra MP. Osteoinduction by Foamed and 3D-Printed Calcium Phosphate Scaffolds: Effect of Nanostructure and Pore Architecture. ACS Appl Mater Interfaces 2017;9:41722-36.

[19]   Ripamonti U, Crooks J, Kirkbride AN. Sintered porous hydroxyapatites with intrinsic osteoinductive activity: geometric induction of bone formation. S Afr J Sci 1999;95:335-43.

[20]   Bidan CM, Kommareddy KP, Rumpler M, Kollmannsberger P, Bréchet YJ, Fratzl P, Dunlop JW. How linear tension converts to curvature: geometric control of bone tissue growth. PLoS One 2012;7:e36336.

[21]   Bidan CM, Kommareddy KP, Rumpler M, Kollmannsberger P, Fratzl P, Dunlop JW. Geometry as a factor for tissue growth: towards shape optimization of tissue engineering scaffolds. Adv Healthc Mater 2013;2:186-94.

[22]   National Research Council. Guide for the Care and Use of Laboratory Animals; National Academy Press: Washington, DC, 1996; pp 41-194.

[23]   Directive 2010/63/EU of the European Parliament and of the Council of 22 September 2010 on the Protection of Animals Used for Scientific Purposes. Available at http://data.europa.eu/eli/dir/2010/63/oj.

[24]   Lewin S, Barba A, Persson C, Franch J, Ginebra MP, Öhman-Mägi C. Evaluation of bone formation in calcium phosphate scaffolds with μCT – method validation using SEM. Biomed Mater 2017;12:65005.

[25]   Yuan H, Li Y, de Bruijn JD, de Groot K, Zhang X. Tissue responses of calcium phosphate cement: a study in dogs. Biomaterials 2000;21:1283-90.

[26]   Bourgeois B, Laboux O, Obadia L, Gauthier O, Betti E, Aguado E, Daculsi G, Bouler JM. Calcium-deficient apatite: a first in vivo study concerning bone ingrowth. J Biomed Mater Res A 2003;65:402-8.

[27]   Okuda T, Ioku K, Yonezawa I, Minagi H, Gonda Y, Kawachi G, Kamitakahara M, Shibata Y, Murayama H, Kurosawa H, Ikeda T. The slow resorption with replacement by bone of a hydrothermally synthesized pure calcium-deficient hydroxyapatite. Biomaterials 2008;29:2719-28.

[28]   Gonda Y, Ioku K, Shibata Y, Okuda T, Kawachi G, Kamitakahara M, Murayama H, Hideshima K, Kamihira S, Yonezawa I, Kurosawa H, Ikeda T. Stimulatory effect of hydrothermally synthesized biodegradable hydroxyapatite granules on osteogenesis and direct association with osteoclasts. Biomaterials 2009;30:4390-400.

[29]   Guo H, Su J, Wei J, Kong H, Liu C. Biocompatibility and osteogenicity of degradable ca-deficient hydroxyapatite scaffolds from calcium phosphate cement for bone tissue engineering. Acta Biomater 2009;5:268-78.

[30] Ambrosio L, Guarino V, Sanginario V, Torricelli P, Fini M, Ginebra MP, Planell JA, Giardino R. Injectable calcium-phosphate-based composites for skeletal bone treatments. Biomed Mater 2012;7:024113.

[31] Cuzmar E, Perez RA, Manzanares MC, Ginebra MP, Franch J. In vivo osteogenic potential of biomimetic hydroxyapatite/collagen microspheres: comparison with injectable cement pastes. PLoS One 2015;10:e0131188.

[32] Yuan H, van Blitterswijk CA, de Groot K, de Bruijn JD. A comparison of bone formation in biphasic calcium phosphate (BCP) and hydroxyapatite (HA) implanted in muscle and bone of dogs at different time periods. J Biomed Mater Res A 2006;78:139-47.

[33] Habibovic P, Yuan H, van den Doel M, Sees TM, van Blitterswijk CA, de Groot K. Relevance of osteoinductive biomaterials in critical-sized orthotopic defect. J Orthop Res 2006;24:867-76.

[34] Yuan H, Fernandes H, Habibovic P, de Boer J, Barradas AMC, de Ruiter A, Walsh WR, van Blitterswijk CA, de Bruijn JD. Osteoinductive ceramics as a synthetic alternative to autologous bone grafting. Proc Natl Acad Sci USA 2010;107:13614-19.

[35] Habibovic P, Juhl MV, Clyens S, Martinetti R, Dolcini L, Theilgaard N, van Blitterswijk CA. Comparison of two carbonated apatite ceramics in vivo. Acta Biomater 2010;6:2219-26.

[36] Heo SJ, Kim SE, Wei J, Kim DH, Hyun YT, Yun HS, Kim HK, Yoon TR, Kim SH, Park SA, Shin JW, Shin JW. In vitro and animal study of novel nano-hydroxyapatite/poly(epsilon-caprolactone) composite scaffolds fabricated by layer manufacturing process. Tissue Eng Part A 2009;15:977-89.

[37] Seol YJ, Park JY, Jung JW, Jang J, Girdhari R, Kim SW, Cho DW. Improvement of bone regeneration capability of ceramic scaffolds by accelerated release of their calcium ions. Tissue Eng Part A 2014;20:2840-9.

[38] Simon JL, Michna S, Lewis JA, Rekow ED, Thompson VP, Smay JE, Yampolsky A, Parsons JR, Ricci JL. In vivo bone response to 3D periodic hydroxyapatite scaffolds assembled by direct ink writing. J Biomed Mater Res A 2007;83:747-58.

[39] Lin KF, He S, Song Y, Wang CM, Gao Y, Li JQ, Tang P, Wang Z, Bi L, Pei GX. Low-Temperature Additive Manufacturing of Biomimic Three-Dimensional Hydroxyapatite/Collagen Scaffolds for Bone Regeneration. ACS Appl Mater Interfaces 2016;8:6905-16.

[40] Ripamonti U, Klar RM, Renton LF, Ferretti C. Synergistic induction of bone formation by hOP-1, hTGF-beta3 and inhibition by zoledronate in macroporous coral-derived hydroxyapatites. Biomaterials 2010;31:6400-10.

[41] Klar RM, Duarte R, Dix-Peek T, Dickens C, Ferretti C, Ripamonti U. Calcium ions and osteoclastogenesis initiate the induction of bone formation by coral-derived macroporous constructs. J Cell Mol Med 2013;17:1444-57.

[42] Davison NL, Gamblin A-L, Layrolle P, Yuan H, de Bruijn JD, Barrère-de Groot F. Liposomal clodronate inhibition of osteoclastogenesis and osteoinduction by submicrostructured beta-tricalcium phosphate. Biomaterials 2014;35:5088-97.

[43] Garimella R, Tague SE, Zhang J, Belibi F, Nahar N, Sun BH, Insogna K, Wang J, Anderson HC. Expression and synthesis of bone morphogenetic proteins by osteoclasts: a possible path to anabolic bone remodeling. J Histochem Cytochem 2008;56:569-77.

[44] Pederson L, Ruan M, Westendorf JJ, Khosla S, Oursler MJ. Regulation of bone formation by osteoclasts involves Wnt/BMP signaling and the chemokine sphingosine-1-phosphate. Proc Natl Acad Sci USA 2008;105:20764-69.

[45] Kreja L, Brenner RE, Tautzenberger A, Liedert A, Friemert B, Ehrnthaller C, Huber-Lang M, Ignatius A. Non-resorbing osteoclasts induce migration and osteogenic differentiation of mesenchymal stem cells. J Cell Biochem 2010;109:347-55.

[46] Akiyama N, Takemoto M, Fujibayashi S, Neo M, Hirano M, Nakamura T. Difference between dogs and rats with regard to osteoclast-like cells in calcium-deficient hydroxyapatite-induced osteoinduction. J Biomed Mater Res A 2011;96:402-12.

[47] Takeshita S, Fumoto T, Matsuoka K, Park K, Aburatani H, Kato S, Ito M, Ikeda K. Osteoclast-secreted CTHRC1 in the coupling of bone resorption to formation. J Clin Invest 2013;123:3914-24.

[48] Davison NL, Su J, Yuan H, van den Beucken JJ, de Bruijn JD, Barrère-de Groot F. Influence of surface microstructure and chemistry on osteoinduction and osteoclastogenesis by biphasic calcium phosphate discs. Eur Cell Mater 2015;29:314-29.

[49] Beck Jr GR. Inorganic phosphate as a signaling molecule in osteoblast differentiation. J Cell Biochem 2003;90:234-43.

[50] Dvorak MM, Riccardi D. Ca^{2+} as an extracellular signal in bone. Cell Calcium 2004;35:249-55.

[51] Kondo N, Ogose A, Tokunaga K, Umezu H, Arai K, Kudo N, Hoshino M, Inoue H, Irie H, Kuroda K, Mera H, Endo N. Osteoinduction with highly purified beta-tricalcium phosphate in dog dorsal muscles and the proliferation of osteoclasts before heterotopic bone formation. Biomaterials 2006;27:4419-27.

[52] Zayzafoon M. Calcium/calmodulin signaling controls osteoblast growth and differentiation. J Cell Biochem 2006;97:56-70.

[53] Habibovic P, Bassett DC, Doillon CJ, Gerard C, McKee MD, Barralet JE. Collagen biomineralization in vivo by sustained release of inorganic phosphate ions. Adv Mater 2010;22:1858-62.

[54] Barradas AM, Fernandes HA, Groen N, Chai YC, Schrooten J, van de Peppel J, van Leeuwen JP, van Blitterswijk CA, de Boer J. A calcium-induced signaling cascade leading to osteogenic differentiation of human bone marrow-derived mesenchymal stromal cells. Biomaterials 2012;33:3205-15.

Chapter 4
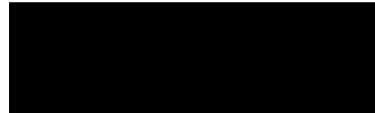
OSTEOINDUCTION AND OSTEOGENESIS BY NANOSTRUCTURED CALCIUM PHOSPHATE SCAFFOLDS: EFFECT OF NANOCRYSTAL MORPHOLOGY AND CARBONATE DOPING

4.1 Introduction

Bone is a nanocomposite material whose major constituents are collagen microfibrils and nanocrystallites of a CaP with apatite structure. The mineral phase represents, in fact, around 65 wt% of the bone extracellular matrix.[1] This is the reason why CaPs have been the preferred option when designing synthetic bone grafts, most bone substitutes currently in the market being either HA, β-TCP or a combination of both (BCP).[2,3]

However, although it is true that in a broad sense these materials bear some resemblance with the bone mineral, a closer look reveals major differences.[1] The bone apatite is a highly carbonate-substituted, calcium deficient form of hydroxyapatite ($Ca_{10}(PO_4)_6(OH)_2$), with a high vacancy content,[4,5] and containing, in addition to carbonate, other trace elements such as Mg^{2+}, Fe^{2+}, Zn^{2+}, K^+, Na^+, $(HPO_4)^{2-}$, F^- and Cl^-.[1,6] This results in a distorted network with poor crystallinity.[1] The carbonate ions can substitute both hydroxyl or phosphate groups in the apatite crystal structure, originating the A-type and B-type carbonation, respectively, B-type being the preferred form in biological apatite.[4,5,7,8] Bone mineral is produced by precipitation from the supersaturated extracellular fluids, resulting in plate-shaped nanocrystals of variable lengths (30-50 nm) and thickness (average about 5 nm), located both within the collagen fibres, and also in the extrafibrillar space.[9] Recent studies, moreover, have shown evidence that the extrafibrilar mineral has the form of elongated plates about 5 nm thick, 60 nm wide and several hundreds of nm long.[10-13]

This is in contrast to conventional CaP bone substitutes, which are commonly obtained by high temperature sintering processes, resulting in a lack of nanostructure, and of a chemical composition far from biological apatites.[1] In this work, we propose mimicking much more closely the chemical and nanostructural properties of biological apatite as a strategy to enhance the performance of synthetic bone grafts. In fact, there is an imperative necessity to find more effective synthetic bone grafts[14] since their biological performance is still inferior to that of autografts, especially regarding the initiation of bone growth and the synchronized graft resorption.[3,15] This is evidenced by the fact that autologous bone grafts are still considered the gold standard treatment, despite the serious drawbacks associated to the need of a second harvesting surgery.[16]

The relevance of nanostructure for the *in vivo* performance of CaPs was demonstrated in the previous study (Chapter 2).[17] Nanostructured CDHA foams, obtained through a biomimetic process, were shown to possess superior osteoinductive properties than conventional sintered ceramic foams, fostering the differentiation of MSCs to bone forming cells. This was a clear indication that biomimicry is a promising strategy for the design of bone substitutes. However, only one nanostructure and chemical composition was analyzed. In the present work, we intend to exploit the versatility of the biomimetic process used to produce the above mentioned

scaffolds, which allows tuning the size and shape of the CDHA crystals.[18,20] Moreover, in order to increase the chemical similarity to natural bone, carbonate can be introduced in the apatite by a novel biomimetic process to obtain carbonated nanostructured CDHA foams.

Although different *in vitro* studies have highlighted that the size and shape of nanocrystals in nanostructured biomaterials exert a direct effect on cells involved in osteoinduction,[21-26] little is known about the role of nanocrystal shape and size in terms of the *in vivo* performance of these materials. Similarly, the presence of carbonate in the apatite structure is known to increase the chemical reactivity of HA by disturbing its crystal lattice,[7,27-31] and it has been shown to foster osteoclastogenesis,[32-36] a critical event in the intrinsic osteoinduction cascade of biomaterials.[17,37-40] However, most *in vivo* studies investigating the behavior of carbonated apatites have focused on high temperature ceramics, with absence of nanostructure and limited carbonate content,[7,8,41-50] as the sintering process, in addition to fusing the nanometric crystals, causes a severe thermal decomposition of carbonate into CO_2 resulting in high carbonate losses.[43,51-57]

The aim of the present work was to investigate the role of nanocrystal morphology (plate *vs.* needle) and the effect of carbonate doping of nanostructured CDHA foamed scaffolds on their intrinsic osteoinduction and degradation behaviour *in vivo*, and to assess if there is a direct correlation with their bone healing capacity. To this end, the performance of nanostructured CDHA foams with two different crystal sizes and morphologies were compared using canine ectopic and orthotopic implantation models. Plate-shaped nanocrystals were compared with needle-shaped CDHA foams evaluated in our previous studies (Chapter 2 and 3).[17,58] To further mimic bone mineral, carbonated CDHA nanostructured foams obtained under biomimetic conditions were included as a third group. Moreover, the *in vitro* response of rMSCs cultured in direct contact with the same biomaterials used in the *in vivo* assays was investigated.

4.2 Materials and Methods

4.2.1 Calcium phosphate materials

4.2.1.1 *Synthesis of alpha-tricalcium phosphate*

α-TCP (α-Ca$_3$(PO$_4$)$_2$,) was used as precursor of the CDHA foams. Briefly, α-TCP was obtained by heating calcium hydrogen phosphate (CaHPO$_4$, Sigma-Aldrich, St. Louis, MO) and calcium carbonate (CaCO$_3$, Sigma-Aldrich, St. Louis, MO) at a 2:1 molar ratio. The powder mixture was heated up to 1400ºC for 15 h and quenched in air. The α-TCP obtained was milled in an agate ball mill (Pulverisette 6, Fritsch GmbB, Markt Einersheim, Germany), using two different milling protocols in order to obtain two different sizes of α -TCP powder. A coarse powder (5.2 μm median size) was obtained by milling with 10 balls (d = 30 mm) for 15 min at 450 rpm, and a fine powder (2.8 μm median size) by milling first with 10 balls (d = 30 mm) for 60 min at 450 rpm followed by a second milling for 70 min at 500 rpm with 100 balls (d = 10 mm).

4.2.1.2 *Preparation of foams and discs*

CDHA foams were obtained by hydrolysis of α-TCP foams. They were prepared by mixing a solid phase consisting of 98 wt% of α-TCP and 2 wt% of precipitated hydroxyapatite (PHA,

Merck KGaA, Darmstadt, Germany) with a liquid phase consisting of an aqueous solution of 1 wt% Polysorbate 80 (Tween 80[®], Sigma-Aldrich, St. Louis, MO) as foaming agent.[59] Fine or coarse α-TCP powders were used to obtain Fine-CDHA or Coarse-CDHA foams, respectively. The liquid to powder ratio was adjusted to obtain similar macroporosities for both type of foams, being ratios of 0.65 and 0.55 mL/g for fine and coarse α-TCP powders, respectively. Foaming was performed with a customized hand mixer for 30 s at 7000 rpm and the resulting foams were transferred to Teflon cylindrical moulds (5 mm diameter and 10 mm height), which were left in humid atmosphere at 37 ℃ for 8 h to ensure cohesion of the foamed structures. Afterwards, the scaffolds were immersed in water for 10 days at 37 ℃ to allow for the hydrolysis of α-TCP to CDHA. The carbonated CDHA foams (CO_3-CDHA) were obtained by immersing the coarse α-TCP foams in a saturated sodium bicarbonate ($NaHCO_3$, Sigma-Aldrich, St. Louis, MO) solution instead of water, in this case for 17 days to complete the hydrolysis reaction.[26]

For the *in vitro* studies, 5 mm diameter x 0.3 mm height discs were prepared of all three groups, following the procedure described above for the foamed scaffolds, except for the foaming step, which was substituted by mixing in a mortar for 1min.

4.2.1.3 *Materials characterization*

Phase characterization of the different samples was performed by X-ray diffraction (D8 Advance, Bruker Corp., Billerica, MA) using a Cu Kα anode operated at 40 kV and 40 mA. Data were collected in 0.02° steps over the 2θ range of 10°-80° with a counting time of 2 s per step. The experimental patterns were compared to those of HA (JCPDS 09-0432) and α-TCP (JCPDS 09-0348). Samples were analysed also by Attenuated Total Reflectance Fourier-transform infrared spectroscopy analysis (ATR-FTIR, Nicolet 6700FTIR, Thermo Fisher Scientific Inc., Waltham, MA). Data were acquired in 64 scans with a resolution of 4 cm^{-1} from 4000 to 575 cm^{-1} with a Germanium crystal. Carbonate quantification was performed by bulk combustion element analyzer (TC/EA, Thermo EA 1108, Thermo Fisher Scientific Inc., Waltham, MA) as previously reported.[26] The SSA was determined by nitrogen adsorption (ASAP 2020, Micrometrics Instrument Corp., Norcross, GA), using the BET method. Porosity and pore entrance size distribution were measured MIP (AutoPore IV, Micrometrics Instrument Corp., Norcross, GA). The microstructure was characterized by SEM (Zeiss Neon40 EsBCrossBeam, Zeiss, Oberkochen, Germany). Prior to imaging, samples were coated with carbon to impart conductivity. Finally, the macroporosity of the foamed scaffolds was assessed by micro-CT (SkyScan 1172, BrukermicroCT, Kontich, Belgium) at a voltage of 90 kV and a current of 112 µA, with a Cu−Al filter.

4.2.2 In vitro study

4.2.2.1 *Cell culture*

To better understand the role of nanocrystal morphology and carbonate doping, rMSCs were cultured on the surface of discs of all three materials. The discs, previously sterilized by immersion in 70% ethanol and rinsed three times with PBS (Gibco, Thermo Fisher Scientific Inc., Waltham, MA), were placed in a 24-well plate and incubated with 2.5 mL medium/well overnight. rMSCs were isolated from tibias and femurs of Lewis rats and characterized by flow

cytometry.[60] Afterwards, cells were expanded in AdvDMEM supplemented with 10% FBS, 20 mMHEPES buffer, 2 mM L-glutamine and penicillin/streptomycin (50 U/mL and 50µg/mL, respectively), all from Thermo Fischer Scientific Inc. (Waltham, MA). Cells at passages 3-4 were used in all experiments.

4.2.2.2 Cell proliferation

For the proliferation assay, all samples were tested at 6 h, 3, 7 and 14 days. The experiments were performed with three replicates of each sample and TCPS was used as control. Cells were seeded at a density of 300 cells/mm^2. Samples were changed into another plate at each specified time and cell lysis was performed using 300 µl of M-PER® (Mammalian Protein Extraction Reagent, Thermo Scientific Inc., Waltham, MA). Subsequently, cell number was evaluated using the Cytotoxicity Detection KitPLUS (Hoffmann-La Roche, Basel, Switzerland) and lactate dehydrogenase (LDH) activity was measured spectrophotometrically at 492 nm (Synergy HTX, BioTek Instruments Inc., Winooski, VT). A calibration curve with decreasing number of cells was prepared to express the results. The values were normalized by total seeded area.

4.2.2.3 Cell morphology

Cell seeded discs were observed by SEM (Zeiss Neon40 EsBCrossBeam, Zeiss, Oberkochen, Germany) after 14 days. Samples were washed with PBS three times and fixed for 1 h at 4ºC in a 2.5% glutaraldehyde (Sigma-Aldrich, St. Louis, MO) solution in PBS. Subsequently, fixed samples were washed three times with PBS and dehydrated in increasing series of ethanol solutions. Complete dehydration was performed in hexamethyldisilazane (HMDS,Thermo Scientific Inc., Waltham, MA) and discs were stored in desiccator. Dried disks were covered with a thin gold-palladium layer using vapor deposition.

Cell morphology was further analyzed by confocal microscopy using immunofluorescent staining to visualize nuclei, actin stress fibres and osteocalcin after 14 days of culture. The attached cells were rinsed with PBS (x3) and fixed in 4% paraformaldehyde (PFA, Sigma-Aldrich, St. Louis, MO) solution in PBS. Afterwards, cells were permeabilized with 0.1% Triton X-100 (Sigma-Aldrich, St. Louis, MO) in PBS for 15 min and blocked with 1% bovine serum albumin (BSA, Sigma-Aldrich, St. Louis, MO) in PBS for 1 h. Then, discs were incubated for 1 h with rabbit anti-osteocalcin (G-5, Santa Cruz Biotechnology Inc., Dallas, TX) (1:100 in 1% BSA in PBS). Subsequently, Alexa Fluor 488 chicken anti-rabbit and Alexa Fluor 546 phalloidin (Thermo Scientific Inc., Waltham, MA) were added and incubated for 1 h (1:1000 and 1:300 in 0.1% Triton X-100 in PBS, respectively). For nuclei staining, discs were incubated with 4',6-diamidino-2-phenylindole (DAPI) for 2 min. Three rinses of 5 min each in 0.15 % glycine (Sigma-Aldrich, St. Louis, MO) in PBS were done between all steps. Sample discs were mounted in Mowiol 4-88 (Sigma-Aldrich, St. Louis, MO) and visualized in a confocal microscope (Leica TCS SPE, Leica Microsystems, Wetzlar, Germany). Digital images were processed using an image analysis software (Fiji/Image-J package, open source software).

4.2.2.4 Cell differentiation

The osteoblastic differentiation was assessed by measuring the expression of osteogenic genes by RT-qPCR. Cells were seeded on the discs (300 cells/mm^2) and incubated for 6 h and 1 and 3 days. Additionally, for OCN late marker, 7 and 14 days were also monitored. Prior to RNA

extraction, samples were transferred into a new well plate and rinsed with PBS (Gibco, Thermo Fisher Scientific Inc., Waltham, MA). Total RNA was extracted using RNeasy Mini Kit (Qiagen GmbH, Hilden, Germany) and quantified by NanoDrop ND-1000 spectrophotometer (NanoDrop Products, Thermo Fisher Scientific Inc., Waltham, MA). Equal amounts of RNA (120 ng) were retrotranscribed to cDNA using the QuantiTect Reverse Transcription Kit (Qiagen GmbH, Hilden, Germany) and then specifically amplified using selective primers (**Table 4.1**) by QuantiTect SYBR Green RT-PCR Kit (Qiagen GmbH, Hilden, Germany) in an RT-PCR StepOnePlus (Applied Biosystems, Thermo Fisher Scientific Inc., Waltham, MA). The expression values of studied genes were normalized by expression of β-actin (housekeeping gene) and relative fold changes (FC) were related to TCPS at 6 h of culture. The following formula was used: $FC = E_{target}^{\Delta Cq\ target\ (TCPS\ 6h\ -\ sample)} / E_{housekeeping}^{\Delta Cq\ housekeeping\ (TCPS\ 6\ h\ -\ sample)}$, where C_q is the median value of the quantification cycle of the triplicate of each sample and E corresponds to the efficiency of amplification and is determined from the slope of the log-linear portion of the calibration curve, as $E=10^{(-1/slope)}$. The experiment was performed in two independent runs.

Table 4.1. Primers' sequences used for RT-qPCR

Gene	Gene symbol	Forward primer sequence (5' to 3')	Reverse primer sequence (5' to 3')
β-actin	ACTB	CCCGCGAGTACAACCTTCT	CGTCATCCATGGCGAACT
Bone morphogenetic protein-2	BMP-2	CCCCTATATGCTCGACCTGT	AAAGTTCCTCGATGGCTTCTT
Alkaline phosphatase	ALP	GCACAACATCAAGGACATCG	TCAGTTCTGTTCTTGGGGTACAT
Collagen I	Col I	CATGTTCAGCTTTGTGGACCT	GCAGCTGACTTCAGGGATGT
Osteonectin	ONN	GTTTGAAGAAGGTGCAGAGGA	GGTTCTGGCAGGGGTTTT
Osteopontin	OPN	CGGTGAAAGTGGCTGAGTTT	GGCTACAGCATCTGAGTGTTTG
Osteocalcin	OCN	ATAGACTCCGGCGCTACCTC	CCAGGGGATCTGGGTAGG

4.2.3 In vivo study

Ethical approval for the animal procedures was obtained from the local ethic committee (CEAAH 2338) and all procedures were performed in compliance with the Guide for Care and Use of Laboratory Animals[61] as well as the European Community Guidelines (Directive 2010/63/EU) for the protection of animals used for scientific purposes.[62]

Twelve adult beagle dogs (body weight 14-17 kg) were purchased from a professional stock breeder (Isoquimen S.L., Barcelona, Spain). The animals were randomly divided into 2 groups of six dogs each, corresponding to two different experimental times (6 weeks/12 weeks) and acclimatized for 2 weeks prior to surgery. All surgical procedures were carried out under standard anesthetic and analgesic protocols.

4.2.3.1 *Intramuscular implantation*

The intrinsic osteoinductive potential of the materials was evaluated in a standardized intramuscular canine model (described in Chapter 2). Briefly, once the animals were anesthetized, one skin incision was performed on the lumbar region and fascia incisions were

created in the paraspinal muscles bilaterally. Subsequently, three intramuscular pockets were created on each dog, which were filled with one of the three above-mentioned cylindrical foamed scaffolds (5 mm of diameter x 10 mm of length).

4.2.3.2 *Intraosseous implantation*

To study the bone healing capacity of the same scaffolds, their potential to repair a femoral monocortical bone defect was evaluated in a standardized intraosseous canine model (described in Chapter 3), in the same group of animals. Briefly, the lateral aspect of the femur was approached and three round monocortical bone defects (5 mm of diameter) were drilled on the mid-shaft femoral diaphysis. Then, one scaffold (5 mm of diameter x 10 mm of length) was inserted in each defect by press-fit.

During the postoperative period, the animals received a long-acting antibiotic and a non steroidal anti-inflammatory drug for 7 days, which is routinely prescribed after orthopedic surgeries. The animals were euthanized at 6 and 12 weeks post-implantation respectively, by an overdose of pentobarbital sodium, after sedation of medetomidine for animal welfare reasons.

To sum up, one scaffold of each group was implanted intramuscularly and intraosseously in each dog, resulting in three intramuscular and three intraosseous scaffolds per animal (**Table 4.2**).

Table 4.2. Summary of implanted foamed scaffolds

Materials	Intramuscular implantation		Intraosseous implantation	
	6 weeks	12 weeks	6 weeks	12 weeks
Fine-CDHA	6	6	6	6
Coarse-CDHA	6	6	6	6
CO_3-CDHA	6	6	6	6

4.2.3.3 *Sample harvest and histological processing*

After euthanasia, samples were immediately harvested and fixed in a buffered formalin solution for 72 h. The specimens were then dehydrated in a graded ethanol series, and embedded in ascending graded mixtures of ethanol and methylmethacrylate resin (Technovit 7200, Heraeus Kulzer GmbH, Hanau, Germany) under vacuum conditions that photopolymerized under white and ultraviolet light for 2 and 4 h, respectively. The resulting blocks were analyzed by X-ray micro-CT. After micro-CT scanning, each block was divided into two equal pieces. Intramuscular samples were divided transversally and intraosseous samples longitudinally to evaluate the full thickness of the cortical bone defect. One half of each sample was polished (EXAKT Cutting & Grinding System, EXAKT Advanced Technologies GmbH, Norderstedt, Germany) and subsequently coated with carbon for BS-SEM. The other half was sliced and grinded (Cutting & Grinding System, EXAKT Advanced Technologies GmbH, Norderstedt, Germany) to obtain histological sections (50 μm). Sections were then stained with Goldner-Masson trichrome (GMT) and toluidine blue (TB) for histological evaluation under light microscopy.

4.2.3.4 *Histology and histomorphometry*

The samples were analyzed by micro-CT (SkyScan 1172, Bruker Corp., Billerica, USA) using the same settings as for the scaffolds scanning described above. The specimen was rotated through 180º with a rotation step of 0.40º, an acquisition time of 2.1 s per scan and anisotropic pixel size of 5 µm for the intramuscular samples and 10 µm for the intraosseous samples. The 3D evaluation of the samples was performed following a previously established protocol[63] and the same histomorphometric parameters were measured in both groups of samples:

a) Percentage of newly formed bone within the initial available macropore space:

% newly formed bone = (bone volume / initial available macropore volume) * 100

b) Percentage of scaffold degradation, calculated by subtracting the remaining scaffold volume from the initial scaffold volume prior to implantation:

% scaffold degradation = [(initial scaffold volume – final scaffold volume) / initial scaffold volume] * 100

For the intramuscular samples, both parameters were quantified in the entire scaffold volume, whereas for the intraosseous samples they were quantified only in the monocortical bone defect volume, without considering the intramedullarly portion of the scaffolds.

The localization and maturity of the newly formed bone were determined based on tissue morphology and the different gray levels by BS-SEM imaging (Zeiss Neon40 EsBCrossBeam, Zeiss, Oberkochen, Germany) at a voltage of 20 kV.

The stained histological sections were observed under light microscopy (Nikon Eclipse E800, Nikon Corp.,Tokyo, Japan) to evaluate histological qualitative parameters such as the degree of peri-implant inflammatory reaction, neovascularization, fibrous-tissue infiltration and osteoclastic activity.

4.2.4 Statistical analysis

The histomorphometric and *in vitro* results are presented as mean values ± standard error. All analyzed data were normally distributed according to Anderson-Darling and Kolmogorov-Smirnov tests and showed homogeneity of variances according to Levenne's and Barralet's tests. Statistical comparisons among experimental groups at each time point were performed using one-way repeated measures ANOVA followed by Tukey's post hoc test in GraphPad Prism software (GraphPad Software Inc., La Jolla, CA). A pair-wise comparison result of $p<0.05$ was considered statistically significant.

4.3 Results

4.3.1 Materials characterization

XRD analysis showed that both the foamed cylinders and the discs consisted of low crystallinity hydroxyapatite containing in some cases small amounts of unreacted α-TCP (less than 2%) (**Fig. 4.1A**). The ATR-FTIR spectra showed the typical phosphate bands at 570, 600, 960 and 1030 cm^{-1} for all three groups (**Fig. 4.1B**).[64,65] The detection of bands at 1471 and 1419 cm^{-1}in the CO_3-CDHA samples proved the B-type carbonate substitution in the apatite crystal lattice in these specimens.[5,66,67]

The pore entrance size distribution of the different samples, as determined by MIP, is displayed in **Fig. 4.1C**. The presence of open macroporosity centered at 70 μm was confirmed in the three foamed scaffolds, together with pores in the micrometric and nanometric range. As expected, the discs, which had not been subjected to the foaming step, showed only submicrometric and nanometric pores. SEM images in **Fig. 4.1D** revealed similar pore size and spherical geometry of the macropores in the three foamed materials, and marked differences in micro- and nanostructure. Whereas Fine-CDHA scaffolds showed the typical network of entangled needle-like nanocrystals, Coarse-CDHA and CO_3-CDHA showed entangled plate-like crystals, significantly smaller in the latter.

A detailed quantification of the textural properties as well as carbonate incorporation levels is given in **Table 4.3**. SSA values varied in accordance with the nanocrystal morphology, being the highest for Fine-CDHA samples and the lowest for the Coarse-CDHA group due to the larger crystal size (**Fig. 4.1D**). The carbonate content reached 11-12 wt% in the carbonated samples regardless of their dense or foamed nature, being almost negligible for the non-carbonated counterparts (Fine-CDHA and Coarse-CDHA).
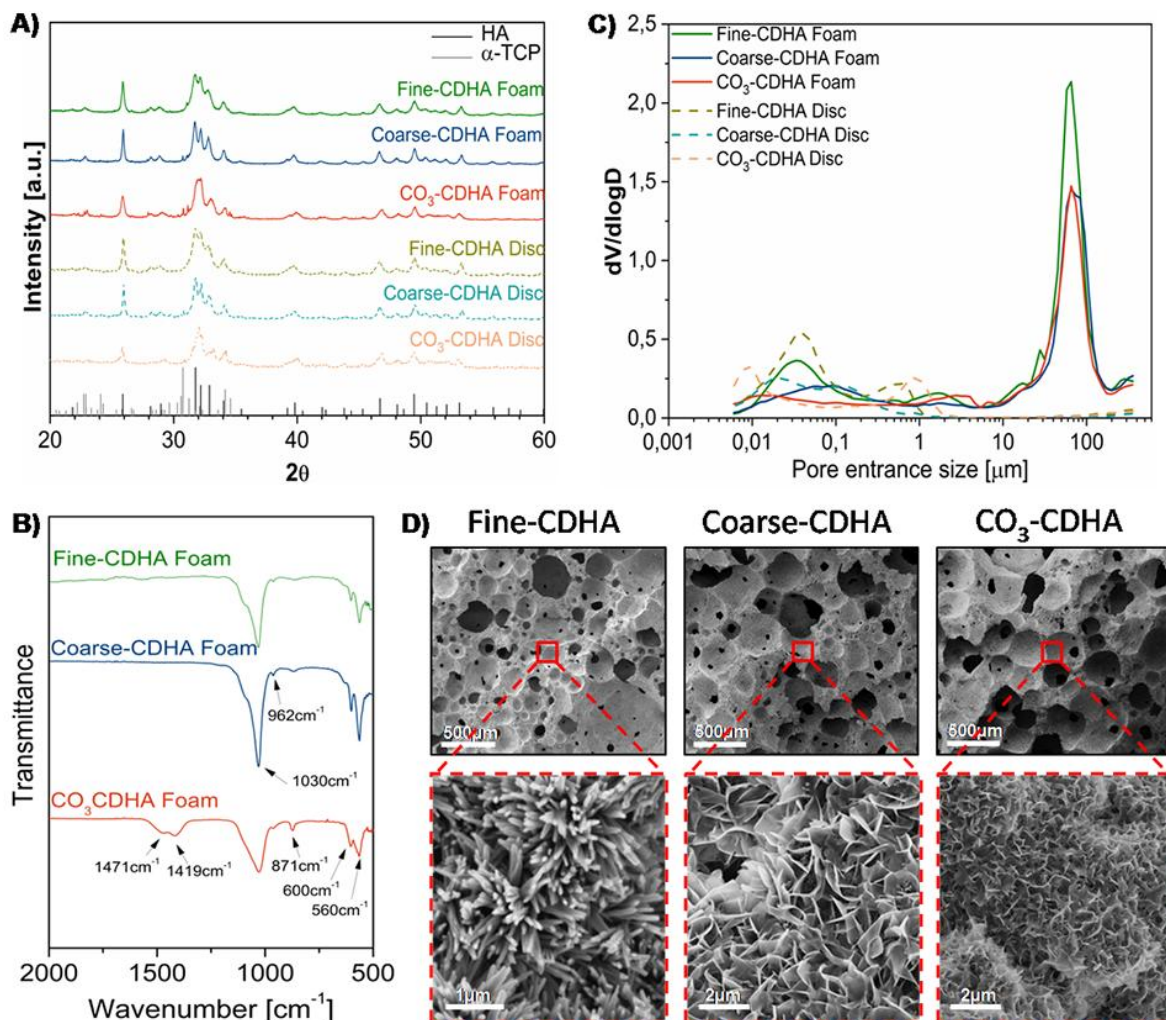
Figure 4.1. Physicochemical characterization of Fine-CDHA, Coarse-CDHA and CO_3-CDHA foams and discs: **(A)** XRD patterns. **(B)** ATR-FTIR spectra **(C)** Pore entrance size distributions determined by MIP. **(D)** Low magnification SEM images of the implanted foams showing the interconnected spherical concave macropores in all groups and high magnification images showing the nanostructure consisting of the typical network of entangled needle-shaped nanocrystals for the Fine-CDHA foams and the plate-shaped nanocrystals for the Coarse-CDHA and CO_3-CDHA foams, significantly smaller in the carbonated samples.

Table 4.3. Porosity, SSA and carbonate content of the different samples

Materials		Porosity					SSA (m²/g)	CO₃²⁻ content (wt%)
		Total Porosity by MIP (%)	Macroporosity by MIP (%)	Macroporosity by micro-CT (%)	Macropore entrance size by MIP (µm)	Macropore size by micro-CT (µm)		
Fine-CDHA	Disc	57.7	-	-	-	-	40.18	0.05
	Foam	76.5	49.5	52.3	70	227.0	38.49	0.03
Coarse-CDHA	Disc	51.8	-	-	-	-	21.96	0.05
	Foam	71.1	47.6	49.3	70	302.1	19.26	0.02
CO₃-CDHA	Disc	48.0	-	-	-	-	29.81	11.33
	Foam	69.7	46.7	49.1	70	264.0	30.33	12.33

4.3.2 In vitro results

4.3.2.1 *Cell adhesion and proliferation*

rMSC adhesion after 6 h was very similar in all groups (**Fig. 4.2A**). However, from this time point cell number progressively decreased on Fine- and Coarse-CDHA, whereas it significantly increased on CO_3-CDHA, with statistically significant differences between groups at 3, 7 and 14 days of culture.

4.3.2.2 *Cell morphology*

Morphological studies performed by SEM after 14 days of culture showed that the cells seeded on all three substrates had similar morphologies and were well spread in all cases (**Fig. 4.2B**). The main difference between groups was the density of cells, in accordance with the results obtained in the proliferation assay, with lower cell density on the Coarse- and Fine-CDHA groups compared with CO_3-CDHA samples.

Immunofluorescence assays performed at 14 days revealed that actin filaments were not well developed in the cells seeded on the Coarse- and Fine-CDHA discs (**Fig. 4.2B**). In contrast, cells seeded on the CO_3-CDHA discs showed clearly defined actin filaments, as well as a superior osteocalcin activity (**Fig. 4.2B**), suggesting improved cell differentiation compared with the Fine- and Coarse-CDHA groups.

4.3.2.3 *Cell differentiation*

The results obtained by RT-qPCR analysis are displayed in the Appendix (**Fig A4.1**). In general terms, cells seeded on all three materials showed a superior osteogenic gene expression compared to those cultured on TCPS, showing significant differences at 6 h for BMP-2, Col I and OPN, at 1 day for all osteogenic markers except for ALP, and at 3 days for OPN and OCN. Moreover, the expression of OCN at 7 and 14 days was significantly higher for the cells cultured on the three CDHA discs than for those cultured on TCPS. Among the three nanostructured CDHA materials, the non-carbonated CDHA groups showed a slightly superior osteogenic gene expression than CO_3-CDHA samples, although no statistically significant differences were consistently found between groups.
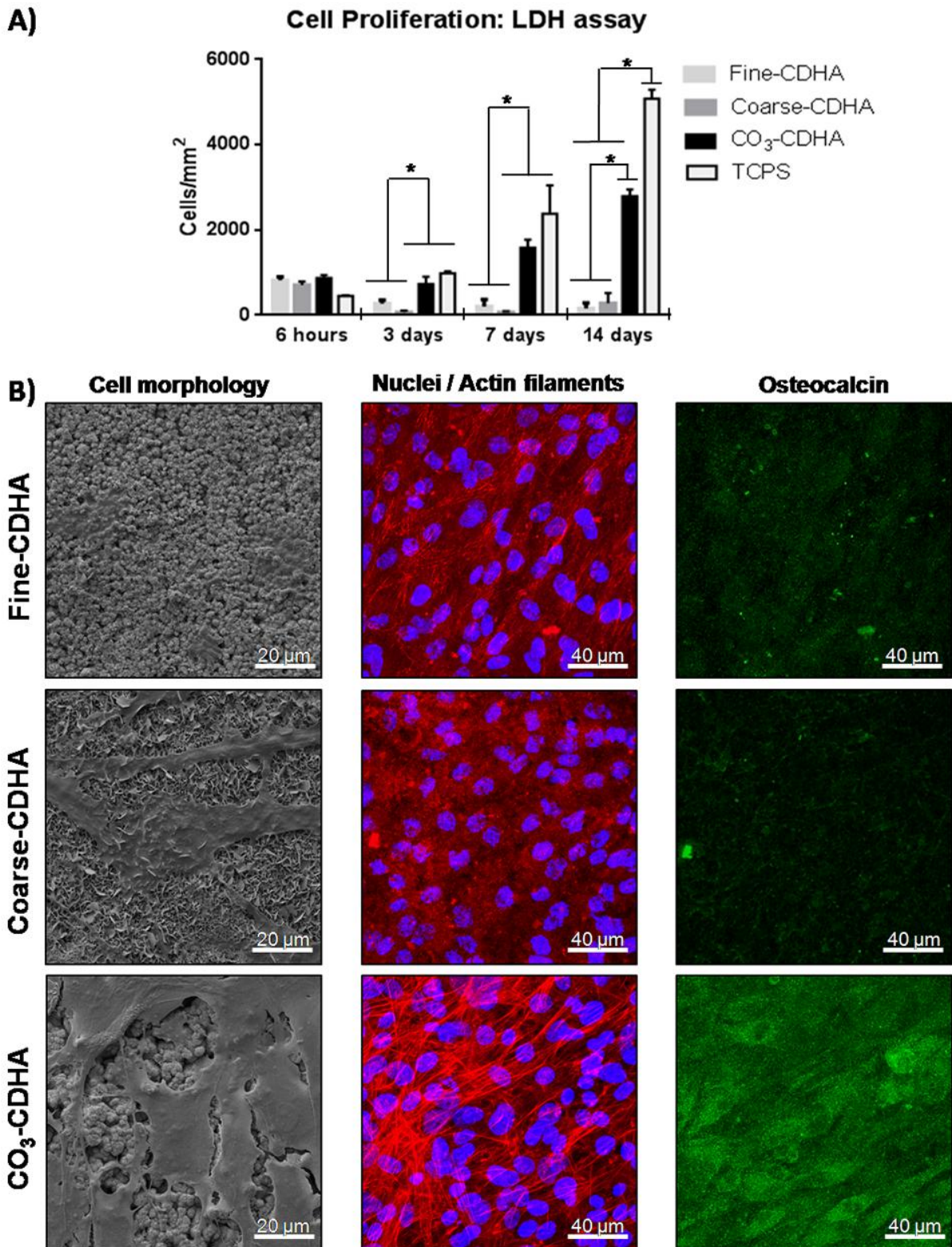
Figure 4.2. (A) LDH assay: rMSCs proliferation after 6 h, 3, 7 and 14 days. (*) denotes groups with statistically significant differences (p < 0.05). **(B)** Morphology of rMSCs at 14 days observed by SEM (first column) and by confocal microscopy (second and third columns). Nuclei in blue, actin fibers in red and osteocalcin in green.

4.3.3 In vivo results

There were no surgical and postoperative complications. All the intramuscular and orthotopic implanted scaffolds were retrieved and processed for histological evaluation and no adverse

foreign body reaction was observed in any case, confirming the good biocompatibility of all scaffolds in both implantation sides.

4.3.3.1 *Intramuscular implantation*

At 6 weeks, loose connective-tissue infiltration and abundant blood vessel ingrowth were observed within the interconnected macropores of all three groups (**Fig. 4.3**). However, significant differences were noted regarding new ectopic bone formation.
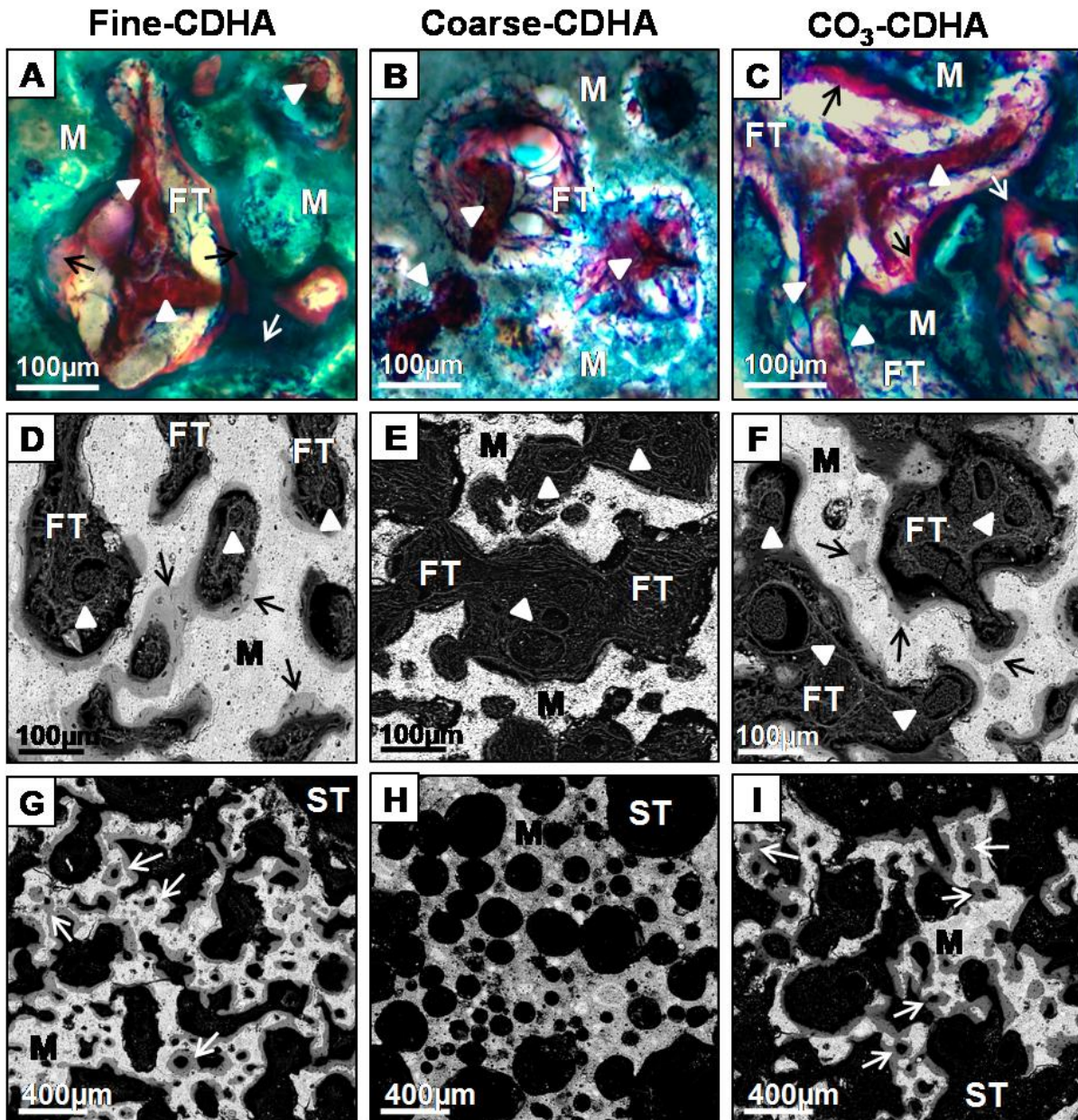
Figure 4.3. Undecalcified Goldner-Masson trichrome stained sections **(A,B,C)** and backscattered scanning electron micrographs **(D,E,F)** after 6 weeks of intramuscular implantation. All groups showed loose fibrous-tissue (FT) infiltration and abundant blood vessel (arrow heads) ingrowth within the interconnected macropores. Note the new osteoid in pink and the well-mineralized bone matrix in dark green in the GMT stained sections. In BS-SEM images the calcified bone appears in light grey. Interestingly, only Fine-CDHA and CO$_3$-CDHA groups showed new ectopic bone formation (arrows) at this time point, always in direct contact with the material (M) concave surfaces. **(G,H,I)** Backscattered scanning electron micrographs showing some haversian structures (white arrows), in which new bone is arranged concentrically surrounding a central blood vessel replicating the osteonic structure of cortical bone. ST=Soft tissue, M=Material.

Whereas newly formed bone was observed in the Fine-CDHA group in four out of six animals and in the CO_3-CDHA group in five out of six animals, no signs of bone formation were found in the Coarse-CDHA scaffolds (**Fig. 4.3** and **Fig. 4.4**). The bone found at 6 weeks mainly consisted in woven bone firmly attached to the concave surfaces of scaffold macropores. Moreover, a few haversian structures were observed, in which the lamellar bone was arranged concentrically surrounding a central blood vessel, replicating the osteonic structure of cortical bone (**Fig. 4.3**).
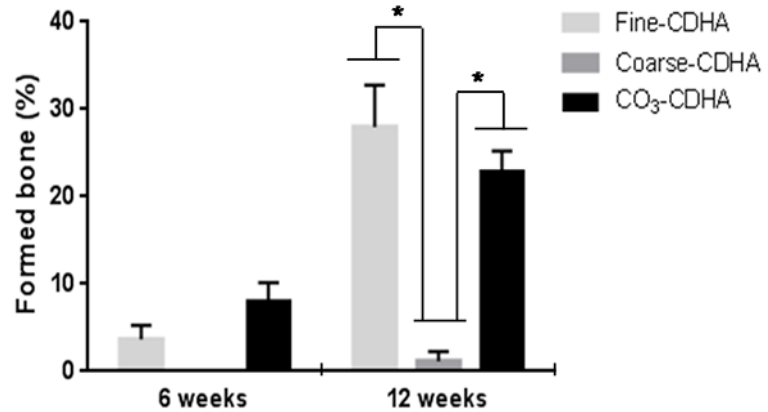

Figure 4.4. (A) Bone incidence after 6 and 12 weeks of intramuscular implantation. **(B)** Histomorphometrical results: percentage of newly formed bone within the available macropore space after 6 and 12 weeks of intramuscular implantation, as measured by micro-CT. (*) denotes groups with statistically significant differences at the same time point (p < 0.05).

A similar trend was observed after 12 weeks of implantation when a significant amount of new ectopic bone was observed in all animals for Fine-CDHA and CO_3-CDHA groups, while in the Coarse-CDHA group a small amount of bone was observed only in two out of six animals (**Fig. 4.4**). At this time point mature lamellar bone was formed on the Fine-CDHA and CO_3-CDHA scaffolds while mainly woven bone was observed in Coarse-CDHA constructs (**Fig. 4.5**). No chondrocytes or any evidence of endochondral ossification was detected during ectopic bone formation in either group.

Histological evaluation also showed the presence of multinucleated osteoclast-like resorbing cells in all groups (**Fig. 4.6C**). However, a larger amount of osteoclast-like cells were observed at both time points in the Fine-CDHA scaffolds, and especially in the CO_3-CDHA scaffolds, than in the Coarse-CDHA ones. This was in agreement with the superior degradation rate shown by the CO_3-CDHA and Fine-CDHA foams compared with the Coarse-CDHA (**Fig. 4.6A**), which was more pronounced in the carbonate-containing scaffolds (**Fig. 4.6A/B**), although in all cases the differences were statistically significant only after 12 weeks of implantation. It is worth noting that, contrary to the other two groups, the degradation of Coarse-CDHA constructs did not progress overtime (**Fig. 4.6A**).
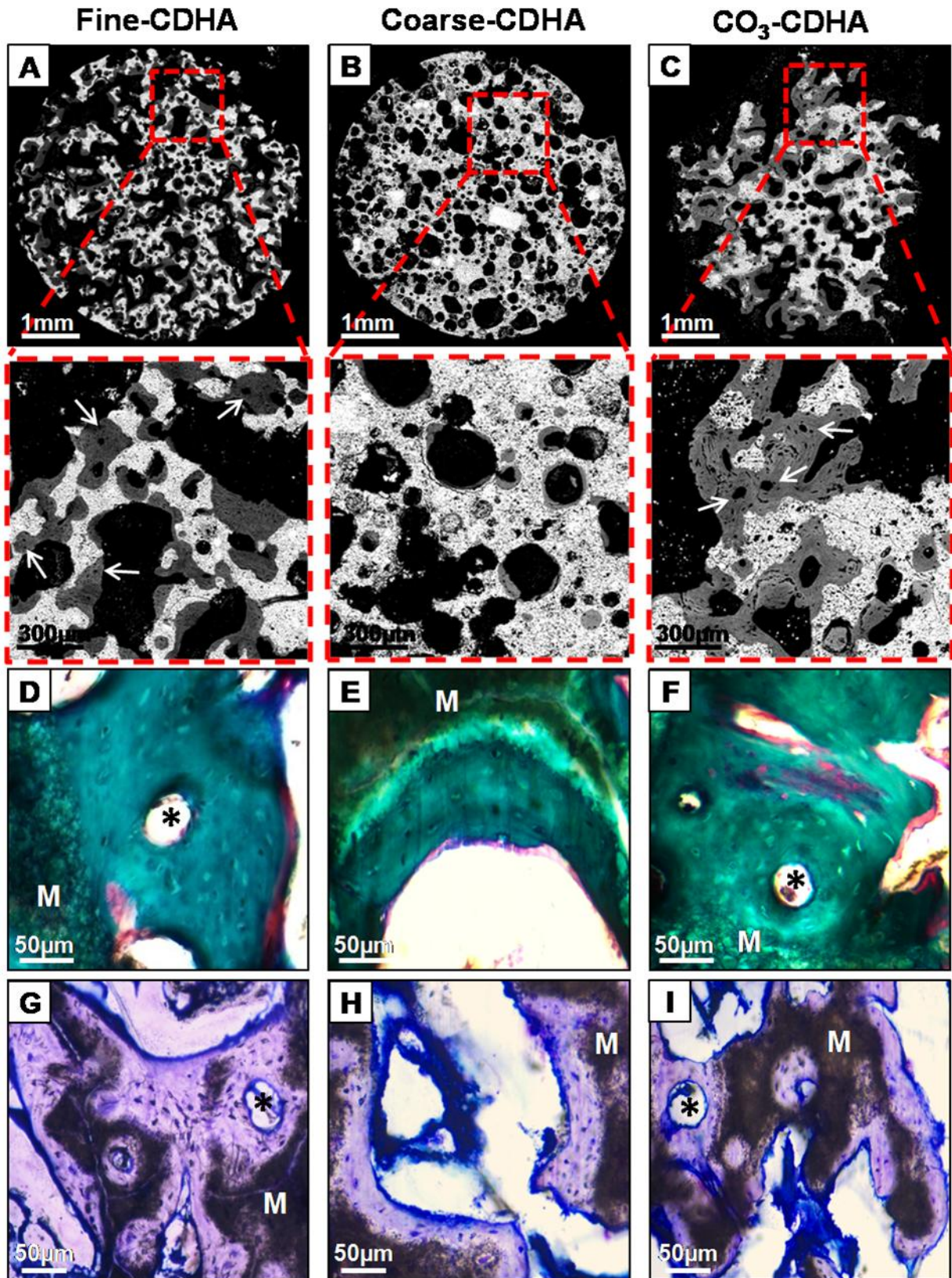
Figure 4.5. Histological images of the studied scaffolds after 12 weeks of intramuscular implantation. **(A,B,C)** Backscattered scanning electron images. **(D,E,F)** Undecalcified Goldner-Masson trichrome stained sections. **(G,H,I)** Toluidine blue stained sections. A significant amount of well-calcified bone matrix (grey in the BS-SEM, green in GMT and purple in TB) and some osteon-like structures (arrows) with the characteristic haversian canals (asterisks) in the centre were indentified in the Fine-CDHA and CO$_3$-CDHA foams. In contrast, small amounts of ectopic bone were observed in the Coarse-CDHA scaffolds. Note the new osteoid (pink in GMT and blue in TB) and osteocytes inside lacunae (light green in GMT and blue in TB). M=Material.

Figure 4.6. (A) Histomorphometrical results: percentage of scaffold degradation 6 and 12 weeks after intramuscular implantation, as measured by micro-CT. (*) denotes groups with statistically significant differences at the same time point (p <0.05). **(B)** Micro-CT 3D reconstructions of studied foams 12 weeks after intramuscular implantation. **(C)** Undecalcified toluidine blue stained sections of implanted scaffolds after 12 weeks of intramuscular implantation showing multinucleated osteoclast-like cells and macrophages resorbing the materi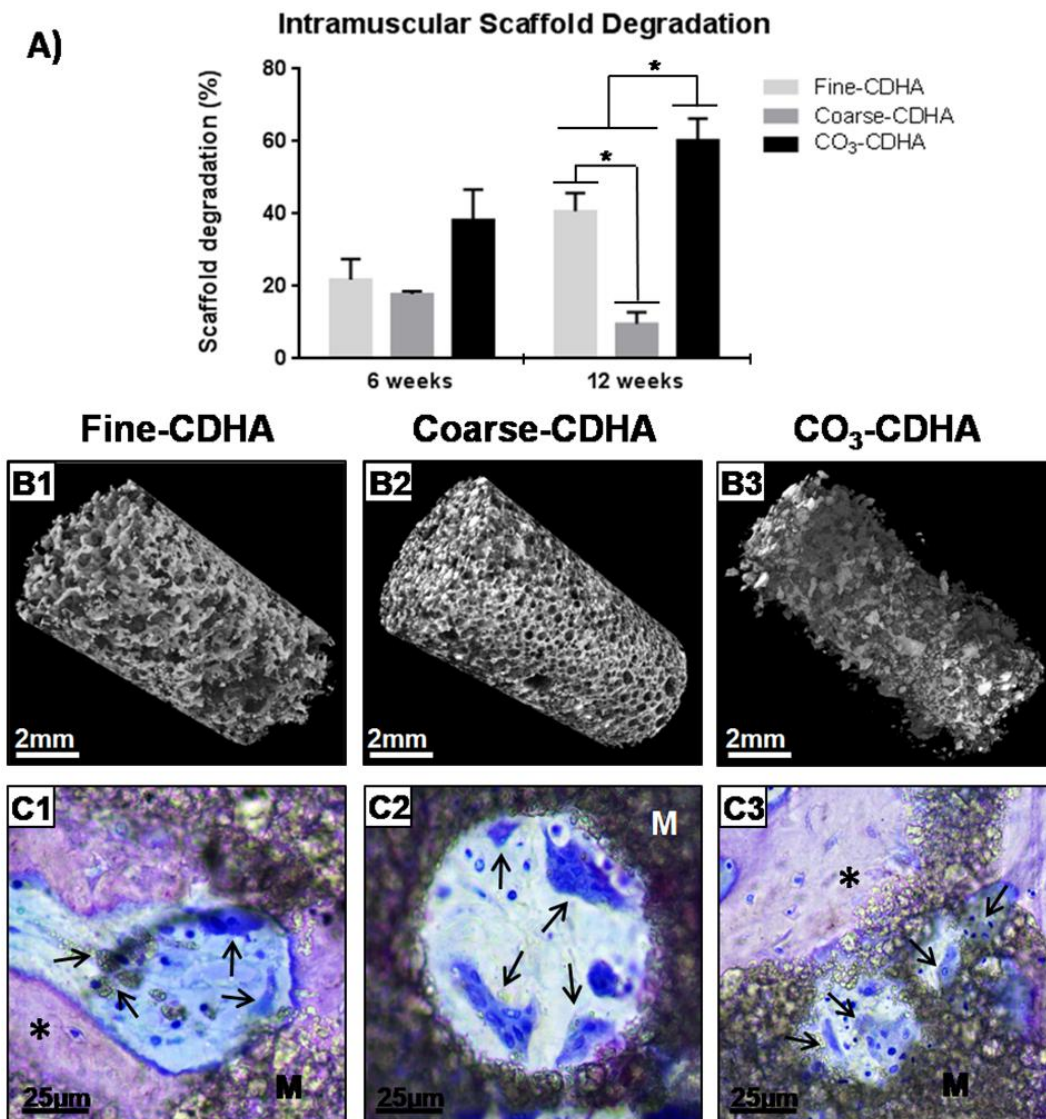als (arrows). Note intracellular material particles visible in some resorbing cells (C1,C3). M=Material, Asterisk=Ectopic bone

4.3.3.2 *Intraosseous implantation*

Histological analysis of the scaffolds implanted orthotopically revealed new bone tissue ingrowth within open macropores of all three scaffolds, in close contact with the material surfaces and without any intervening layer of fibrous tissue at the host cortical bone-material interface (Appendix, **Fig. A4.2A/B/C**). Moreover, all groups showed a high degree of neovascularization, as observed in the Goldner-Masson trichrome stained sections (Appendix, **Fig. A4.2D/E/F**).

The main histological finding, however, was that Fine-CDHA and CO_3-CDHA scaffolds stimulated bone ingrowth further, with newly formed bone present in the centre of the scaffolds already at 6 weeks postimplantation (**Fig. 4.7A1/A3**). Conversely, in the Coarse-CDHA scaffolds at this early time point new bone was formed only in the peripheral areas of the defects (**Fig. 4.7A2**).
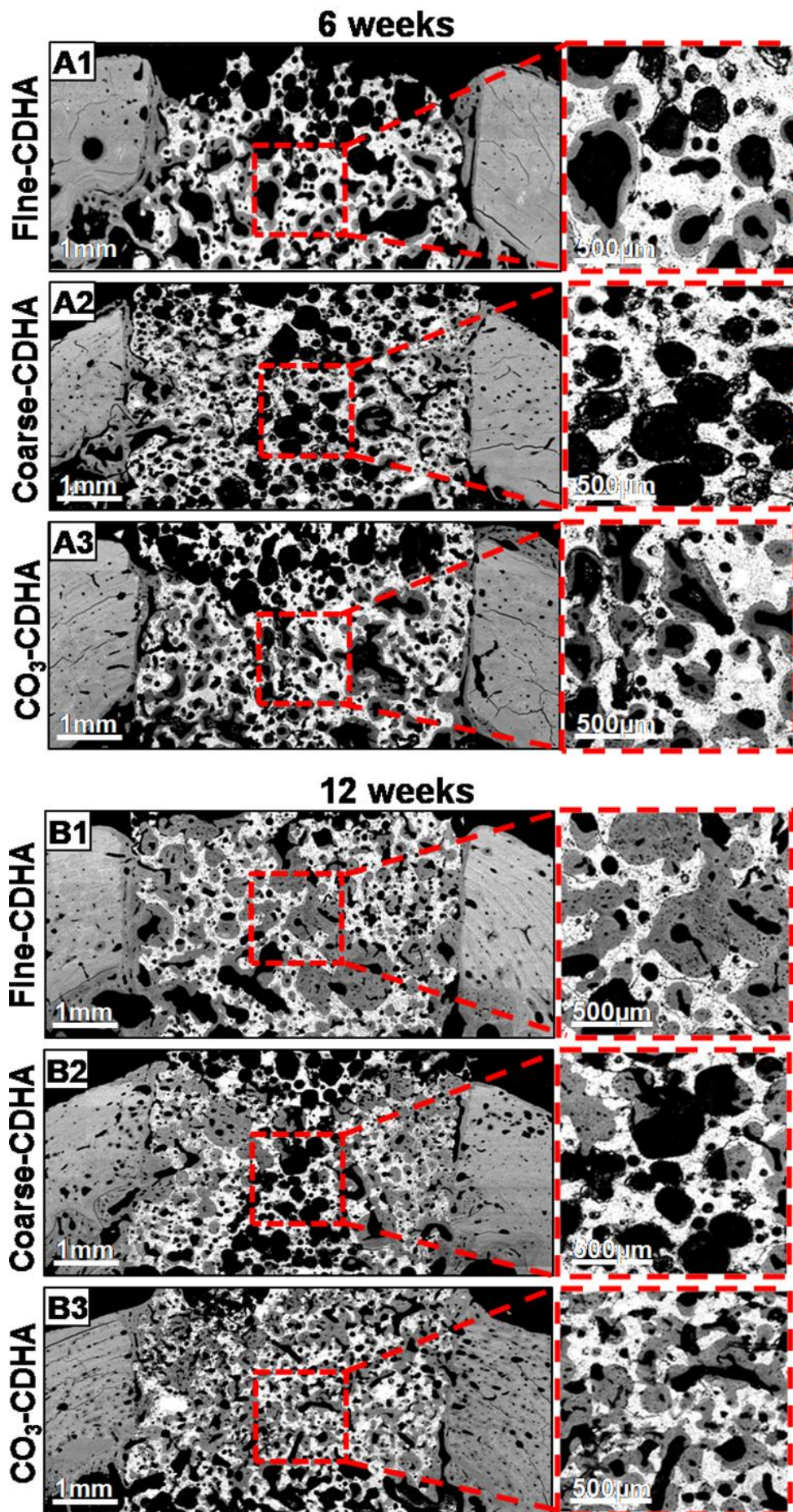
Figure 4.7. Backscattered scanning electron micrographs of a section of the femoral diaphysis, showing the cortical bone containing the studied scaffolds, after 6 **(A)** and 12 weeks **(B)** of implantation.

After 12 weeks, complete bridging of bone defects were found for the Fine-CDHA and CO$_3$-CDHA scaffolds (**Fig. 4.7B1/B3**), whereas bone formation was more limited in Coarse-CDHA scaffolds and some empty pores were still observed in the central regions of the defects (**Fig. 4.7B2**).

These histological observations were confirmed by the histomorphometric results obtained by micro-CT (**Fig. 4.8**). The percentage of newly formed bone was significantly higher in the Fine-CDHA and CO$_3$-CDHA groups than in the Coarse-CDHA group, at both time points, as shown in **Fig. 4.8A**. Moreover, Fine-CDHA and CO$_3$-CDHA groups showed a significantly higher degradation than the Coarse-CDHA scaffolds at 12 weeks (**Fig. 4.8B**). Similarly to what happened intramuscularly, the CO$_3$-CDHA scaffolds showed a higher resorption than Fine-CDHA constructs, especially at 12 weeks, and the resorption of Coarse-CDHA scaffolds did not progress significantly overtime (**Fig. 4.8B**).
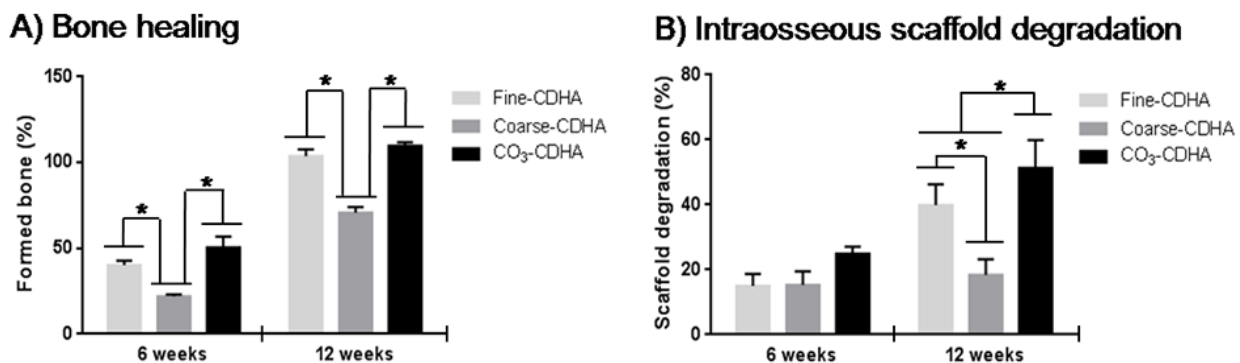

Figure 4.8. Histomorphometrical results obtained by micro-CT after 6 and 12 weeks of intraosseous implantation: **(A)** Percentage of newly formed bone within the monocortical bone defect. **(B)** Percentage of scaffold degradation. (*) denotes groups with statistically significant differences at the same time point (p < 0.05).

The consistent observation of cutting cones and multinucleated osteoclast-like cells in all groups was a clear indication of cell-mediated scaffold resorption and the integration of the material in the bone remodelling process (Appendix, **Fig. A4.2G/H/I**). However, similarly to the intramuscular study, a larger number of osteoclast-like cells was observed in the Fine-CDHA, and especially in the CO$_3$-CDHA scaffolds, than in the Coarse-CDHA foams at both time points.

4.4 Discussion

The fabrication of CaP scaffolds using biomimetic routes, based on the hydrolysis of α-TCP to a CDHA at body temperature, and avoiding high temperature sintering processes, allowed mimicking the properties of bone mineral. As shown in **Fig. 4.1**, it was possible to tune the microstructure and the chemical composition of the biomimetic CDHA, modifying crystal shape and size, and consequently the textural properties of the materials. Using α-TCP powders of different sizes, either fine or coarse, allowed obtaining CDHA nanocrystals with different morphologies, either thin needles several hundreds of nm long or thin submicrometric plates respectively, with a consequent change in the SSA from 40 m^2/g to 20 m^2/g (**Fig. 4.1D** and **Table 4.3**). Although the crystals obtained were still slightly larger than the ones found in the bone mineral, the biomimetic route allowed approaching closely the size and morphology of biological apatite.

Concerning chemical composition, in order to increase the biomimetism of the foams, carbonation of the scaffolds was achieved by performing the setting reaction of the coarse α-TCP foams in a carbonate-containing solution. This resulted in the incorporation of carbonate in the CDHA structure as revealed by the displacement of the XRD peaks and the appearance of the bands in the ATR-FTIR spectra corresponding to B-type carbonated CDHA, the preferred type of carbonate substitution in bone apatite.[4,5,7,8] The amount of carbonate introduced in the CDHA was 11-12%, slightly higher than the amount contained in bone apatite, which ranges between 4 and 8% [4-6] depending on the age.[68] This was accompanied with a change in microstructure, since small plate-like nanocrystals with intermediate SSA (around 30 m^2/g) were obtained (**Fig. 4.1D** and **Table 4.3**), in agreement with previous studies.[26]

The effects of both nanostructure and carbonate substitution in terms of osteoinduction and bone healing potential are discussed in the following sections.

4.4.1 Effect of nanostructure and carbonate doping on osteoinduction

The foams analyzed in the present study presented similar macropore architecture, that is, similar percentage of total porosity, macropore volume, macropore architecture, macropore entrance size and macropore size values (**Fig. 4.1D** and **Table 4.3**). The good macropore interconnectivity fostered a fast neovascularization in all scaffolds (**Fig. 4.3**). In contrast, very different trends were observed in terms of osteoinduction depending on nanostructure and chemical composition. After the intramuscular implantation of the scaffolds for 6 weeks, Coarse-CDHA scaffolds did not show any sign of ectopic bone formation, while both Fine-CDHA and CO_3-CDHA exhibited high incidences of ectopic bone formation, being slightly higher for the carbonated foams (**Fig. 4.3** and **Fig. 4.4**). Moreover, at 12 weeks postimplantation, these two groups showed a significant amount of ectopic bone formation in all animals, whereas only a small amount of newly formed ectopic bone was observed in 2 out of 6 animals in the Coarse-CDHA group (**Fig. 4.4** and **Fig. 4.5**). Considering that the three groups shared the same macropore features, the significant differences observed in their osteoinductive potential should be ascribed to the nanostructure and composition of the materials. The smaller nanocrystals of the Fine-CDHA and CO_3-CDHA scaffolds, with the associated larger SSAs compared to the Coarse-CDHA scaffolds, are known to enhance surface reactivity increasing the capacity to release calcium and phosphate ions upon cell-mediated degradation. The reactivity is moreover further promoted by the presence of carbonate ions. These findings go in the same direction as previous *in vivo* studies,[40,69-72] in which it was shown that increasing the microporosity fostered osteoinduction of CaPs, although the range of SSAs analyzed were significantly smaller than the ones studied in the present work.

The *in vitro* study with rMSCs showed some contradictory results. A higher cell proliferation (**Fig. 4.2A**) and more mature cell morphology (**Fig. 4.2B**) was observed for the cells cultured on CO_3-CDHA discs compared with both Fine- and Coarse-CDHA discs. However, the RT-qPCR analysis showed, as a general trend, higher expression of osteogenic genes for the cells cultured on Fine- and Coarse-CDHA than on CO_3-CDHA samples, with no significant differences between the two undoped CDHA substrates (Appendix, **Fig. A4.1**).

These results, which can seem contradictory when compared with the ectopic bone formation, are a clear indication of the limitations of the static *in vitro* cell cultures to model the *in vivo* scenario, and reveal that the mechanism leading to osteoinduction cannot be reduced to a simple

and direct interaction between material and MSCs. The mechanism is in fact far more complex and involves numerous intermediate processes and interactions, which are overlooked in a simple *in vitro* MSC cell culture study.[73] The active involvement of macrophages and osteoclasts in osteoinduction has been demonstrated in previous studies.[37-40,70,74,75] The osteogenic growth factors secreted by these cells,[76-80] together with the release of calcium and phosphate ions when resorbing the materials,[80-84] are deemed to trigger the osteogenic differentiation of MSCs.

In this respect, large differences were observed in the degradation behavior of the different foams, despite the identical or similar chemical composition between groups. Coarse-CDHA foams, with the lowest SSA, were the least resorbable scaffolds, being the only group where scaffold resorption did not progress overtime (**Fig. 4.6**). In contrast, Fine-CDHA and CO_3-CDHA scaffolds showed a superior and progressive resorption, with statistically significant differences at 12 weeks compared with Coarse-CDHA constructs (**Fig. 4.6**). Since the physiological fluid is supersaturated with respect to CDHA and CO_3-CDHA, the degradation observed should be attributed to cell activity. In fact, a larger number of osteoclast-like cells was identified in both groups compared with that observed in Coarse-CDHA samples.

Two different parameters can contribute to a higher cell-mediated degradation of a scaffold: i) the presence of a larger number of bone-resorbing cells, in this case osteoclast-like multinucleated cells; ii) the higher sensitivity of the material to the acidic pH produced by the bone-resorbing cells. Regarding the first factor, a higher number of osteoclast-like cells were observed both in the Fine- and CO_3-CDHA foams compared with the Coarse-CDHA scaffolds in the histological analysis, which would contribute to the higher degradation rate observed in that groups. On top of this, the susceptibility of the biomaterial to acidic degradation is clearly dependent on the chemical composition and SSA of the substrate. The foams with higher SSA (Fine-CDHA) and carbonate content (CO_3-CDHA) are more reactive, and therefore more susceptible to acidic degradation.[7,8,28,30,85-86] In this respect, it is clear that the presence of carbonate contributed to the highest degradation observed in the carbonate containing foams, since the SSA of the CO_3-CDHA was smaller than that of Fine-CDHA and in spite of this the degradation was higher. Previous *in vitro*[32-34,36,87] and *in vivo*[7,35,43,45,48,88] studies already reported the promotion of the osteoclastic activity by natural or synthetic carbonated apatites. The results found in the present work demonstrate that both carbonate content and SSA can be used to tune degradation. However, the fact that carbonate doping entails also a change in crystal size and SSA precludes the possibility to evaluate independently the effect of carbonate doping and textural properties.

Interestingly, the higher activity of osteoclastic-like cells observed in the Fine- and CO_3-CDHA foams was associated to a superior osteoinductive potential compared to the Coarse-CDHA constructs. This in fact is in contrast to previous studies, in which the high resorption rate showed by carbonated apatite scaffolds, far from being beneficial for osteoinduction, clearly hindered it.[8,46,47] Carbonated apatites with a SSA of 7-10 m^2/g and 3-8 wt% of carbonate were claimed to lack the stable three-dimensional macrostructure required to facilitate new bone growth, [8,46,47] and it was hypothesized that there was a limit in the increase of SSA to positively influence osteoinduction.[46] In contrast, the nanostructured Fine- and CO_3-CDHA analyzed in this work, with much higher SSA values (30-40 m^2/g), as well as a higher carbonate content (12 wt%) in the case of CO_3-CDHA, simultaneously presented high rates of resorption and large amounts of bone formation in an ectopic site.

4.4.2 Effect of nanostructure and carbonate doping on bone healing

In order to assess the correlation between the osteoinductive potential and bone healing capacity, the same biomaterials were implanted orthotopically in the same dogs used for the intramuscular implantation study. Histological evaluation indicated that all scaffolds were well integrated in the cortical bone without any inflammatory adverse reaction (Appendix, **Fig. A4.2**). Similarly to what was observed intramuscularly, all groups showed a rich widespread blood vessel network within the constructs (Appendix, **Fig. A4.2**), which confirmed the appropriate pore interconnectivity, as well as the good biocompatibility of all three types of scaffolds, as previously reported in similar *in vivo* studies were CDHA[89-94] and carbonated hydroxyapatite[8,35,43,45,47-49,88] were evaluated orthotopically.

The main finding was that the scaffolds with higher osteoinductivity, namely Fine-CDHA and CO_3-CDHA, accelerated and promoted osteogenesis orthotopically (**Fig. 4.7**), as demonstrated by the significantly higher percentage of newly formed bone after 6 and 12 weeks compared with the poorly osteoinductive Coarse-CDHA constructs (**Fig. 4.8A**). Interestingly, whereas considerable bone ingrowth was observed in the peripheral regions of all scaffolds, as a result of their excellent osteoconductive properties triggered by the open and interconnected macropores, negligible amounts of bone were detected in the centre of the Coarse-CDHA scaffolds at 6 weeks (**Fig. 4.7A2**). In contrast, the early presence of new bone formation in the centre of the bone defects treated with the Fine- and CO_3-CDHA scaffolds (**Fig. 4.7A1/A3**) could be ascribed to the high intrinsic osteoinductive capacity of these materials, demonstrated in the ectopic implantation experiment, although, it cannot be ruled out that the better performance of these two scaffolds could derive also from an increased osteoconductive capacity besides their higher intrinsic osteoinductive potential.[46] At 12 weeks, the results followed the same trend, as Fine- and CO_3-CDHA scaffolds showed a full-thickness cortical bone bridging, with the complete repair of the bone defects, whereas bone formation was significantly inferior in the Coarse-CDHA scaffolds (**Fig. 4.7B** and **Fig. 4.8A**). It is worth mentioning that a good correlation between osteoinduction and osteogenic capacity was previously reported by other authors for sintered ceramics.[8,95-98]

A good match was found also when comparing the resorption behaviour in orthotopic and ectopic sites (**Fig. 4.6A** and **Fig. 4.8B**). Fine-CDHA scaffolds showed a significantly higher cell-mediated resorption than Coarse-CDHA scaffolds after 12 weeks of implantation, being even higher in the CO_3-CDHA group (**Fig. 4.8B**). The resorption of Coarse-CDHA constructs implanted intraosseously did not progress overtime (**Fig. 4.8B**), as already observed intramuscularly. The high cell-mediated resorption exhibited by the Fine-CDHA and, especially, by the CO_3-CDHA scaffolds, in conjunction with their high osteoconductive and osteoinductive properties enabled an excellent synchronization between biomaterial resorption and new bone formation. The simultaneous degradation and bone formation is the reason for having a percentage of newly formed bone at 12 weeks over a hundred per cent in these two groups (**Fig. 4.8A**), since the percentage was calculated over the initial macropore volume, and the final macropore volume was larger than the initial one and it was almost completely filled with new bone.

Overall, the present results highlight on one side the importance of the nanocrystal morphology and SSA and suggest that there is a threshold value in terms of SSA necessary to activate the cell-mediated resorption and the associated osteoinductive potential, which determine the

osteogenic capacity of the materials in a bony environment. Regarding the effect of carbonate doping, although it is not possible to separate it from the textural properties since its inclusion in the apatite entails also a change in crystal morphology and an increase in SSA, it clearly increases degradation without impairing the osteoinductive properties.

4.5 Conclusions

The results obtained in the present study demonstrate that the idea of mimicking the mineral phase of bone is a very powerful approach to design bone substitutes with enhanced performance. The size and morphology of the nanocrystals, as well as the presence of carbonate, allow tuning the osteoinductive and osteogenic properties as well as the degradation profile of the CDHA. Moreover, the materials with textural and compositional properties closer to the biological apatite exhibited better results in terms of the synchronization between bone formation and material degradation. This suggests that biomimetic CDHA is able to enter the natural bone remodeling process, being transformed by the cells using the same mechanisms by which they remodel the extracellular matrix. Further studies are required in order to verify this hypothesis and clarify the underlying mechanisms, and the interactions of the material with the host tissue at a cellular and molecular level.

4.6 Appendix

4.6.1 <u>Gene expression of osteogenic markers of rMSCs cultured on planar discs</u>

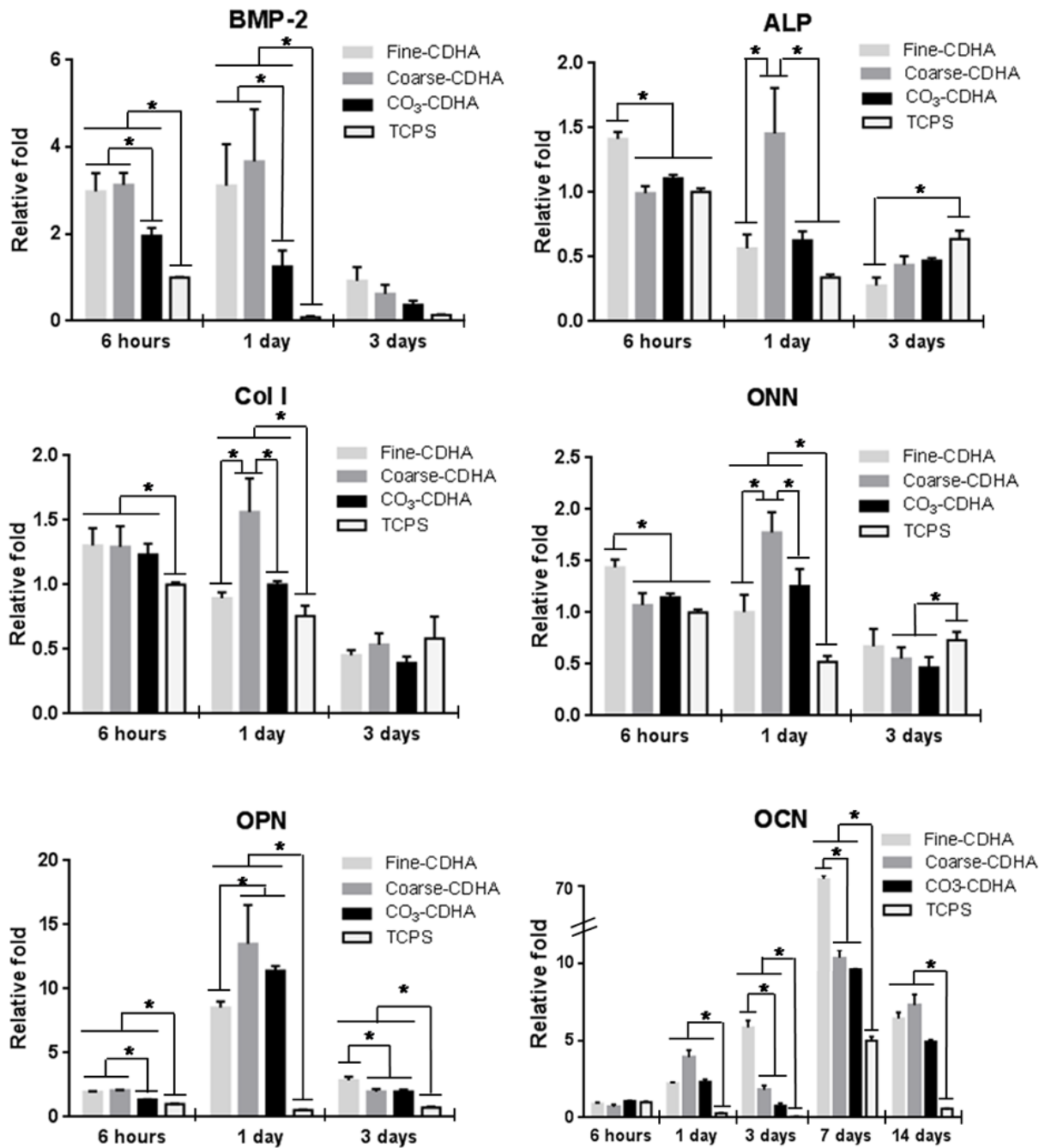**Figure A4.1.** Gene expression of osteogenic markers of rMSCs cultured on planar discs of the different materials used to fabricate the scaffolds (Fine-CDHA, Coarse-CDHA, CO_3-CDHA) and measured by RT-qPCR. TCPS was used as a reference. Cells were cultured in basic medium. Statistical comparisons were performed between CaP materials. (*) denotes groups with statistically significant differences at the same time point ($p < 0.05$).

4.6.2 Histological images of the intraosseoulsy implanted scaffolds
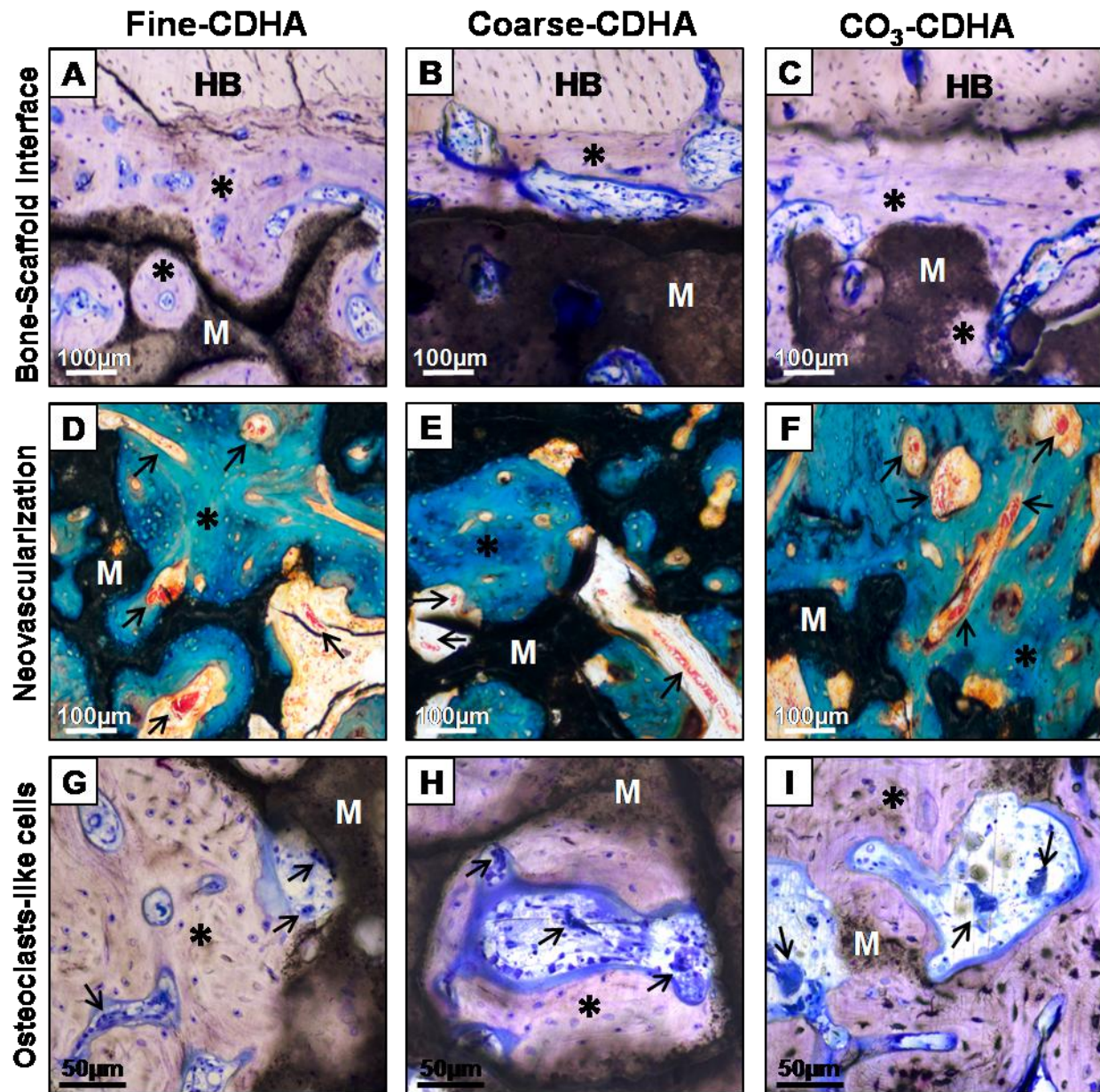
Figure A4.2. Histological images of studied scaffolds after 6 **(A,B,C,D,E,F)** and 12 weeks **(G,H,I)** of intraosseous implantation. **(A,B,C)** Toluidine blue stained sections showing the absence of fibrous capsules at the host cortical bone (HB) and material (M) interfaces in all groups. Note the newly formed bone (asterisks) tight bonded to material surfaces in all three groups of scaffolds. **(D,E,F)** Goldner-Masson trichrome stained sections showing abundant blood vessel (arrows) neoformation within the macropores of materials (M). Asterisks denote newly formed calcified bone matrix. **(G,H,I)** Toluidine blue stained sections showing multinucleated osteoclast-like cells (black arrows), which were consistently observed in all groups, as a clear indication of cell-mediated material (M) resorption. Asterisks denote newly formed calcified bone matrix.

4.7 References

[1]   Wopenka B, Pasteris JD. A mineralogical perspective on the apatite in bone. Mater Sci Eng C 2005;25:131-143.

[2]   Chai YC, Carlier A, Bolander J, Roberts SJ, Geris L, Schrooten J, Van Oosterwyck H, Luyten FP. Current views on calcium phosphate osteogenicity and the translation into effective bone regeneration strategies. Acta Biomater 2012;8:3876-87.

[3]   LeGeros RZ. Calcium phosphate-based osteoinductive materials. Chem Rev 2008;108:4742-53.

[4]   Biltz RM, Pellegrino ED. The nature of bone carbonate. Clin Orthop 1977;129:279-92.

[5]   Rey C, Collins B, Goehl T, Dickson IR, Glimcher M. The carbonate environment in bone mineral: a resolution-enhanced Fourier Transform Infrared Spectroscopy study. Calcif Tissue Int 1989;45:157-64.

[6]   Bigi A, Cojazzi G, Panzavolta S, Ripamonti A, Roveri N, Romanello M, Noris Suarez K, Moro L. Chemical and structural characterization of the mineral phase from cortical and trabecular bone. J Inorg Biochem 1997;68:45-51.

[7]   Landi E, Celotti G, Logroscino G, Tampieri A. Carbonated hydroxyapatite as bone substitute. J Eur Ceram Soc 2003;23:2931-7.

[8]   Habibovic P, Juhl MV, Clyens S, Martinetti R, Dolcini L, Theilgaard N, van Blitterswijk CA. Comparison of two carbonated apatite ceramics in vivo. Acta Biomater 2010;6:2219-26.

[9]   Reznikov N, Shahar R, Weiner S. Bone hierarchical structure in three dimensions. Acta Biomater. 2014;10:3815-26.

[10] McNally E, Schwarcz HP, Botton GA, Arsenault AL. A model for the ultra-structure of bone based on electron microscopy of ion-milled sections. PLos One 2012;7:e29258.

[11] McNally E, Nan F, Botton GA, Schwarcz HP. Scanning transmission electron microscopic tomography of cortical bone using Z-contrast imaging. Micron 2013;49:46-53.

[12] Schwarcz HP, McNally EA, Botton GA. Dark-field transmission electron microscopy of cortical bone reveals details of extrafibrillar crystals. J Struct Biol 2014;188:240-8.

[13] Schwarcz HP. The ultrastructure of bone as revealed in electron microscopy of ion-milled sections. Semin Cell Dev Biol 2015;46:44-50.

[14] Habibovic P. Strategic directions in osteoinduction and biomimetics. Tissue Eng Part A 2017;23:1295-6.

[15] Barradas AMC, Yuan H, van Blitterswijk CA, Habibovic P. Osteoinductive biomaterials: current knowledge of properties, experimental models and biological mechanisms. Eur Cell Mater 2011;21:407-29.

[16] Younger EM, Chapman MW. Morbidity at bone graft donor sites. J Orthop Trauma 1989;3:92-5.

[17] Barba A, Diez-Escudero A, Maazouz Y, Rappe K, Espanol M, Montufar EB, Bonany M, Sadowska JM, Guillem-Marti J, Öhman-Mägi C, Persson C, Manzanares MC, Franch J, Ginebra MP. Osteoinduction by Foamed and 3D-Printed Calcium Phosphate Scaffolds: Effect of Nanostructure and Pore Architecture. ACS Appl Mater Interfaces 2017;9:41722-36.

[18] Ginebra MP, Driessens FCM, Planell JA. Effect of the particle size on the micro and nanostructural features of a calcium phosphate cement: a kinetic analysis. Biomaterials 2004; 25:3453-62.

[19] Ginebra MP, Espanol M, Montufar EB, Perez RA, Mestres G. New processing approaches in calcium phosphate cements and their applications in regenerative medicine. Acta Biomater 2010;6:2863-73.

[20] Pastorino D, Canal C, Ginebra MP. Multiple characterization study on porosity and pore structure of calcium phosphate cements. Acta Biomater 2015;28:205-14.

[21] Dalby MJ, Gadegaard N, Tare R, Andar A, Riehle MO, Herzyk P, Wilkinson CD, Oreffo RO. The control of human mesenchymal cell differentiation using nanoscale symmetry and disorder. Nat Mater 2007;6:997-1003.

[22] Engel E, Del Valle S, Aparicio C, Altankov G, Asin L, Planell JA, Ginebra MP. Discerning the role of topography and ion exchange in cell response of bioactive tissue engineering scaffolds. Tissue Eng Part A. 2008;14:1341-51.

[23] Kilian KA, Bugarija B, Lahn BT, Mrksich M. Geometric cues for directing the differentiation of mesenchymal stem cells. Proc Natl Acad Sci USA 2010;107:4872-7.

[24] Danoux C, Pereira D, Döbelin N, Stähli C, Barralet J, van Blitterswijk C, Habibovic P. The effects of crystal phase and particle morphology of calcium phosphates on proliferation and differentiation of human mesenchymal stromal cells. Adv Healthc Mater 2016;5:1775-85.

[25] Dobbenga S, Fratila-Apachitei LE, Zadpoor AA. Nanopattern-induced osteogenic differentiation of stem cells - A systematic review. Acta Biomater 2016;46:3-14.

[26] Diez-Escudero A, Espanol M, Beats S, Ginebra MP. In vitro degradation of calcium phosphates: Effect of multiscale porosity, textural properties and composition. Acta Biomater 2017;60:81-92.

[27] LeGeros RZ. Effect of Carbonate on the Lattice Parameters of Apatite. Nature 1965;206:403-4.

[28] Nelson DG, Featherstone JD, Duncan JF, Cutress TW. Paracrystalline disorder of biological and synthetic carbonate-substituted apatites. J Dent Res 1982;61:1274-81.

[29] LeGeros RZ, Tung MS. Chemical stability of carbonate- and fluoride-containing apatites. Caries Res 1983;17:419-29.

[30] Okazaki M, Moriwaki Y, Aoba T, Doi Y, Takahashi J. Solubility behavior of CO3 Apatites in relation to crystallinity. Caries Res 1981;15:477-83.

[31] Gibson IR, Bonfield W. Novel synthesis and characterization of an AB-type carbonate substituted hydroxyapatite. J Biomed Mater Res 2001;59:697-708.

[32] Doi Y, Shibutani T, Moriwaki Y, Kajimoto T, Iwayama Y. Sintered carbonate apatites as bioresorbable bone substitutes. J Biomed Mater Res 1998;39:603-10.

[33] Doi Y, Iwanaga K, Shibutani T, Moriwaki Y, Iwayama Y. Osteoclastic responses to various calcium phosphates in cell cultures. J Biomed Mater Res 1999;47:424-33.

[34] Spence G, Patel N, Brooks R, Bonfield W, Rushton N. Osteoclastogenesis on hydroxyapatite ceramics: the effect of carbonate substitution. J Biomed Mater Res A 2010;92:1292-300.

[35] Ayukawa Y, Suzuki Y, Tsuru K, Koyano K, Ishikawa K. Histological Comparison in Rats between Carbonate Apatite Fabricated from Gypsum and Sintered Hydroxyapatite on Bone Remodeling. Biomed Res Int 2015;2015:579541.

[36] Pernelle K, Imbert L, Bosser C, Auregan JC, Cruel M, Ogier A, Jurdic P, Hoc T. Microscale mechanical and mineral heterogeneity of human cortical bone governs osteoclast activity. Bone. 2017;94:42-9.

[37]   Ripamonti U, Klar RM, Renton LF, Ferretti C. Synergistic induction of bone formation by hOP-1, hTGF-beta3 and inhibition by zoledronate in macroporous coral-derived hydroxyapatites. Biomaterials 2010;31:6400-10.

[38]   Akiyama N, Takemoto M, Fujibayashi S, Neo M, Hirano M, Nakamura T. Difference between dogs and rats with regard to osteoclast-like cells in calcium-deficient hydroxyapatite-induced osteoinduction. J Biomed Mater Res A 2011;96:402-12.

[39]   Davison NL, Gamblin A-L, Layrolle P, Yuan H, de Bruijn JD, Barrère-de Groot F. Liposomal clodronate inhibition of osteoclastogenesis and osteoinduction by submicrostructured beta-tricalcium phosphate. Biomaterials 2014;35:5088-97.

[40]   Davison NL, Luo X, Schoenmaker T, Everts V, Yuan H, Barrère-de Groot F, et al. Submicron-scale surface architecture of tricalcium phosphate directs osteogenesis in vitro and in vivo. Eur Cell Mater 2014;27:281-97.

[41]   Ellies LG, Carter JM, Natiella JR, Featherstone JD, Nelson DG. Quantitative analysis of early in vivo tissue response to synthetic apatite implants. J Biomed Mater Res 1988;22:137-48.

[42]   Manjubala I, Sivakumar M, Sureshkumar RV, Sastry TP. Bioactivity and osseointegration study of calcium phosphate ceramic of different chemical composition. J Biomed Mater Res 2002;63:200-08.

[43]   Hasegawa M, Doi Y, Uchida A. Cell-mediated bioresorption of sintered carbonate apatite in rabbits. J Bone Joint Surg Br 2003;85:142-7.

[44]   Porter A, Patel N, Brooks R, Best S, Rushton N, Bonfield W. Effect of carbonate substitution on the ultrastructural characteristics of hydroxyapatite implants. J Mater Sci Mat Med 2005;16:899-907.

[45]   Kogaya Y, Hasegawa M, Uchida A, Doi Y. Ultrastructural characterization of tissue response to sintered carbonate apatite in rabbit bone. Dent Mater J 2006;25:487-492.

[46]   Habibovic P, Sees TM, van den Doel MA, van Blitterswijk CA, de Groot K. Osteoinduction by biomaterials-physicochemical and structural influences. J Biomed Mater Res A 2006;77:747-62.

[47]   Habibovic P, Kruyt MC, Juhl MV, Clyens S, Martinetti R, Dolcini L, Theilgaard N, van Blitterswijk CA. Comparative in vivo study of six hydroxyapatite-based bone graft substitutes. J Orthop Res 2008;26:1363-70.

[48]   Keiichi K, Mitsunobu K, Masafumi S, Yutaka D, Toshiaki S. Induction of new bone by basic FGF-loaded porous carbonate apatite implants in femur defects in rats. Clin Oral Implants Res 2009;20:560-565.

[49]   Hayakawa T, Mochizuki C, Hara H, Yang F, Shen H, Wang S, Sato M. In vivo evaluation of composites of PLGA and apatite with two different levels of crystallinity. J Mater Sci Mater Med 2010;21:251-8.

[50]   Kasai T, Sato K, Kanematsu Y, Shikimori M, Kanematsu N, Doi Y. Bone tissue engineering using porous carbonate apatite and bone marrow cells. J Craniofac Surg. 2010;21:473-8.

[51]   Ellies LG, Nelson DG, Featherstone JD. Crystallographic structure and surface morphology of sintered carbonated apatites. J Biomed Mater Res 1988;22:541-53.

[52]   Doi Y, Koda T, Adachi M, Wakamatsu N, Goto T, Kamemizu H, Moriwaki Y, Suwa Y. Pyrolysis-gas chromatography of carbonate apatites used for sintering. J Biomed Mat Res 1995;29:1451-7.

[53] Tônsuaadu K, Peld M, Leskelä T, Mannonen R, Niinistö L, Veiderma M. A thermoanalytical study of synthetic carbonate-containing apatites. Themochim Acta 1995;256:55-65.

[54] Barralet JE, Best SM, Bonfield W. Effect of sintering parameters on the density and microstructure of carbonate hydroxyapatite. J Mater Sci Mater Med 2000;11:719-24.

[55] Barralet JE, Knowles JC, Best SM, Bonfield W. Thermal decomposition of synthesised carbonate hydroxyapatite. J Mater Sci Mater Med 2002;13:529-33.

[56] Rau JV, Cesaro SN, Ferro D, Barinov SM, Fadeeva IV. FTIR study of carbonate loss from carbonated apatites in the wide temperature range. J Biomed Mater Res B Appl Biomater 2004;71:441-7.

[57] Barinov SM, Rau JV, Cesaro SN, Durisin J, Fadeeva IV, Ferro D, Medvecky L, Trionfetti G. Carbonate release from carbonated hydroxyapatite in the wide temperature rage. J Mater Sci Mater Med 2006;17:597-604.

[58] Barba A, Maazouz Y, Diez-Escudero A, Rappe K, Espanol M, Montufar EB, Persson C, Öhman-Mägi C, Fontecha P, Manzanares MC, Franch J, Ginebra MP. Osteogenesis by foamed and 3D-printed nanostructured calcium phosphate scaffolds: effect of pore architecture. Acta Biomater 2018;79:135-47.

[59] Montufar EB, Traykova T, Gil C, Harr I, Almirall A, Aguirre A, Engel E, Planell JA, Ginebra MP. Foamed surfactant solution as a template for self-setting injectable hydroxyapatite scaffolds for bone regeneration. Acta Biomater 2010;6:876-85.

[60] Gonzalez-Vazquez A, Planell JA, Engel E. Extracellular calcium and CaSR drive osteoinduction in mesenchymal stromal cells. Acta Biomater 2014;10:2824-33.

[61] National Research Council. Guide for the Care and Use of Laboratory Animals; National Academy Press: Washington, DC, 1996; pp 41-194.

[62] Directive 2010/63/EU of the European Parliament and of the Council of 22 September 2010 on the Protection of Animals Used for Scientific Purposes. Available at http://data.europa.eu/eli/dir/2010/63/oj.

[63] Lewin S, Barba A, Persson C, Franch J, Ginebra MP, Öhman-Mägi C. Evaluation of bone formation in calcium phosphate scaffolds with μCT – method validation using SEM. Biomed Mater 2017;12:65005.

[64] Berzina-Cimdina L, Borodajenko N. Research of Calcium Phosphates Using Fourier Transform Infrared Spectroscopy. In: Theophile T, ed. Infrared Spectroscopy - Materials Science, Engineering and Technology. First edition. London: IntechOpen Ltd;2012: pp. 123-48.

[65] Wilson RM, Elliott JC, Dowker SEP, Rodriguez-Lorenzo LM. Rietveld refinements and spectroscopic studies of the structure of Ca-deficient apatite. Biomaterials 2005;26:1317-27.

[66] Fleet ME. The carbonate ion in hydroxyapatite: recent X-ray and infrared results. Front Biosci (Elite Ed) 2013;5:643-52.

[67] Sader MS, Lewis K, Soares GA, LeGeros RZ. Simultaneous incorporation of magnesium and carbonate in apatite: effect on physico-chemical properties. Materials Research 2013;16:779-84.

[68] Rey C, Renugopalakrishnan V, Collins B, Glimcher MJ. Fourier transform infrared spectroscopic study of the carbonate ions in bone mineral during aging. Calcif Tissue Int 1991;49:251-8.

[69] Habibovic P, Yuan H, van der Valk CM, Meijer G, van Blitterswijk CA, de Groot K. 3D microenvironment as essential element for osteoinduction by biomaterials. Biomaterials 2005;26: 3565-75.

[70] Davison NL, Su J, Yuan H, van den Beucken JJ, de Bruijn JD, Barrère-de Groot F. Influence of surface microstructure and chemistry on osteoinduction and osteoclastogenesis by biphasic calcium phosphate discs. Eur Cell Mater 2015;29:314-29.

[71] Zhang J, Luo X, Barbieri D, Barradas AMC, de Bruijn JD, van Blitterswijk CA, Yuan H. The size of surface microstructures as an osteogenic factor in calcium phosphate ceramics. Acta Biomater 2014;10:3254-63.

[72] Chan O, Coathup MJ, Nesbitt A, Ho CY, Hing KA, Buckland T, Campion C, Blunn GW. The effects of microporosity on osteoinduction of calcium phosphate bone graft substitute biomaterials. Acta Biomater 2012;8:2788-94.

[73] Habraken W, Habibovic P, Epple M, Bohner M. Calcium phosphates in biomedical applications: materials for the future? Mater Today 2016;19:69-87.

[74] Kondo N, Ogose A, Tokunaga K, Umezu H, Arai K, Kudo N, Hoshino M, Inoue H, Irie H, Kuroda K, Mera H, Endo N. Osteoinduction with highly purified beta-tricalcium phosphate in dog dorsal muscles and the Proliferation of osteoclasts before heterotopic bone formation. Biomaterials 2006;27:4419-27.

[75] Klar RM, Duarte R, Dix-Peek T, Dickens C, Ferretti C, Ripamonti U. Calcium ions and osteoclastogenesis initiate the induction of bone formation by Coral-Derived macroporous constructs. J Cell Mol Med 2013;17:1444-57.

[76] Garimella R, Tague SE, Zhang J, Belibi F, Nahar N, Sun BH, Insogna K, Wang J, Anderson HC. Expression and synthesis of bone morphogenetic proteins by osteoclasts: a possible path to anabolic bone remodeling. J Histochem Cytochem 2008;56:569-77.

[77] Pederson L, Ruan M, Westendorf JJ, Khosla S, Oursler MJ. Regulation of bone formation by osteoclasts involves Wnt/BMP signaling and the chemokine sphingosine-1-phosphate. Proc Natl Acad Sci USA 2008;105:20764-9.

[78] Kreja L, Brenner RE, Tautzenberger A, Liedert A, Friemert B, Ehrnthaller C, Huber-Lang M, Ignatius A. Non-resorbing osteoclasts induce migration and osteogenic differentiation of mesenchymal stem cells. J Cell Biochem 2010;109:347-55.

[79] Guihard P, Danger Y, Brounais B, David E, Brion R, Delecrin J, Richards CD, Chevalier S, Rédini F, Heymann D, Gascan H, Blanchard F. Induction of osteogenesis in mesenchymal stem cells by activated monocytes/macrophages depends on oncostatin M signaling. Stem Cells 2012;30:762-72.

[80] Takeshita S, Fumoto T, Matsuoka K, Park K, Aburatani H, Kato S, Ito M, Ikeda K. Osteoclast-secreted CTHRC1 in the coupling of bone resorption to formation. J Clin Invest 2013;123:3914-24.

[81] Beck Jr GR. Inorganic phosphate as a signaling molecule in osteoblast differentiation. J Cell Biochem 2003;90:234-43.

[82] Dvorak MM, Riccardi D. Ca^{2+} as an Extracellular Signal in Bone. Cell Calcium 2004;35:249-55.

[83] Habibovic P, Bassett DC, Doillon CJ, Gerard C, McKee MD, Barralet JE. Collagen biomineralization in vivo by sustained release of inorganic phosphate ions. Adv Mater 2010;22:1858-62.

[84] Barradas AMC, Fernandes HAM, Groen N, Chai YC, Schrooten J, van de Peppel J, van Leeuwen JP, van Blitterswijk CA, de Boer J. A calcium-induced signaling cascade leading

to osteogenic differentiation of human bone marrow-derived mesenchymal stromal cells. Biomaterials 2012;33:3205-15.

[85] Legeros RZ, Trautz OR, Legeros JP, Klein E, Shirra WP. Apatite crystallites: effects of carbonate on morphology. Science 1967;155:1409-11.

[86] Yokota R, Hayashi H, Hirata I, Miake Y, Yanagisawa T, Okazaki M. Detailed consideration of physicochemical properties of CO3Apatites as biomaterials in relation to carbonate content using ICP, X-ray diffraction, FT-IR, SEM and HR-TEM. Dent Mater J 2006;25:597-603.

[87] Spence G, Patel N, Brooks R, Rushton N. Carbonate substituted hydroxyapatite: resorption by osteoclasts modifies the osteoblastic response. J Biomed Mater Res A 2009;90:217-24.

[88] Nagayama M, Takeuchi H, Doi Y. Comparison of carbonate apatite and beta-tricalcium phosphate (resorbable calcium phosphates) implanted subcutaneously into the back of rats. Dent Mater J 2006;25:219-25.

[89] Ambrosio L, Guarino V, Sanginario V, Torricelli P, Fini M, Ginebra MP, Planell JA, Giardino R. Injectable calcium-phosphate-based composites for skeletal bone treatments. Biomed Mater 2012;7:024113.

[90] Okuda T, Ioku K, Yonezawa I, Minagi H, Gonda Y, Kawachi G, Kamitakahara M, Shibata Y, Murayama H, Kurosawa H, Ikeda T. The slow resorption with replacement by bone of a hydrothermally synthesized pure calcium-deficient hydroxyapatite. Biomaterials 2008;29:2719-28.

[91] Gonda Y, Ioku K, Shibata Y, Okuda T, Kawachi G, Kamitakahara M, Murayama H, Hideshima K, Kamihira S, Yonezawa I, Kurosawa H, Ikeda T. Stimulatory effect of hydrothermally synthesized biodegradable hydroxyapatite granules on osteogenesis and direct association with osteoclasts. Biomaterials 2009;30:4390-400.

[92] Guo H, Su J, Wei J, Kong H, Liu C. Biocompatibility and osteogenicity of degradable Ca-deficient hydroxyapatite scaffolds from calcium phosphate cement for bone tissue engineering. Acta Biomater 2009;5:268-78.

[93] Sponer P, Strnadová M, Urban K. In vivo behaviour of low-temperature calcium-deficient hydroxyapatite: comparison with deproteinised bovine bone. Int Orthop 2011;35:1553-60.

[94] Cuzmar E, Perez RA, Manzanares MC, Ginebra MP, Franch J. In Vivo Osteogenic Potential of Biomimetic Hydroxyapatite/Collagen Microspheres: Comparison with Injectable Cement Pastes. PLoS One 2015;10:e0131188.

[95] Habibovic P, Yuan H, van den Doel M, Sees TM, van Blitterswijk CA, de Groot K. Relevance of osteoinductive biomaterials in critical-sized orthotopic defect. J Orthop Res 2006;24:867-76.

[96] Yuan H, van Blitterswijk CA, de Groot K, de Bruijn JD. A comparison of bone formation in biphasic calcium phosphate (BCP) and hydroxyapatite (HA) implanted in muscle and bone of dogs at different time periods. J Biomed Mater Res A 2006;78:139-47.

[97] Yuan H, Fernandes H, Habibovic P, de Boer J, Barradas AMC, de Ruiter A, Walsh WR, van Blitterswijk CA, de Bruijn JD. Osteoinductive ceramics as a synthetic alternative to autologous bone grafting. Proc Natl Acad Sci USA 2010;107:13614-9.

[98] Davison NL, Yuan H, de Bruijn JD, Barrere-de Groot F. In vivo performance of microstructured calcium phosphate formulated in novel water-free carriers. Acta Biomater 2012;8:2759-69.

Chapter 5

GENERAL CONCLUSIONS

This thesis was devoted to investigate the role of different intrinsic physicochemical parameters of CaP scaffolds on their osteoinductive, osteoconductive and osteogenic properties, as well as on their resorption profile in order to enhance their clinical performance as bone substitutes. The main conclusions are summarized below:

Chapter 2. Osteoinduction by foamed and 3D-printed calcium phosphate scaffolds: effect of nanostructure and pore architecture

➤ Nanostructure and reactivity of the CaP substrate were critical factors for osteoinduction and material degradation of the foamed scaffolds implanted intramuscularly.

- The high reactivity of biomimetic CDHA, which resulted from its chemical composition, poor crystallinity, nanostructured nature (needle-like nanocrystals) and high SSA combined with the concave macroporosity produced by a foaming process, resulted in accelerated osteoinduction when compared with conventional sintered ceramics with the same macropore architecture, but with higher crystallinity, lack of nanostructure and significantly lower SSAs, due to the high temperature processing.

- The high cell-mediated resorption of CDHA foams, contrary to being an obstacle for osteoinduction, clearly promoted it. The progressive scaffold resorption resulted in a simultaneous replacement by new ectopic bone, homogeneously distributed within the entire construct, including the periphery.

- A different ectopic bone formation pattern was found when comparing BCP and CDHA foams. Contrary to what was found in the CDHA scaffolds, where ectopic bone replaced the biomaterial, in the BCP scaffolds bone was deposited on the surface of the material, progressively filling the pore space, and mainly concentrated in the centre of the constructs with minimal bone formation in the peripheral regions. This was attributed to the slower degradation of BCP foams, which could also explain the delayed ectopic bone formation compared to the CDHA foams.

- The β-TCP foams showed a high and heterogeneous degradation pattern. The loss of a stable three-dimensional macrostructure was probably the main reason for the poor intrinsic osteoinduction showed by this group, despite having the same macroporosity, microstructure and SSA than BCP foams.

➤ Pore architecture also played a crucial role in osteoinduction and material resorption of CDHA scaffolds implanted intramuscularly.

- The concave macropores with small entrance sizes of the foamed scaffolds stimulated the intrinsic osteoinduction of CDHA when compared with the prismatic macropores with convex surfaces and large entrance sizes of the robocast scaffolds. This was associated to the distinct microenvironments created in the different scaffolds.

- Pore geometry had also a significant effect on material degradation. Foamed scaffolds showed a higher cell-mediated resorption than the robocast counterparts, suggesting that osteoclastic activity was influenced by the different microenvironments created by the distinct macropore architectures. This, in turn, confirmed the close connection between osteoclastic activity and osteoinduction.

- Within the ranges analyzed in the present study (200-400 µm), macropore size of the robocast scaffolds was not a critical parameter, since no differences were found between the robocast scaffolds with different pore dimensions.

➢ Tailoring both nanostructure and macropore geometry is a good strategy to enhance the osteoinduction of calcium phosphates. Specifically, designing nanostructured biomimetic CDHA with convex macropores allowed pushing the osteoinduction potential beyond the limits obtained for the microstructured CaP ceramics.

Chapter 3. Osteogenesis by foamed and 3D-printed nanostructured calcium phosphate scaffolds: effect of pore architecture

➢ Pore geometry played a crucial role in the *in vivo* performance of biomimetic CDHA scaffolds implanted intraosseously. Both bone healing capacity and material degradation of chemically identical materials (CDHA) with the same nanostructure (needle-like nanocrystals) and similar SSAs ($\approx$35 m^2/g) and pore volumes ($\approx$70%) were drastically affected by the macropore architecture of the scaffolds.

- Although CDHA was highly osteoconductive both in the robocast and foamed scaffolds, CDHA foams showed a superior bone healing capacity than the robocast counterparts.

- Foamed scaffolds showed an early presence of new bone formation in the centre of bone defects, whereas very small amounts of bone were detected in the central macropores of the robocast scaffolds at six weeks. The superior bone healing capacity of the foamed scaffolds correlated well with their higher intrinsic osteoinductive potential, demonstrated previously in the ectopic implantation experiment.

- Fibrous-tissue infiltration was significantly more extensive within the central macropores of the robocast samples than in the foams. This could partly explain the lower values of newly formed bone and, especially, the lack of new bone formation in the central regions of the robocast scaffolds compared with the CDHA-Foam group at 6 weeks.

- The contribution of both osteoconduction and osteoinduction accelerated the complete healing of the bone defects in the foamed group.

- The foamed scaffolds showed a superior cell-mediated resorption than the robocast constructs, triggering the simultaneous and progressive scaffold replacement by new bone, which correlated well with the degradation results obtained intramuscularly.

- Within the ranges analyzed in the present study (200-400 µm), the different macropore size between the two robocast scaffolds did not have any significant effect neither on new bone formation nor on degradation, as observed in the intramuscular implantation study.

➢ The control of macropore architecture of CDHA nanostructured bone susbtsitutes allows tuning both material degradation and new bone formation. Specifcally, the foamed scaffolds showed a superior bone regeneration potential and higher resorption than the 3D-printed scaffolds.

Chapter 4. Osteoinduction and osteogensis by nanostructured calcium phosphate scaffolds: effect of nanocrystal morphology and carbonate doping

➢ Nanocrystal morphology and the associated SSA played a key role in the *in vivo* performance of biomimetic CDHA-based bone substitutes.

- Fine-CDHA foams with needle-like nanocrystals and a high SSA (40 m^2/g) showed a higher osteoinductive potential and a superior cell-mediated resorption than Coarse-CDHA foams with plate-shaped crystals and a SSA of 20 m^2/g.

- The early presence of new bone formation in the centre of bone defects and the superior bone healing capacity showed by the Fine-CDHA scaffolds correlated well with their superior osteoinduction observed ectopically. Moreover, they were progressively resorbed and simultaneously replaced by new bone when implanted intraosseously.

- In contrast, the Coarse-CDHA foams implanted intraosseously showed a limited bone healing capacity and their resorption did not progress overtime, similarly to that observed intramuscularly.

- These findings suggested that there is a threshold in terms of SSA that is required to activate the cell-mediated resorption and the associated osteoinductive potential, which determine the osteogenic capacity of the materials in a bony environment.

➢ Carbonate dopping of CDHA, which resulted in small plate-shaped crystals and a SSA of 30 m^2/g, enhanced the biological performance of scaffolds.

- Carbonation of CDHA accelerated both the intrinsic osteoinduction and the bone healing capacity compared with the Fine-CDHA scaffolds despite having a lower SSA.

- The carbonation of CDHA significantly increased the cell-mediated resorption of scaffolds despite having a lower SSA than Fine-CDHA scaffolds in both ectopic and orthotopic implantation sites.

- These findings demonstrated that it is possible to have simultaneously high rates of resorption with large amount of bone formation, which allows for a gradual replacement of the material by the newly formed autologous bone tissue.

➢ Developing materials that mimic the mineral phase of bone allows introducing the material in the physiological bone remodelling cycle, this resulting in a tight synchronization of material degradation and bone formation, and ultimately, obtaining bone substitutes with enhanced bone regeneration capacities.

Chapter 6
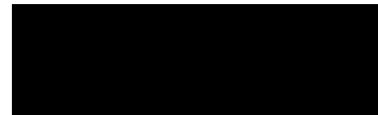
FUTURE PERSPECTIVES

The results obtained in the present thesis showed that biomimetic routes based on the self-setting reaction of CPCs represent a promising platform to obtain synthetic bone grafts with enhanced biological performance.

The enhanced osteoinductive potential and, hence, the accelerated bone healing capacity of the nanostructured CDHA foams with needle-like crystals and the carbonated CDHA foams, together with their progressive and homogenous resorption behaviour, make them better candidates as bone substitutes than sintered CaPs.

The next step toward the clinical application of these novel biomimetic bone substitutes would be to perform a comparative critical-seized orthotopic implantation study with a positive control (autograft), a negative control (empty defect) and the most widely used commercial bone grafts (sintered ceramics and allografts). In the proposed study would be critical also to evaluate their mechanical stability, since a too rapid scaffold resorption may be detrimental for bone regeneration, especially in the centre of the bone defect. The optimization of the mechanical properties of these biomimetic, macroporous foams would represent a significant benefit towards their clinical application.

Although we used a standardized animal model, establishing direct comparisons with other studies and drawing general conclusions was challenging due to the differences found in the experimental protocols, including different animal models, implantation sites, implantation times, evaluation techniques and histomorphometrical analysis. To solve these problems, standardized experimental protocols for the *in vivo* evaluation of bone substitutes should be established enabling the direct comparison between preclinical studies. Eventually, only prospective randomized clinical trials will be able to provide the conclusive evidence that these novel biomimetic bone substitutes can act as a valid alternative to autologous bone grafts in human patients.

Moreover, in future *in vivo* studies would be also interesting to work with decalcified tissue samples embedded in paraffin, which allow performing several immuno-histochemical tests (e.g. TRAP for osteoclasts, inflammatory markers, osteogenic markers) in order to shed further light on the cellular signaling occurring at the bone-biomaterials interface, and to better understand the underlying mechanisms responsible for bone induction. In the present thesis, it was not possible since the high temperature resin-embedding and polymerization procedures did not allow for this type of immuno-histochemical investigation. However, it is a line of research that deserves further attention to compose a larger picture of what is the exact biological response of such biomimetic substrates.

Another advantage of these novel biomimetic foams compared with the conventional sintered ceramics is that through a setting reaction at body temperature they are able to harden *in vivo* while preserving their hierarchical porosity. Thus, they can be obtained as an injectable paste-like material suitable for minimally invasive surgery applications. In this context, it would be crucial to investigate if they preserve the observed intrinsic osteoinductive potential and the enhanced bone healing capacity when used as an injectable foaming paste in an ectopic and orthotopic implantation models, respectively.

The design of biomimetic smart matrices able to instruct the endogenous expression of osteogenic growth factors, as those developed in the present thesis, has been proposed as one of the most promising approaches to obtain effective, affordable, safe and readily available off-the-shelf synthetic bone substitutes to replace autografts. However, their intrinsic osteoinductive and osteogenic capacities could be insufficient in certain compromised clinical scenarios. Moreover, depending on the clinical problem different types of substitutes or combinations (polytherapy) are necessary. Therefore, this new family of low-temperature biomimetic bone grafts emerges as a promising starting point to find the ideal carrier for drugs, bioactive molecules or even cells without protein thermal denaturalization or loss of activity associated with the high-temperature processing techniques. For instance, their high SSAs, their increased protein entrapment capacity, and their boosted intrinsic osteoinduction could avoid the use of expensive and unsafe megadoses of exogenous growth factors and may simplify the regulatory path towards the clinical application of these bone tissue engineering strategies.

Finally, although the optimized robocast scaffolds showed a limited osteoinductive potential, they demonstrated excellent osteoconductive capacities. Moreover, 3D printing technology enables a fast fabrication of individual complex geometrical scaffolds with high precision on the internal architecture and on the outer shape and with a high reliable reproducibility, which constitute a remarkable clinical advantage. Robocast scaffolds can be built in the shape of the pacient-specific bone tissue defect given by the computer-aided design specifications based on computerized tomography or magnetic resonance imaging 3D data files of patients. This matching of the shape should help to reduce the surgical time, as well as the bone healing time. On the other hand, the superior control on the internal architecture allows exploring new insights into the cell-material interactions, such as the importance of macropores surface curvature.While in the present work we chose the simplest geometrical pattern with orthogonal struts, the osteoinductive and osteogenic potentials of other patterns, with more complex internal architectures should be assessed in future studies. An alternative strategy to improve the biological performance of these biomimetic robocast scaffolds would be to combine them with bioactive molecules and MSCs during the 3D-printing process thanks to the beneficial low-temperature setting reaction, which avoids the harmful sintering step. Therefore, the results obtained in the present thesis, far from going against 3D-printing, stress the importance of pushing the enormous possibilities of this technique in the right direction.

Annex

Publications and conferences

PUBLICATIONS

- Lewin S, Barba A, Persson C, Franch J, Ginebra MP, Öhman-Mägi C. Evaluation of bone formation in calcium phosphate scaffolds with μCT – method validation using SEM. Biomed Mater 2017;12:65005.

- Barba A, Diez-Escudero A, Maazouz Y, Rappe K, Espanol M, Montufar EB, Bonany M, Sadowska JM, Guillem-Marti J, Persson C, Öhman-Mägi C, Manzanares MC, Franch J, Ginebra MP. Osteoinduction by foamed and 3D-printed calcium phosphate scaffolds: effect of nanostructure and pore architecture. ACS Appl Mater Interfaces 2017;9:41722-36.

- Barba A, Maazouz Y, Diez-Escudero A, Rappe K, Espanol M, Montufar EB, Persson C, Öhman-Mägi C, Fontecha P, Manzanares MC, Franch J, Ginebra MP. Osteogenesis by foamed and 3D-printed nanostructured calcium phosphate scaffolds: effect of pore architecture. Acta Biomater 2018;79:135-47.

- Barba A, Diez-Escudero A, Espanol M, Fontecha P, Bonany M, Sadowska JM, Guillem-Marti J, Persson C, Öhman-Mägi C, Manzanares MC, Franch J, Ginebra MP. Osteoinduction and osteogenesis by nanostructured calcium phosphate scaffolds: effect of nanocrystal morphology and carbonate doping. ACS Nano. **(Under revision, September 2018)**

CONFERENCE PARTICIPATION

- Barba A, Rappe K, Fontecha P, Diez-Escudero A, Maazouz Y, Montufar EB, Espanol M, Manzanares MC, Franch J, Ginebra MP. Osteoinducción intrínseca de sustitutos óseos biomiméticos con diferentes nano-, micro- y macroporosidades para su aplicación clínica en el tratamiento de defectos óseos críticos. Poster: XV Jornadas GEVO, Ibiza (Spain), 29th April - 2nd May 2015.

- Barba A, Rappe K, Maazouz Y, Ginebra MP, Franch J. 3D-printed β-TCP scaffold loaded with rhBMP-2 as treatment for a severe atrophic non-union of the radius in a Yorkshire Terrier. Poster: IX Southern European Veterinary Conference / 21st Federation of European Companion Animals Veterinary Associations Eurocongress / XII Congreso Federación Iberoamericana de Asociaciones Veterinarias, Barcelona (Spain), 15th-17th October 2015. **AWARD FOR THE BEST STUDENT PRESENTATION**

- Barba A, Rappe K, Fontecha P, Diez-Escudero A, Maazouz Y, Montufar EB, Espanol M, Manzanares MC, Ginebra MP, Franch J. Biomimetic calcium phosphate scaffolds with intrinisic osteoinductive activity for the treatment of critical-sized bone defects. Poster: IX Southern European Veterinary Conference / 21st Federation of European Companion Animals Veterinary Associations Eurocongress / XII Congreso Federación Iberoamericana de Asociaciones Veterinarias, Barcelona (Spain), 15th-17th October 2015.

- Barba A, Rappe K, Diez-Escudero A, Maazouz Y, Montufar EB, Espanol M, Manzanares MC, Franch J, Ginebra MP. Osteoinducción intrínseca de sustitutos óseos biomiméticos con diferentes nano-, micro- y macroporosidades. Poster: XXXVIII Congreso de la Sociedad Ibérica de Biomecánica y Biomateriales. Barcelona (Spain), 6th-7th November 2015.

- Barba A, Rappe K, Fontecha P, Diez-Escudero A, Maazouz Y, Espanol M, Öhman-Mägi C, Persson C, Manzanares MC, Ginebra MP, Franch J. Evaluación del potencial osteogénico de sustitutos óseos biomiméticos con diferentes nano-, micro- y macroporosidades para su aplicación clínica en el tratamiento de defectos óseos críticos. Poster: XVI Jornadas GEVO, Baiona (Spain), 4th-7th May 2016.

- Franch J, Barba A, Rappe K, Maazouz Y, Ginebra MP. Tratamiento de una no-unión atrófica severa de radio en un Yorkshire Terrier mediante uso combinado de injerto sintético robocasted de β-TCP y rhBMP-2. Aplicación clínica y desarrollo de nuevos biomateriales con osteoinducción intrínseca. Oral communication: XVI Jornadas GEVO, Baiona (Spain), 4th-7th May 2016.

- Barba A, Rappe K, Fontecha P, Diez-Escudero A, Maazouz Y, Montufar EB, Espanol M, Manzanares MC, Ginebra MP, Franch J. Intrinsic osteoinduction of biomimetic nanostructured calcium phosphate scaffolds. Oral communication: 10th World Biomaterials Congress, Montreal (Canada), 17th-22nd May 2016.

- Barba A, Rappe K, Fontecha P, Diez-Escudero A, Maazouz Y, Espanol M, Öhman-Mägi C, Persson C, Manzanares MC, Franch J, Ginebra MP. Biomimetic nanostructured calcium phosphate scaffolds: osteoinduction and osteogenesis. Oral communication: 2016 eCM XVII: Stem cells, Bone Fixation, Repair & Regeneration. AO Foundation, Davos (Switzerland), 20th-23rd June 2016. **ROBERT MATHYS STUDENT AWARD FOR THE BEST ORAL PRESENTATION**

- Franch J, Barba A, Rappe K, Fontecha P, Maazouz Y, Ginebra MP. Long-term evaluation of a radius atrophic non-union treated with rh-BMP-2 and a β-TCP robocasted synthetic bone graft. Oral communication: 18th European Society of Veterinary Orthopaedics and Traumatology (ESVOT) Congress, London (UK), 8th-10th September 2016.

- Barba A, Rappe K, Fontecha P, Diez-Escudero A, Maazouz Y, Espanol M, Manzanares MC, Ginebra MP, Franch J. Intrinsic osteoinduction of biomimetic nanostructured calcium phosphate scaffolds for the treatment of critical-sized bone defects. Poster: 41st World Small Animal Veterinary Association Congress, Cartagena (Colombia), 27th-30th September 2016.

- Barba A, Rappe K, Diez-Escudero A, Maazouz Y, Franch J, Manzanares MC, Ginebra MP. Nanostructured calcium phosphate scaffolds trigger osteoinduction and osteogenesis. Poster: Internation Association for Dental research (IADR) Oral health Research Congress 2017, Vienna (Austria), 21st-23rd September 2017.

- Lewin S, Barba A, Persson C, Franch J, Ginebra MP, Öhman-Mägi C. Assessment of bone formation in CaP scaffolds - μCT method development. Oral communication: 29th Symposium and Annual Meeting of the International Society for Ceramics in Medicine (Bioceramics 29), Tolouse (France), 25th-27th October 2017.